Synthesis and Application of Hybrid Nanocomposites for the Removal of Heavy Metals and Bacteria from Contaminated Water

Thesis submitted to the
University of Calicut
in partial fulfilment of the requirements
for the award of the degree of

DOCTOR OF PHILOSOPHY IN CHEMISTRY

By

Hridya T K

Under the guidance of
Dr. P.S. HARIKUMAR
Chief Scientist (Retd.)

KSCSTE Centre for Water Resources Development and Management
Kozhikode - 673 571, Kerala
June 2023

KSCSTE-CWRDM

KSCSTE - CENTRE FOR WATER RESOURCES DEVELOPMENT AND MANAGEMENT
ജലവിഭവ വികസന വിനിയോഗ കേന്ദ്രം

An Institution of Kerala State Council for Science, Technology & Environment, Govt. of Kerala
കേരള ശാസ്ത്ര സാങ്കേതിക പരിസ്ഥിതി കൗൺസിൽ സ്ഥാപനം, കേരള സർക്കാർ

KSCSTE

Dr. P.S. Harikumar
Chief Scientist (Retd.)
CWRDM.

CERTIFICATE

This is to certify that the thesis entitled **"Synthesis and Application of Hybrid Nanocomposites for the Removal of Heavy Metals and Bacteria from Contaminated Water"** submitted by Hridya T K to the University of Calicut for the award of Doctor of Philosophy in Chemistry under the faculty of science, is an authentic record of the research work carried out at the Ecology and Environment Research Group, Centre for Water Resources Development and Management (CWRDM), Kozhikode, India, under my guidance and supervision. The contents of the thesis have been checked for plagiarism using the software 'Urkund' and the similarity index falls within the permitted limit. I further certify that the content of this thesis has not been submitted elsewhere for the award of any degree or diploma.

CWRDM
March 2023

P S Harikumar
(Research Guide)

Kunnamangalam, Kozhikode-673571, Kerala, India | കുന്ദമംഗലം, കോഴിക്കോട്-673571, കേരളം, ഇന്ത്യ
E-mail: ed@cwrdm.org, registrar@cwrdm.org | Website: www.cwrdm.org
Phone: (91) 495 235 1800, 235 1801 | Fax: (91) 495 235 1808, 235 7827

KSCSTE-CWRDM

KSCSTE - CENTRE FOR WATER RESOURCES DEVELOPMENT AND MANAGEMENT
ജലവിഭവ വികസന വിനിയോഗ കേന്ദ്രം

An Institution of Kerala State Council for Science, Technology & Environment, Govt. of Kerala
കേരള ശാസ്ത്ര സാങ്കേതിക പരിസ്ഥിതി കൗൺസിൽ സ്ഥാപനം, കേരള സർക്കാർ

KSCSTE

Dr. P.S. Harikumar
Chief Scientist (Retd.)
CWRDM.

CERTIFICATE

This is to certify that the thesis entitled **"Synthesis and Application of Hybrid Nanocomposites for the Removal of Heavy Metals and Bacteria from Contaminated Water"** submitted by Hridya T K to the University of Calicut for the award of Doctor of Philosophy in Chemistry under the faculty of science, is an authentic record of the research work carried out at the Ecology and Environment Research Group, Centre for Water Resources Development and Management (CWRDM), Kozhikode, India, under my guidance and supervision. The contents of the thesis have been checked for plagiarism using the software 'Urkund' and the similarity index falls within the permitted limit. I further certify that the content of this thesis has not been submitted elsewhere for the award of any degree or diploma.

CWRDM
March 2023

P S Harikumar
(Research Guide)

Kunnamangalam, Kozhikode-673571, Kerala, India | കുന്ദമംഗലം, കോഴിക്കോട്-673571, കേരളം, ഇന്ത്യ
E-mail: ed@cwrdm.org, registrar@cwrdm.org | Website: www.cwrdm.org
Phone: (91) 495 235 1800, 235 1801 | Fax: (91) 495 235 1808, 235 7827

DECLARATION

I hereby declare that, the work presented in this thesis entitled **"Synthesis and Application of Hybrid Nanocomposites for the Removal of Heavy Metals and Bacteria from Contaminated Water"** is the result of the investigations carried out by me in the Ecology and Environment Research Group, Centre for Water Resources Development and Management (CWRDM), Kozhikode, India, under the supervision of Dr. P S Harikumar, Chief Scientist (Retd.), Ecology and Environment Research Group, CWRDM, Kozhikode, India, and that it has not been submitted elsewhere for the conferment of any degree or diploma of any Institute or University.

CWRDM
June 2023

Hridya T K

ACKNOWLEDGEMENTS

The completion of this Ph.D. thesis would never have been possible without the help and support of these people. It is my pleasure to acknowledge everyone who contributed to the journey towards the successful completion of this Ph.D. thesis.

First and foremost, I would like to express my sincere gratitude to my research supervisor, Dr. P S Harikumar, for giving me the opportunity to work under his guidance. He has always motivated me by giving me freedom of work. He encouraged me to learn new things and techniques which are not directly related to my active research. Apart from being an excellent scientist, he is also a wonderful human being. An energetic and dynamic person, who is always active from the start of the day till the end of the day. I am grabbing this opportunity to thank him for his supervision and constant support. It is his constant encouragement and guidance that helped me to present this thesis in its present form. I will be forever obliged for his guidance, patience, and continuous encouragement.

I wish to express my sincere gratitude to the former Executive Director of Centre for Water Resources Development and Management (CWRDM), Dr. A B Anitha, and the present Executive Director,
Dr. Manoj P. Samuel for providing me the necessary facilities for the successful completion of this research work. My sincere acknowledgement goes to all the scientists and technical staff members of the Ecology and Environment Research Group for their support and

cooperation during all this time. It is a pleasure for me to thank Dr. Shiji M, who were simply great enough to help me with my struggles to keep on with my research.

I gratefully acknowledge the Council of Scientific & Industrial Research (CSIR), India, for providing financial assistance during my Ph.D. tenure. Also, I express my sincere thanks to the CWRDM, Kozhikode, for providing the research facility.

I am also grateful to STIC Cochin University, NIIST Trivandrum, and CSIF University of Calicut for helping with the characterisation part and RGCB Trivandrum for Bacterial Sequencing.

I would like to thank all the past and present members of my research group including Nimmi N, Navaneeth A, Sachin V M, Sreedevi M A, Ajith, Sandra, Adarsh, Sudhin, Aswin, Sanusree, Thara, Nayana, Haritha, Dr. Sreeda ,Shalna, Jiji, lamya and Manjusha for providing a warm and cheerful atmosphere in the lab.

The real strength and support I enjoyed at every instance of my career could be credited to my family members, especially my parents, Jagannathan T K and Anila M S, who always dreamt of me reaching golden heights. I am forever indebted to them for giving me the opportunities, inspiration, and motivations that have made me who I am. I express my deep sincere gratitude to my parents for being with me during my ups and downs and also for their continuous help and efforts to make me able to lead a life of my own. I would like to extend my sincere thanks to my brother Akshay T K and cousins Navya Babu,

Akhil Babu, Sarang and Gowtham for their love and support. They simply transformed those stressed moments of research into the most beautiful pages of my life filled with everlasting memories of bliss, care, and trust. I express my immense love and affection to my best friend Anupriya Babu who always bestowed positive radiance on me with her inherent innocence and care.

Above all, I would like to share my heartfelt gratitude to Jayakrishnan P, my life partner, during these years for bearing with me and being with me while everything seemed to be falling apart. He inspires me to pursue my goals and always be there to listen and share all my happy and sad moments. He supported me without any complaint or regret that enabled me to complete my thesis. Thanks for all of the sacrifices that you made on my behalf and for all your support, without which I would not have completed my PhD. I am extremely grateful to my motherin-law, Sujatha, and father-in-law, Prabhakaran, for their care and support.

Apart from the ones mentioned here, there are many well-wishers who have helped me throughout my life. I record my warm thanks to all those who have helped me directly or indirectly in making this thesis successful.

Hridya T K

ABBREVIATIONS

AAS	:	Atomic Absorption Spectrophotometer
BET	:	Brunauer–Emmett–Teller
BIS	:	Bureau of Indian Standards
BNC	:	Bimetallic Nanocomposite
BNPs	:	Bimetallic Nanoparticles
Cd	:	Cadmium
CFU	:	*Colony-Forming Unit*
Cu	:	Copper
DBPs	:	Disinfection by-Products
EDS	:	Energy Dispersive X-ray Spectroscopy
HR-TEM	:	High-Resolution Transmission Electron Microscopy
ISO	:	International Organization for Standardization
MCL	:	Maximum Contaminant Level
Mn	:	Manganese
MNPs	:	Monometallic Nanoparticles
MTZ	:	Mass Transfer Zone
NB	:	Nutrient broth
Ni	:	Nickel
NMs	:	Nanomaterials
NPs	:	Nanoparticles
P(St–DVB)	:	Porous (styrene–divinylbenzene)
Pb	:	Lead
PNCs	:	Polymer-based nanocomposites
PXRD	:	Powder X-ray Diffraction

ROS	:	Reactive Oxygen Species
rpm	:	Revolutions per minute
SEM	:	Scanning Electron Microscopy
St–DVB	:	styrene–divinylbenzene
TAP Medium	:	Tris-Acetate-Phosphate Medium
UNICEF	:	United Nations International Children's Emergency Fund
USEPA	:	United States Environment Protection Agency
WHO	:	World Health Organization
Zn	:	Zinc

CONTENTS

LIST OF TABLES

LIST OF FIGURES

ABSTRACT

Clean and fresh water is the most essential element for the survival of all forms of life on the earth. It is considered as the most precious resource in this world and its scarcity, in terms of quantity and quality, has become a significant threat to the well-being of people. Contamination from microbes, heavy metals, and fluoride has been identified as the highest concerned parameter for global monitoring of drinking water quality. A significant burden on water quality and, consequently, public health is the proliferation of heavy metals and microbiological pollution. Consumption of such contaminated water can cause the most devastating effects on communities and individuals. To address the problem rapid, energy efficient decontamination, and disinfection processes are required.

Nanotechnology is an important emerging field in several applications, such as optoelectronics, chemistry, device storage, physics, medicine, biology, and environmental restoration. Among the wide group of nanotechnology, the use of nanoparticles for environmental remediation can be considered a novel application of nanotechnology. Recent advances in nanotechnology have explored the use of nanoparticles as an adsorbent in drinking water treatment systems and have received increasing interest. These materials have been chosen because nanoparticle-based remediations have the specific potential to minimize the need for treatment and disposal of contaminated water by removing or transforming organic or inorganic contaminants into harmless forms and also due to the high surface area

that they offer in a very small volume. Currently, bimetallic nanoparticles, composed of two different metal elements, have drawn great interest in drinking water treatment among various types of nanoparticles. Bimetallic nanoparticles have a greater surface area which increases their adsorption power as compared to their monometallic counterparts.

The purpose of the present study is to develop an efficient and affordable organo-inorganic hybrid nanocomposite material for the treatment of water contaminated with heavy metals and bacteria. The thesis focuses on the synthesis and characterisation of porous(Styrene-divinylbenzene)/CuNi bimetallic nanocomposite, their application as adsorbents for the removal of heavy metals, and their potential use as an antibacterial agent. Development of a portable water purification device using the synthesised hybrid nanocomposites for their application in addressing the aforementioned water quality challenges in a simple and cost-effective manner. The impact of nanoparticles on the selected flora and fauna species was also attempted

The first chapter of the thesis introduces the current world scenario on water, water crisis and water pollution, especially in the case of microbial and heavy metal contamination. The occurrence, sources of contamination and corresponding health effects, with different types of bacteria, and heavy metals such as lead, cadmium, manganese, and zinc have been studied. Fundamentals of their remediation and conventional water treatment techniques are also discussed. Additionally, this chapter provides an overview of the different types of nanomaterials, their classification, synthesis

techniques, and applications in water treatment as disinfectants and adsorbents.

The importance of metal nanoparticles in water purification is described in Chapter 2. Special emphasis has been put on the water treatment using bimetallic nanoparticles. This chapter also covers the unique features and applications of Cu nanoparticles, Ni nanoparticles, and CuNi bimetallic nanoparticles.

Chapter 3 describes the synthesis, characterisation, and antibacterial activity of the CuNi bimetallic nanoparticle. The structural and chemical analysis of the synthesised nanoparticle has been determined using SEM, TEM, EDS, PXRD, and surface area studies. Experiments are performed with multiple bacterial strains such as *Escherichia coli* (*E.coli*), *Aeromonas hydrophila* (*A.hydrophila*) and *Vibrio alginolyticus (V. alginolyticus)* by spread plate counting method. The BNP showed remarkable antibacterial activity against all the three tested bacteria. Furthermore, we demonstrate that, the antibacterial activity of CuNi BNPs is higher than that of individual Cu and Ni NPs.

Chapter 4 reports the adsorption behaviour of CuNi bimetallic nanoparticle and its ability to remove lead, cadmium, manganese, and zinc ions from aqueous solutions. Batch mode adsorption studies have been carried out, and the effect of several physico-chemical parameters on the removal efficiency such as contact time, pH, initial metal ion concentration, and adsorbent dosage, has been investigated. The adsorption isotherms were described by Freundlich and Langmuir isotherm models. Pseudo-first and Pseudo-second order models were

used to evaluate the mechanism of adsorption, and the results showed that the adsorption reaction fitted very well with the Langmuir isotherm model and the pseudo-first-order kinetic model. Then, we investigated the heavy metal removal efficiency of individual Cu NPs and Ni NPs and compared it with CuNi BNPs.

Chapter 5 reports a method for the immobilization of metallic NPs using styrene and divinylbenzene co-polymer by oil-in-water emulsion polymerization of styrene and divinylbenzene in the presence of NPs. Here, we investigated the antibacterial activity of the synthesised P(St-DVB)/CuNi BNC againest *Escherichia coli* (*E.coli*), *Aeromonas hydrophila* (*A.hydrophila*) and *Vibrio alginolyticus (V. alginolyticus).*

Chapter 6 describes the batch scale adsorption studies with P(St-DVB)/CuNi BNC for the removal of heavy metals such as Pb^{2+}, Cd^{2+}, Mn^{2+} and Zn^{2+}. We explored the effects of contact time, pH, adsorbent mass, and initial metal concentration on the adsorption characteristics of the adsorbent. Batch experiments indicate that the pseudo-first-order kinetic model is more appropriate to explain the adsorption kinetics and the Langmuir adsorption isotherm closely fits to the experimental data than the Freundlich model. Desorption studies were carried out by using 0.5 M NaOH solution. Immobilization of CuNi BNPs into porous polymeric material leads to the more efficient, simpler, and low-cost separation of these used materials from the treated solution.

Chapter 7 illustrates the fixed-bed column study using P(St-DVB)/CuNi BNC microspheres for the removal of Pb^{2+}, Cd^{2+}, Mn^{2+}

and Zn^{2+} from water. We investigated how the initial metal concentration, flow rate, and bed height affected the adsorption characteristics of the adsorbent. The obtained breakthrough and the column kinetic parameters were successfully predicted with three mathematical models; Thomas, Yoon–Nelson, and Adams–Bohart models. Both Thomas and Yoon–Nelson models were shown good agreement with the experimental results for all operating conditions studied. Successful desorption of heavy metals from the P(St-DVB)/CuNi BNC microspheres was performed using 0.5 M NaOH solution.

Chapter 8 describes the fabrication of a low-cost, portable, and simple device for water purification by the application of the synthesised P(St-DVB)/CuNi BNC microspheres. Here, we report that, the device can effectively remove Pb^{2+}, Cd^{2+}, Mn^{2+}, and Zn^{2+} from about 66 L of water with an average flow rate of 25 mL/min using 20 g of the composite without any regeneration of the material.

Chapter 9 describes the impact of synthesised P(St-DVB)/CuNi BNC microspheres and CuNi BNPs on different species like Chlorella vulgaris, Mosquito ferns, Water Hyacinth, Water Hyssop, Ostracods and Guppy. The impact on each species has been assessed by evaluating the morphological changes that have occurred in them. The P(St-DVB)/CuNi BNC had shown less detrimental effects on both flora and fauna than CuNi BNPs at the same dose.

Chapter 10 summarizes the entire work of the thesis along with a proposal for future research in this area. We hope that this thesis will be of great interest to the community and would result in a better

understanding of the various aspects of water purification using nanomaterials.

CHAPTER 1
INTRODUCTION

Clean and fresh water is the most essential element for the survival of all forms of life on the earth. It is considered the most precious resource in this world and its scarcity, in terms of quantity and quality, has become a significant threat to the well-being of people (Rijsberman, 2006). Prior to 1800, water resources were considered enough for human use and ecosystems. The progressive explosion of global population growth increases the demand for clean and potable water (Sandia, 2003; Chen et al., 2016). Moreover, the ever-expanding increase in industrialization, rapid urbanization, and increase in water contamination adds enormously to the existing problems of water scarcity by contaminating large volumes of available water and it doesn't seem easy to make further improvements (McNabb, 2019; Omer et al., 2020). Approximately 80% of the municipal and industrial wastewater have been discharged without prior treatment in developing areas (Water UN, 2018). The impact of climate change, such as higher temperatures and changes to the water cycle, are another factor that may significantly affect the quality and quantity of potentially available drinking water and it may alter the water availability patterns in the world by increased flooding and more severe droughts (Milly et al., 2002; Noyes et al., 2009; Xi et al., 2017; Boholm et al., 2017). Emerging and priority contaminants are recurrently detected in natural waters, sewage effluents, and drinking water sources, and a

leapfrogging increase in the concentration of such toxic chemical contaminants has been occurred recently.

The percentage of chronic water shortage level increased by years and 2% of the total population was become under water scarcity by 1900. By 1960, the percentage further increased to 9%, and by 2005, it reached 35% (Kadhom and Deng, 2018). It was found that human population affected water scarcity four times as much as the effect of climate change (Kummu et al., 2010). The World Health Organization (WHO) estimates that 884 million people still lack access to adequate potable water and that 2.2 million people die each year because of the consumption of contaminated water, and 90% of these deaths are children under 5 years of age (WHO, 2019; WHO, 2017).

Today, most of the countries are facing formidable challenges, especially the developing countries, in meeting the rising demands of clean water as the available supplies of freshwater are depleting. In India, almost 70% of the water bodies are contaminated by microbes, inorganic substances, organic compounds, heavy metals, and other pollutants due to the addition of industrial wastes, urban wastes, pesticides and related pollutants. Moreover, over four billion people, primarily in India and China, experience acute water scarcity for at least one month each year (Kummu et al., 2016; Mekonnen and Hoekstra, 2016). In addition to India and China, people in Bangladesh, Pakistan, Nigeria, Mexico, and arid and semi-arid areas of the United States also experience water shortages. Hence, the management and control of contaminants have become a primary environmental concern

for national and international organizations, governments, and researchers across the world (Olvera et al., 2017).

An enormous number and various kinds of pollutants such as trace chemicals, organic and inorganic particles, biologicals, microorganisms, and heavy metals were contained in the uncontrolled wastewater discharge during domestic, industrial, commercial, and agricultural activities (Sarma et al., 2019; Jun et al., 2018). Both chemical and microbiological pollutants can be harmful to humans and surrounding flora and fauna. These pollutants can change the colour, taste, and odour of the water. Since the consumption of water, which is polluted with these contaminants via irrigation of plants with contaminated water, the consumption of toxins in aquatic organisms, or the use of contaminated surface water can cause the most devastating effects on communities and individuals. The solution to which is the treatment of wastewater discharged from various anthropogenic activities such as shipping, industries (including nuclear, metallurgical, battery, chemical, mining, and tannery), agriculture and others, and degrade the pollutants to fewer toxic forms.

In a study by the WHO along with the United Nations International Children's Emergency Fund (UNICEF), it has been identified that contamination from microbes, heavy metals, and fluoride as the highest priority parameters for global monitoring of drinking water quality (WHO and UNICEF, 2017). A significant burden on water quality and, consequently, public health is the proliferation of heavy metals and microbiological pollution. The

commonly found microorganisms in drinking water include bacteria, viruses, protozoans, and parasites. Hence, the present study is mainly attributed to microbial contamination and inorganic class of pollutants especially heavy metals.

1.1. Microbial contamination

Among the various water contaminants, biological contamination arising from bacteria is considered as one of the greatest threats to human health. Even a low concentration of pathogenic bacteria exists in drinking water can cause acute and chronic health problems which include cholera, dysentery, diarrhea, hepatitis A, typhoid, and malaria among several others (Lewis and Gattie, 2002; Agdi et al., 2000; Al-Ghouti et al., 2003; Alberts et al., 2017). However, waterborne diseases remain the leading cause of death in many developing nations and their outbreaks continue to occur at unexpected high levels. Among various waterborne diseases, diarrhoeal diseases alone result in the death of two million people each year (World health organization) (Pruss-Ustun et al., 2014). Thus, an adequate supply of microbial safe water is the top priority among others. The highest microbial risks are associated with consuming water, which is contaminated with humans or animal feces (WHO, 2011). Unlike the risk of contamination from chemical pollutants, which is a concern in some parts of the world, bacterial contamination of drinking water is a universal concern. Because bacteria (unlike chemical compounds) can grow very fast and they reproduce at rapid rate, which results in their out-of-control spreading in water. According to WHO recommendation, in any 100 mL of drinking

water, faecal and total coliform counts should be zero (Tiwari et al., 2008). Therefore, prevention and removal of the growth of dangerous pathogenic bacteria from water is the most important step to obtain safe and clean water (Pradeep, 2009).

Recently, there is an increase in the emergence of multidrug-resistant bacterial strains which are resistant to conventional treatment methods. The design and development of novel antibacterial agents with enhanced activity and not susceptible to bacterial resistance are necessary to solve this issue (Udikovic-Kolic et al., 2014).

The most essential feature of the bacteria is its cell wall, and it can provide rigidity, strength, shape and protection from mechanical damage. According to the bacterial cell wall structure, they can be categorized as gram-positive and gram negative as depicted in Figure 1.1 (Wolny-Koładka and Malina, 2017). Gram positive strains have a spherical shape as gram-negative are rod-shaped. Cell wall of Gram-positive bacteria is made up by a thick negatively charged peptidoglycan layer (~22–52 nm) whereas, Gram-negative bacteria have a very thin layer of peptidoglycan and encloses an additional outer membrane of lipopolysaccharide to protect the surface membrane (Scott and Barnett, 2006).

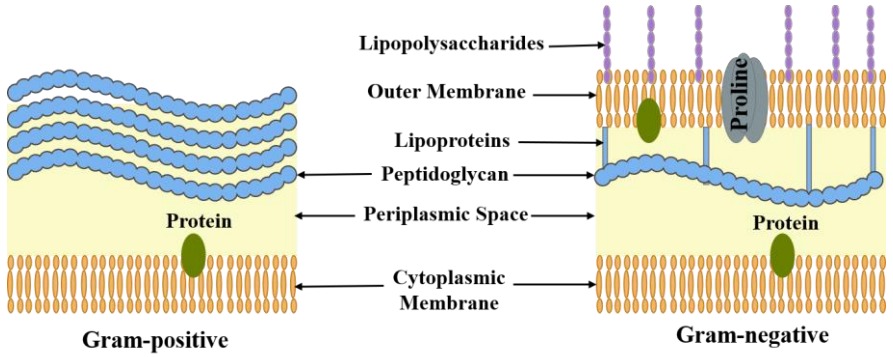

Figure 1.1: Schematic structure of gram-positive and gram-negative bacterial cell wall.

In the present work, different types of bacteria, that are known to cause water borne diseases, such as *Escherichia coli* (*E.coli*), *Aeromonas hydrophila* (*A.hydrophila*) and *Vibrio alginolyticus (V. alginolyticus)* have been selected for studying the removal of pathogenic bacteria from water.

E.coli are rod-shaped, Gram-negative bacteria that typically found in the gastrointestinal tract of animals. They colonise in the intestinal tract of human infants within a few hours after birth. Some of the E. coli strains are pathogenic and cause various intestinal and extra-intestinal diseases such as diarrhoea, urinary tract infections, meningitis, septicemia and pneumonia (Hilbert et al., 2011). They are associated with the faecal contamination of water.

A.hydrophila is the Gram negative, non-spore forming, rod shaped bacteria. They have received particular attention due to their emergent human pathogenic properties. *A.hydrophila* can cause septicaemia, diarrhoeal illness, and wound infection (Hänninen and

Siitonen, 1995). It is commonly found in contaminants of human foodstuffs and different water bodies.

V. alginolyticus is a comma shaped Gram-negative bacterium. It causes wound infections, septicemia, endophthalmitis, and gastrointestinal infections. The main vehicle of transmission is contaminated water and commonly found in saltwater (Maheshwari et al., 2011). *V. alginolyticus* can survive in the environment longer than any other faecal organism. Most people become infected with the bacteria by drinking water contaminated with infected human sewage.

1.2. Heavy Metal contamination

During the last decades, the presence of elevated heavy metal concentrations in aqueous resources raised as a problem of worldwide concern. Contrary to organic contaminants, heavy metals are toxic, carcinogenetic, and non-biodegradable. Besides, they can accumulate in living tissues due to their non-biodegradable character and become concentrated in the internal organs such as the brain, kidneys, and liver (Pehlivan et al., 2008; Schwarzenbach et al., 2010). These concentrated metals can affect the functioning of such vital body organs. Moreover, heavy metals are considered as conservative pollutants that are not subjected to bacterial attack or other break-down or degradation process and hence, they are permanent addition to the environment.

Discharge of untreated and inadequately treated effluents in the water, which contains toxic heavy metals, have wide impact on the ecosystem by getting transferred into the food chain. Among various metal ions, the aqueous soluble forms of lead, mercury, cadmium, zinc,

manganese, and chromium are considered as emerging water pollutants (Simeonidis et al., 2019) and the accumulation of these metals in elevated concentrations in industrial wastewater has alarming effects. The presence of these heavy metals even in trace quantities can cause deleterious health effects on humans and animals (Al-Othman et al., 2012; Singh et al., 2011). Heavy metals pave their way into human tissues through various absorption pathways such as food chain, direct ingestion, inhalation, oral intake, and dermal contact (Singh and Prasad, 2015). Thus, the treatment of industrial effluents containing toxic metals, before they are discharged, is becoming a crucial issue (Wang and Chen, 2009).

Release of hazardous metals like Cr, Cd, Hg, Zn, Pb, and Mn into the environment by both natural and anthropogenic sources have been reported in India and it became an important national issue at present (Marg, 2011). The natural sources of heavy metals include volcanic activities, aerosols, geochemical processes, mineral weathering, soil erosion, urban runoff, etc. While, untreated or partially treated wastewater discharges from industries like metal plating industries, mining, leather tanning, textile dyeing, paints, pigment manufacturing, batteries, fertilisers, water cooling and electroplating are the prime root of heavy metal contamination by human contribution (Tchounwou et al., 2012). Emissions from vehicles and other urban activities also contribute to it (Pandey and Pandey, 2009; Prasse et al., 2012). Moreover, these heavy metals, released from such contaminated areas, can easily be transported through the environment and leached to the nearby surface and groundwater. This can be usually

results in the spreading of these metals over vast areas and form large-scale contamination (Nriagu and Pacyna, 1988).

Concerning about their potential health effects on human beings, United States Environment Protection Agency (USEPA) issued the Maximum Contaminant Level (MCL), *i.e*., the highest level of a contaminant that is allowed in drinking water, of heavy metals in drinking water based on their toxicity (USEPA, 2019; Babe and Kurniawan, 2003). Many of the drinking water treatment techniques which are commonly used, including chlorination, boiling, and solar disinfection, are ineffective at removing these heavy metals (De Kwaadsteniet et al., 2013). Therefore, treatment of heavy metals is of special concern for the substantial growth of human and environment. There is an urgent need for developing cost-effective, eco-friendly, in-situ treatment technologies for the removal of heavy metals in water. Due to their highly toxic nature, even at very low concentrations, and non-biodegradable properties, USEPA has prescribed certain regulatory standards for the discharge of heavy metals in wastewater and in drinking water. The important sources of heavy metals and their potential health effects are tabulated in Table 1.1. Table 1.2 represents the MCL of heavy metals in drinking water according to USEPA and WHO.

Table 1.1

Characteristics of common heavy metals

Lead (Pb)	Carcinogenic, anemia, joint pain, kidney problems, high blood	Lead acid batteries, paints, coal-based thermal power plants,

	pressure, damage in circulatory system and nervous system.	ceramics, household plumbing system.
Cadmium (Cd)	Kidney damage, renal disorder, Carcinogenic, and chronic lung disease.	Zinc smelting, waste batteries, paint sludge, incinerations, and fuel combustion.
Manganese (Mn)	Toxic, causes growth retardation, muscles fatigue, eye blindness, and sexual impotence.	Coal mining, production of dry battery cells, matches, fireworks, glass-bonding materials.
Zinc (Zn)	Stomach cramps, respiratory disorders, nausea, vomiting, skin irritations, anemia.	Smelting, mining and metal production, dye, wood preservatives, ointments and electroplating industries.

Table 1.2

Maximum Contaminant Level (MCL) of heavy metals according to USEPA and WHO.

Heavy metal	**Maximum contaminant level**		
	USEPA[a] (mg/L)	**WHO[b] (mg/L)**	**BIS IS:10500[c] (mg/L)**
Lead (Pb)	0.015	0.01	0.01
Cadmium (Cd)	0.005	0.003	0.003
Manganese (Mn)	0.05	0.4	0.1
Zinc (Zn)	5	5	5

[a] Value by United States Environment Protection Agency (USEPA, 2019; USEPA, 2008)

[b] Values prescribed by World Health Organization (WHO chronicle, 2011; WHO, 2008)

[b] Values prescribed by Bureau of Indian Standards (BIS, 2012)

In the present study, four heavy metals including lead, cadmium, manganese and zinc have been selected for studying their removal. The presence of lead at a higher concentration in the drinking

water may cause diseases such as anaemia, hepatitis, encephalopathy, and nephritic syndrome (Lo et al., 1999; Kataria and Garg, 2018). Lead poisoning mainly affects the nervous, kidneys, bones, and blood circulation systems. The WHO and BIS guidelines for drinking water quality standard recommended the maximum limit of lead concentration in drinking water to be 0.01 mg/L (WHO chronicle, 2011; BIS, 2012).

Cadmium is highly toxic to the human body and it affects the lungs, kidneys, liver, and skeletal system (Marg, 2011). It has been classified as a suspected human carcinogen (International Agency for Research on Cancer, 1993). Industrial waste from metallurgical plants, plating works, plants that make cadmium pigments, textile operations, cadmium-stabilized plastics, nickel-cadmium batteries, or by effluents from sewage treatment plants are the main sources of chromium in aquatic ecosystems. The maximum permissible limit of Cd (II) in drinking water is 0.003 mg/L, recommended by WHO and BIS (WHO chronicle, 2011; BIS, 2012).

Manganese is a very abundant transition metal in the earth's crust and one of the most common contaminants found in natural waters, predominantly in the groundwater. The presence of manganese in drinking water can cause turbidity, black-brown colour, odour, and taste problems to drinking water (Alvarez-Bastida et al., 2013). Manganese is an essential nutrient yet its high levels of exposure is problematic from an aesthetic, operational, and economic point of view. The WHO has set 0.4 mg/L as the maximum permissible limit for manganese concentration and BIS recommends it as 0.1 mg/L (WHO chronicle, 2011; BIS, 2012).

Zinc is vastly found in natural waters and the municipal incineration and discharge of industrial wastewaters, like paint, pipes, galvanic industries, fungicides, and insecticides, may increase zinc contents in the source water. The maximum permissible level stipulated for zinc in the drinking water is 5 mg/L because of no adverse health effects at natural concentrations of this metal (WHO chronicle, 2011; BIS, 2012; USEPA, 2019). Zinc is essential for human metabolism, but its regular exposure can cause stomach cramps, skin irritations, anaemia, nausea, and vomiting (Lu et al., 2009).

1.3. Water Treatment

Understanding the negative effect of specific water pollutants on life expectancy, research efforts had oriented towards the improvement of water treatment strategies which are extremely resourceful in eradicating toxicants from water and wastewater. Therefore, in recent years several wastewater treatment techniques have been developed to mitigate the problem of heavy metal contamination and microbial pollution from aqueous medium. The primary goal of such process is the reduction of residual contaminant concentration below the regulation limit set by international organizations. However, these methods are still having some limitations especially that of high operation cost, incomplete removal, and low efficiency (Barakat, 2011). This can be overcome by decreasing the amount of wastewater produced and improving the quality of the treated effluent. Cheaper and efficient approaches have been under research to advance the quality of effluents.

1.3.1. Antibacterial activity-Disinfection

Materials that destruct pathogenic bacteria or slow down their development without being destroy the other organisms in water or environment are known as antibacterial agents and that process is called disinfection. Water disinfection can be accomplished in various forms. But is most commonly carried out by chlorine, and sometimes by more expensive methods, such as exposure to high-intensity ultraviolet radiation and ozonation. A combination of decontamination methods is usually used in conventional systems. The advantages and disadvantages of such techniques are presented in Table 1.3. Additionally, chemical disinfection methods using oxidizing agents is always accompanied by the formation of toxic disinfection by-products (DBPs) (e.g., halogenated disinfection by-products, carcinogenic nitrosamines, bromate, etc.), which are highly harmful and also carcinogenic in several cases (Li et al., 2008). Moreover, due to the emergence of multidrug-resistant bacterial strains and the increasing prevalence of their resistance to current antibacterial treatments, the search for an alternative method, that are not susceptible to bacterial resistance, has been increased.

Table 1.3

Various disinfection techniques with their advantages and disadvantages.

Methodology	Advantages	Disadvantages
Chlorination	Chlorination is effective, reliable, and inexpensive, it has high oxidation potential, the residual formed were remains in water and continues to combat with bacterial contamination.	Due to chlorine's ability to bind to nitrogen and organic compounds, resulting in highly toxic disinfection by-products.

Ozonation	Very powerful oxidant, it is used to remove colour, odour and bad taste,	High capital and running cost, generate toxic disinfection by-products, the distribution system should be contamination free.
Ultraviolet Light	Highly efficient against many microorganisms (even viruses), free from disinfection by-products,	Does not possess residual disinfection ability, limited to small treatment systems, suspended solids may contaminate the UV lamp, which results in reduced intensity of light

1.3.2. Methods for the removal of heavy metal ions

Many conventional methods have been used to remove heavy metals from water and industrial wastewater, including chemical precipitation (Meunier et al., 2006; Matlock et al., 2002), reverse osmosis (Akin et al., 2011; Weber and Holz, 1991), ion exchange (Xing et al., 2007; Alyüz et al., 2009), membrane filtration (Ersahin et al., 2012), coprecipitation (Kameda et al., 2014), electrochemical treatment (Feng et al., 2007; Walsh and Reade, 1994) and adsorption (Sun et al., 2015; Alluri et al., 2007). Other than these, some methods include reduction and oxidation, screening, neutralization and remineralization, crystallization, fluidization, sedimentation, gravity separation, flotation, solvent extraction, evaporation, distillation and so on. The overview of such techniques, along with advantages and disadvantages, are presented in Table 1.4.

Table 1.4

Techniques for the removal of heavy metal ions along with their advantages and disadvantages.

Methodology	Advantages	Disadvantages
Chemical precipitation	Low capital cost, simple operation, effective for removal of large quantities of metals.	Sludge generation, extra operational cost for sludge disposal, removal of only a few metals.
Ion exchange	High selectivity and efficiency, low sludge volume, and high regeneration efficiency.	High initial capital cost, high maintenance cost.
Membrane filtration	Transport selectivity of the membrane, low chemical consumption, needs low energy, facile	Relatively expensive to install, ease of membrane blocking, prone to fouling, scaling or membrane

	in operation and small space requirement.	degradation, and limited flow rates.
Electrochemical treatment	Rapid process capable of selective removal of metals.	High maintenance and operation costs, large generation of by products, filtration process for flocs.
Coagulation and flocculation	Economically feasible, bacterial inactivation capability.	High sludge formation and chemical consumption.
Adsorption	Flexibility and simplicity of design, high surface area, accessible surface sites, low cost, a wide verity of target pollutants, high capacity, and fast kinetics.	Adsorbent requires regeneration, performance depends on type of adsorbent.

1.3.2.1. Adsorption

Among all these techniques, adsorption occupies an important position because of its good performance, high efficiency, minimization of secondary wastes, and economically feasible character (Wang et al., 2019; Ren et al., 2014). It can apply for the removal of soluble and insoluble pollutants. For this reason, adsorption is one of the most widely used technologies for removing heavy metal ions from wastewater, since it is the simplest removal method and it shows higher efficiency towards the removal of trace levels of heavy metal ions (Zamboulis, 2011). Also, adsorption can be reversible, that involves the transfer of adsorbate ions from the adsorbent surface to the solution and the regenerated adsorbent can be reused after desorption (Mishra, 2014).

The adsorption process is a surface phenomenon in which the pollutant (liquid or gas) molecules bind to the solid surface either by chemical or physical bonds. It is commonly used to remove substances from liquid phase. The adsorbent is the solid surface on which adsorption takes place and the adsorbed substance is known as adsorbate. The adsorption process as well as the components involved on such procedure are schematically described in Figure 1.2. Adsorption is frequently escorted with the desorption and the regeneration efficiency of adsorbent is dependent on the adsorbate amount desorbed from the solid: when the desorption increases, the regeneration of the adsorbent also increases depending on the applied conditions. In practice, the adsorption studies are performed as an operation, either in batch or continuous mode, in a column packed with porous adsorbents.

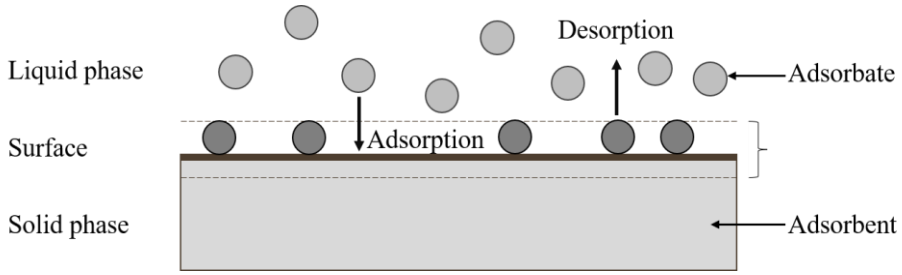

Figure 1.2: Schematic representation of the adsorption process.

Adsorption arises as a result of the unbalanced force of attraction on the surface of the adsorbate. Thus, when adsorbent is brought into contact with a liquid or gas, there will be an interaction between the field of forces of the adsorbent surface and that of liquid

or gas. The adsorbent surface tends to satisfy these residual forces by attracting and retaining the molecules, atoms, or ions of the gas or liquid on its surface. In the case of physical adsorption or physisorption, the adsorbate binds to the surface by weak van der Waals forces, hydrogen bonding, or electrostatic attraction. Chemical adsorption or chemisorption is produced by chemical reactions between adsorbate and the surface sites, through covalent or ionic bonding (Figure 1.3). It involves the exchange or sharing of electrons between adsorbate and the adsorbent. Physisorption is nonspecific, reversible in nature and has a low heat of adsorption ranging from 15-30 kJ/mol. On the other hand, chemisorption is selective, irreversible, and the heat of adsorption has a range of 10-100 of kJ/mol (Tripathi et al., 2015; Singh and Gupta, 2016; Tyagi et al., 2017).

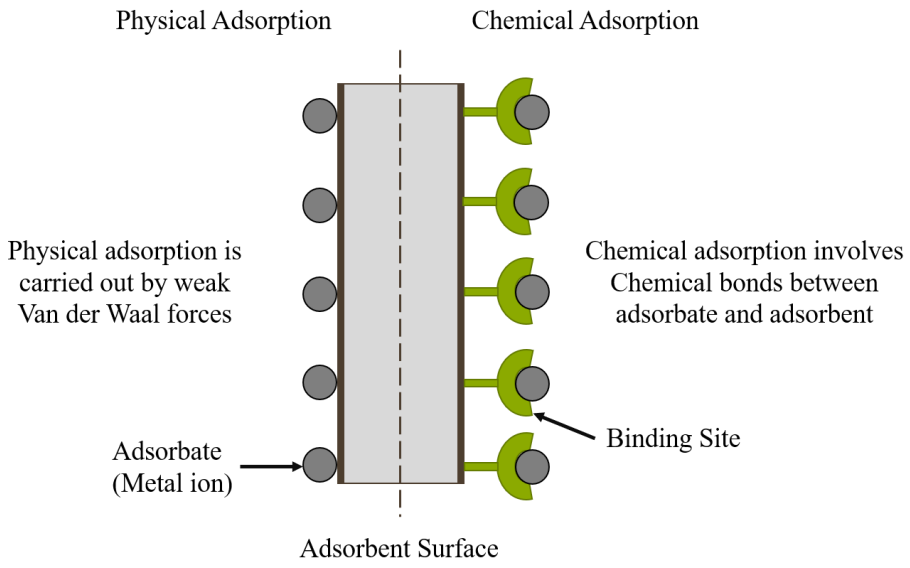

Figure 1.3: Physical and chemical adsorption on the adsorbent.

The adsorption of pollutants on the surface of adsorbent takes place in three steps:

Step 1: Film diffusion-the transportation of the pollutant molecules from the bulk solution to the external surface of adsorbent.

Step 2: Pore diffusion-transport of material by diffusion from the external surface into the pores of the adsorbent.

Step 3: Adsorption on the internal surface of the adsorbent by physical/chemical adsorption.

Where the first two steps are transport steps, and the last step is a reaction step, and Figure 1.4 represents the step 1 and 2 of an adsorbate molecules during adsorption.

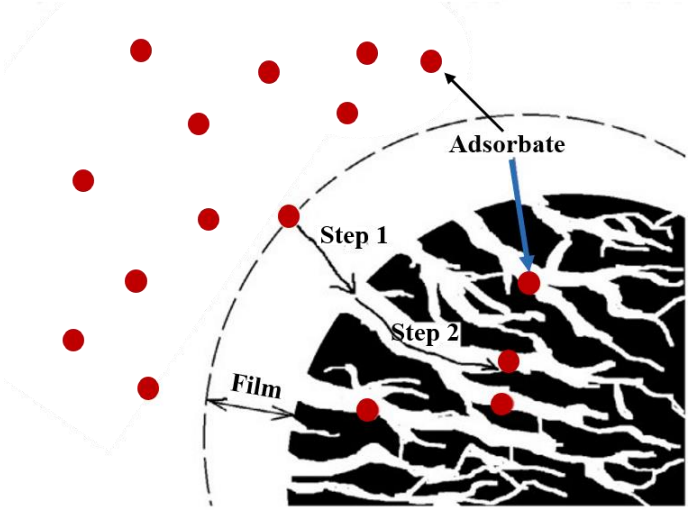

Figure 1.4: Trajectory of an adsorbate molecule during adsorption.

Currently, various adsorbents such as activated carbon, graphene oxide, metal oxides, chitosan, zeolite, alumina, nanoparticles, nanocomposites etc have been reported to be used as adsorbents for removing heavy metals from aqueous solutions and wastewaters (Vodyanitskii, 2010; Wang et al., 2012; Wang and Peng, 2010). The main difference in their adsorption method is the interaction between adsorbates and adsorbents, which depends on their physicochemical properties such as particle size, surface area, surface charge, morphology, surface coating, and so forth. Hence, discovery for an effective novel adsorbent material to ensure the availability of quality drinking water to the mass at an affordable cost has always been a hot topic among researchers.

1.4. Nanotechnology

Nanotechnology, often referred as the science of the small, is a novel and emerging technology that dominating the various fields of research. It is considered as an interdisciplinary branch of science integrating engineering aspects with physics, biology, chemistry, medicine, and material science. Hence, it enhanced the area of scientific as well as industrial research.

1.4.1. Nanomaterials– at a Glance

The original idea of nanotechnology came from a speech entitled “There is a plenty of room at the bottom” by Nobel laureate Richard Feyman, an American physicist who is known as the ‘‘Father of nanotechnology,” during a meeting of the American Physical

Society held in December 1959 (Feynman, 1959). He also explained how things behave at small scale and different techniques that makes it possible to transform particles to their minute forms (Feynman, 1960).

The "nanometre" is a unit of measurement of length that is equal to one billionth (10^{-9}) of a meter and nanomaterials (NMs) are defined as objects with at least one dimension fall within the range of 1-100 nm *i.e.*, whose size is above molecular dimensions and below macroscopic ones (Clifford et al., 2020). Materials below 100 nm in diameter exhibit physical and chemical properties in between those of the bulk material and the atomic or molecular structures (Tarafdar et al., 2013). This phenomenon is in association with the quantum effects and surface effects, which are the main highlight of nanotechnology, due to their large surface area to volume ratio experienced at these dimensions, high number of particles per mass unit, presence of large fraction of atoms at the surface, higher surface-reactive sites, high surface free energy and surface interactions (Roduner, 2006; Buzea et al., 2007).

Physical qualities of bulk materials are independent of size, whereas in the case of NMs, physicochemical properties including its chemical, electrical, mechanical, and optical properties can vary depending on the parameters like size, morphology, surface features and inner structure of NMs. The active surface area is a crucial factor for various processes, including catalysis and adsorption, and it will increase when a material's size is reduced to the nanometer range. The little modifications and control in the size, shape, and composition of

NMs will results into the magnificent transitions in their properties. This provides a variety of surprising and interesting uses of NMs and promptly gaining importance in a number of areas such as medicine, optics, chemical industries, electronics, ceramics, magnetics, catalysis, and water treatment (Li et al., 2011; Pal et al., 2011). Thus, strategies are developed to exploit the regime of size-controlled properties so to form either novel or superior physical, chemical, and biological properties that are not attainable by conventional bulk particles of similar composition.

When discussing nanomaterials, a variety of words are frequently used, which might be confusing for less-experienced researchers or those who are new to the topic. In specifically, nanomaterials include hollow spheres, nanotubes, nanowires, nanospheres, nanofibres, nanofilms, nanofluids, nanoribbons, nanorods, and quantum dots in addition to NPs, which could be the most popular one (Kuhn et al., 2022).

1.4.2. Classification of Nanomaterials

There are several methods for categorising nanomaterials. On the basis of dimensionality, morphology, composition, uniformity, and agglomeration, NMs are generally classified as follows (Saleh, 2020).

1.4.2.1. Dimensionality

On the basis of dimensionality, nanomaterials can be categorised as zero dimensional materials (0D), one dimensional

materials (1D), two dimensional materials (2D), and three-dimensional materials (3D) (Pokropivny and Skorokhod, 2008).

(1) **Zero-dimensional nanomaterials (0D)**: This class of nanomaterials have all their three dimensions at the nanoscale level. e.g., quantum dots, nanoparticles, and fullerenes.

(2) **One-dimensional nanomaterials (1D)**: This class of nanomaterials have one dimension outside the nanometer scale while the other two dimensions are in nanoscale. e.g., nanotubes (like carbon nanotubes (CNTs)), nanofibers (like carbon nanofibers), nanorods, nanowires, and nanocore shells.

(3) **Two-dimensional nanomaterials (2D)**: This class of nanomaterials have two dimensions outside the nanometer scale. e.g., nanosheets (graphene), nanofilms, and nanolayers (multilayered nanosheets).

(4) **Three-dimensional nanomaterials (3D) or bulk nanomaterials**: Nanomaterials which are not confined to the nanoscale in any dimension. They create hybrid structures as a result of their unique confinement in a three-dimensional space. e.g., bulk powders, hybrid nanostructures, arrays of nanowires, carbon nanobuds, and nanotubes, etc.

1.4.2.2. Morphology

(1) **High aspect ratio**: The length exceeds the width by many folds. Nanotubes and nanowires fall under this category.

(2) **Low aspect ratio**: This covers spherical, oval, cubic, prism, helical, and pillar forms. e.g., nanospheres, nanocubes, nanopyramids, etc.

In addition to the aspect ratio, NMs' morphological characteristics also include sphericity and flatness.

1.4.2.3. Uniformity

Depending on their uniformity, NMs can be categorised as dispersed and agglomerated or isometric and inhomogeneous.

1.4.2.4. Chemical Composition

NMs can be categorised into a number of groups according to their chemical composition, including organic, carbon-based, and inorganic, which in turn have further varieties (Joudeh and Linke, 2022).

(1) **Organic nanomaterials**: NMs consisting of proteins, carbohydrates, lipids, polymers, or any other organic substances are generally known as organic NMs. They are most commonly employed in the biomedical industry for example, drug delivery system and cancer therapy. e.g., dendrimers, micelles, liposomes and ferritin, etc. (Figure 1.5).

(2) **Carbon-based nanomaterials**: NMs which mainly formed of carbon are known as carbon based, e.g., fullerenes, CNTs, carbon nanofibers, carbon black, and graphenes. Carbon-based NMs combine the distinct features of sp^2-hybridized carbon

bonds with their unique physicochemical properties at the nanoscale. Carbon-based NMs play a key role in several interdisciplinary fields and employed in a variety of applications, including drug delivery, energy storage, bioimaging, adsorption, photovoltaic devices, and environmental sensing to identify microbial pathogens (Mauter and Elimelech, 2008).

(3) **Inorganic nanomaterials**: Inorganic nanomaterials are those made of metals or metal oxides. e.g., metal, ceramic, and semiconductor NPs. Metal NPs are purely composed of metal precursors and can be monometallic, bimetallic, or polymetallic. It is possible to synthesise nanoparticles from almost all the metals. Aluminum (Al), iron (Fe), silver (Ag), copper (Cu), gold (Au), Nickel (Ni), cobalt (Co), lead (Pb), and zinc (Zn) are the most frequently utilized metals to synthesize nanoparticles. As compared to bulk materials, metal NPs have peculiar chemical, optical, and electrical characteristics. To modify the characteristics of the corresponding metal nanoparticles, metal oxide-based nanoparticles are synthesised. e.g., Aluminium oxide (Al_2O_3), Magnetite (Fe_3O_4), Iron oxide (Fe_2O_3), Zinc oxide (ZnO), Cerium oxide (CeO_2), Silicon dioxide (SiO_2), Titanium oxide (TiO_2), etc. Due to the change in its surface properties, these nanoparticles exhibit a high reactivity and efficiency when compared to their metal counterparts.

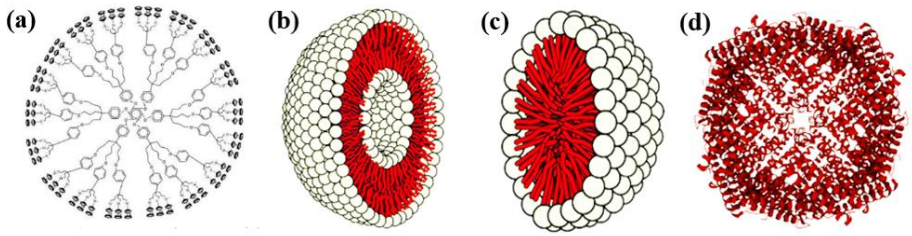

Figure 1.5: Types of organic NMs - (a) dendrimers; (b) liposomes; (c) micelles; and (d) ferritin.

1.4.3. Nanoparticles

The International Organization for Standardization (ISO) defines nanoparticles (NPs) as "nano-objects having all external dimensions at the nanoscale, where the lengths of the longest and the shortest axes of the nano-object do not differ significantly" (Haydon, 2015). If the dimensions differ significantly (usually by more than three orders of magnitude), words such as nanofibers or nanoplates may be chosen over the term NPs. Apart from their composition, nanoparticles vary in terms of shapes, sizes, and structures. NPs can be spherical, cylindrical, tubular, conical, hollow core, spiral, flat, etc., or irregular and their size can be anywhere from 1 to 100 nm (Ealia and Saravanakumar, 2017). As previously indicated, the distinct physical and chemical characteristics of NPs, which do not present in their larger-dimension counterparts of the same materials, make them suitable for a wide range of applications.

1.4.3.1. Methods for the synthesis of nanoparticles

A wide range of conventional and modern methods have been developed to produce nanoparticles with enhanced properties and

reduced production costs. There are three different approaches for synthesising NPs s including top-down, bottom-up, and hybrid method. In the first one, bulk material at the macroscopic level is reduced significantly to nanometric scale using physical or chemical methods and is known as top-down or destructive approach. Mechanical milling, nanolithography, laser ablation, sputtering, and thermal decomposition are the most commonly used top-down methods for NP production. Making connections at the macroscopic level and producing structures with long-range order are two frequent uses of the top-down method (Kuhn et al., 2022). In the second case, NPs are prepared via the assembly of atoms, molecules or smaller particles to clusters or NPs and termed as bottom-up or constructive approach. Sol-gel, chemical synthesis, chemical vapour deposition (CVD), pyrolysis, spinning, and biosynthesis are the most commonly used bottom-up methods. These methods are frequently employed to produce short-range orders, such as complex molecular devices, and also in the fabrication of structural composite nanomaterials. Figure 1.6 represents a simplified illustration of the above procedures. A hybrid technique that combines top-down and bottom-up approaches is an alternate tactic that addresses technical issues that arise with these two approaches (Kargozar and Mozafari, 2018). The hybrid method mostly results in hybrid materials, i.e., the integration of organic and inorganic materials, which have recently gained a lot of attention (Kuhn et al., 2022).

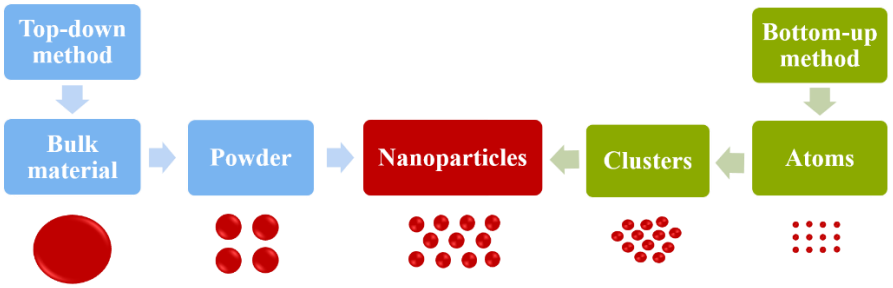

Figure 1.6: Schematic representation of the top-down and bottom-up methods for nanoparticle preparation.

1.4.4. Engineered nanoparticles for clean water

Owing to its uniqueness, there were many opportunities to use engineered NPs for water treatment. As a result, increased uses of nanomaterials in wastewater treatment have been noticed during the last two decades and various types of nanomaterials have been found to be successful at removing heavy metals, organic pollutants, inorganic anions, and microorganisms (Zhang et al., 2016; Abdelbasir and Shalan, 2019). The growing importance of NPs in water purification has resulted in the appearance of an ever-increasing volume of scientific and technical literature on novel NPs in this field.

The US Environmental Protection Agency has provided data on 25 locations that have used nanotechnology directly for site remediation (Morris and Willis, 2007). The National Nanotechnology Initiative includes a significant water programme, with 1.04% of the entire $1.4 billion 2020 budget allotted to water sustainability using nanotechnology (NNI, 2020). Additionally, water is on the agenda of the European Union's Horizon 2020 initiative, which is focused on

Preserving Freshwater: Recycling Industrial Waters Industry (IA) (ID: CE-SPIRE-07-2020) and New Biotechnologies for Environmental Remediation (RIA) (ID: CE-BIOTEC-04-2018), and which incorporates nanotechnology in each section (European Commission, 2017).

1.4.4.1. Nanoparticles for water disinfection

Researchers have developed novel NPs which have emerged as feasible alternatives to centuries-old conventional water treatment processes, due to its potential to overcome bacterial resistance facing the world because of the overexploitation of antibiotics (Jian et al., 2019; Shannon et al., 2010). Recently, several engineered nanomaterials have shown strong antimicrobial properties. Among all, metal NPs have been extensively studied in a wide range of disinfection applications and proposed as the most promising NPs with bacteriostatic and bactericidal characteristics (Qu et al., 2013; Wang et al., 2017). The antimicrobial characteristics of metal NPs are attributed to their unique physicochemical properties such as small size, chemical nature, functional groups present on the solution–solid interface, high surface to volume ratio and photo-sensitivity, which allow them to interact closely with microbial membranes. The mechanism of this antibacterial activity varies from metal to metal and cannot be exploited using conventional methods. For all varieties of metallic nanoparticles, the antibacterial mechanism is not fully understood. Metallic NPs can have multiple antibacterial mechanisms which include cell membrane degradation through electrostatic interaction

(Wang et al., 2015), cell wall disruption (Ivanova et al., 2013), generation of reactive oxygen species (ROS) and oxidative stress (Zhang et al., 2010), disruption of proteins and enzymes (Xiu et al., 2012) and signal transduction inhibition (Baptista et al., 2018). Unlike conventional chemical disinfectants, these metallic NPs are not strong oxidants and are relatively inert in water. Therefore, they are not expected to produce harmful DBPs. Moreover, most of the antibiotic resistance mechanisms are irrelevant for metallic NPs because the mode of action of NPs is direct contact with the bacterial cell wall, this raises the hope that metallic NPs would have high potential to solve the problem of the emergence of bacterial multidrug resistance. However, due to their small size and nature, Metallic NPs with antibacterial activity require immobilization on support materials for them to be safely used in water treatment systems.

1.4.4.2. Nanoparticles as Adsorbents

The implementation of nanotechnology in the field of wastewater treatment has recently received much research attention due to their distinct characteristics such as higher surface area, large number of particles, chemical and thermal stability, enhanced reactivity, increased surface to volume ratio and magnetic separation (Hristovski et al., 2007; Kahrizi et al., 2016; Simeonidis et al., 2018; Adeleye et al., 2016). Compared to traditional adsorbents, adsorption by nanomaterial is accepted to be the best available technology for the reduction of contaminants because they offer chemical and thermal stability, small size, large surface area, high adsorption capacity and

regeneration efficiency for pollutants and faster rates in water treatment.

Recent advances in nanotechnology have stimulated the development and use of novel and cost-effective technologies for heavy metal remediation. Hence, the development of engineered nanoparticles which are capable of removing heavy metals from wastewater appears as the most promising application of nanotechnology in drinking water treatment. The number of publications on nanoparticles for heavy metal removal has shown an exponential increase over the past 2 decades and this reflects the research interest of the scientific community in using nanoparticles for heavy metal removal (Figure. 1.7). As of now, adsorption by nanomaterial is accepted to be the best available technology for the reduction of heavy metals because they offer high adsorption and regeneration efficiency for heavy metals. Different types of NPs have been explored for heavy metal removal such as metal oxides, CNTs, silica nanoparticles, chitosan, and various noble metals (Kaushal and Singh, 2017; Wang et al., 2012).

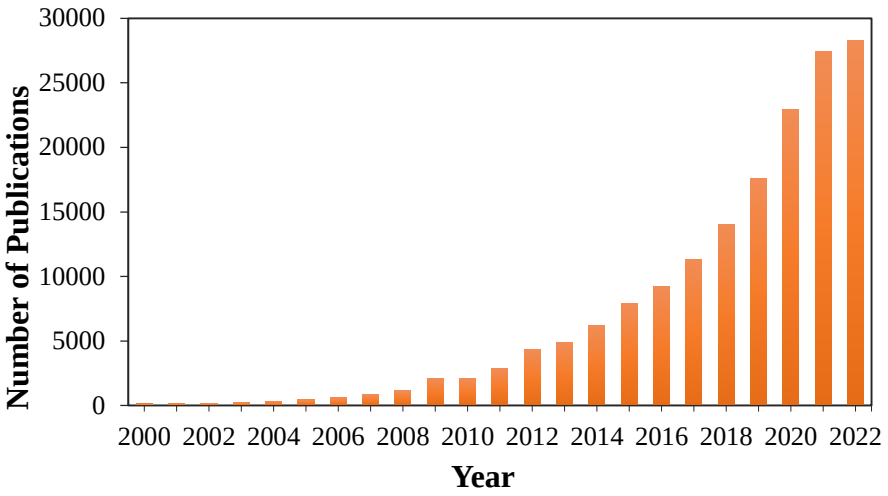

Figure 1.7: Distribution of the number of publications per year from 2000 to 2022 with the keyword's "nanoparticles", "water" and "heavy metal" from Google Scholar.

1.5. Objectives of the investigation

The goal of clean water can only be accomplished when we investigate potential and cost-effective treatment technologies. Continuous efforts are being made to encourage the development of novel technologies that could offer clean and safe water. It is recognized that low-cost, efficient solutions that can be easily implemented at the household or community level are crucial for achieving this goal. The current thesis investigates an efficient, affordable, and eco-friendly method for removing bacteria and heavy metals from polluted water using engineered bimetallic nanomaterials for achieving better performance. Effort was given to take the experiments from laboratory to prototype scale. This study also focuses on the potential future impact of nanoparticles on the environment by measuring the nano-ecotoxicity on various aquatic species, which will help to understand the probable impacts of nanoparticles on the aquatic

environment. To achieve this general objective, the work presented in the thesis has been organised to meet the following particular goals:

- ❖ To develop an efficient and cost-effective bimetallic nanoparticle for the removal of heavy metals from water and study its antibacterial activity against various bacterial isolates.
- ❖ To develop an organo-inorganic hybrid nanocomposite material in the form of granular media without losing the efficiency, adsorption capability, and antibacterial activity of bimetallic nanoparticle.
    - To study its antibacterial activity against various drinking water bacterial isolates.
    - To investigate on their application for the adsorptive removal of heavy metals from water in batch and continuous flow column system and optimise the impact of different operational variables.
- ❖ To fabricate simple, low-cost, and portable water purification device based on the developed hybrid nanocomposite for the removal of heavy metals.
- ❖ To evaluate the environmental impact of synthesised hybrid nanocomposite on morphological aspects of different plant and animal species.

Chapter 2

REVIEW OF LITERATURE

2.1. Metal Nanoparticles in Water Purification

In the past few decades, the concept of nanotechnology fangled its roots towards the water treatment research and have developed into the next-generation wastewater treatment technique. Nanoparticles, especially metal NPs, purely made of metal precursors, are expected to play an important role in water purification. There are various reasons for using metal NPs for water treatment, for example, they appear to be very compatible with the aqueous chemistry, have multipronged use in drinking water purification (removal of organic compounds, heavy metals, and microorganisms) and they provide superior material properties with functional adaptability. Furthermore, Metal NPs may be created using relatively low-cost preparation processes and their great adsorption capacity and ease of separation and regeneration make them technologically and economically advantageous.

Moreover, they are known for their distinctive properties such as nanoscalar size, high surface area to volume ratio, modifiable surface area, and antimicrobial properties (Musee et al., 2011). As the size of the metal NP is reduced to nanometre regime, a high percentage of the atoms exist on the surface than those available inside. This vastly increases the surface energy and surface area for chemical reactions to occur, because the unsaturated surface atoms can bind with

other atoms very easily (Liu et al., 2005; Xu et al., 2012). Because of their high surface energy, the system tries to reduce it by aggregation, chemical modification, or protection. Therefore, a variety of different species are likely to adsorb on the surface of NPs. It may create highly active adsorption sites and increased rate of potential for chemical reactions compared with the bulk material. This leads to the new possibilities in surface-based sciences.

Metal NPs have enormous potential to be used as antimicrobial agents in a variety of applications, including dentistry, synthetic fabrics, food packaging, and wastewater treatment (Zhao et al., 2011; Cheng et al., 2012; Montazer et al., 2012; Zhang et al., 2012). They have been studied for antibacterial action against a variety of pathogenic bacteria, most notably *Escherichia coli*, *Vibrio cholerae*, *Salmonella*, *Staphylococcus aureus*, and *Pseudomonas aeruginosa*, which are primarily responsible for many human epidemics (Moritz and Geszke-Moritz, 2013). There is a rising curiosity about the role of metal NPs as adsorbents for the decontamination of wastewater due to their remarkable physiochemical properties, ease of synthesis, and modification. Hence, these surface properties and the high reactivity of metal NPs can be utilized to inhibit pathogenic bacteria and remove heavy metals from water.

Metal NPs can be monometallic, bimetallic, or polymetallic depending on how many component particles are present (Hassan and Ghadam, 2020).

2.1.1. Monometallic Nanoparticles

Monometallic NPs (MNPs), as the name suggests, have a single distinct metal as their only component. The properties of these NPs depend on the metal atoms which make them up. According to the type of metal atom present, MNPs can be classified as magnetic, metallic, transition metal nanoparticles, etc. These NPs have been employed extensively in a variety of fields, including adsorption (Zhang et al., 2016), optical (Maruthupandy et al., 2017), catalysis (Gawande et al., 2016), and as antibacterial agents against a select number of pathogens, including *Escherichia coli* (Ribeiro et al., 2018) and *Streptococcus* (Lima et al., 2020). The same characteristics as that of metal NPs (increased surface area, chemical reactivity, etc.) give them the special capacity to destroy hazardous species existing in the water. Therefore, they offer tremendous advantages in the purification of drinking water. Over the years, several synthesis techniques have been studied for the preparation of MNPs, out of which chemical methods are the most commonly used. MNPs have several drawbacks, including easy deactivation, slow absorption efficiency for impurities, and the sensitivity of removal efficiency to pH, etc (Huang et al., 2013; Lin et al., 2009; Huang et al., 2015; Wang et al., 2015).

2.1.2. Bimetallic Nanoparticles

In order to increase the reactivity and to overcome the limitations of MNPs, bimetallic NPs (BNPs) were created by the combination of two distinct metals where at least one of them has a nanoscale structure. Extensive investigations on BNPs were began

barely a decade ago and have been studied for a variety of applications including sensors, optoelectronics, catalysis, medicine, and UV protection gels, etc. Numerous BNPs with controlled size, morphology, and compositions have been created because of their unusual magnetic (Singh, 2003; Mattei et al., 2002), electronic (Jo et al., 2005), catalytic (Fortunelli and Velasco, 2002) and biological properties (Hong et al., 2005; Kim et al., 2005).

The characteristics of BNPs can be determined by their composition, nanometric size, and shape (Rao et al., 2003). In comparison to their monometallic counterparts, BNPs display some unexpected new features that expand their functionality and range of applications (Luo et al., 2011). For example, due to the interaction between the two metals present, BNPs exhibit remarkable properties such as improved optical, electrical, magnetic, antibacterial, and catalytic activities (Arora et al., 2020; González et al., 2011; Omori et al., 2011; Er et al., 2020; Yadav et al., 2018). And also, they show greater stability and selectivity (Ali et al., 2010; Carrillo-Torres et al., 2016). These unique features of BNPs are mostly influenced by the synergistic or multifunctional effect induced by the two metals (He et al., 2020; Sharma et al., 2019). It is possible to get a multifunctional BNP by choosing the right combination of metals with different characteristics (Srinoi et al., 2018). We can also improve and tune the physical and chemical characteristics of BNPs by simply altering their individual components and geometrical layouts (Sobal et al., 2003; Kodama et al., 2006).

Furthermore, due to the presence of two metals, BNPs can be prepared in a variety of morphologies and structures (Belenov et al., 2017). Based on their structural features, they can be classified as multi-shell, core-shell, segregated, intermetallic (alloyed), and heterogeneous structures (Ferrando and Jellinek, 2009; Zaleska-Medynska et al., 2016). The diversity of these nanostructures is mostly governed by the character of the combining metals, which is primarily influenced by parameters such as surface energy, charge transfer, atomic dimensions, relative bond strength, and their electronic and magnetic effects (Liu et al., 2014). They are often created by either simultaneous reduction or successive reduction of two metal ions, and the simultaneous/co-reduction of two metal ions generally results in the formation of alloys, whereas successive reduction of one metal ion after the other typically produces core shell NP. When compared to their bulk samples, the alloyed nanoparticles exhibit improved structural and physical characteristics, such as increased solid solubility with decreasing particle size.

2.1.2.1. Application of BNPs in Water treatment

The number of articles dealing with the BNPs has dramatically grown in recent years and an enormous number of scientific information are available on the synthesis and characterisation of BNPs that utilising various metal combinations. BNPs have been thoroughly investigated for the removal of a wide range of pollutants from wastewater and have gained a lot of attention from scientists in recent years (Li et al., 2020; Hassan and Ghadam, 2020; Fang et al.,

2015; Wang et al., 2015). So far, numerous studies have been discussed the removal of various organic and inorganic pollutants from water and wastewater and some of them are highlighted in Table 2.1. To the best of our knowledge, most of these studies are limited within iron based BNPs.

Table 2.1

Selected examples of BNPs for water treatment.

Sl. No.	Type of BNPs	Method of synthesis	Application	References
1	Fe–Ni	Green synthesis	As (V) removal from aqueous solution.	(Lin et al., 2022)
2	Cu/Fe	Liquid-phase chemical reduction	Removal of hexavalent chromium (Cr(VI)) from wastewater.	(Ye et al., 2021)
3	Fe/Cu	Chemical reduction	Removal of Cr(VI)	(Mondal et al., 2022)
4	Fe/Cu	Co-reduction	Co-removal of As(V) and Sb(V) from aqueous solution.	(Wang et al., 2022)
5	Cu/Ag	Chemical reduction	Antibacterial Agents	(Cruces et al., 2022)
6	Fe/Bi	Co-reduction	Removal of Cr(VI) from aqueous environment	(Mahar et al., 2022)
7	Fe–Cu-chitosan	Coprecipitation	Antimony removal	(Wang et al., 2022)
8	Fe–Cu	Successive reduction	Coal mine wastewater treatment.	(Dlamini et al., 2021)
9	Fe/Al and Al/Fe	Chemical liquid-phase deposition and co-reduction	Remediation of Cr^{6+} contaminated groundwater.	(Ou et al., 2020)
10	Chitosan–Fe/Ag	Co-reduction	Simultaneous removal of cadmium, nickel, and lead from aqueous solution.	(Van der Horsta et al., 2021)
11	Mg–Zn	-	Removal of Chromium (VI) from industrial wastewater	(Rahimi et al., 2021)
12	Fe/Cu	Co-reduction	Removal of arsenic from synthetic contaminated water	(Babaee et al., 2018)
13	Fe–Cu	Co-reduction	Removal of As(V) from aqueous solutions.	(Sepúlveda et al., 2018)

14	Montmorillonite-Supported Fe/Ni	Co-reduction	Removal of Cr(VI) from Wastewater	(Lu et al., 2017)
15	NiFe nanocomposite	Successive reduction	Removal of tetracycline (TC) from aqueous solutions.	(Ravikumar et al., 2020)
16	Ni–Al	Co-precipitation method	Adsorptive removal of fluoride from aqueous solution.	(Raghav et al., 2019)
17	Fe–Ni	Co-reduction	Degradation of Tetracycline (TC) in aqueous solution.	(Dong et al., 2018)
18	Ni/Fe	Liquid-phase chemical reduction	Cr(VI) Removal from aqueous solutions	(Zhou et al., 2014)
19	Ni/Fe	Co-reduction	Remediation of Pb(II)	(Saberi, 2012)
20	Au–Fe	Successive reduction	Simultaneous removal of Cd and nitrate in aqueous media	(Su et al., 2014)
21	Ni–Fe	Co-reduction	Used for groundwater decontamination and Trichloroethylene (TCE) reduction.	(Han and Yan, 2014)
22	Calcium alginate encapsulated Ni–Fe	Co-reduction	Simultaneous removal of Cu(II) and monochlorobenzene (MCB) from aqueous solution.	(Kuang et al., 2015)
23	Kaolin-supported Fe/Ni	Liquid-phase reduction method	Remediation of Direct Black G (DBG) from wastewater	(Liu et al., 2013)
24	Fe/Ni	-	Degradation of scarlet 4BS in aqueous solution	(Lin et al., 2012)
25	Fe–Pd	Reductive deposition	Degradation of lindane (γ-hexachlorocyclohexane) in aqueous solution.	(Nagpal et al., 2010)
26	Pd–Fe	Reductive deposition	Treatment of 2,4-dichlorophenol (2,4-DCP)	(Zhang et al., 2010)
27	Graphene–Fe–Ag	Chemical reduction	Antibacterial activity for Bacillus subtilis, Escherichia coli, and Staphylococcus aureus	(Ahmad et al., 2016)
28	Fe–Ag	Sonochemical synthesis	Antibacterial and antifungal activities as well as phosphorous removal from water.	(Markova et al., 2013)
29	Chitosan stabilized Fe/Ni	Liquid-phase reduction	Simultaneous removal of amoxicillin and Cd (II) from aqueous solutions.	(Weng et al., 2013)
30	Ni–Fe immobilized on cation exchange	-	Debromination	(Ni and Yang, 2014)

	resin			
31	Pt–Cu	Co-reduction	Reduction of Rhodamine B dye	(Singh et al., 2013)
32	Ag–Cu	Co-reduction	Antimicrobial for *Escherichia coli* / *Staphylococcus aureus*	(Singh et al., 2014)
33	Au–Ag	Co-reduction	Degradation of methyl orange and reduction of 2/3/4–Nitrophenols	(Kumari et al., 2015)
34	Ag–Au	Wet chemical method	Antibacterial activity	(Bankura et al., 2014)
35	Ag–Se	Biosynthesis method	Antibacterial activity for *Escherichia coli* / *Bacillus subtilis.*	(Mittal et al., 2014)
36	Cu–Ni	Simple chemical method	Antibacterial activity for *Staphylococcus* aureus, *Escherichia coli*, and *Streptococcus* mutans.	(Argueta-Figueroa et al., 2014)
37	Au–Ag core–shell	Simple chemical method	Antibacterial activity for *Staphylococcus aureus.*	(Ding et al., 2017)
38	Pt–Ag	Hydrothermal	Antibacterial activity for *Escherichia coli* / *Staphylococcus aureus*	(Cai et al., 2017)
39	Graphene–Cu–Ag	Successive reduction	Antibacterial activity	(Perdikaki et al., 2016)

Currently, BNPs have been used as a new line of defence against microbial resistance among various types of NPs due to their enhanced and synergistic bactericidal activity and better efficiency compared to the constituent ingredients (Taner et al., 2011). And also, it has been reported that low concentration of bimetallic nanoparticles can exhibit better bactericidal activity than single metallic nanoparticle against the multidrug-resistant bacteria and fungi (Eremenko et al., 2016).

Recent advances in nanotechnology have also explored the use of BNPs as a novel class of adsorbents in drinking water treatment

systems and have drawn great interest among various types of NPs. Many efforts have been made up to this point to remove or separate various heavy metals from water using different BNPs (Table 2.1). BNPs have a greater surface area as compared to their monometallic counterparts, which increases their adsorption power and also the interaction between two metals plays a vital role in the unique properties of BNPs (Sharma et al., 2015; Toshima and Yonezawa, 1998; Sharma et al., 2017; Wadhawan et al., 2020). The selection of an appropriate metallic combination and the optimisation of the metallic arrangement are essential for the engineering of the properties and activity of a BNP and which in turn determines how well the pollutants are removed (Arora et al., 2020)

2.2. Cu and Ni Nanoparticles

2.2.1. Cu nanoparticles

Copper nanoparticles (Cu NPs) have attained much attention by the scientific community due to their unique physical, chemical, and optical properties such as low toxicity, good biocompatibility, and excellent photostability (Momeni et al., 2017; Ojha et al., 2017; Raffi et al., 2010; Chatterjee et al., 2012) and therefore find applications in water treatment, biomedicine, optical imaging, and in catalysis. Cu NPs are very attractive due to their high natural abundance and low cost, and they are also simple to make using a wet chemical process. Hence, they have extensively studied over the past several years. Compared to other metal NPs, Cu NPs have more advantages because they are less expensive, provide greater yields under mild reaction

conditions, and have short reaction times than traditional nanoparticles. Furthermore, it has been long known that copper, especially in nanoparticle form, is an effective antimicrobial and bactericidal agent and works for a wide spectrum of bacteria and viruses (Cioffi et al., 2005; Chatterjee et al., 2012; Raffi et al., 2010). Cu is also a natural constituent of living tissues and human body can resist copper toxicity to some extent (Cady et al., 2011; Turnlund, 1998). USEPA has recently recognised it as the first antimicrobial substance (USEPA, 2021; García et al., 2021). Another important aspect is the utilisation of various cost-efficient synthesis methods to generate copper-based compounds with adjustable properties.

Several methods, including physical and chemical methods, can be used to produce copper NPs. Due to their ease of operation, minimal equipment requirements, and good particle quality, chemical methods like wet chemical reduction (Dang et al., 2011), reverse micelles (Lisiecki et al., 1995), microemulsions, electrochemical techniques (Silva, et al., 2019), laser irradiation (Sadrolhosseini et al., 2016), thermal decomposition (Effenberger et al., 2014) and vapor deposition (Safonov et al., 2017) have been used more frequently.

The ability of Cu NPs to suppress the development of harmful bacteria makes it an excellent candidate for use as an active biocide agent. Various hypotheses have been proposed to describe the mechanism of antimicrobial activity of Cu NPs (Sistemática et al., 2016). There are two ways that copper toxicity may happen: (1) direct contact death, which relies on how close the microbe is to surfaces that

contain copper, and (2) toxic effects generated by copper ions produced by copper dissolution (Vincent et al., 2018). According to several studies, depolarization of the cellular membrane is the main way that copper NPs cause toxicity in bacteria (Chang et al., 2012; Grass et al., 2011). In addition, they may also interact with biomolecules within cells, dislodging metal-binding protein sites and lowering or inactivating the activity (Chang et al., 2012). Both methods enhance the oxidative stress of the cell membrane by producing reactive oxygen species (ROS) (Quezada et al., 2020; Midander et al., 2009). In mammalian cells, Cu NPs have been shown to be around fifty times less hazardous than the ionic version. Cu NPs, on the other hand, are more harmful to bacteria than its ionic forms because of the previously described capacity of contact killing and quick disintegration in comparison to the bulk (García et al., 2021).

Giannousi *et al.* investigated the antibacterial activity of copper-based nanoparticles against Gram-positive (*Bacillus subtilis*, *Bacillus cereus*, *Staphylococcus aureus*) and Gram-negative (*Xanthomonas campestris*, *Escherichia coli*) bacteria. A hydrothermal process has been used to create copper-based nanoparticles (Cu, Cu_2O and Cu/Cu_2O NPs) of various compositions and sizes. The NPs were found to induce plasmid DNA degradation in a dose-dependent manner and verified the production of ROS and peroxidation of lipids. However, the ionic contribution to the bactericidal action of NPs cannot be validated since the released ions were below the critical value of limiting bacterial growth. Hence, it was concluded that the

nanoparticle size was more crucial for the antibacterial action than the quantity of discharged ions (Giannousi et al., 2014).

Yoon *et al*. reported preliminary studies on the toxicity of Ag and Cu NPs on *E. Coli* and *B. Subtilis*, where the Cu nanoparticles demonstrated superior antibacterial activity compared to the silver nanoparticles (Yoon et al., 2007). In addition, *B. subtilis* showed higher sensitivity than *E. coli* to Cu NPs. Many more recent investigations have confirmed the antibacterial activity of copper nanoparticles and their possible utility against infections (García et al., 2021; Rajesh et al., 2018; Thakur et al., 2018; Gutiérrez et al., 2017; Maqbool et al., 2017).

In a study, silver and copper nanoparticles were synthesised from plant extracts and were used as adsorbent to remove naphthalene from spiked aqueous medium. Three different plant precursors such as *Aloe barbedensis*, *Azadirachta indica* and *Coriandrum sativum* were used to synthesise nanoparticles. Based on these results, the authors concluded that copper nanoparticles synthesised from *Azadirachta indica* have more adsorption power as compared to silver nanoparticles (Abbas et al., 2020).

Similarly, Husein *et al*. synthesised Cu NPs by green synthesis method and used it as nano-adsorbent for the removal of Non-Steroidal Anti-Inflammatory drugs (NSAIDs) such as Ibuprofen (Ibu), Naproxen (Nab) and Diclofenac (Dic). High removal efficiency was achieved under the following circumstances: temperature-298 K, pH-4.5, Cu NPs-10.0 mg, and time-60 min. Under these conditions, the removal

efficiencies of Ibu, Nap, and Dic were 74.4, 86.9, and 91.4%, respectively. The adsorption data were fitted very well to the Langmuir isotherm model and pseudo-second-order kinetic model. The findings supported the effectiveness and application of green-biosynthesised Cu NPs in the treatment of aquatic systems polluted with NSAIDs (Husein et al., 2019).

2.2.2. Ni nanoparticles

Nanoparticles of Ni as well as their composite materials are also exciting and have a wide range of applications, including catalysis, magnetic fluid, magnetic storage, environmental remediation, water pollutant adsorption, fuel cell electrodes, biological medicine, and photocatalysis etc (Liu et al., 2018; Hajipour and Abolfathi, 2018; Cárdenas-Triviño et al., 2017). Compared to noble metal NPs like silver, nickel NP is chemically more stable, due to its relative abundance in the earth's crust, the metal salts of Ni are more affordable and easily accessible in comparison to the majority of other transition metal salts. Moreover, nickel exhibits fascinating properties when combined with other metals (Kumar and Deka, 2014).

In general, nickel NPs are produced by utilising microwave aided synthesis (Xu et al., 2008; Eluri and Paul, 2012), chemical reduction approaches employing appropriate reducing agents like sodium borohydride and hydrazine hydrate (Hou et al., 2005; , Pandey and Manivannan, 2015; Wu and Chen, 2003; Wu et al., 2012; Sudhasree et al., 2014; Roselina and Azizan, 2012), micro-emulsion synthesis (Chen and Wu, 2000; Ai et al., 2003), thermal degradation of

nickel (II) acetylacetonate in alkylamines (Chen et al., 2007), reversed micelles method (Harish et al., 2011), and sol-gel techniques (Jia et al., 2008). Among all these, chemical reduction procedures are the economically efficient and most convenient technique. Nickel chloride, nickel sulphate, nickel acetate, nickel nitrate, nickel carboxylate, etc. are among the frequently used precursors for NP synthesis and sodium hypophosphite, sodium borohydride, sodium hydride, hydrazine hydrate, organic amine (oleyl amine), primary aliphatic amines (dodecylamine), etc. are some of the reducing agents.

It has already been reported that Ni NPs have antimicrobial activity and, they can act as good adsorbent due to its chemical and magnetic properties (Pang et al., 2009; Mahmoud et al., 2015). Compared to the extensive literature on their uses in other study areas, such as catalysis, antimicrobial, bio-medical, electrochemistry, sensor, etc., the nano particles of Ni or NiO are less studied in the treatment of contaminated water.

Kumar *et al*. reported the antibacterial effects of Ni nanoparticles against six different bacteria (*Escherichia Coli, Lactobacillus, Stephilococcus Aureus, Pseudomonas Aeruginosa and Bacillus Subtitles)* and noticed, superior antibacterial activity at a very low concentration. Furthermore, antibacterial activity of Ni Nanoparticles was compared with seven well known antibiotics and demonstrated that, nickel nanoparticles show almost similar zone of inhibition as compared to the seven investigated antibiotics (Kumar et al., 2010).

Antibacterial activity of Ni NPs against *Staphylococcus aureus*, *Escherichia coli*, *Klebsiella sp*, *Enterococcus faecalis* and *Pseudomonas aeruginosa* were studied by Gomaji Chaudhary *et al*. using well diffusion method. And the antibacterial activities were compared with four antibiotics, *i.e*., Amikacin, Ciprofloxacin, Gentamicin and Norfloxacin. In their study, *pseudomonas aeruginosa* (21 mm), *Staphylococcus aureus* (21 mm), and *Klebsiella sp* (20 mm) were shown the highest zone of inhibition. The results revealed that even at lower concentrations, Ni NPs had potent antibacterial activity against all the tested pathogens (Gomaji Chaudhary et al., 2015).

Jeyaraj Pandian *et al.* examined the antimicrobial effectiveness of Ni NPs, which were made using Ocimum sanctum leaf extract, against harmful Gram-positive (*Bacillus subtilis*, *Staphylococcus epidermidis*), Gram-negative (*Escherichia coli*, *Klebsiella pneumoniae*, and *Salmonella typhi*), and fungal bacteria (*Candida albicans*, *Candida tropicalis*, *Aspergillus fumigatus*, *Aspergillus clavatus*, and *Aspergillus niger*). Among the tested pathogens, *E. coli* (25 mm) and *C. albicans* (23 mm) exhibited higher zone of inhibition at 100 μg/mL of NiGs. Jeyaraj Pandian *et al.* proposed that, the enhanced antimicrobial activity was due to the active production of ROS, which resulted in the loss of cellular proteins and Lactate Dehydrogenase (LDH) by damaging the cell membrane and finally caused cell death. According to this study, NiGs have the potential to be an antimicrobial agent at a concentration of 50 g/mL. As a result, they might be used as antimicrobial coatings on the surfaces of materials for a variety of

biomedical and environmental applications (Jeyaraj Pandian et al., 2016).

The simplicity of synthesis and the ability to create a very high surface area structure make Ni NP a potential adsorbent. While only a few studies have reported the application of Ni and NiO-based nanoparticles as adsorbent in the elimination of hazardous compounds from water (Wang et al., 2020; Bhardwaj and Sarkar, 2020).

Zhang *et al.* synthesised Ni NPs by reducing Ni^{2+} with $NaBH_4$ at room temperature and their capacity to adsorb organic dyes from industrial effluent was quantitatively examined using Congo red (CR) as an adsorbate. According to their findings, Ni nanoparticles exhibited a high adsorption capacity of 966.7 mg/g and a rapid adsorption rate of 83% in just 5 minutes. The magnetic experiments also revealed that the Ni nanoparticles have ferromagnetic characteristics and can be effortlessly separated from the dispersion system using a magnetic bar. Finally concluded that, the synthesised NPs can be employed in its current state as a possible adsorbent in the treatment of industrial effluent, particularly when it contains CR (Zhang et al., 2015).

Nickel nanoparticles encapsulated in porous carbon/carbon nanotube hybrids (Ni/PC-CNT) were used for the removal of malachite green (MG), congo red (CR), rhodamine B (Rh B), methylene blue (MB) and methyl orange (MO) from aqueous solution (jin et al., 2018). The created Ni/PC-CNT composites had a high surface area (999 m^2g^{-1}), large pore volume (0.86 cm^3g^{-1}) and it exhibited outstanding dye adsorption behaviour and high adsorption capacity. Moreover, Ni/PC-

CNT composites are readily separable by an external magnetic field and could be easily regenerated by washing with ethanol. Therefore, the Ni/PC-CNT composites would be a good choice for the removal of dyes from aqueous solution.

2.2.3. Cu-Ni Bimetallic Nanoparticle

In consideration of the adsorption and bactericidal properties of Cu and Ni NPs, we expect that, the combination of these two nanoparticles would increase its potential for removing the heavy metals and reducing the bacterial content from water. Several methods have been used for the preparation of Bimetallic Cu–Ni NPs such as hydrothermal method (Niu et al., 2004; Hashemizadeh and Biglari, 2018; Seethapathy et al., 2019), microemulsion method using sodium dodecyl sulfate (as anionic surfactant) and oleic acid (Feng and Zhang, 2006; Wen et al., 2009), precipitation method (Riaz et al., 2012), co-reduction method (Argueta-Figueroa et al., 2014) etc.

In a study by Argueta-Figueroa et al., synthesised Cu, Ni and bimetallic Cu–Ni NPs via chemical precipitation method and were examined their antimicrobial activity against *Staphylococcus aureus, Escherichia coli* and *Streptococcus mutans*. All the three NPs exhibited antibacterial property and were effectively reduced the bacterial concentrations. They observed a higher antibacterial activity for bimetallic Cu–Ni nanoparticles than Cu and Ni NPs and postulated that the obtained results are promising for the potential use of bimetallic Cu–Ni NP in dental materials science (Argueta-Figueroa et al., 2014).

Seethapathy et al. reported the hydrothermal synthesis method for Cu-Ni bimetallic nanoparticles with different Cu-Ni molar ratios (Cu25Ni75, Cu50Ni50 and Cu75Ni25) and their catalytic activity was compared with the monometallic nickel and copper. It has been shown that CuNi bimetallic NPs possess more catalytic activity for the

degradation of 4-nitrophenol in comparison to individual Cu and Ni NPs. Moreover, Cu75Ni25 bimetallic alloy also shown good recyclability and 24 times higher catalytic activity than monometallic copper which have similar surface area and size. The difference in the catalytic activity was attributed to the better electron transfer rate of Cu75Ni25, which was confirmed by the higher oxidation current obtained by the cyclic voltammetry studies. They also mentioned about the effective recyclability of Cu-Ni bimetallic nanoparticles with the help of a magnet, thereby reducing the material loss during the collection of nanoparticles for repeated usage. Hence, they proposed that, the synthesised catalyst can be efficiently used in industries for treating effluent waters (Seethapathy et al., 2019).

Cu-Ni BNPs were also used for the photodegradation of methyl orange and methylene blue. In this study, Cu-Ni BNPs were prepared via the simple hydrothermal method and characterized by X-ray diffraction, energy-dispersive X-ray spectroscopy, scanning electron microscope, and vibrating sample magnetometer. The obtained NPs exhibited a magnetic feature with a suitable magnetization, and it is an essential characteristic required for a re-generable and reusable magnetic heterogeneous catalyst. Then the catalytic activity for the photodegradation of dyes were studied and showed that methylene blue and methyl orange were degraded about 98 and 72% in 60 min, respectively (Hashemizadeh and Biglari, 2018).

Riaz *et al*. studied the photodecolorization of Orange II under visible light using bimetallic Cu–Ni/TiO_2. Photocatalysts with different

Cu:Ni mass compositions were prepared via precipitation method and calcined at different temperatures. Results showed that, Cu–Ni/TiO_2 photocatalysts displayed high percentage removal of Orange II as compared to bare TiO_2 and the monometallic photocatalysts. It was found that, the best performing photocatalyst has 9:1 Cu:Ni mass composition. 100% Orange II removal was achieved with 16.1 ppm TOC value (Riaz et al., 2012).

A study by Liu *et al.* investigated the catalytic activities of three types of bimetallic Cu–Ni nanoparticles supported on Chromium(III) terephthalate metal organic framework (MIL-101), titanium dioxide (TiO_2), and carbon (C) in the selective oxidation of benzyl alcohol to benzaldehyde. All the catalysts were synthesised by co-immobilization followed by H_2 reduction. Where the CuNi/MIL-101catalysts displayed a high functional group (electron-donating and electron-withdrawing groups) tolerance and the supported catalysts with Cu:Ni mole ratio of 1:1 exhibited the highest yield of 47%. The highest benzaldehyde yields were achieved with CuNi/TiO_2, CuNi/MIL-101, and CuNi/C catalysts respectively at 100 °C within 4 h (Liu et al., 2019).

Several literatures are available which have focused on the adsorption behaviour of Cu and Ni NPs separately. As far as our knowledge and our literature survey indicates that, the removal of heavy metals from solutions using CuNi bimetallic NPs has not been so far reported. Therefore, the present work is a novel one to investigate the effect of CuNi bimetallic NPs on the adsorption of

metal from contaminated water and its antibacterial efficiency. Moreover, in the case of nanoparticles, factors like ease of preparation, kinetics of reaction, pH, effective separation from treated water, etc. can affect the effective pollutant removal. The CuNi BNPs can be prepared very quickly in the lab or *in situ* and also it is quite stable in different pHs. Hence, CuNi bimetallic NPs have been prepared to achieve more potent antibacterial and adsorption properties.

2.3. Immobilization of bimetallic nanoparticle

Despite that, this small size of NPs is one of the main obstacles in their successful implementation into water treatment units because of the difficulty in separation from wastewater, risk of particle leaching, and high replacement cost. The recovery of NPs from an aqueous medium has normally been carried out by nanofiltration, magnetic separation, and ultracentrifugation methods. But referring to common water purification strategies these methods are practically tedious and may become the cost-determining step of the whole process. Generally, these limitations can be overcome by immobilization/stabilization of NPs. Several methods are available for the immobilization of NPs. By using proper materials for encapsulation, it is possible to decrease and control the release rate of NPs and provide an effective protection from the oxidation and agglomeration of NPs. However, majority of these techniques are less environment-friendly and less cost effective, and most of them result in the loss of adsorption capability due to the usage of binders and high temperature processing. Therefore, it is necessary to fabricate

immobilized NPs with good stability, higher efficiency, easy synthesis, economy, and reusability for the potential removal of heavy metals available in water and wastewater.

A wide range of solid support organic or inorganic materials have been used for the immobilization of metal NPs, these include silica (Li et al., 2016; Tabakci and Yilmaz, 2008), alumina (Mallick and Scurrell, 2003), metal oxides (Li and Tang, 2014), activated carbon (Silva et al., 2002; Li et al., 2014), chitosan, alginate beads (You et al., 2014) etc. Among all, polymers have become one of the most promising substrate candidates due to its non-toxic, non-volatile, simple, stable, flexible, and reusable character (Burguete et al., 2005; King and Twyman, 2002). Because of their excellent mechanical properties, adaptable porosity structure, and chemically attached functional groups, polymers provide excellent support to the nanomaterials (Salem et al., 2022).

Polymer-based nanocomposites (PNCs) are being explored as attractive materials for water and wastewater treatment because they usually incorporate the inherent benefits of both nanoparticles and the polymeric matrix (Bustamante-Torres et al., 2021). Particularly, the porous polymer microsphere has gained significant attention for immobilization of metallic NPs due to its porous character which determines the efficiency of the adsorption, provides better accessibility for adsorbates by increasing the contact area between the adsorbent and adsorbate and larger specific surface area (Yang et al., 2015). Zha et al. showed that the multi-porous sulfonated

polystyrene/chitosan/Ag microspheres could efficiently adsorb chromium ions and have a higher catalytic degradation rate than that of non-porous solid structured composite particles (Zha et al., 2015).

Research in recent years has indicated that the porous polymer styrene–divinylbenzene (St–DVB) microbeads exhibit high surface area, controllable particle size, good chemical and physical stability, easy functionalization, and tuneable pore structures (Tian et al., 2016; Albuszis et al., 2016). Especially in the case of water treatment, the porous structure and surface area have an important role in determining the efficiency of adsorption and release (Wang et al., 2010; Lin et al., 2013; Ali and Gupta, 2006). Therefore, in this investigation, the immobilization of the synthesised nanoparticles was accomplished using the styrene-divinylbenzene (St-DVB) copolymer.

Chapter 3

Synthesis, characterisation, and antibacterial activity of CuNi bimetallic nanoparticles

3.1. Introduction

Recently, there is an increase in the emergence of multidrug-resistant bacterial strains which are resistant to conventional treatment methods. Therefore, design and development of novel antibacterial agents with enhanced activity and not susceptible to bacterial resistance are necessary to solve this issue (Udikovic-Kolic et al., 2014). To this extent, nanotechnology can offer an attractive method for synthesising alternative antimicrobial agents that can overcome the bacterial resistance (Fernando et al., 2018; Beyth et al., 2015; Pelgrift et al., 2013). Recent progress in the field of nanotechnology has paved the way for innovative approaches for development of novel bacteriostatic and bactericidal agents. Nanomaterials have shown broad spectrum antimicrobial activity against Gram positive and Gram-negative bacteria, fungi, and mycobacteria (Wang et al., 2017). A new class of antimicrobial materials based on noble metal NPs has been developed due to their tremendously large surface area, high reactivity, and many reactive surface sites. The antimicrobial activity of heavy metal-based nanoparticles can find various applications in the field of antimicrobial fabric manufacturing, water disinfection, food packaging, industry and medicine. Their antibacterial effect has been attributed to

their small size, large surface area, and increased surface to volume ratio, which allows them to attach closely with microbial membranes. The bactericidal effect of metal NPs may vary with their individual properties such as particle size, particle shape, morphology, zeta potential, surface coatings, stability, etc. which enable scientists to develop novel antimicrobial agents.

However, the specific antibacterial mechanisms of metal NPs are poorly understood, and the same types of NPs often present contrasting effects. It is suggested that multiple mechanisms such as oxidative stress induction (Gurunathan et al., 2012), metal ion release (Nagy et al., 2011), and non-oxidative (Leung et al., 2014) mechanisms may contribute to its antibacterial mechanisms. Certain studies have proposed that, the cell membranes of bacteria contain pores of nanometer range and it can be overcome by the NPs which have smaller size than that of pores of bacteria. They act directly on bacterial walls and the structure of the bacterial cell membranes can be altered noticeably when in contact with NPs, that leads to the leakage of intracellular constituents and cause bacterial cell death. Most of the antibiotic resistance mechanisms are irrelevant for metal NPs because of its specific mode of action against bacteria. This raises the hope that, these heavy metal-based NPs would be less prone to promoting resistance in bacteria than antibiotics and can find many applications in the field of medicine and industry in the future and provide a solution to the current challenges of antimicrobial resistance to conventional treatment methods.

Currently, bimetallic NPs, composed of two different metal elements, have been used as a new line of defence against microbial resistance among various types of NPs due to their enhanced bactericidal activity and better efficacy compared to the constituent ingredients (Taner et al., 2011). And also, it has been reported that low concentration of bimetallic nanoparticles can exhibit better bactericidal activity than single nanoparticle against the multidrug-resistant bacteria and fungi (Eremenko et al., 2016). The interaction among two metals plays a vital role in the unique properties of bimetallic NPs. Furthermore, bimetallic NPs have greater surface area as compared to those of monometallic NPs (Toshima and Yonezawa, 1998; Sharma et al., 2015; Sharma et al., 2019) and which results in novel properties, such as greater interaction with cells due to a larger surface area-to-mass ratio.

Cu and Ni NPs have excellent antimicrobial and bactericidal activity (Chatterjee et al., 2012; Raffi et al., 2010). Copper nanoparticles (Cu NPs), on the other hand, have unique physical and chemical properties and it have been widely used as an effective antibacterial agent (Cioffi et al., 2005). Cu is also a natural constituent of living tissues and human body can resist copper toxicity to some extent (Cady et al., 2011; Turnlund, 1998). Various hypotheses have been proposed to describe the mechanism of antimicrobial activity of Cu NPs (Sánchez-Sanhueza et al., 2016). Yoon *et al*. reported preliminary studies on the toxicity of Ag and Cu nanoparticles on *E. Coli* and *B. Subtilis*, where the Cu nanoparticles demonstrated superior

antibacterial activity compared to the silver nanoparticles (Yoon et al., 2017). While only a few studies have reported the antibacterial properties of Ni nanoparticles. Harish Kumar *et al*. reported the antibacterial effects of Ni nanoparticles against six different bacteria (*Escherichia Coli, Lactobacillus, Stephilococcus Aureus, Pseudomonas Aeruginosa and Bacillus Subtitles)* and found that, superior antibacterial activity at a very low concentration. Further, antibacterial activity of Ni Nanoparticles was compared with seven well known antibiotics and demonstrated that, nickel nanoparticles show almost similar zone of inhibition as compared to the seven investigated antibiotics (Kumar et al., 2010). In consideration of the bactericidal activity of Cu and Ni NPs, we expect that, the combination of these two nanoparticles would offer a potential remediation method for bacterial reduction from water. So CuNi bimetallic NPs have been prepared to achieve more potent antibacterial properties.

This chapter focuses on the preparation and characterisation of CuNi bimetallic nanoparticle followed by its antibacterial activity studies against three different pathogenic bacteria, namely *Escherichia coli* (*E.coli*), *Aeromonas hydrophila* (*A.hydrophila*) and *Vibrio alginolyticus (V. alginolyticus)*, by using the spread plate counting method. The NPs were synthesised by "chemical reduction method" and it is commonly used as a simple, cost-effective, and efficient technique for the production of metallic NPs. And also, this approach can produce NPs in high yield and uniformity in shape and size. The NPs were then characterised to reveal their composition, morphology,

and size by various characterisation techniques such as Scanning Electron Microscopy (SEM), Transmission Electron Microscopy (TEM), Energy Dispersive X-ray Spectra (EDS), Powder X-ray Diffraction (PXRD) and surface area studies. Then determined the effects of contact time, NP dose, and initial bacterial concentration on the bactericidal rate through batch experiments.

3.2. Experimental

3.2.1. Materials

All chemicals used in the study were of analytical reagent grade and purchased from Merck, India. Ultrapure water, with a resistivity of 18.2 MΩ from a Milli-Q water filtration system purchased from Millipore, was used throughout the experiment for all solution and media preparation. The bacterial strains used in this study were isolated from the water samples collected from Canoli Canal, Kozhikode. All bacterial strains were characterised and identified based on biochemical tests as well as 16S rDNA sequencing from Rajiv Gandhi Centre for Biotechnology (RGCB). Nutrient broth (NB) medium containing peptone, Sodium Chloride, Yeast Extract, and Beef Extract were purchased from HiMedia, India, and were used without further purification. EMB Agar, Chromogenic Coliform Agar, Bismuth Sulphite Agar and TCBS Agar, were purchased from HiMedia, India. Sterilisation of all the glassware and media were carried out in a Rotek RAV01 autoclave for 20 min at 121°C. Agar plates were prepared in a laminar flow hood and the plates were streaked in an aseptic area around a Bunsen burner. All worktops and benches were sterilised by

washing with 70 % (v/v) ethanol/water prior to use. Bacterial cell density was recorded using a Spectrophotometer.

3.2.2. Preparation of CuNi bimetallic nanoparticle

The CuNi BNPs used in this study was synthesised via in situ chemical precipitation method. The chemical precipitation methods are simple, easy to operate, cost effective, and allows high purity of the products with reproducible results. Moreover, this procedure can be applied at room temperature under ordinary pressure and in aqueous solution.

A solution of equal mole amount of copper sulfate pentahydrate ($CuSO_4 \cdot 5H_2O$) and nickel sulfate hexahydrate ($NiSO_4 \cdot 6H_2O$) metal salts were used to complete 1×10^{-2} M. The pH of the solution was fixed to 8 with NaOH. After that, 4×10^{-2} M Sodium borohydride ($NaBH_4$) as a reducing agent, was added to the metal solution. After the addition of the reducing agent, the solution was stirred for 30 min to complete the reaction and the precipitate was filtered, washed with distilled water. Then it was rinsed with acetone to displace deionized water and stored.

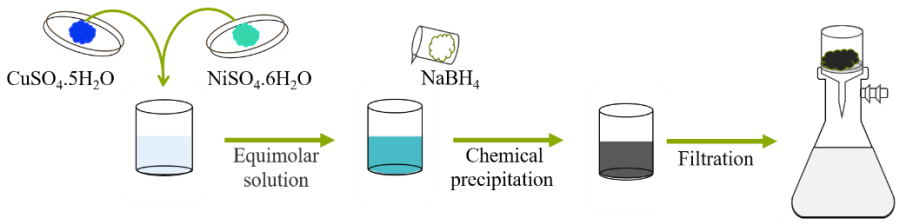

Figure 3.1: Schematic representation of the synthesis of CuNi BNPs.

3.2.3. Characterisation of CuNi BNPs

The synthesised CuNi BNPs were characterised using Scanning Electron Microscopy (SEM), Transmission Electron Microscopy (TEM), Energy Dispersive X-ray Spectroscopy (EDS), powder X-ray diffraction (PXRD) and surface area studies. The surface morphology and size of the NPs were examined by SEM (SEM-EDX, **ZEISS GeminiSEM 300)** and TEM (HR-TEM, **Jeol/JEM 2100**). The crystal structure was determined by PXRD (PXRD, **Bruker D8 Advance**) and EDS was used for the determination of elemental composition and purity of the samples by atom percentage of metal. The surface area of the samples was analysed using Brunauer–Emmett–Teller (BET) method from N_2 adsorption desorption data (BET, **BELSORP-max**).

3.2.4. Antibacterial activity

The potential antibacterial activity of the CuNi Bimetallic nanoparticle was tested against three different strains of bacteria, namely *Escherichia coli* (*E.coli*), *Aeromonas hydrophila* (*A.hydrophila*) and *Vibrio alginolyticus (V. alginolyticus)* by using the spread plate counting method described by *Pan, et al.*(Figure 3.2)(Pan et al., 2019). Streak culture method was used for isolation of organisms in pure culture from the collected water samples. Selective media were chosen to culture each strain according to the type of bacterial strains. For culturing *E.coli*, *A.hydrophila* and *V. alginolyticus* the agars used were: Chromogenic Coliform agar, Bismuth Sulphite agar (BSA), and Thiosulfate-citrate-bile salts-sucrose (TCBS) agar respectively.

Approximately, 25ml of molten and cooled agar media were poured in the sterilized petri dishes. The plates were left over night at room temperature to check for any contamination to appear. The NB medium was used for growing and maintaining the bacterial liquid cultures and prepared as per the manufacturer's instructions in sterilised water.

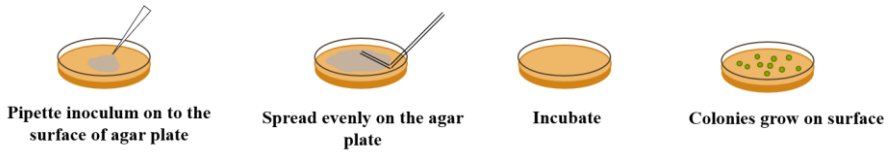

Figure 3.2: Schematic representation of the spread plate counting method.

A series of batch scale experiments were conducted to investigate the antibacterial activity of the CuNi Bimetallic nanoparticle. Experimental conditions as per **Table 3.1** were varied to quantitatively evaluate their effects on antibacterial activity.

Table 3.1

Experimental conditions for batch study.

Bacteria	Contact time (min)	Nanoparticle dose (µg/ml)	Initial bacterial concentration
Escherichia coli	15-180	10-50	10^6
	60	10-50	10^6
	60	50	10^4-10^8
Aeromonas hydrophila	15-180	10-50	10^6
	60	10-50	10^6
	60	50	10^4-10^8
Vibrio alginolyticus	15-180	10-50	10^6
	60	10-50	10^6

60	50	10^4-10^8

3.2.4.1. Preparation of Synthetic Contaminated Water

A representative microbe colony was picked off with a wire loop, placed in NB, and then initially incubated at 37°C for 24 hrs for bacterial culture. The inoculation of each bacterial culture was maintained at 4 ± 1˚C for short term storage and were routinely sub-cultured within every 4-6 weeks of time intervals. Sterilized physiological saline (0.85% NaCl) solution was prepared and appropriate amount of previously prepared bacterial culture were suspended in to separate 1000 mL of the saline water under sterile conditions. The spiked saline water were then incubated at 37°C until a level of approximately 10^6 CFU/mL of *E.coli, A. hydrophila* and *V. alginolyticus* were reached and shaken vigorously for several times. 100 µL of 10^6 CFU/mL bacterial suspensions of each bacterial organism were spread onto the agar plates and incubated at 37°C for 24 hrs. The initial CFU/ml of the target organism was determined by counting the number of colonies using a Digital Colony Counter **(Interscience, Scan 1200)** and the remaining contaminated water was used for the batch study. It should be noted that the input bacterial concentration may change significantly in experiments lasting several weeks, therefore the cultures are made on a daily basis.

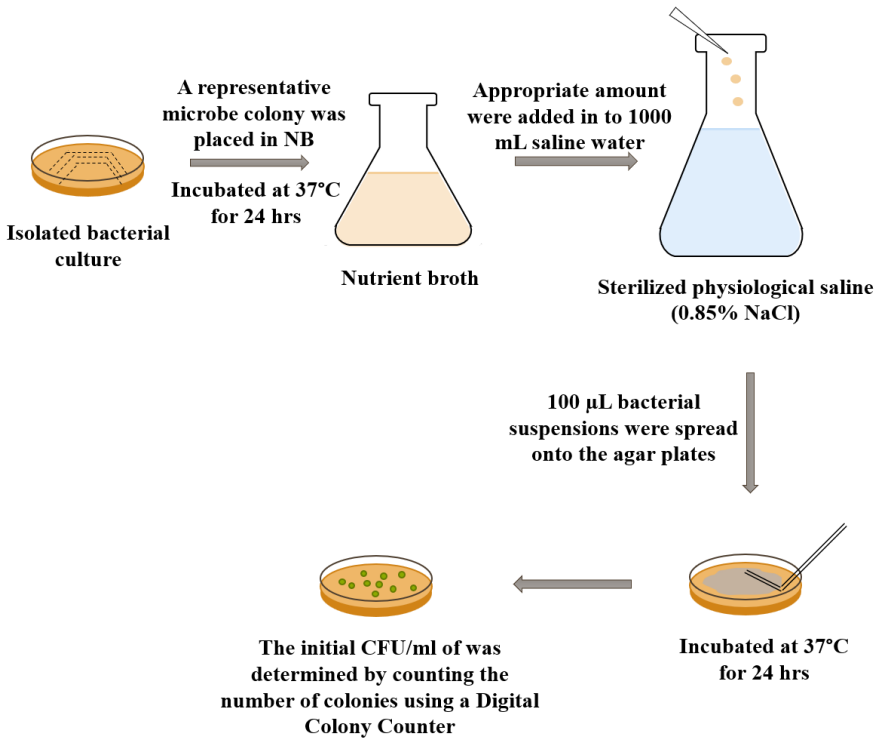

Figure 3.3: Schematic representation of the preparation of the synthetic contaminated water.

3.2.4.2.Dose-dependent antibacterial activity of CuNi BNPs

The experiments were conducted in 500 mL sterilized stoppered bottles. Different amounts of the synthesised BNPs (10, 20, 30, 40, and 50 µg/ml) were added into 250 mL spiked saline samples with an initial bacterial concentration of approximately 10^6 CFU/mL. The saline water without nanoparticles were used as negative control. All the bottles were then shaken for 1 hr in an incubator shaker with continuous stirring at 200 rpm and 37℃. After this period of time, an aliquot of 100 µL were withdrawn and were inoculated in

corresponding agar plates by the spread plate method (three plates for one sample). The control sample was tested in every run by the same method and used as a standard for comparison. All plates were incubated at 37 °C for 24 h and the grown colonies were counted. The average value was obtained and expressed as CFU/mL.

3.2.4.3. Bacterial growth kinetics in the presence of CuNi BNPs

Bacterial growth curve was monitored by treating the saline water with BNPs at different exposition times. 10 to 50 µg/ml of the BNPs were added into a 250 mL spiked saline water samples of each bacterial saline water with initial bacterial concentration of approximately 10^6 CFU/mL. A negative control was carried out in flasks without BNPs. Each flasks were then shaken for 2 hrs and an aliquot of 100 µL of the treated samples was withdrawn at every 15 min time interval. The aliquots were transferred into the petri plates and were incubated at 37℃ for 24 h. Then the final CFU was determined by counting the number of colonies on each plate and the results were plotted in function of the time of aliquot withdrawal.

3.2.4.4. Bactericidal activity of CuNi BNPs

Sterilized saline (0.85% NaCl) solution was prepared with variable number of initial bacterial concentrations (10^4-10^8 CFU/mL) for each bacterial strain. 50 µg/ml of the synthesised CuNi BNPs was added to 250 mL of each bacterial solution and shaken for 60 min in an incubator shaker with continuous stirring at 200 rpm at 37℃. Finally,

100 µL of each sample was spread on the petri plates followed by recording the number of colonies on each plate.

3.2.4.5. The bactericidal rate of CuNi BNPs

The bactericidal rate of every sample was calculated according to the following equation.

$$\text{Bactericidal rate } (\%) = \frac{B - A}{B} \times 100$$

Where A represents the number of colonies of the tested plate (CFU/mL), B represents the number of colonies of the Initial/controlled plate (CFU/mL).

3.3. Results and Discussion

3.3.1. Characterisation of CuNi BNPs

The SEM images showed that the appearance of the particles is spherical in shape and also it was homogeneous in size to a certain extent (Figure 3.4). Figure 3.5 presents the TEM images of NPs and it showed that the NPs exhibited the morphology of spherical particles with an average size of 38.4 nm. The high-resolution TEM (HR-TEM) image shows the lattice fringes with the interplanar distance of 0.21 nm, which corresponds to the (111) plane of the bimetallic NP. The substitution of Ni atoms in the lattice locations of Cu to produce a bimetallic alloy is confirmed by the absence of discrete lattice fringes belonging to either Cu or Ni.

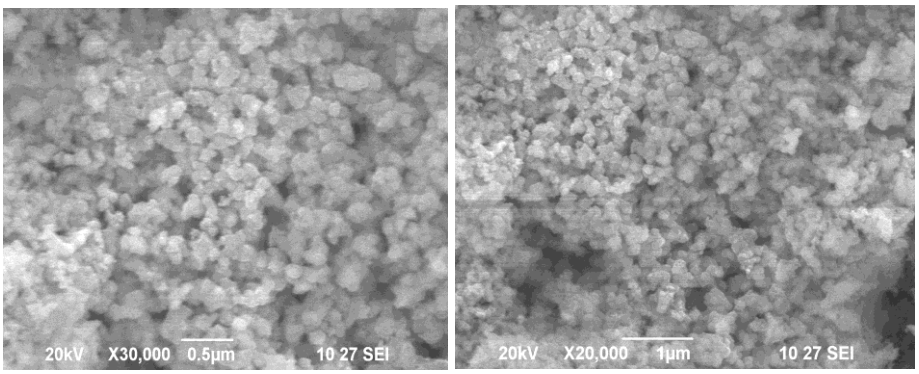

Figure 3.4: SEM images of CuNi bimetallic nanoparticle.

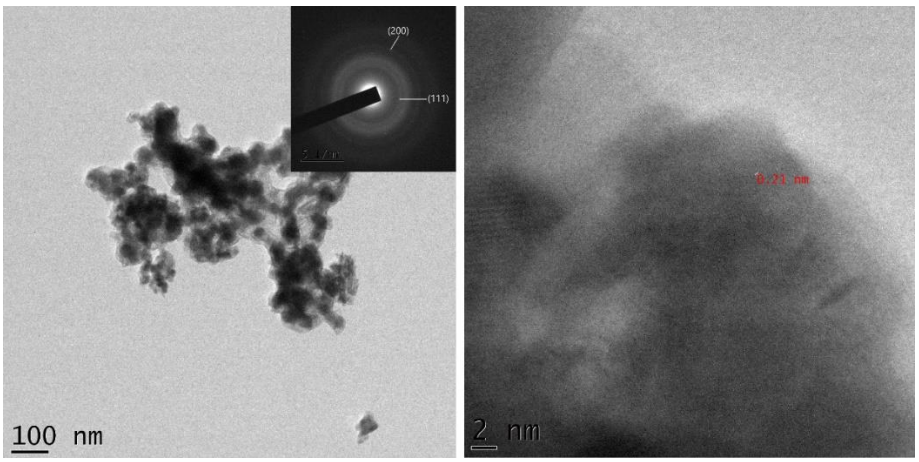

Figure 3.5: TEM micrograph of (a) CuNi bimetallic nanoparticle, the inset shows selected area diffraction pattern and (b) HR-TEM image with lattice spacing.

EDS analysis (Figure 3.6) was carried out to confirm the elemental composition of the samples and which confirms the ratio (1:1) whose weight % of Cu and Ni is found to be 36.60 and 36.45. Results obtained from EDS analysis reflect that Cu (II) and Ni (II) salts are almost reduced to their zero-valent metals.

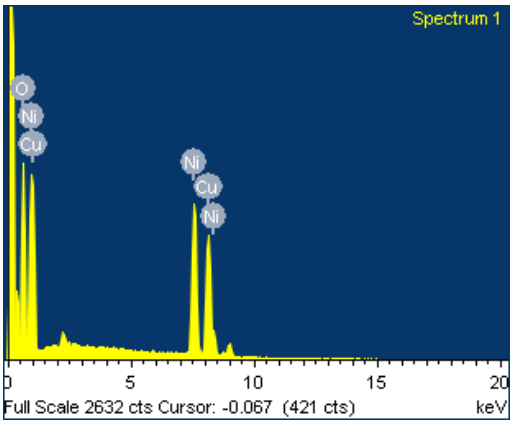

Figure 3.6: EDS image of CuNi bimetallic nanoparticle.

Figure 3.7 shows the PXRD pattern of prepared CuNi bimetallic NPs. It can be seen that there is strong diffraction peaks at 43.2°, 50.4° and 74° which correspond to the (111), (200) and (220) plates, respectively, which is similar to that reported for CuNi (1:1) bimetallic nanoparticles (JCPDS # 3- 065-7246).

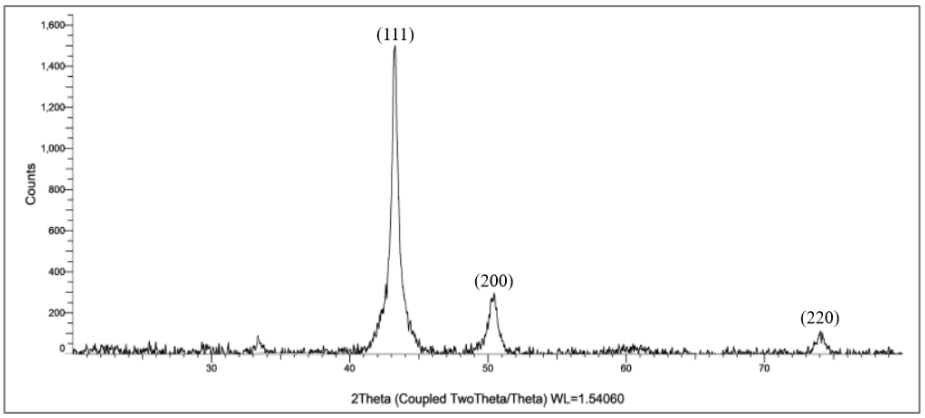

Figure 3.7: Powder X-ray diffraction pattern of synthesised CuNi bimetallic nanoparticles.

The surface area analysis was carried out by BET method. The BET experimental results of the CuNi bimetallic NPs were summarized in Table 3.2 and the N_2 adsorption-desorption isotherm plot is shown in Figure 3.8. According to the IUPAC classification, the isotherm exhibited is intermediate between type IV and type II with H3-type hysteresis loop, indicating the presence of large mesopores with a broad size distribution that continues into the macropore domain. The specific surface area was found to be 31.28 m^2/g. This value is higher than that of metallic Cu (7.61m^2/g) and Ni (10.15 m^2/g) nanoparticle

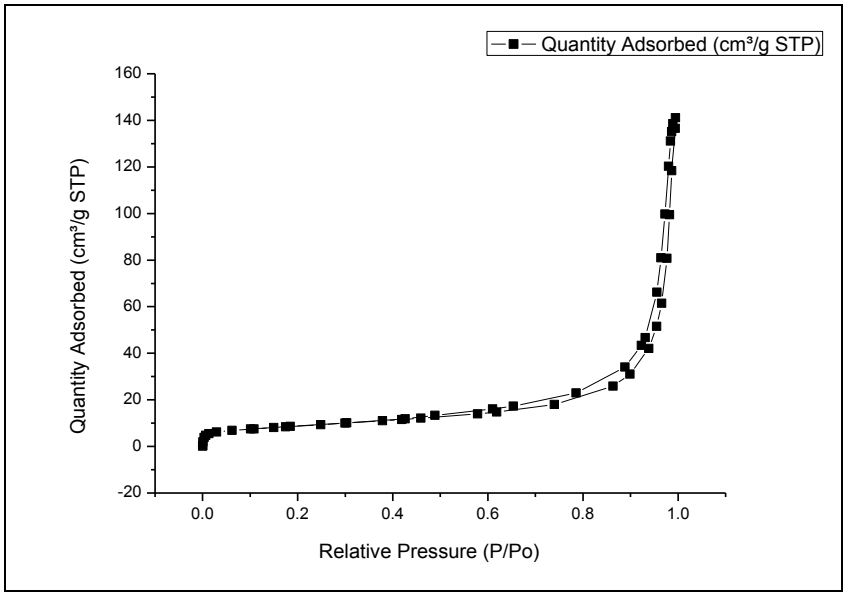

Figure 3.8: N_2 adsorption-desorption isotherms of CuNi bimetallic nanoparticles.

Table 3.2: BET experimental results of CuNi bimetallic nanoparticles

BET surface area S_{BET} (m^2/g)	**Average pore diameter (nm)**	**Total pore volume (cm^3/g)**
31.28	18.79	0.14

3.3.2. Antibacterial activity

Spread plate counting method was used to assess the sensitivity of the BNPs against three of the most ubiquitous bacteria, namely *Escherichia coli* (*E.coli*), *Aeromonas hydrophila* (*A. hydrophila*) and *Vibrio alginolyticus* (*V. alginolyticus*). It was observed that CuNi BNPs exhibited effective antibacterial activity against all three types of bacteria.

3.3.2.1. Dose-dependent antibacterial activity of CuNi BNPs

In the experiment, different amounts of BNPs (10, 20, 30, 40, and 50 µg/ml of saline solution) were added in each stoppered bottles containing the bacterial saline solution with an initial concentration of approximately 10^6 CFU/mL. The bottles were shaken for 1 hr and an aliquot of 100 µL of the bacteria suspensions was inoculated in agar plates. Number of surviving bacteria in each agar plates was counted after 24 h of incubation at 37°C. Figure 3.9 shows the bactericidal rate (%) of CuNi BNPs at different investigated concentrations against all the three bacteria. Dose dependent study of nanoparticles showed that, CuNi BNPs with different concentration had different antimicrobial effects and the effectiveness of the bacterial growth inhibition increased linearly with increasing amount of nanoparticles. At lower concentrations, the CuNi BNPs exhibited a relatively weak

antibacterial effect. But a significant decrease on the cellular viability was observed with an increase in the amount of NPs up to 30 µg/ml for *A. hydrophila* and *V. alginolyticus,* and up to 40 µg/ml for *E. coli*. This indicates that, the bactericidal activity increased with increasing concentration of BNPs and the higher concentrations were able to kill more number of cells. This might be attributed to the increased ability of NPs to eliminate the bacteria at higher NPs concentration. This is because at higher concentrations more nanoparticles exist in the solution, which in turn increases the probability of nanoparticles coming into contact with the microorganism. This situation leads to the killing of more number of bacteria at higher concentrations in comparison with low concentrations. Negative control (without nanoparticles) did not show any growth inhibition.

It is evident from the figures that, with increasing concentration of nanoparticles from 10 to 30 µg/ml, the bacterial growth inhibition of *E. coli*, *A. hydrophila* and *V. alginolyticus* were increased respectively from 0 to 77%, from 70 to 99% and from 80 to 100%. Thereafter, the bactericidal rate increased slightly and reached its maximum. 100% of *A. hydrophila* and *V. alginolyticus* cells were inactivated after the contact with 40 µg/ml and 30 µg/ml of CuNi BNP respectively. The maximum bactericidal rate of CuNi BNPs to *E. coli* was found to be 97% and it was attained at 60 min of contact time with 50 µg/ml of NPs. Prior to this, 50 µg/ml was chosen as the optimum dosage of BNP for further analysis and research. Hence, we have confirmed that the bacterial growth inhibition by CuNi BNPs is dose dependent.

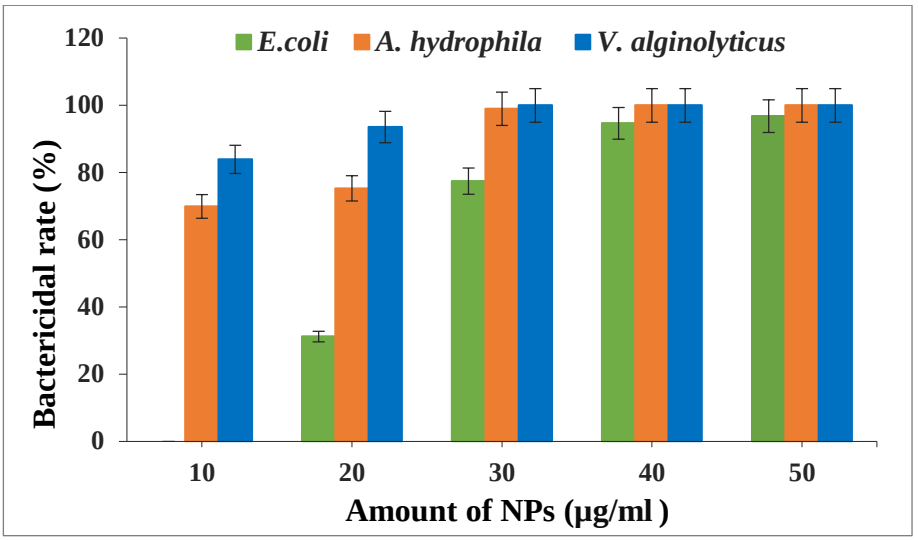

Figure 3.9: Bactericidal rate (%) of CuNi BNPs at different investigated concentrations against *E. coli*, *A. hydrophila* and *V. alginolyticus* (contact time, 60 min; initial bacterial concentration, 10^6 CFU/mL; 200 rpm).

The bactericidal rate of CuNi BNP is also varied depending on the organism tested. Results of antimicrobial studies showed relatively higher sensitivity of CuNi BNPs for *A. hydrophila* and *V. alginolyticus* compared to that of *E. coli* and that can be attributed to the different cell wall composition of bacteria. The bacterial cell wall plays a vital role in resistance or susceptibility (Hajipour et al., 2012). This observation is in concurrence with the other antibacterial studies carried out with other NPs (Sondi et al., 2004).

3.3.2.2. Bacterial growth kinetics in the presence of CuNi BNPs

Bacterial growth kinetics experiments were carried out to see how exposure time affects the antibacterial activity of CuNi BNP.

Experiments for longer incubation periods were performed in order to examine whether there is any change in the activity profiles of the NPs and to test the ability of the BNPs to keep bacterial growth suppressed for a longer time. Figures 3.10 to 3.12 are showing the inhibitory effects on *E. coli*, *A. hydrophila* and *V. alginolyticus* after exposure to NP up to 3 hr at different NPs concentrations (10, 20, 30, 40, and 50 µg/ml). The progressive decline in the number of grown colonies in each petri plate after the incubation period, confirms the antimicrobial activity of the nanoparticle. It is evident from the figure that the concentrations tested (10–50 µg/ml) caused complete inhibition of bacterial growth within 135 min for all types of bacteria. Whereas, the control plate loaded with sterile saline water did not show any growth inhibition.

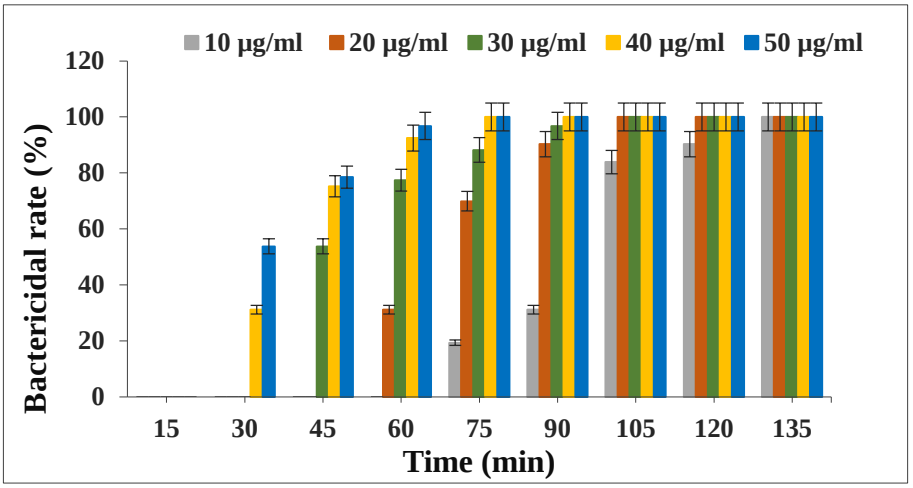

Figure 3.10: Effect of contact time on bactericidal rate of *E. coli* at different NP concentrations (initial bacterial concentrations, 10^6 CFU/mL; 200 rpm).

The bactericidal rate was measured after different exposition times between *E. coli* and the BNPs as shown in Figure 3.10. At 10 µg/ml, the inhibition of *E. coli* was not detectable up to 60 min of exposure, but continued to increase from 75 min onwards and the complete hindering of the *E. coli* growth at this NPs concentration was attained within 135 min (Figure 3.7). No bacterial growth was observed after the contact with 20 and 30 µg/ml of BNPs for 105 min. A significant decrease on the cellular viability of *E. coli* was observed at concentrations of 40 and 50 µg/ml and 100% of *E. coli* cells were inactivated after 75 min of contact with the NPs.

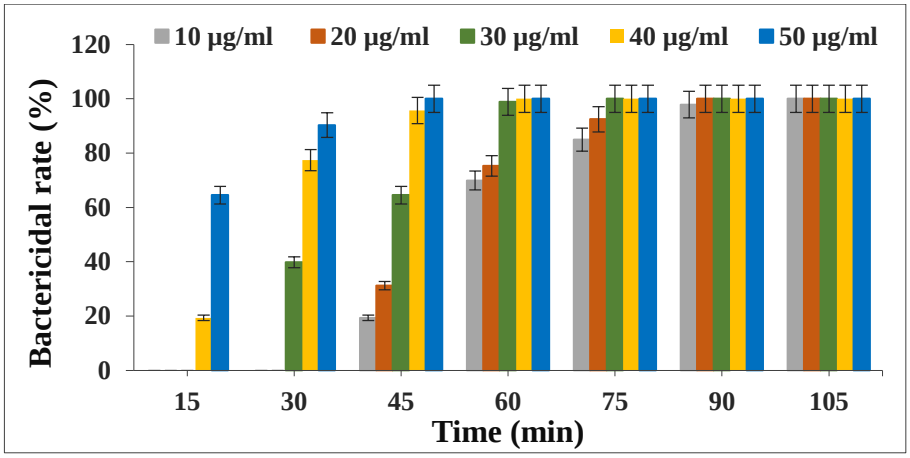

Figure 3.11: Effect of contact time on bactericidal rate of *A. hydrophila* at different NP concentrations (initial bacterial concentrations, 10^6 CFU/mL; 200 rpm).

In the same way, the viability of *A. hydrophila* cells was evaluated after different times of exposure to CuNi BNPs and the results are shown in Figure 3.11. At 40 µg/ml, the percent inhibition of *A. hydrophila* increases from exposure time of 15 to 45 min, and it

reaches 100% at 60 min of contact time. In the case of 10 and 20 µg/ml, a significant suppression in the growth of *A. hydrophila* was observed only after 45 min of contact with BNPs. While at 50 µg/ml concentration, these nanoparticles were able to inhibit 100% of bacterial growth on petri plates by 45 min of contact time.

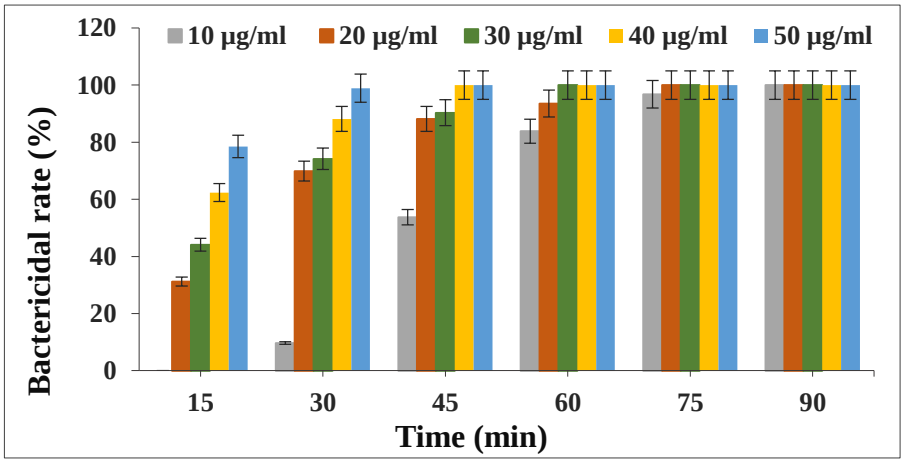

Figure 3.12: Effect of contact time on bactericidal rate of *V. alginolyticus* at different NP concentrations (initial bacterial concentrations, 10^6 CFU/mL; 200 rpm).

The antibacterial activity of CuNi BNPs towards the *V. alginolyticus* was superior compared to *E. coli* for all NPs concentrations tested (figure 3.12). In the case of 10 µg/ml, the bactericidal rate was increased from 0 to 96% with increasing contact time from 15 to 75 min, respectively, and the complete inhibition of bacterial growth was occurred within 90 min. The concentrations of 20 and 30 µg/ml were able to eliminate 100% of bacterial growth after 75 min and 1 hr of contact, respectively. The 100% bacterial growth

inhibition for both 40 and 50 µg/ml of NPs were achieved at 45 min of exposure time.

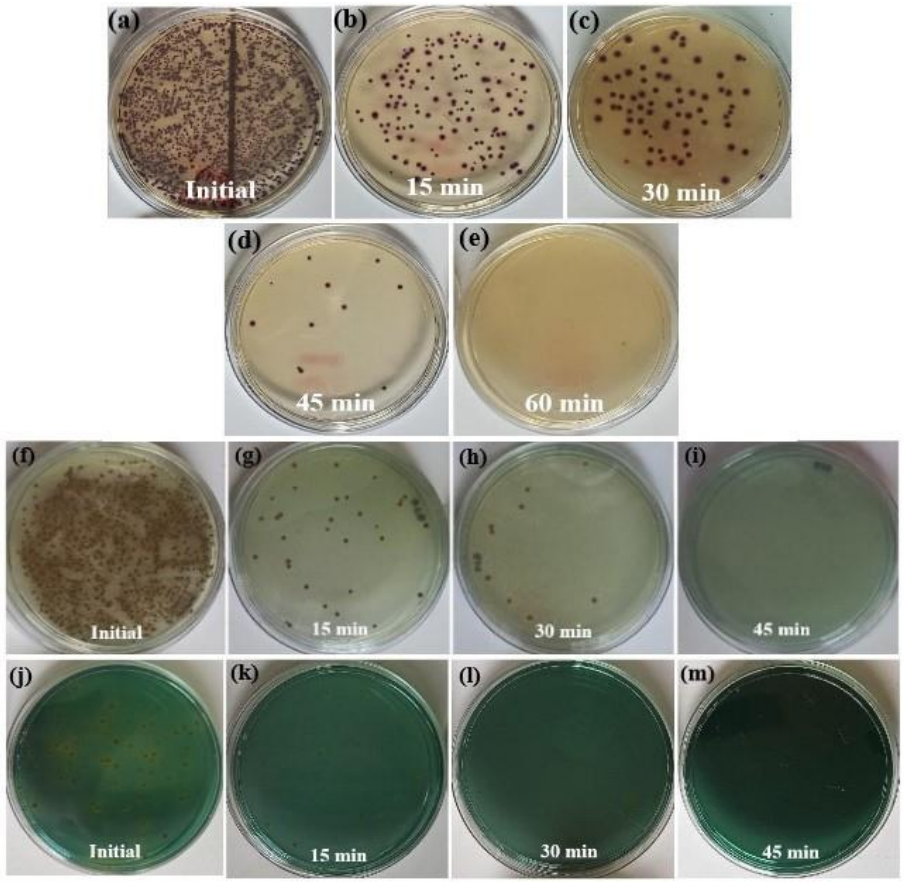

Figure 3.13: Agar plate photographs of bacterial colonies formed by (a-e) *E. coli*, (f-i) *A. hydrophila* and (j-m) *V. alginolyticus* cells in the presence of CuNi BNPs at different contact times (amount of CuNi BNP, 50 µg/ml; initial bacterial concentrations, 10^6 CFU/mL; 200 rpm).

It is evident from the bacterial growth profiles that all samples suppressed bacterial growth, with the effect being more and more significant as CuNi BNPs concentration in the bacterial solution and

the contact time increases. For the optimum antibacterial activity, a contact time of 60 minutes was fixed for further investigation.

3.3.2.3. Bactericidal activity of CuNi BNPs

To elucidate the effect of initial bacterial concentration, bacterial solutions with variable number of initial CFU/mL were used as per Table 3.1. The number of surviving bacteria in agar plates was counted and the results are shown in the bar chart graph (figure 3.14). CuNi BNPs at lower bacterial concentrations achieved almost 100% inhibition of bacterial growth but it exhibited a relatively weak antibacterial effect against all bacteria at higher bacterial concentrations.

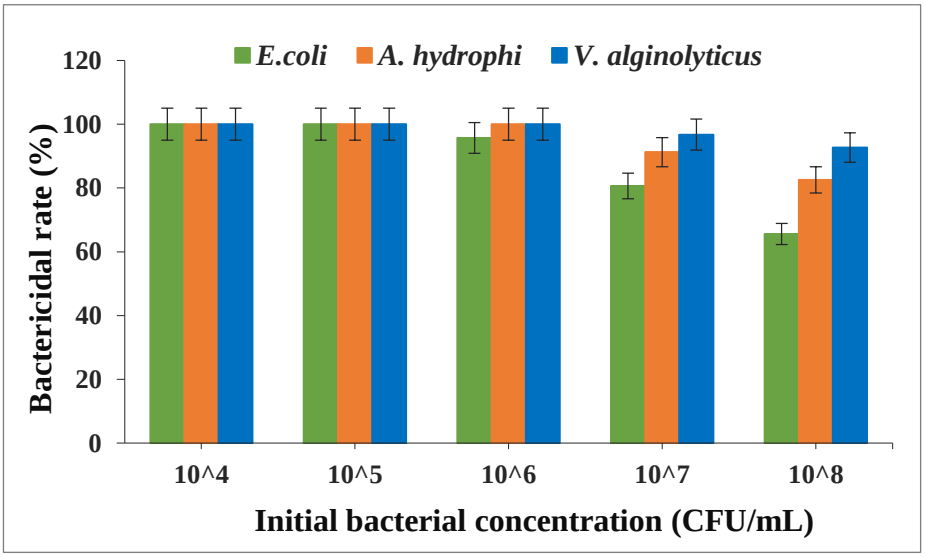

Figure 3.14: Effect of initial bacterial concentration on bactericidal rate of CuNi BNPs (amount of NP, 50 µg/ml; contact time, 60 min; 200 rpm).

Results demonstrated that, *A. hydrophila* and *V. alginolyticus* were nearly completely eliminated from the contaminated saline solution within 60 min for all initial concentrations. The synthesised CuNi bimetallic NPs have a high potential to eliminate these bacteria from their solutions of 10^4 to 10^8 CFU/mL with a bactericidal rate of more than 80%. However, the bactericidal rate of *E. coli* was apparently affected by the change in initial *E. coli* concentration. The bactericidal rate of *E. coli* was found to be maximum at the initial concentration of 10^4 to 10^5 CFU/mL. When 10^7 CFU/mL *E. coli* solution was used, 80% of *E. coli* growth was inhibited within 60 min; whereas, only 65% of *E. coli* growth was inhibited from 10^8 CFU/mL in 60 min. In the case of *A. hydrophila* the maximum bactericidal rate for 10^7 and 10^8 CFU/mL initial concentrations were 91% and 82%, respectively. With increasing the initial *V. alginolyticus* concentration from 10^6 to 10^7 CFU/mL and 10^7 to 10^8 CFU/mL, the bactericidal rate was decreased from 100% to 96% and 96% to 92% respectively.

3.3.2.4. Antibacterial activity of Cu NPs, Ni NPs and CuNi BNPs

Then we analysed the antibacterial activity of individual Cu and Ni NPs under similar experimental conditions as previously described. The obtained results were then compared with the antibacterial activity of CuNi BNPs (Figure 3.15). From the graph it is clear that the CuNi BNPs exhibited higher antibacterial activity than individual Cu and Ni NPs at similar experimental conditions. The complete elimination of bacteria was not occurred even after 60 min of exposure with the Cu NPs and Ni NPs. Whereas, in the case of CuNi

BNP 100% bactericidal rate was achieved within 60 min for *A. hydrophila* and *V. alginolyticus*, and in the case of *E. coli*, the maximum bactericidal rate was found to be 97%.

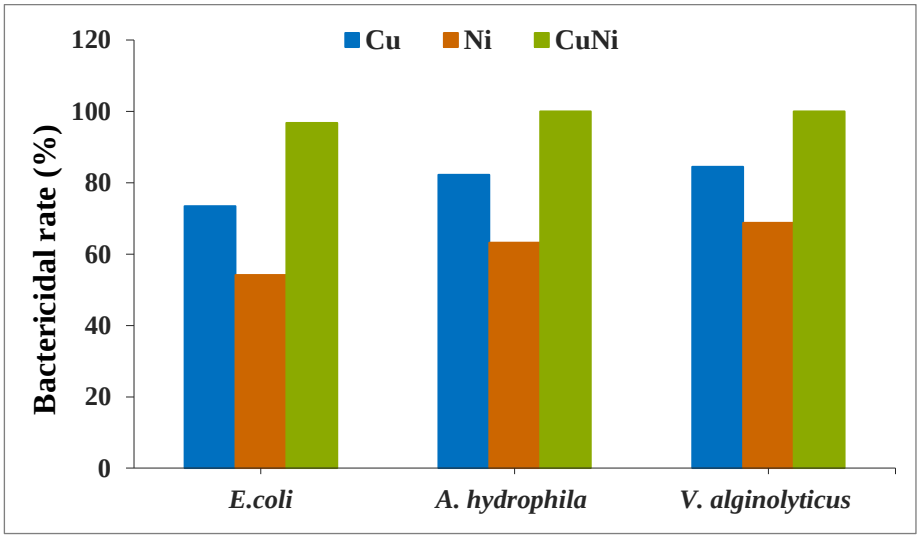

Figure 3.15: Antibacterial activity of Cu NPs, Ni NPs and CuNi BNPs (Amount of NP, 50 µg/ml; contact time, 60 min; initial bacterial concentrations, 10^6 CFU/mL; 200 rpm).

3.3.2.5. Mechanism

The antibacterial mechanism is primarily attributed to the adsorption of NPs on the bacterial membrane, and which leads to the leakage of intracellular material cause bacterial cell death due to the permeabilization of the cell surface. Cu and Ni NPs have excellent antimicrobial and bactericidal activity. Copper nanoparticles (CuNPs), on the other hand, have been widely used as effective antibacterial agents. Various hypotheses have been proposed to describe the mechanism of antimicrobial activity of Cu NPs. Cu NPs affect the

bacterial cell functions in numerous ways, including adhesion to Gram-negative bacterial cell wall through electrostatic interaction (Grass et al., 2011), denaturation of intracellular proteins by binding to the sulfhydryl amino and carboxyl groups of amino acids (Santo et al., 2008), affecting the protein structure in the cell membrane, generation of Reactive Oxygen Species (ROS) in bacteria (Kornblatt et al., 2016), and production of hydroxyl radicals, which bind with DNA molecules and lead to distortion of the helical structure and eventually causes cell death (Mahmoodi et al., 2018). While only a few studies have reported the antibacterial properties of Ni nanoparticles. The mode of action of Ni NPs is influenced by many factors and they were also responsible for the antibacterial activity of the NPs. Though, the mechanism by which the Ni nanoparticles penetrates into bacteria is not understood completely, but it was observed that, when the bacteria was treated with Nickel NPs, changes took place in its membrane morphology and produced a significant increase in its permeability. Which in turn increases the penetrating power of Ni NPs and leaving the bacterial cells incapable of properly regulating transport through the plasma membrane (Kumar et al., 2010). Moreover, inactivation of bacterial DNA by interacting with the phosphorous and sulphur containing moieties and which ultimately leads to the death of the bacteria (Morones et al., 2005). Another reason would be that, Ni NPs after penetration into bacteria inactive their enzymes, generate hydrogen peroxide and cause bacterial cell death.

The resulting antibacterial effect of CuNi BNP can be explained through the combined effect of Cu and Ni NP. According to existing research, the major steps in the mechanism of the bactericidal activity of heavy metal-based NPs are divided into four steps. The first is the disruption of the bacterial cell membrane. The second step is the generation of ROS. The third step consists of the disruption of the electron transport chain. Finally, the induction of intracellular antibacterial effects, including interactions with DNA and proteins (Figure 3.16).

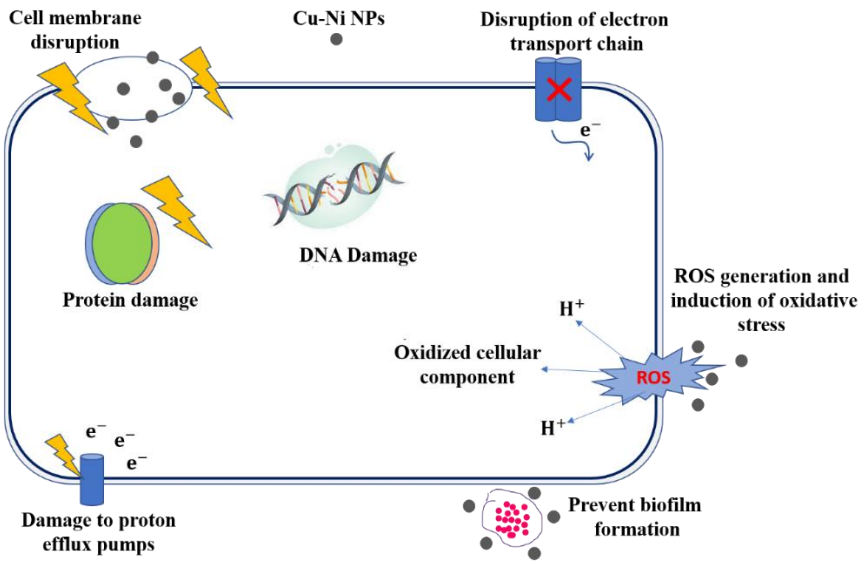

Figure 3.16: Major steps in the mechanism of the bactericidal activity of Cu-Ni BNPs.

Even though they have multiple antibacterial mechanisms, the main mechanism by which these particles showed antibacterial activity might be via strong adsorption of Cu-Ni BNPs to the pores of bacterial cell membranes by interacting with the bacterial membrane, thus

resulting in subsequent release of lipopolysaccharides, membrane proteins and intracellular biomolecules and it also interrupt the biochemical processes of the bacterial cells, which ultimately leads to the cell death. This results in antibacterial efficacy in a concentration-dependent manner. The significantly superior antibacterial activity of the CuNi BNP is attributed to the synergistic treatment of Cu and Ni NPs towards the bacteria (Argueta-Figueroa et al., 2014) as well as the surface area of CuNi BNPs, which is larger than the Cu and Ni NPs. The ultrasmall size and increased surface area are the major contributing factors in the antibacterial effect of NPs, through which they damage the cell membrane, cross the body of the microbe, and cause intracellular damage. The enhancing effect of bimetallic species has also been reported in other antibacterial systems (Jena et al., 2020; Perdikaki et al., 2016) and some investigations have already been shown that, the properties of the bimetallic nanomaterials are better with respect to those of the pure metals (Kumar et al., 2019).

3.4. Conclusion

In conclusion, successful preparation of the CuNi bimetallic nanoparticles were demonstrated by co-reduction of copper and nickel salts in the presence of a strong reducing agent, sodium borohydride, under ambient conditions. The prepared CuNi bimetallic nanoparticles were characterised by Scanning Electron microscopy (SEM), Transmission Electron Microscopy (TEM), Energy Dispersive X-ray Spectroscopy (EDS), powder X-ray diffraction (PXRD) and surface area studies. The SEM images showed that the appearance of the

particles is spherical in shape and also it was homogeneous in size. From the BET experimental results, the specific surface area was found to be 31.28 m^2/g and it is higher than the surface area of individual Cu and Ni nanoparticles.

The antibacterial activity of the CuNi BNP was systematically evaluated against three different strains of bacteria, namely *Escherichia coli* (*E.coli*), *Aeromonas hydrophila* (*A.hydrophila*) and *Vibrio alginolyticus (V. alginolyticus)* by using the spread plate counting method. The results demonstrates that CuNi BNP is strongly antibacterial against all the three tested bacteria. It is evident from the bacterial growth kinetics that all samples achieved complete bacterial growth inhibition within 135 min for all types of bacteria, with the effect being more and more significant as the concentration of the CuNi BNPs increases. 100% of *A. hydrophila* and *V. alginolyticus* cells were inactivated after the contact with 40 µg/ml and 30 µg/ml of CuNi BNP respectively, for 60 min. The maximum bactericidal rate of CuNi BNPs to *E. coli* was attained at 75 min of contact time with 50 µg/ml of NPs. This striking performance is attributed to the synergistic effect of Cu and Ni NP that coexist on the surface. From the data, it is also evidenced that, the parameters like length of treatment, amount of CuNi BNPs, and initial bacterial concentration have significant effect on the bactericidal activity of CuNi BNPs and also it varies slightly with the type of bacteria. The relatively higher antimicrobial activity against *A. hydrophila* and *V. alginolyticus* compared with *E. coli* can be attributed to the different cell wall composition of bacteria. The

antibacterial activity of individual Cu and Ni NPs was then analysed and compared with that of the CuNi BNPs, and it was observed that the BNPs exhibited more antibacterial activity than the individual Cu and Ni NPs. A direct comparison between the studies is difficult due to variation in the strains employed and variation in the initial bacterial concentration.

This preliminary result demonstrates the potential application of CuNi BNPs as an effective antibacterial agent against *E. coli, A. hydrophila* and *V. alginolyticus*. The results presented herein open the route to the next generation of antimicrobial agents and it would have a bright future in practical application.

Chapter 4

Application of CuNi bimetallic nanoparticles as an adsorbent for the removal of heavy metals from aqueous solution

4.1 Introduction

The rapid growth of industrialization results in the release of wastewater polluted with toxic metals into the environment. The treatment of heavy metals is of special concern due to their highly toxic nature, even at very low concentrations and non-biodegradable properties. These toxic pollutants can be accumulated in living organisms and pose a stern risk to the environment and living organisms (Schwarzenbach et al., 2010). Thus, the treatment of industrial effluents containing toxic metals, before they are discharged, is becoming a crucial issue (Wang and Chen, 2009).

Currently, bimetallic NPs (BNPs), composed of two different metal elements, have drawn great interest in drinking water treatment among various types of NPs. BNPs have a greater surface area as compared to those of monometallic NPs (Toshima and Yonezawa, 1998; Sharma et al., 2015; Sharma et al., 2019), which increases their adsorption power and also the interaction among the two metals plays a vital role in the unique properties of BNPs. Unfortunately, to the best of our knowledge, most of these studies are limited within iron based BNPs.

Both Cu and Ni NPs can act as good adsorbent due to their unique chemical and magnetic properties (Ojha et al., 2017; Mahmoud et al., 2017; Chatterjee et al., 2012). Several literatures are available which have focused on the adsorption behaviour of Cu and Ni NPs separately. The synergic effect of these two NPs in the CuNi BNPs would increase its potential for removing the heavy metals and reducing the bacterial content from water. As far as our knowledge and our literature survey indicates that, the removal of heavy metals from solutions and the mechanisms of metals absorption using CuNi BNPs have not been so far reported. Moreover, in the case of nanoparticles, factors like ease of preparation, kinetics of reaction, pH, effective separation from treated water, etc. can affect the effective pollutant removal. The CuNi BNPs can be prepared very quickly in the lab or *in situ* and also it is quite stable in different pHs. Therefore, the present work is a novel one to investigate the effect of CuNi BNPs on the adsorption of metal contaminated water.

The aim of this work is to quantify and predict the adsorption behaviour of CuNi BNPs towards Pb^{2+}, Cd^{2+}, Zn^{2+}, and Mn^{2+} under different conditions (pH, contact time, adsorbent dosage and concentration of metals). To evaluate the adsorption capacity of the BNP and to investigate the adsorption equilibrium and kinetics of the heavy metal ions from aqueous solutions for examine the adsorption mechanism.

4.2. Experimental

4.2.1. Materials

All chemicals used were of analytical reagent grade and purchased from Merck. Heavy metal analysis was conducted using a Thermofisher M series atomic absorption spectrophotometer (AAS) with air/acetylene flame and deuterium background correction was applied in all measurements. Distilled water, prepared by a water purifier (Synergy-Merck, India) was used throughout the experiment for all solution preparation. Stock solutions of heavy metals were purchased from Merck. Contaminated aqueous solutions were artificially prepared by diluting the metal stock solution with deionized water to bring the desired concentration.

4.2.2. Batch Adsorption study

Batch adsorption experiments were performed to investigate the adsorption behaviour of heavy metals (Pb^{2+}, Cd^{2+}, Zn^{2+} and Mn^{2+}) under different conditions (contact time, pH, adsorbent dosage and initial metal concentration). The experiments were conducted in 500 mL stoppered bottles which contained 250 mL metal solution of desired concentration. The stoppered bottles were shaken in an electric shaker with continuous stirring at 200 rpm at room temperature (25 ± 0.5°C). After the reaction time, the solution was filtered by using 0.2 µm syringe filters and analysed by AAS. All experiments were conducted in triplicate. Experimental conditions as per Table 4.1 were varied to quantitatively evaluate their effects on metal adsorption.

The percentage of metal removal/ the quantity of adsorbed heavy metal ions was calculated using the equation:

$$\%\text{Adsorption (Removal)} = \frac{C_0 - C_e}{C_0} \times 100$$

Where C_0 is the initial heavy metal concentration (mg/L) and C_e is the heavy metal concentration at final equilibrium (mg/L).

Table 4.1

Experimental conditions for batch adsorption study.

Metals	Contact time (min)	Adsorption dose (g/L)	Initial metal concentration (mg/L)	pH
Pb	10-120	0.5	1, 5, 10	7
	100	0.1-0.5	1	7
	100	0.5	1-10	7
	100	0.5	1	3-11
Cd	10-120	0.5	1, 5, 10	7
	100	0.1-0.5	1	7
	100	0.5	1-10	7
	100	0.5	1	3-11
Mn	10-120	0.5	1, 5, 10	7
	100	0.1-0.5	1	7
	100	0.5	1-10	7
	100	0.5	1	3-11
Zn	10-120	0.5	1, 5, 10	7
	100	0.1-0.5	1	7
	100	0.5	1-10	7
	100	0.5	1	3-11

4.2.2.1. Effect of contact time on adsorption

In order to investigate the effect of contact time, 0.5 g of synthesised NPs was added into heavy metal solutions of three different initial concentrations (1, 5, and 10 ppm) and were kept in the

shaker for 2 hours. An aliquot of metal solution was withdrawn at every 5 minutes time interval and analysed.

4.2.2.2. Effect of pH on adsorption

The effect of solution pH on the heavy metal removal was examined by varying the initial pH of the solution from pH 3 to 11using 1M HCl and 0.1M NaOH. All other parameters such as initial concentration of heavy metals, adsorbent dosage, and contact time were kept constant.

4.2.2.3. Effect of adsorbent dosage

The effect of adsorbent dosage on heavy metal adsorption was evaluated by using different amounts of NPs (0.1, 0.2, 0.3, 0.4, and 0.5 g) and by and keeping other parameters constant.

4.2.2.4. Effect of initial metal concentration

To elucidate the effect of initial metal concentration, different concentrations of heavy metal solutions (ranging from 1ppm to 10ppm) were used. All prepared solutions were treated for 100 minutes at room temperature.

4.2.3. Adsorption isotherms

Isotherm adsorption experiments were conducted to understand the mechanism of adsorption, to describe the affinity of adsorbate–adsorbent, to find the maximum adsorption capacity of CuNi BNPs towards different heavy metals. It is also useful to understand the

distribution of metal ions between the liquid phase and the solid phase and offer a theoretic maximum adsorption capacity, which have great significance for the optional design of adsorption device and the analysis of adsorption mechanism. The adsorption isotherm indicates the distribution of adsorbate between the adsorbed phase and the solution phase when the adsorption process is at equilibrium. All the isotherm adsorption experiments were conducted under optimal conditions. In order to study the adsorption isotherms, 0.5 g of adsorbent was added to a series of 250 mL heavy metal solutions, with concentrations ranging from 1ppm to 10ppm and was kept in the shaker for 100 min. Langmuir and Freundlich isotherms were employed to analyse the adsorption equilibrium.

4.2.3.1. Langmuir adsorption isotherm

Langmuir isotherm (Langmuir, 1918) assumes that the adsorption takes place at specific homogeneous sites by monolayer adsorption without any interaction between adsorbed molecules. The linearized form of the equation is as follows:

$$\frac{C_e}{q_e} = \frac{1}{K_L q_{max}} + \frac{C_e}{q_{max}}$$

where C_e is the equilibrium concentration of heavy metal in the solution (mg/L), q_e is the amount of metals adsorbed at equilibrium (mg/g), q_{max} is the maximum adsorption capacity of the adsorbent corresponding to complete monolayer coverage on the surface (mg/g), and K_L is the Langmuir adsorption constant (L/mg) and is related to

the free energy of adsorption. The constants q_{max} and K_L can be calculated from the intercept and the slope of the linear plot of C_e/q_e versus C_e.

4.2.3.2. Freundlich adsorption isotherm

The Freundlich isotherm describes the adsorption equation for both multilayer adsorptions and sorption on heterogeneous surface (Freundlich, 1906). It is applicable for describing non-ideal and reversible adsorption. The linear form of Freundlich isotherm equation can be expressed as:

$$ln\, q_e = ln\, K_F + {}^{1}/_{n}\, lnC_e$$

where K_F and 1/n are Freundlich constants representing the adsorption capacity and adsorption intensity of the system, respectively. The values of K_F and 1/n are obtained from the linear plot of lnq_e versus lnC_e.

4.2.4. Adsorption kinetics

Kinetic study is important for understanding the mechanism of metal adsorption processes and it can also interpret the rate at which a pollutant was removed from aqueous solutions. To determine the adsorption rate and the maximum efficiency of CuNi BNPs on adsorption, adsorption kinetics was investigated. The initial concentrations of heavy metals were fixed at 1, 5, and 10 mg/L. 0.5g of synthesised nanoparticle was added into 250 mL of metal solutions and was shaken in a mechanical shaker at 200 rpm for 2 h at 25°C.

Sampling was performed by removing aliquots at every five minutes. Pseudo-first -order and pseudo-second -order kinetics models were tested to define the adsorption kinetics. The adsorbed heavy metal amount at equilibrium (q_e) per unit absorbent mass was calculated from the following equation:

$$q_e = \frac{C_o - C_e}{W} \times V$$

where Co and Ce are the initial and equilibrium concentrations of heavy metal ions (mg/L), respectively, W is the adsorbent dosage (g) and V is the volume of the solution (L) used.

4.2.4.1. Pseudo-first-order kinetic model

The pseudo-first-order rate equation of Lagergren (Li et al., 2015) is represented as:

$$ln\,(q_e - q_t) = ln\,q_e - k_1 t$$

where q_e and q_t are the amounts of heavy metal ions adsorbed on the sorbents in mg/g, at equilibrium and at time t (min), respectively, and k_1 (min^{-1}) is the pseudo-first-order rate constant. Value of k_1 was calculated from the plot of ln ($q_e - q_t$) versus t.

4.2.4.2. Pseudo-second-order kinetic model

The rate equation for Ho's pseudo-second-order model (Ho, 2006) can be represented in the linear expression as:

$$\frac{t}{q_t} = \frac{1}{k_2 {q_e}^2} + \frac{t}{q_e}$$

where k_2 (g/(mg min)) is the pseudo-second-order rate constant and its value can be obtained from the plot of t/q_t versus t.

4.2.5. Method validation

Method validation was performed by assessing Limit of Detection (LOD) and Limit of Quantification (LOQ), defined as the lowest concentration of analyte that generates a signal significantly different from zero, but not necessarily quantified and the lowest analyte concentration that can be calculated quantitatively under the described experimental conditions with an acceptable level of precision and accuracy, respectively (Gonzales and Herrador, 2007). The LOD and LOQ were determined by analysing 10 blank samples and were calculated using the following equations

$$LOD = 3.3\ SD/b$$

$$LOQ = 10\ SD/b$$

where SD is the mean standard deviation of blanks and b is the slope of the calibration curve. The obtained values were described in Table 4.2.

Table 4.2

LOD and LOQ of the flame atomic absorption spectroscopy method.

Metal	**LOD (mg/L)**	**LOQ (mg/L)**

Pb	0.013	0.073
Cd	0.0028	0.013
Zn	0.016	0.19
Mn	0.0016	0.020

4.3. Results and Discussion

4.3.1. Effect of contact time on adsorption

The effect of contact time was examined to determine the kinetics of the adsorption process and to find the appropriate time for the saturation of NPs at which the adsorption is at equilibrium. For that, the variation of the adsorption capacity of CuNi BNPs towards different metal ion solutions (Pb^{2+}, Cd^{2+}, Zn^{2+}, and Mn^{2+}) with concentrations 1, 5 and 10 mg/L was investigated as a function of contact time. The effect of contact time on the uptake of lead ions on CuNi BNPs was depicted in Figure 4.1. The removal rate increases quickly within the first 60 min and which then increases slightly and reaches its maximum within 100 min. The graph reveals that, the complete removal of 1 mg/L lead solution was attained at 60 min. The maximum percent removal (%) of Pb^{2+} in the case of 5 and 10 mg/L initial concentration was 98.34% and 91.42%, respectively. As shown in Figure, with increasing the initial lead concentration from 1 to 5 mg/L and 5 to 10 mg/L, the removal efficiency was decreased from 100% to 98.34% and 98.34% to 91.42% respectively.

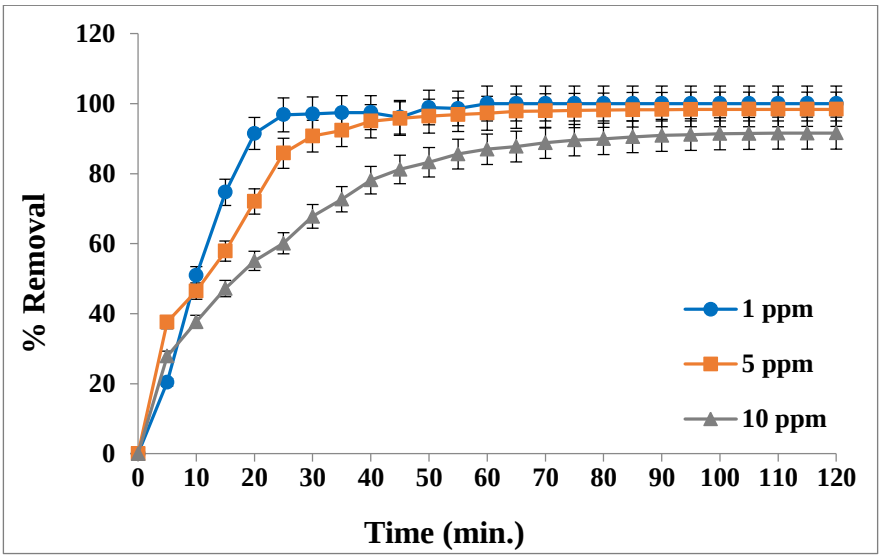

Figure 4.1: Effect of contact time on percentage removal of lead ions (adsorbent dosage, 0.5 g/250 mL; pH, 7;200 rpm).

The effect of contact time on the uptake of Cd ions is shown in Figure 4.2. It is evident from this figure that the percentage removal decreases with the increase in initial Cd concentration. When 1 mg/L cadmium solution was used, 96% of Cd was removed within 120 min; however, 83% of Cd was removed from 5 mg/L cadmium solution within 100 min and only 65 % of Cd was removed from 10 mg/L in 100 min.

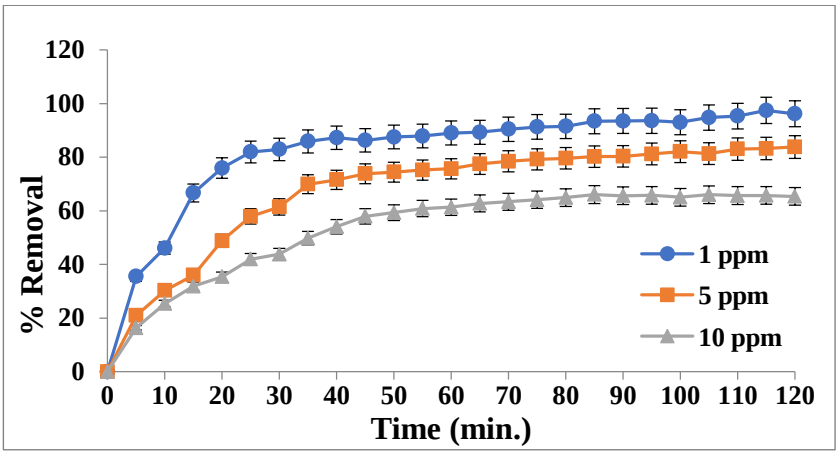

Figure 4.2: Effect of contact time on percentage removal of cadmium ions (adsorbent dosage, 0.5 g/250 mL; pH, 7;200 rpm).

Figure 4.3 shows the effect of contact time on the uptake of Zn ions. The maximum percent removal (%) of Zn for 1, 5, and10 mg/L initial concentration was 100%, 98.22% and 96.16% respectively.

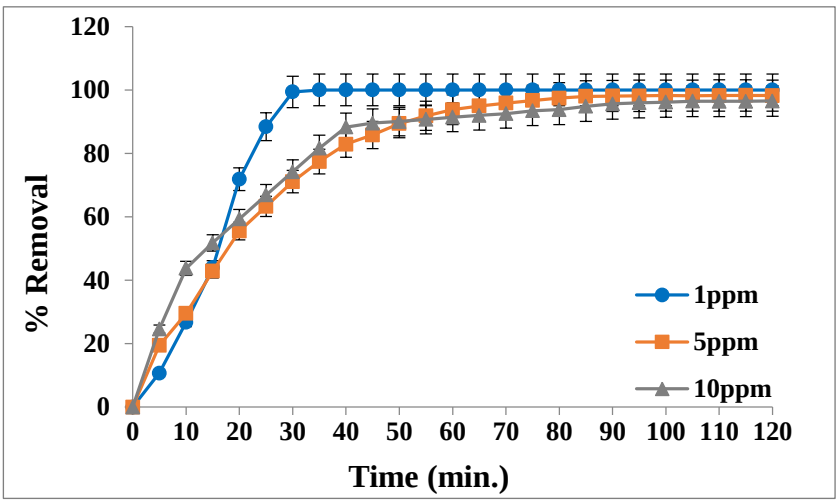

Figure 4.3: Effect of contact time on percentage removal of Zinc ions (adsorbent dosage, 0.5 g/250 mL; pH, 7;200 rpm).

With increasing the initial manganese concentration from 1 to 5 mg/L and 5 to 10 mg/L, the removal efficiency was decreased from 100% to 99% and 99% to 97%, respectively (Figure 4.4). The adsorbent was able to adsorb 100 % of the manganese ions from 1, 5, and 10 mg/L manganese solution, respectively within 45, 105 and 115 min.

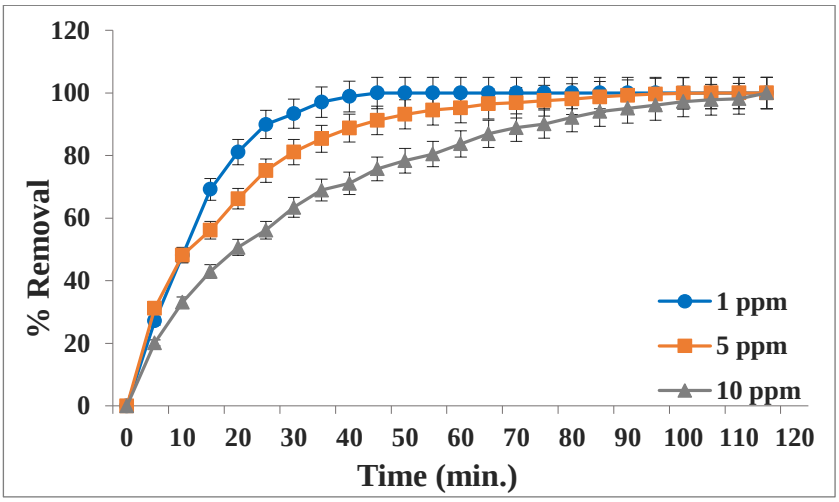

Figure 4.4: Effect of contact time on percentage removal of manganese ions (adsorbent dosage, 0.5 g/250 mL; pH, 7;200 rpm).

The difference in concentration of adsorbate between adsorbent and solution is the main diffusion force of adsorbate. It was observed that heavy metal removal was rapid initially and the percent removal (%) reached its plateau within 100 minutes for all metals. This may be due to the abundant availability of vacant sites on the adsorbent during the initial stages, large adsorption energy of BNP and also large external diffusion rate of metal ions (Doulia et al., 2009). The reason for the followed slow adsorption was attributed to adsorption transfer

from extra diffusion to internal one (Shi et al., 2009), and the gradual occupancy of the vacant sites leads to the saturation of nanoparticles and which in turn decreases the removal efficiency. With further increase in the adsorption time, the removal rate of metal cations did not change significantly, indicating that the adsorption was in dynamic equilibrium. For the optimum removal of heavy metals, a contact time of 100 minutes was fixed as the equilibrium time for further investigation.

Significant variations in adsorption were observed for different heavy metals. Therefore, the difference in the removal percentage of different heavy metal ions at constant initial metal concentrations, adsorbent dose and contact time may be attributed to the type of metals, charge, ion availability, ionic radius, the effective hydrated ion radius, electrovalence of heavy metal cations, the difference in their chemical affinity, changes in the number and type of adsorption sites, ion exchange capacity of adsorbent, etc. (Giammar et al., 2009; Inglezakis et al., 2003; Vidal et al., 2009; Zhou et al., 2017). The removal percentages of heavy metals under test were in the following order

$$Mn^{2+} > Zn^{2+} > Pb^{2+} > Cd^{2+}$$

The effective radius of hydrated ions is a main factor in determining adsorption efficiency. The effective hydrated ionic radius of four heavy metals is in the order as follows: $Pb^{2+} > Cd^{2+} > Mn^{2+} \sim Zn^{2+}$ (Table 4.3) (Marcus, 1988). More is the effective hydrated ion

radius of metal cations; its hydrated ions are more difficult to adsorb on the adsorbent surface. Because the ion with the higher effective hydrated radius exerts weaker forces of attraction and has more difficulty to reach adsorption sites (Tang et al., 2017; Bohli et al., 2017). And also, the cations with small ionic radius are expected to diffuse more rapidly into the adsorption sites while cations with large ionic radius can cause a quick saturation of the adsorbent due to steric effects resulting in a lower adsorption on the adsorbent surface (Gao et al. 2009). Moreover, the charge-to-radius ratio of the cations is also important factor in determining which metal adsorb with the highest performance. According to the charge-to-radius ratio, the order of adsorption should have been Zn^{2+}> Mn^{2+}> Cd^{2+}> Pb^{2+} (Es-Said et al., 2020). But, in the case of Cd^{2+} and Pb^{2+}, the hydration energy of Cd^{2+} (1826.7 kJ/mol) is higher than that of Pb^{2+} (1500.6 kJ/mol) (Zhou et al., 2017). The ions with higher hydrated energy are difficult to dehydrate and the adsorption efficiency of Cd ions decreases. But, Pb^{2+} can easily lose water ligands and become the bare Pb cation when it enters into the interlayer of NPs and thus get easily adsorbed inside the NP. The hydrolysis constant (pKa) values play a key role in predicting how various metals will behave when they are adsorbed. According to certain reports, lower pKa values reduce metal ion solvation and allow them to reach the sorbent surface more easily (Alloway et al., 1995; Reddad et al., 2002). Thus, the higher adsorption selectivity for Pb^{2+} (pKa: 7.7) than Cd^{2+} (pKa:10.1) can be most significantly predicted on the basis of their corresponding pKa values. Furthermore, the

electronegativity of Cd is 1.69, less than 2.33 of Pb, which was also one of the reasons for the lower adsorption of Cd (Tang et al., 2017).

Table 4.3

Ion radius, effective hydrated radius and charge-to-radius ratio of Pb^{2+}, Cd^{2+}, Mn^{2+}, and Zn^{2+}.

Metal ions	**Pb^{2+}**	**Cd^{2+}**	**Mn^{2+}**	**Zn^{2+}**
Radius /nm	0.132	0.097	0.080	0.074
Effective Hydrated radius /nm	0.2655	0.2305	0.2192	0.2165
Charge to radius ratio	1.51	2.11	2.50	2.70

4.3.2. Effect of pH

The effect of pH on the adsorption of heavy metals by CuNi BNPs was evaluated within the pH range of 3-9. Figure 4.5 shows that, with increasing the pH solution from 3 to 7, the percent removal of all metals increased and then decreased with increasing pH from pH 7 to 9 for Pb^{2+}, Mn^{2+} and Zn^{2+}.The maximum removal of lead was found at pH 5-7 and in the case of Cd^{2+}, Mn^{2+} and Zn^{2+} maximum removal was occurred at pH 7. The metal ion uptake was limited in the acidic medium; this may be attributed to the presence of H^+ ions which compete with the metal ions for the adsorption sites. The competing effect of H^+ ions decreased as pH increased, which led to greater heavy metal ion adsorption onto the adsorbent at higher pH values (Kahrizi et al., 2016). However, a sudden increase in the percent removal curve of Cd^{2+}occurred when the pH is beyond 7, and this rapid increase may be due to the precipitation of Cd ions as $Cd(OH)_2$.

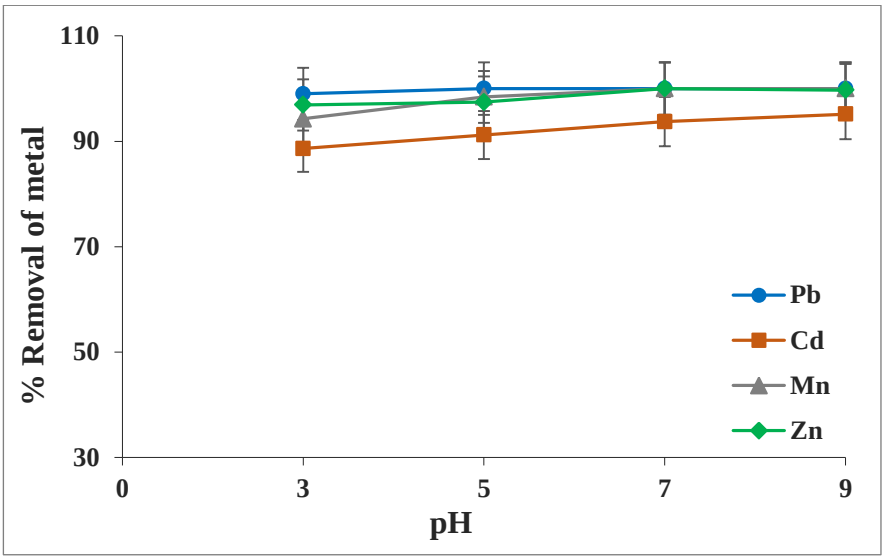

Figure 4.5: Effect of pH on percentage removal of metals (initial concentration, 1ppm; adsorbent dosage, 0.5 g/250 mL; contact time, 100 min; 200 rpm).

4.3.3. Effect of adsorbent dosage

In the experiment, different amounts of adsorbent (0.1, 0.2, 0.3, 0.4, and 0.5 g in 250 mL of solution) were used with an initial concentration of 1mg/L of metals at a contact time of 100 minutes. The effect of adsorbent dosage on the removal of Pb^{2+}, Cd^{2+}, Mn^{2+}, and $Zn^{2+}$is presented in Figure 4.6. when the initial dosage of CuNi BNP were 0.1 g, the removal rate of Mn^{2+} in wastewater was the highest, followed by $Zn^{2+}$and Pb^{2+}, and that of Cd^{2+} was the lowest. The results clearly indicate that the removal efficiency increases with increasing the amount of NPs, which might be attributed to the availability of extra active sites on the surface of the NPs. The optimum dosage of micro absorbent for the removal of Mn^{2+} and Zn^{2+} was 0.4 g, while for

Pb^{2+} and Cd^{2+} it was 0.5 g. With an increase in adsorbent from 0.1 to 0.3 g, the efficiency of cadmium adsorption increased from 68% to 84%, and with further increase in adsorbent dosage, the percent removal became almost fixed. However, when the amount of adsorbent increases from 0.1 to 0.2 g, the rate of increase in the percent removal is higher in comparison with the rate of removal when the amount of adsorbent is increased from 0.3 to 0.5g. This is indicating the saturation of adsorption sites.

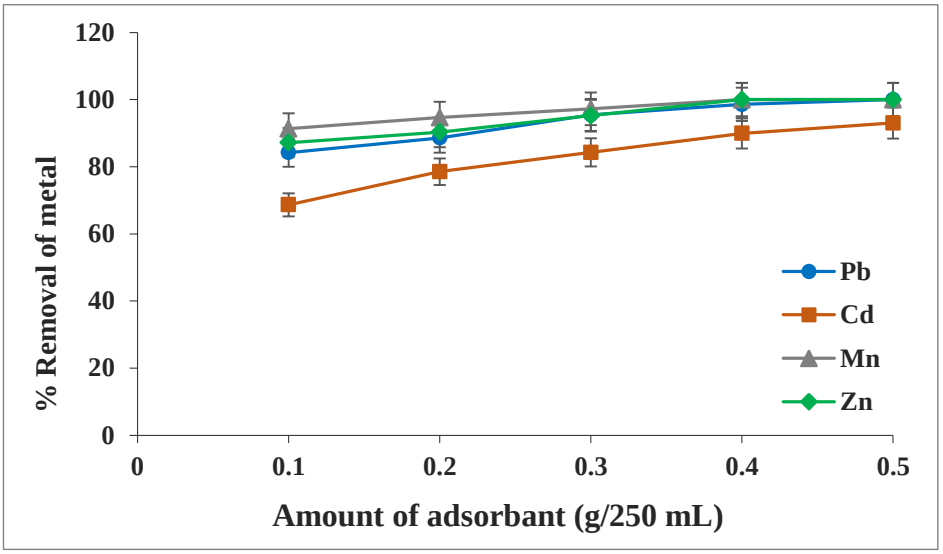

Figure 4.6: Effect of adsorbent dosage on percentage removal of metals (initial concentration, 1ppm; pH, 7; contact time, 100 min; 200 rpm).

4.3.4. Effect of initial metal concentration

A decreasing trend of removal were observed as initial Pb^{2+}, Cd^{2+}, Mn^{2+}, and Zn^{2+} concentration was increased as shown in Figure 4.7. The increase in initial metal concentration results in a relative

reduction of available binding sites on the adsorbent; consequently, it can lead to the reduction of adsorption efficiency in high concentrations.

Results demonstrated that, Pb^{2+}, Mn^{2+}, and Zn^{2+}were nearly completely removed from wastewater within 100 min for all initial concentrations. The synthesised CuNi BNPs have a high potential to remove Pb, Mn, and Zn ions from their solutions of 1 to 10 mg/L with a removal efficiency of more than 90%. However, the percent removal of $Cd^{2+}$was apparently affected by the change in initial Cd^{2+}concentration. The removal efficiency of Cd was found to be maximum at the initial concentration of 1 mg/L of Cd.

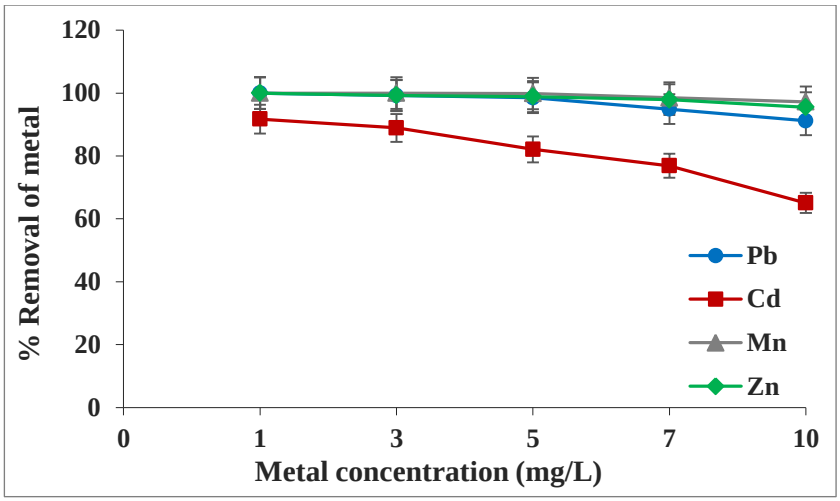

Figure 4.7: Effect of initial metal concentration on percentage removal of metals (adsorbent dosage, 0.5 g/250 mL; pH, 7; contact time, 100 min; 200 rpm).

4.3.5. Adsorption by Cu NPs, Ni NPs and CuNi BNPs

Evaluated the percentage removal of Pb^{2+}, Cd^{2+}, Mn^{2+}, and Zn^{2+} by Cu NPs and Ni NPs under similar experimental conditions as previously described. The obtained results were then compared with the results of adsorption of heavy metals by the CuNi BNPs. The obtained findings are depicted in Figure 4.8, and it is evident from the figure that CuNi BNPs have higher adsorption properties than individual Cu NPs and Ni NPs under similar experimental conditions. This may be due to the increased surface area of the bimetallic nanoparticles as compared to their monometallic counterparts and the synergic effect between the two metals. The maximum % removal obtained for Cu NPs for Pb^{2+}, Cd^{2+}, Mn^{2+}, and Zn^{2+} respectively, was 81%, 76%, 85%, and 82%, respectively. The obtained maximum % removal for Ni NPs was 60%, 59%, 65%, and 68%, respectively, for Pb^{2+}, Cd^{2+}, Mn^{2+} and Zn^{2+}. Whereas, in the case of CuNi BNPs it was nearly 100% for all the heavy metals.

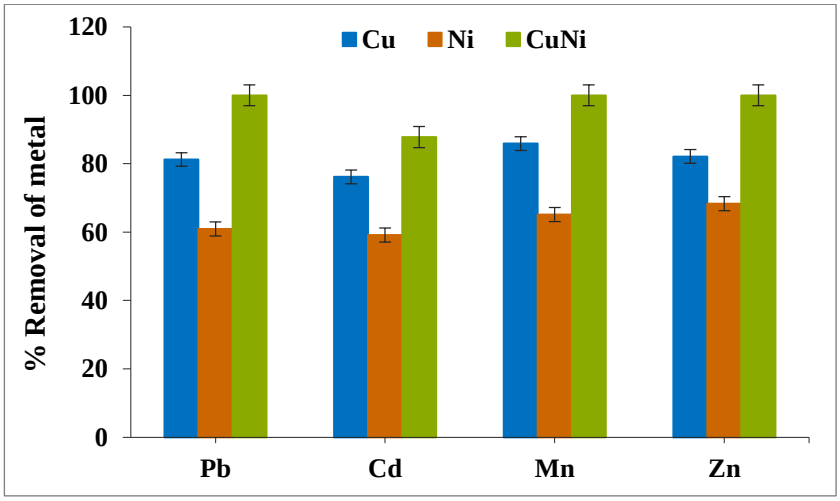

Figure 4.8: Percentage removal of heavy metals by Cu NPs, Ni NPs and CuNi BNPs (adsorbent dosage, 0.5 g/250 mL; initial concentration, 1ppm; pH, 7; contact time, 100 min; 200 rpm).

4.3.6. Adsorption isotherms

Adsorption occurring in a solid–liquid system is a dynamical equilibrium process. Adsorption isotherms are useful for estimating the theoretical maximum adsorption capacity of an adsorbent and can demonstrate the distribution of adsorbate between liquid and solid phases at adsorption equilibrium. The Langmuir and Freundlich isotherm models were used to describe the adsorption of heavy metals by CuNi BNPs and Figure 4.9 shows the equilibrium adsorption isotherm. The adsorption parameters calculated from the slopes and intercepts of isotherms (q_{max}, K_L, K_f, n, and the correlation coefficient values (R^2)) were summarized in Table 4.4. The maximum adsorption capacity q_{max} of CuNi BNPs for Pb, Cd, Mn, and Zn adsorption was 4.03, 3.60, 5.07, and 7.40 mg/g, respectively. The experimental data was well fitted to the Langmuir isotherm model with high correlation coefficient values (R^2), ranked from 0.98–0.99, and this is probably due to the homogeneous distribution of active sites on the surface of CuNi BNPs. Therefore, it concludes that the adsorption of heavy metal ions onto the surface of CuNi BNPs preferably follows monolayer adsorption and adsorption energies are uniform and independent of surface coverage. The essential feature of the Langmuir isotherm can be explained in terms of a dimensionless constant called separation factor (R_L), which can be expressed as:

$$R_L = \frac{1}{1 + K_L C_0}$$

The R_L values lie between 0 and 1 indicate a favourable adsorption. In the present study, the R_L values of adsorption were found to be less than 1 and also the values of Freundlich coefficient (*n*) are in between 1 and 10, both indicating a favorable adsorption. Furthermore, we can observe that the order of maximum metal adsorption capacity of the nanoparticles as follows: Mn^{2+}> Zn^{2+}>Pb^{2+}> Cd^{2+}. The results revealed that the capacity of adsorbent for the adsorption of manganese, which was more than that for the adsorption of zinc, which in turn more than that of lead. The least adsorption capacity was shown towards the cadmium ions.

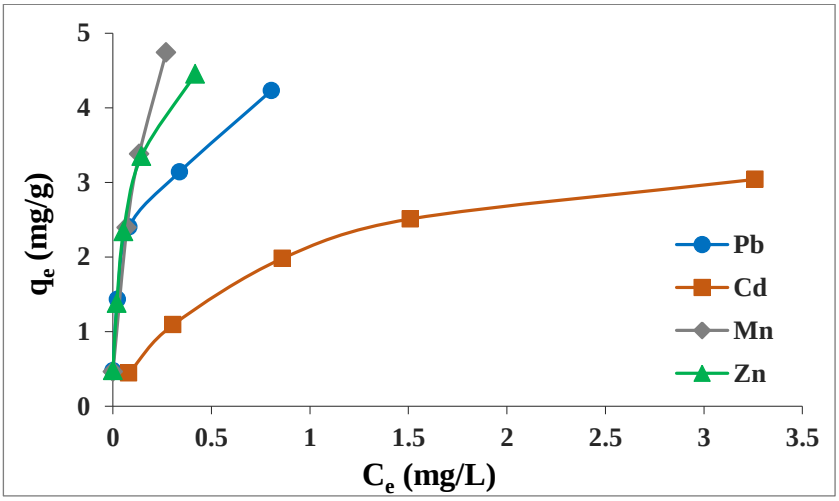

Figure 4.9: Equilibrium isotherm model for heavy metal adsorption (adsorbent dosage, 0.5 g/250 mL; pH, 7; contact time, 100 min; 200 rpm).

Table 4.4

Adsorption isotherm parameters of Langmuir and Freundlich isotherms.

Heavy metals	Langmuir				Freundlich		
	q_{max} (mg/g)	K_L (L/mg)	R_L	R^2	K_f (mg/g) $(L/mg)^{1/n}$	n	R^2
Pb	5.03	19.45	0.051	0.994	4.42	3.60	0.964
Cd	3.60	2.71	0.107	0.988	1.91	5.23	0.986
Zn	6.07	23.86	0.061	0.997	6.60	2.62	0.976
Mn	7.40	24.39	0.043	0.997	9.43	1.95	0.989

4.3.7. Adsorption kinetics

The values of q_e, k_1, k_2, and correlation coefficient (R^2) calculated from the slopes and intercepts of fitted lines of pseudo-first order and pseudo-second -order adsorption data were shown in Table 4.5. High R^2 values were obtained for both pseudo-first -order and pseudo-second-order kinetic models ranked from 0.90–0.99 and 0.89–0.99, respectively, revealing that both kinetic models could fit the data at adsorption equilibrium, especially the pseudo-first-order model. Comparing the calculated q_e values with the experimental q_e value, it is clear that the pseudo-first-order model is more suitable than the pseudo-second-order model and it could describe the whole adsorption process of Pb, Cd, Mn and Zn on CuNi BNPs. The pseudo-first-order rate constant decreased as the initial concentration of heavy metals increased, this may be due to the saturation of the surface sites located

on CuNi nanoparticles at a higher heavy metal concentrations and resulted in a low adsorption rate.

Table 4.5

Calculated parameters of the pseudo-first order and pseudo second order kinetic models.

Heavy metals	C_0 (mg/L)	q_e,exp (mg/g)	Pseudo-first order			Pseudo-second order		
			q_e,cal (mg/g)	K_1 (min^{-1})	R^2	q_e,cal (mg/g)	K_2 (g/mg min)	R^2
Pb	1	1.47	1.47	0.08	0.97	1.70	0.06	0.82
	5	3.39	3.44	0.07	0.99	3.78	0.03	0.99
	10	5.28	5.29	0.05	0.99	6.18	0.01	0.99
Cd	1	1.44	1.44	0.06	0.98	1.54	0.09	0.99
	5	2.74	2.81	0.05	0.98	3.50	0.01	0.98
	10	3.07	3.48	0.04	0.98	4.11	0.005	0.97
Zn	1	1.48	1.31	0.10	0.90	1.51	0.03	0.89
	5	3.32	2.97	0.05	0.98	4.12	0.01	0.98
	10	5.49	5.85	0.06	0.98	6.46	0.01	0.99
Mn	1	1.46	1.46	0.08	0.98	1.53	0.21	0.99
	5	3.42	3.40	0.05	0.98	3.76	0.03	0.98
	10	5.73	5.72	0.03	0.98	7.02	0.005	0.98

4.4. Conclusion

The current study investigated the use of CuNi BNP as sorbents for the removal of Cd^{2+}, Pb^{2+}, Zn^{2+}, and Mn^{2+} from aqueous solutions under various operational conditions. According to the results, maximum adsorption is reached within 100 minutes for all metals. The result revealed that the adsorption of heavy metals follows the order: $Mn^{2+}>Zn^{2+}>Pb^{2+}>Cd^{2+}$. The percentage removal of all ions was strongly dependent on the pH and the removal efficiency is enhanced at higher pH values and as the pH decreases, the adsorption amount

decreases drastically. The optimum dosage of absorbent for the removal of zinc and manganese was 0.4 g while for lead and cadmium it was 0.5 g. With increasing the initial metal concentrations, the adsorption efficiency was reduced. The adsorption isotherms were described by Freundlich and Langmuir isotherm models. Pseudo-first and second-order models were used to evaluate the mechanism of adsorption, and the results showed that the adsorption reaction was fitted very well to the Langmuir isotherm model and the pseudo-first-order kinetic model. In addition, the synthesised CuNi BNPs showed a high efficiency in adsorption than individual Cu and Ni NPs. This may be due to the increased surface area of the bimetallic nanoparticles as compared to their monometallic counterparts and the synergic effect between the two metals. The results illustrated that the synthesised nanoparticle can be used as an efficient sorbent for the removal of heavy metals from aqueous solutions.

Therefore, through our approach, we could synthesise CuNi BNPs by an easy, simple, and straightforward method and which have shown effective antibacterial as well as adsorption properties.

Chapter 5

Synthesis, characterisation, and antibacterial activity of porous (styrene-divinylbenzene)/CuNi bimetallic nanocomposite microspheres.

5.1. Introduction

The small size of NPs is one of the main obstacles in their successful implementation into water treatment units because of the difficulty in separation from wastewater and high replacement cost. The recovery of NPs from an aqueous medium has normally been carried out by nanofiltration, magnetic separation, and ultracentrifugation methods. But referring to common water purification strategies these methods are practically tedious and may become the cost-determining step of the whole process. Moreover, in a real water treatment system, adsorbents in granular form must pack in a column in order to remove impurities. Therefore, granulation of the powder materials is required before using them as a filtration medium. Generally, these can be achieved by immobilization/stabilization of NPs and several techniques are also available. A wide range of solid support, organic or inorganic materials have been used for the immobilization of metal NPs. Among all, polymer microspheres have become one of the most promising substrate candidates due to its non-toxic, non-volatile, simple, stable, flexible, and reusable character (Burguete et al., 2005; King and Twyman, 2002).

Research in recent years has indicated that the porous copolymer styrene–divinylbenzene (St–DVB) exhibit high surface area, controllable particle size, good chemical and physical stability, easy functionalization, and tuneable pore structure, making it an ideal matrix for the nanoparticles (Tian et al., 2016; Albuszis et al., 2016). Especially in the case of water treatment, the porous structure and surface area have an important role in determining the efficiency of adsorption and release (Wang et al., 2010; Lin et al., 2013; Ali and Gupta, 2006). The porous nature allows good contact between the nanoparticles and the heavy metals for adsorption. Furthermore, such composite can be easily recoverable once the adsorption process is complete. Through our approach, we are aiming to demonstrate the idea of an easy, simple, and straightforward method for the encapsulation of BNPs with long-lasting effect by using styrene and divinylbenzene copolymer (figure 5.1).

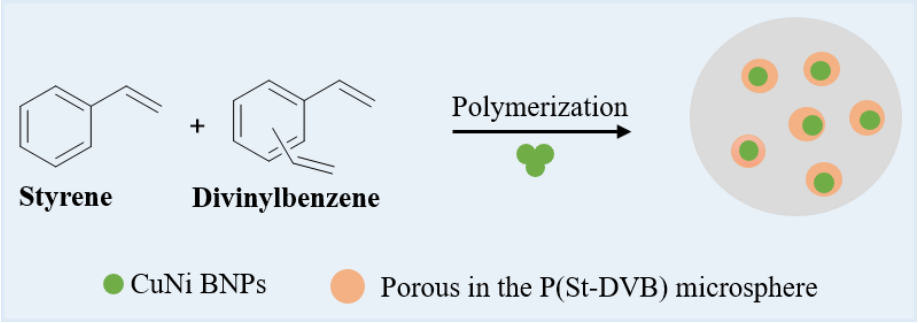

Figure 5.1: Immobilization/encapsulation of CuNi BNPs.

This chapter focuses on the preparation and characterisation of Porous (Styrene-divinylbenzene)/CuNi bimetallic nanocomposite

(P(St-DVB)/CuNi BNC) microsphere followed by its antibacterial activity studies against three different pathogenic bacteria, *E. coli*, *A. hydrophila* and *V. alginolyticus*, by using the spread plate counting method. The bimetallic nanocomposite was synthesised by "oil-in-water emulsion polymerization method" and then characterised to reveal their composition, morphology, and size by various characterisation techniques such as Scanning Electron microscopy (SEM), Transmission Electron Microscopy (TEM), Energy Dispersive X-ray Spectra (EDS), powder X-ray diffraction (PXRD) and surface area studies. Then determined the effects of contact time, dose of nanocomposite and initial bacterial concentrations on the bactericidal rate through batch experiments.

5.2. Experimental

5.2.1. Materials

All chemicals used in the study were of analytical reagent grade and purchased from Merck, India. Distilled water, prepared by a water purifier (Synergy-Merck, India) was used throughout the experiment for all solution preparation. Nutrient broth (NB) medium containing peptone, Sodium Chloride, Yeast Extract, and Beef Extract were purchased from HiMedia, India, and were used without further purification. EMB Agar, Chromogenic Coliform Agar, Bismuth Sulphite Agar and TCBS Agar, were purchased from HiMedia, India. Sterilisation of all the glassware and media were carried out in a Rotek RAV01 autoclave for 20 min at 121°C. Agar plates were prepared in a laminar flow hood and the plates were streaked in an aseptic area

around a Bunsen burner. All worktops and benches were sterilised by washing with 70 % (v/v) ethanol/water prior to use. Bacterial cell density was recorded using a Spectrophotometer.

5.2.2. Preparation of the P(St-DVB)/CuNi BNC microsphere

The porous (St-DVB)/CuNi BNC microspheres were synthesised by oil-in-water emulsion polymerization of styrene and divinylbenzene in the presence of CuNi bimetallic NPs. 3 g of previously prepared CuNi BNPs was added to a 50 ml deionized water and ultra-sonicated for 10 min for better dispersion of bimetallic nanoparticles in water. The reactions were carried out in a 500 mL round bottom flask equipped with a magnetic stir bar and a reflux condenser, in a temperature-controllable oil bath. 300 ml of an aqueous solution of 0.5% (w/v) polyvinyl alcohol was added to the flask along with the deionized water containing CuNi BNP, and the temperature was raised to around 65°C. Then the monomer mixture containing styrene (15 ml), divinylbenzene (0.6 ml), and benzoyl peroxide (0.6 g) as the initiator was added drop-wise by a micropipette to this solution for copolymerization and bead creation. The temperature was then raised to 90°C and kept constant until the polymerization was completed (6 h). After the reaction period, the bead was filtered, washed several times with deionized water (total 2L) and methanol (total 400 ml) and finally dried.

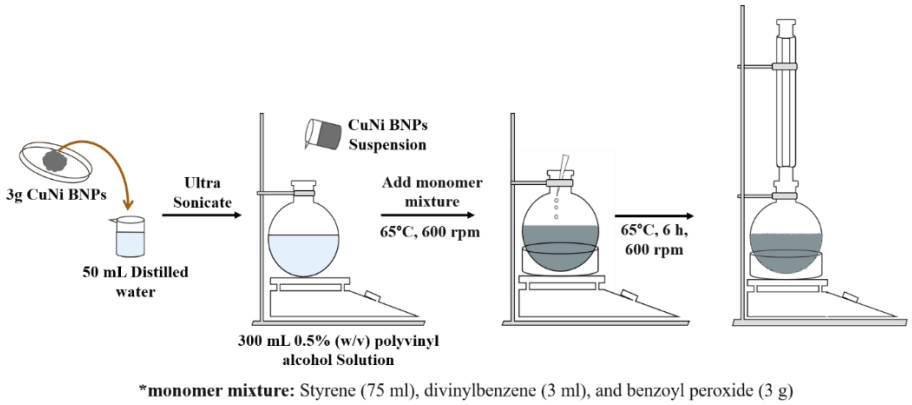

Figure 5.2: Schematic representation of the synthesis of porous (St-DVB)/CuNi BNC microspheres.

The main benefit of this synthetic method is that, they can be synthesised in water at a maximum temperature of 90°C and hence cause no harm to the environment due to solvents during their synthesis and utilisation.

5.2.3. Characterisation of the adsorbent

Surface morphology and the chemical composition of the prepared P(St-DVB)/CuNi BNC microspheres were explored using a Field-Emission Scanning Electron Microscope combined with an Energy Dispersive X-ray detector (FE-SEM-EDX, **ZEISS GeminiSEM 300)** and High-Resolution Transmission Electron Microscope (HR-TEM, **Jeol/JEM 2100**). The crystalline nature of the material was analysed by powder X-ray diffraction (PXRD, **Bruker D8 Advance**). Specific surface area was determined by measuring nitrogen adsorption/desorption isotherms using Brunauer–Emmett–Teller (BET, **BELSORP-max**) method.

5.2.4. Antibacterial activity

A series of batch scale experiments were conducted to investigate the effect of different parameters such as exposure time, dose of P(St-DVB)/CuNi BNC and initial bacterial concentrations on the antibacterial activity of the BNC microspheres. The results were then compared with the CuNi BNP's antibacterial activity to see if the immobilization technique had any impact on the nanoparticle's antibacterial activity. Experimental conditions as per Table 5.1 were varied to quantitatively evaluate their effects on antibacterial activity.

Table 5.1

Experimental conditions for batch study.

Bacteria	Contact time (min)	Dose of BNC (µg/ml)	Initial bacterial concentration
Escherichia coli	15-180	10-50	10^6
	90	10-50	10^6
	90	50	10^4-10^8
Aeromonas hydrophila	15-180	10-50	10^6
	90	10-50	10^6
	90	40	10^4-10^8
Vibrio alginolyticus	15-180	10-50	10^6
	90	10-50	10^6
	90	30	10^4-10^8

5.2.4.1. Dose-dependent antibacterial activity of P(St-DVB)/CuNi BNC

Different amounts of the synthesised BNCs (10, 20, 30, 40, and 50 µg/ml) were added into 250 mL spiked saline samples with initial

bacterial concentration of approximately 10^6 CFU/mL. The saline water without nanoparticles were used as negative control. All the bottles were then shaken for 1 hr in an incubator shaker with continuous stirring at 200 rpm and 37℃. After this period of time, an aliquot of 100 µL were withdrawn and were inoculated in corresponding agar plates by spread plate method (three plates for one sample). The control sample was tested in every run by the same method and used as standard for comparison. All plates were incubated at 37 °C for 24 h and the grown colonies were counted. The average value was obtained and expressed as CFU/mL.

5.2.4.2. Bacterial growth kinetics in the presence of P(St-DVB)/CuNi BNC

Bacterial growth curve was monitored by treating the saline water with BNCs at different exposition times. 10 to 50 µg/ml of the BNPs were added into a 250 mL spiked saline water samples of each bacterial saline water with initial bacterial concentration of approximately 10^6 CFU/mL. A negative control was carried out in flasks without BNC. Each flasks were then shaken for 2 hrs and an aliquot of 100 µL of the treated samples was withdrawn at every 15 min time interval. The aliquots were transferred in to the petri plates and were incubated at 37℃ for 24 h. Then the final CFU was determined by counting the number of colonies on each plate and the results were plotted in function of the time of aliquot withdrawal.

5.2.4.3. Bactericidal activity of P(St-DVB)/CuNi BNC

Sterilized saline (0.85% NaCl) solution was prepared with variable number of initial bacterial concentrations (10^4-10^8 CFU/mL) for each bacterial strain. 50 µg/ml of the synthesised P(St-DVB)/CuNi BNC was added to 250 mL of each bacterial solution and shaken for 90 min in an incubator shaker with continuous stirring at 200 rpm at 37℃. Finally, 100 µL of each sample was spread on the petri plates followed by recording the number of colonies on each plate.

5.3. Results and Discussion

5.3.1. Characterisation of adsorbent

In order to examine the surface morphology of the microsphere, field emission scanning electron microscopy (FE-SEM) micrographs were taken. The SEM images of prepared P(St-DVB)/CuNi BNC microspheres showed that, the particles were spherical in shape. The average diameter of nanocomposite was found to be around 112 µm (Figures 5.3 (a) & (b)). It is interesting to note that P(St-DVB)/CuNi BNC particles with larger size than CuNi bimetallic NPs were formed via encapsulation of CuNi bimetallic NPs by styrene and divinylbenzene co-polymer.

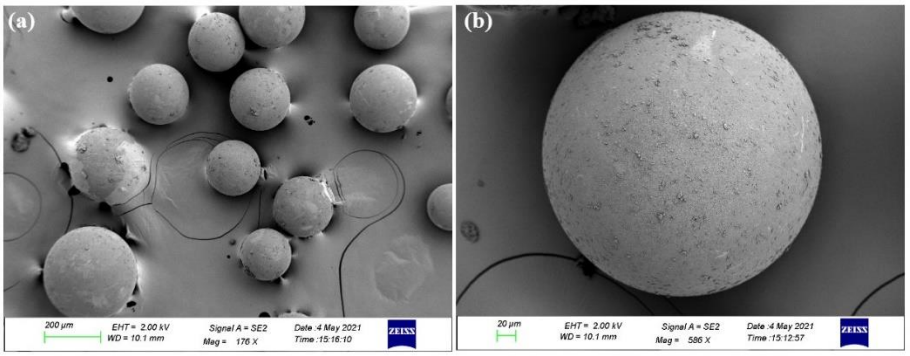

Figure 5.3: SEM images of synthesised P(St-DVB)/CuNi BNC microspheres.

High-resolution transmission electron microscopy (HR-TEM) image was taken and is shown in Figure 5.4. It is indicated that CuNi bimetallic NPs were successfully entrapped in to the P(St-DVB) microspheres. The darker core was CuNi bimetallic NPs and their distribution in the microsphere were non-uniform. The entrapped NPs were almost spherical in shape and separated from each other.

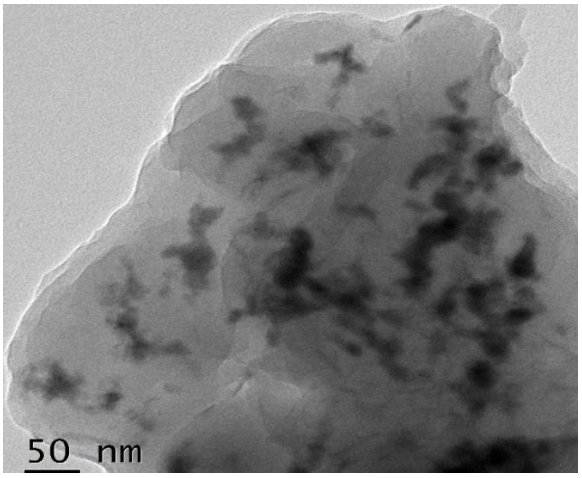

Figure 5.4: TEM image of P(St-DVB)/CuNi BNC microspheres.

Energy dispersive X-ray (EDX) was used to analyse the elemental constituents of the P(St-DVB)/CuNi BNC microspheres. Figure 5.5 represents the EDX spectra of cross-sectional area of the microspheres and the results confirming the existence of Cu and Ni elements inside of the P(St-DVB) microsphere.

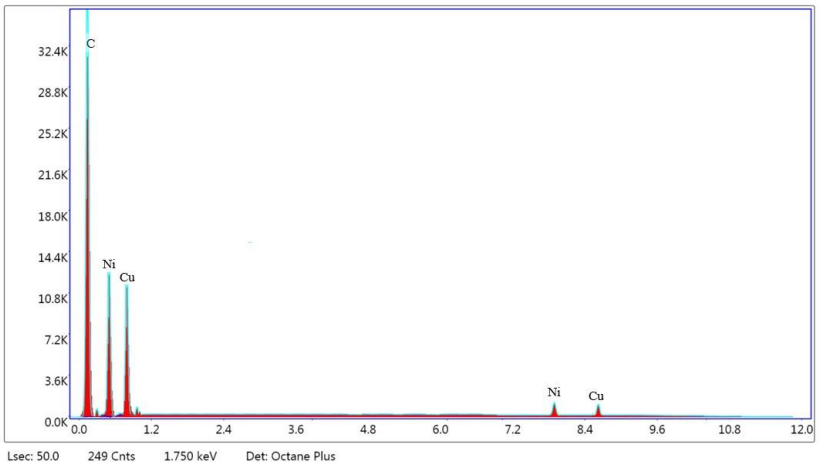

Figure 5.5: EDX image corresponding to the cross section of P(St-DVB)/CuNi BNC microspheres.

The crystalline structure of the nanocomposite was characterised by PXRD as shown in Figure 5.6. The PXRD spectra of P(St-DVB)/CuNi BNC microspheres showed prominent peaks at 44.47° (111), 50.64° (200) and 74.03° (220) confirming the crystal planes of CuNi BNPs (Fig. 1(e)) (JCPDS # 3- 065-7246). These results prove that dispersion of CuNi BNPs occurred in the centre as well as towards the surface of the P(St-DVB) microsphere.

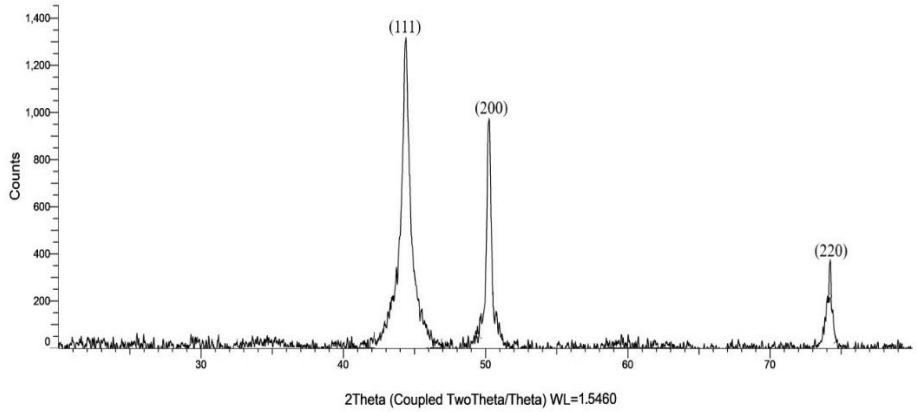

Figure 5.6: Powder X-ray diffraction pattern of P(St-DVB)/CuNi BNC microspheres.

The specific surface areas of microspheres were determined by sorption analysis using nitrogen as the sorbate molecule. The BET experimental results of P(St-DVB)/CuNi BNC microspheres were listed in Table 5.2 and its N_2 adsorption/desorption isotherm plot and corresponding pore size distribution were shown in Figure 5.7. As per IUPAC classification, the sorption isotherm exhibited is a combination of type II and type IV and the H3 type of hysteresis loop indicating the presence of large mesopores and a small number of macropores with a broad size distribution.

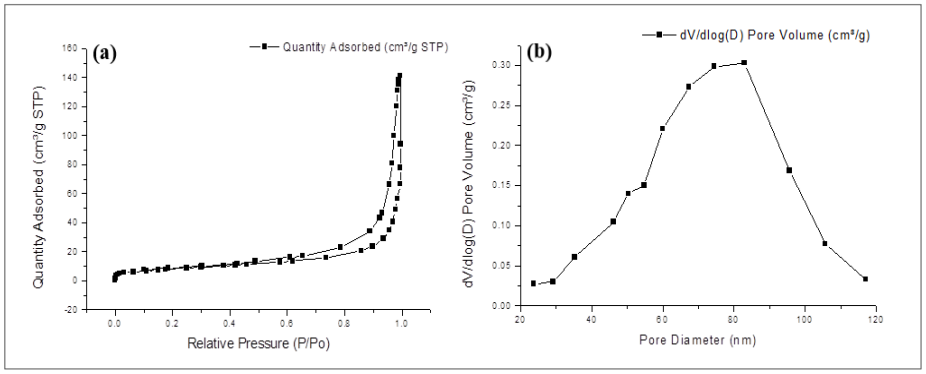

Figure 5.7: (a) N_2 adsorption-desorption isotherm and (b) corresponding pore size distribution of P(St-DVB)/CuNi BNC microspheres.

Table 5.2

BET experimental results of P(St-DVB)/CuNi BNC microspheres.

BET surface area S_{BET} (m^2/g)	**Average pore diameter (nm)**	**Total pore volume (cm^3/g)**
25.88	64.80	0.112

5.3.2. Antibacterial activity

The antibacterial activity of the synthesised P(St-DVB)/CuNi BNC microspheres were analysed against *Escherichia coli* (*E. coli*), *Aeromonas hydrophila* (*A. hydrophila*) and *Vibrio alginolyticus* (*V. alginolyticus*). Effects of different parameters like exposure time, dose of P(St-DVB)/CuNi BNC, and initial bacterial concentrations on the antibacterial activity of the BNC were quantitatively evaluated.

5.3.2.1. Dose-dependent antibacterial activity of P(St-DVB)/CuNi BNC

It is clear from the graphs that, a linear relationship existed between the amount of P(St-DVB)/CuNi BNC and bactericidal rate. The antibacterial activity of the BNC was relatively weak at lower doses. However, increasing the amount of BNC resulted in a significant decrease in cellular viability (Figure 5.8). Bactericidal rates for *E. coli*, *A. hydrophila*, and *V. alginolyticus* were increased, respectively, from 0 to 66%, from 23 to 89%, and from 59 to100%, with nanoparticle concentration rising from 10 to 30 µg/ml at a contact time of 90 min. Complete inhibition of *E. coli* and *A. hydrophila* were occurred after contact with 40 µg/ml of BNC. Therefore, 40 µg/ml was identified as the optimal BNC dose for further study.

According to the findings of this experiment, both the BNP and BNC had shown almost similar antibacterial activity, although BNC required a longer contact time to completely inhibit bacterial growth compared to the BNP. Results were also revealed that *A. hydrophila* and *V. alginolyticus* were considerably more sensitive to CuNi BNC than *E. coli*. This finding is consistent with the antibacterial studies carried out with the CuNi BNPs (chapter 3).

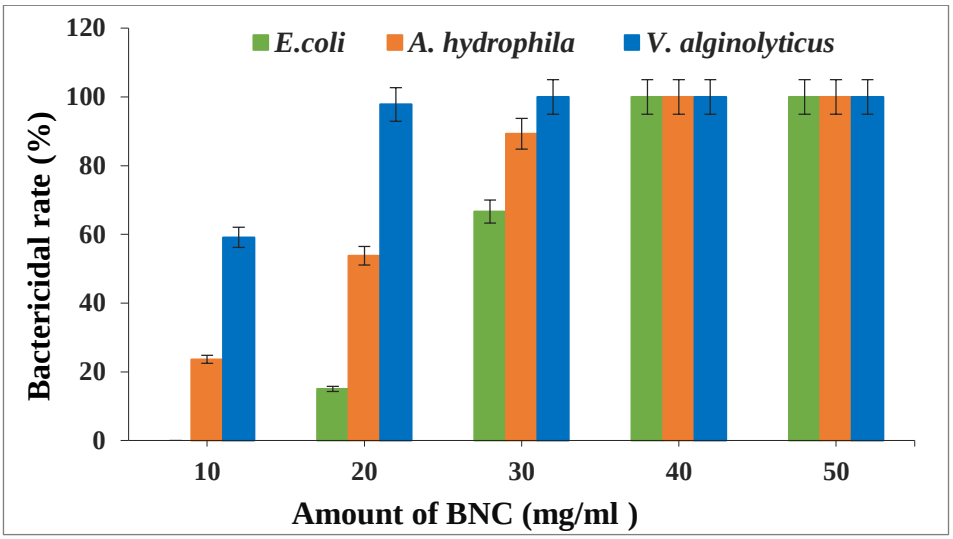

Figure 5.8: Bactericidal rate (%) of P(St-DVB)/CuNi BNC at different investigated concentrations against *E. coli*, *A. hydrophila* and *V. alginolyticus* (contact time, 90 min; initial bacterial concentration, 10^6 CFU/mL; 200 rpm).

5.3.2.2. Bacterial growth kinetics in the presence of P(St-DVB)/CuNi BNC

The effects of exposure time on the antibacterial activity of P(St-DVB)/CuNi BNC were examined against *E. coli*, *A. hydrophila* and *V. alginolyticus* at different BNC concentrations (10, 20, 30, 40, and 50 µg/ml). A gradual increase in the bactericidal rate was found with an increase in the exposure time.

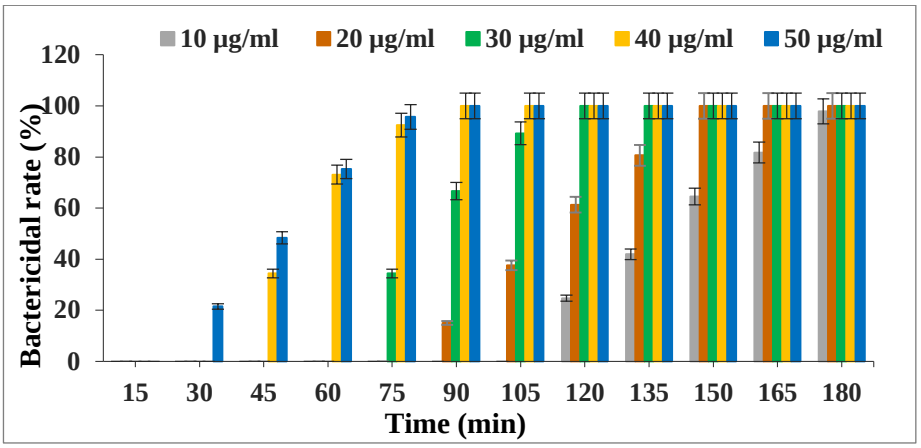

Figure 5.9: Effect of contact time on bactericidal rate of *E. coli* at different P(St-DVB)/CuNi BNC concentrations (initial bacterial concentrations, 10^6 CFU/mL; 200 rpm).

Figure 5.9 illustrates the measurement of the bactericidal rate on *E. coli* at various exposure time with the P(St-DVB)/CuNi BNC. At 10 µg/ml, the inhibition of *E. coli* was not evident up to 105 minutes of exposure time, but the bactericidal rate increased from 120 minutes and attained its maximum rate within 180 minutes of contact time. In the case of 20 and 30 µg/ml of BNCs, complete inhibition of bacterial growth was achieved respectively, within 150 and 120 min of exposure time. The number of grown *E. coli* cells were significantly reduced at doses of 40 and 50 µg/ml of BNC, and 100% of the *E. coli* cells were found inactivated at these concentrations after 90 minutes of exposure. Whereas, in the case of CuNi BNP 100% bactericidal rate was achieved within 75 min of exposure time. Therefore, we can conclude that a slightly longer exposure time was necessary for P(St-DVB)/CuNi BNC microspheres to suppress bacterial growth similar to CuNi BNPs when all other parameters were held constant.

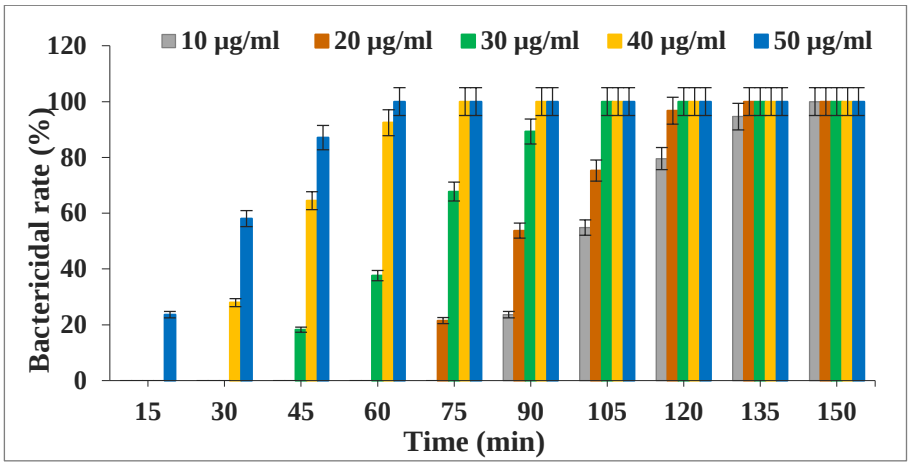

Figure 5.10: Effect of contact time on bactericidal rate of *A. hydrophila* at different P(St-DVB)/CuNi BNC concentrations (initial bacterial concentrations, 10^6 CFU/mL; 200 rpm).

Similarly, the bactericidal rate of *A. hydrophila* was assessed by exposing it with BNCs for different contact times and the findings are depicted in Figure 5.10. A considerable inhibition in the growth of *A. hydrophila* was detected only after 45 minutes of interaction with 10 and 20 µg/ml of BNC and attained its maximum value, i.e., 100% bactericidal rate, within 150 and 135 minutes of exposure with 10 and 20 µg/ml, respectively. In the case of 30 and 40 µg/ml of BNC, 100% bactericidal rate was attained with an exposure time of 105 and 30 min, respectively. Whereas only a 60 min of contact time was enough to completely suppress the growth of *A. hydrophila* from water containing 50 µg/ml of BNC. While at 50 µg/ml concentration of CuNi BNPs, 100% of bacterial growth was inhibited by 45 min of contact time at similar experimental conditions.

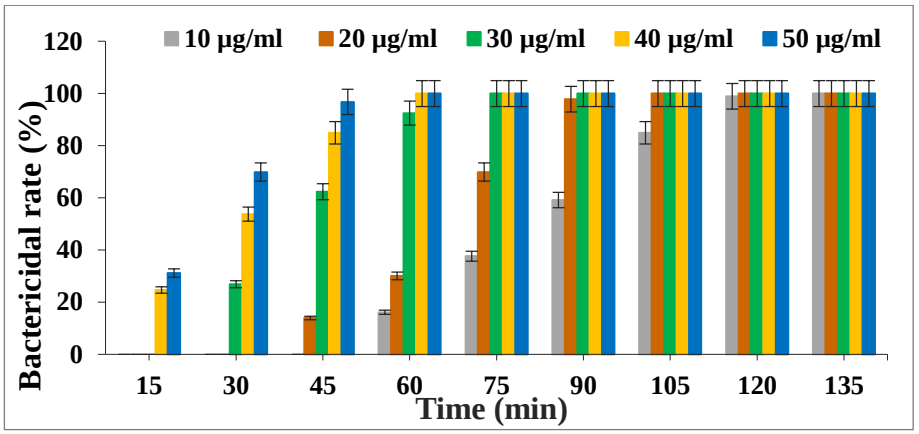

Figure 5.11: Effect of contact time on bactericidal rate of *V. alginolyticus* at different P(St-DVB)/CuNi BNC concentrations (initial bacterial concentrations, 10^6 CFU/mL; 200 rpm).

The antibacterial activity of P(St-DVB)/CuNi BNC microspheres was evaluated against *V. alginolyticus* and found that, with an increase in contact time from 15 to 120 minutes the bactericidal rate increased from 0 to 98% in the case of 10 µg/ml concentration, and the total suppression of bacterial growth was occurred within 135 minutes (figure 5.11). The concentrations of 20, 30, and 40 µg/ml were able to eliminate 100% of bacterial growth after 105, 75 min, and 1 hr of exposure with BNC, respectively. Whereas, for 50 g/ml of BNC, 100% bactericidal rate was attained after 60 min of treatment. In the case of CuNi BNPs, it was attained within 45 min of contact time.

The bacterial growth profiles show that every sample inhibited bacterial growth, and the impact was stronger when the amount of P(St-DVB)/CuNi BNC microspheres in the bacterial solution and

exposure time increased, which was similar with our earlier investigation. For further research, a contact time of 90 minutes was chosen for the optimum antibacterial activity.

5.3.2.3. Bactericidal activity of P(St-DVB)/CuNi BNC

Bactericidal activity of P(St-DVB)/CuNi BNC microspheres were analysed by using bacterial solutions with different initial bacterial concentrations ranging from 10^4-10^8 and the results are shown in the bar chart graph (figure 5.12). A decreasing trend in the bactericidal rate was observed with an increase in the initial bacterial concentration. 100% of bactericidal rate was obtained by BNCs at lower bacterial concentrations, but at higher bacterial concentrations, it only had a moderately good antibacterial impact on all bacteria.

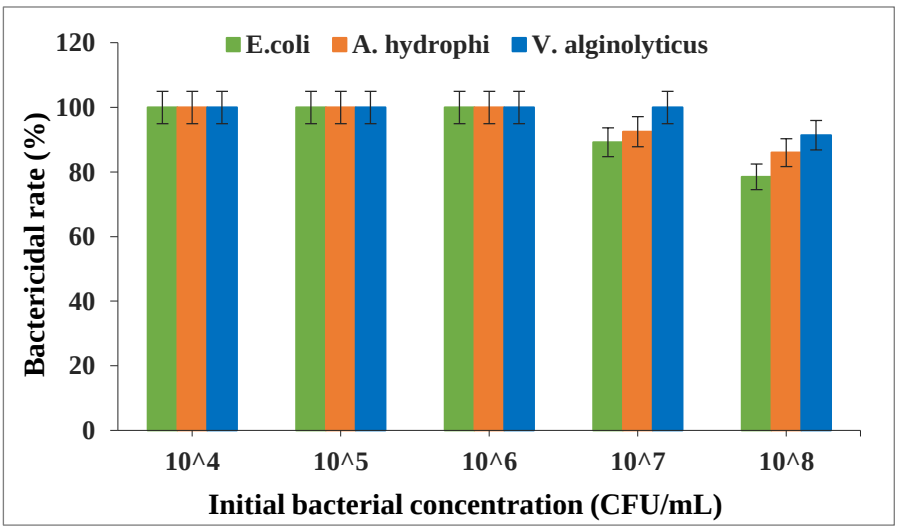

Figure 5.12: Effect of initial bacterial concentration on bactericidal rate of P(St-DVB)/CuNi BNC (amount of NP, 50 µg/ml; contact time, 90 min; 200 rpm).

A bactericidal rate of more than 80% was achieved by the produced P(St-DVB)/CuNi BNC microspheres from solutions containing 10^4 to 10^8 CFU/mL initial concentrations of *A. hydrophila*, and *V. alginolyticus*. *A. hydrophila* and *V. alginolyticus* were completely eliminated from the contaminated saline solution within 90 min for 10^4 to 10^6 CFU/mL initial concentrations. In the case of *A. hydrophila* the maximum bactericidal rate for 10^7 and 10^8 CFU/mL initial concentrations were 92% and 86%, respectively. Whereas, with increasing the initial *V. alginolyticus* concentration from 10^7 to 10^8 CFU/mL, the bactericidal rate was decreased from 100% to 91%. The bactericidal rate against *E. coli* was found to be at its highest at the initial concentration of 10^4 to 10^6 CFU/mL, and it fell from 89% to 78% when the concentration increased from 10^7 to 10^8 CFU/mL.

5.4. Conclusion

In this study, the immobilization of the CuNi BNPs were carried out using styrene and divinylbenzene co-polymer. The immobilized microspheres were successfully synthesised by oil-in-water emulsion polymerization of styrene and divinylbenzene in the presence of CuNi BNPs. The SEM image of P(St-DVB)/CuNi BNC indicates the formation of spherical shaped particles with average diameter of 110 µm. HR-TEM images indicated that CuNi bimetallic NPs were successfully encapsulated with in the P(St-DVB) microspheres. EDX spectra showed that Cu and Ni elements were present inside the P(St-DVB) microsphere. The crystalline structure of the nanocomposite was characterised by PXRD and showed prominent peaks at 43.26◦ (111), 50.44◦ (200) and 74.03◦ (220) confirming the crystal planes of CuNi

BNPs. According to the BET analysis, nanocomposite had a specific surface area of 45.88 m^2/g with an average pore diameter of 64.80 nm.

Similar to CuNi BNPs, P(St-DVB)/CuNi BNC were also shown remarkable antibacterial activity towards *E. coli*, *A. hydrophila*, and *V. alginolyticus*, although BNC required a longer contact time to completely inhibit bacterial growth compared to the CuNi BNPs. The bacterial growth kinetics experiment has shown that, complete inhibition of bacterial growth was occurred within 195 min for all species of bacteria and the impact become increased with the BNC concentration increased. Complete inhibition of *E. coli* and *A. hydrophila* were occurred after contact with 40 µg/ml of BNC and 100% of *V. alginolyticus* cells were inactivated after the contact with 30 µg/ml of BNC all for 90 min of exposure time.

The composites were efficient in the removal of bacteria from water and also, they can be easily synthesised in water at a maximum temperature of 90°C and hence cause no harm to the environment due to solvents during their synthesis and utilisation. Most of the NP immobilization techniques result in a partial loss of their activity proportional to the reduction in their active surface area. Whereas, in the case of P(St-DVB)/CuNi BNC, the porous nature of the poly(styrene-divinylbenzene) allows good contact between the CuNi BNPs and the bacteria. Therefore, they could able to exhibit good antibacterial activity comparable to that of CuNi BNPs. Moreover, their enlarged size makes it possible to recover the used composites very easy from the aqueous media and therefore it is expected that these novel composites might provide promising opportunities in antibacterial applications in water treatment techniques in the future.

Chapter 6

Removal of heavy metals from aqueous solution using porous (styrene-divinylbenzene)/CuNi bimetallic nanocomposite microspheres.

6.1. Introduction

In the present study, a series of batch scale adsorption experiments were conducted to investigate the adsorption characteristics of Pb^{2+}, Cd^{2+}, Mn^{2+}, and Zn^{2+} on to P(St-DVB)/CuNi BNC microspheres.

As a continuation of our previous research, the objectives of the present study were (1) to determine the effects of contact time, pH, adsorbent dosage and initial concentration for Pb^{2+}, Cd^{2+}, Mn^{2+} and Zn^{2+} removal through batch experiments; (2) to determine the adsorption isotherms for describing the equilibrium adsorption and kinetics models to examine the sorption mechanism.

6.2. Experimental

6.2.1. Materials

All chemicals used in the study were of analytical reagent grade and purchased from Merck, India, except for HCl which was of general reagent (GR) grade. The heavy metal analysis was conducted using Thermofisher M series atomic absorption spectrophotometer (AAS)

with air/acetylene flame and deuterium background correction was applied in all measurements. Distilled water, prepared by a water purifier (Synergy-Merck, India) was used throughout the experiment for all solution preparation. The stock solution of heavy metals was purchased from Merck, India. Contaminated aqueous solutions of heavy metals were prepared by diluting the corresponding metal standard stock solutions. The pH of the solution was measured with a pH meter and the pH of the solution throughout the study was adjusted with 0.1 M HCl or NaOH as required.

6.2.2. Batch Adsorption study

A series of batch scale adsorption experiments were conducted to investigate the adsorption characteristics of Cd(II), Pb(II), Mn(II), and Zn(II) onto P(St-DVB)/CuNi BNC microspheres. Experimental conditions as per Table 6.1 were varied to quantitatively evaluate their effects on metal adsorption. For each experimental run, 250 mL metal solution with a known pH and desired concentration of heavy metals was taken in a 500 ml conical flask. The immobilized nanocomposite was then immersed in the heavy metal solution with continuous shaking at 200 rpm, at room temperature (25 ± 0.5°C). Then the remaining heavy metal concentration was measured at equilibrium and at various time intervals. All the experiments were conducted in triplicate and the average values were considered. The percentages of heavy metal removal/ the quantity of adsorbed heavy metal ions were calculated as described in the following equation:

$$\%\text{Adsorption (Removal)} = \frac{C_0 - C_e}{C_0} \times 100$$

Where C_0 is the initial heavy metal concentration (mg/L) and C_e is the heavy metal concentration at final equilibrium (mg/L).

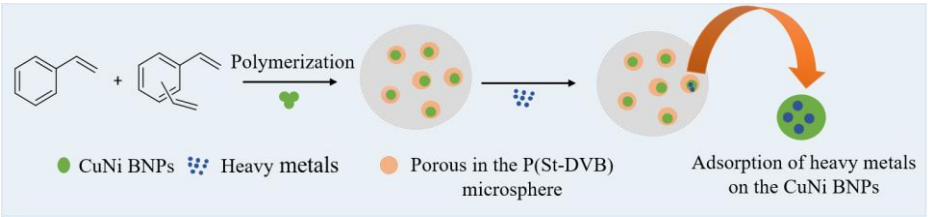

Figure 6.1: Schematic representation of the heavy metal removal using synthesised P(St-DVB)/CuNi BNC microspheres.

Table 6.1

Experimental conditions for batch adsorption study.

Metals	Contact time (min)	Adsorption dose (g/L)	Equilibrium adsorption experiments	pH
Pb	10-200	2	1, 10, 25	5
	120	0-4	10	5
	120	2	1-50	5
	120	2	10	3-9
Cd	10-200	2	1, 10, 25	7
	130	0.5-4	10	7
	130	2	1-50	7
	130	2	10	3-9
Mn	10-200	2	1, 10, 25	7
	110	0.5-4	10	7
	110	2	1-50	7
	110	2	10	3-9
Zn	10-200	1.5	1, 10, 25	7
	140	0.5-4	10	7
	140	1.5	1-50	7
	140	1.5	10	3-9

6.2.2.1. Effect of contact time on adsorption

The effect of contact time on the heavy metal removal was examined with three different initial metal concentrations (5, 10, and 25 mg/L) at an adsorbent dose of 2 g/L and constant pH 5. After shaking, the supernatant was withdrawn at every 10 min time interval, filtrated through a 0.45μm syringe filter, and then analysed.

6.2.2.2. Kinetic adsorption experiments

The experiment was conducted with 10 mg/L metal solutions. The optimal contact time for further analysis was determined from the adsorption kinetics study. The specific amounts of metal adsorbed at equilibrium were calculated from the following equation:

$$q_e = \frac{C_o - C_e}{W} \times V$$

where Co and Ce are the initial and equilibrium concentrations of heavy metal ions (mg/L) respectively, V is the volume of the solution (L) used and W is the adsorbent dosage (g). Pseudo-first-order and pseudo-second-order kinetics models were adopted to define the adsorption rates (Li et al., 2015; Ho, 2006). Table 2 depicted the batch Pseudo-first-order and pseudo-second-order kinetic equations.

6.2.2.3. Effect of pH on adsorption

The effect of pH on metal adsorption and removal was determined between pH 3–9 by keeping other factors such as initial concentration of heavy metals, adsorbent dosage, contact time and

room temperature were constant. The pH of the solutions was adjusted within the range by adding some volume of 1M HCl and 0.1M NaOH.

6.2.2.4. Effect of adsorbent dosage

The influence of adsorbent concentration on the adsorption of heavy metals was studied by varying the amount of P(St-DVB)/CuNi BNCs in a given volume of metal solution and keeping other parameters constant. The concentrations tested were 0.5, 1, 1.5, 2, 3, and 4 g/L.

6.2.2.5. Equilibrium adsorption experiments

All the isotherm adsorption experiments were conducted under optimal conditions. The initial concentrations of the heavy metals were diluted to between 1-50 mg/L. 250 ml of the aqueous solution of each heavy metal was taken in a series of conical flasks and a known amount of the adsorbent was added. The Langmuir and Freundlich adsorption isotherm models were adopted to correlate the experimental and equilibrium adsorption data (Langmuir, 1918; Freundlich, 1906) (Table 6.2).

Table 6.2

Equations of kinetics and isotherm models used in the batch experiments.

Model	**Equation**	**Parameters**
Pseudo-first-order kinetic	$q_t = q_e(1 - e^{-k_1 t})$	q_t = amount of heavy metals adsorbed at any time t (mg/g) q_e = amount of heavy metals adsorbed at equilibrium (mg/g) k_1 = pseudo-first-order rate constant (min^{-1}).
Pseudo-second-order kinetic	$\frac{t}{q_t} = \frac{1}{k_2 q_e^2} + \frac{1}{q_e} t$	k_2 = pseudo-second-order rate constant (g/(mg min))
Langmuir adsorption isotherm	$q_e = \frac{q_{max} b C_e}{1 + b C_e}$	q_e = amount of heavy metals adsorbed at equilibrium (mg/g) C_e = equilibrium concentration of heavy metal in the solution (mg/L) q_{max} = maximum adsorption capacity (mg/g) b = Langmuir constant indicating the affinity of the binding sites for the heavy metal ions (L/mg)
Freundlich adsorption isotherm	$q_e = k_f C_e^{\frac{1}{n}}$	K_f = Freundlich adsorption coefficient n = adsorption intensity (1 < n < 10)

6.2.3. Desorption Studies

Desorption experiment was carried out to investigate whether the heavy metals would be released to the water after they were adsorbed on to the P(St-DVB)/CuNi BNC microspheres. Desorption studies were conducted immediately following the completion of the adsorption experiments with 10 mg/L aqueous solution of Pb, Cd, Mn, and Zn ions. 0.5 g of each metal loaded adsorbent was transferred to 50 mL of 0.10 and 0.5 M NaOH solution and agitated at 200 rpm for 24 h at room temperature using a mechanical shaker. Then the heavy metal concentration in the aliquots of the supernatant was analysed.

6.3. Results and Discussion

6.3.1. Effect of contact time on adsorption

The effect of contact time on the removal of heavy metals (Pb^{2+}, Cd^{2+}, Mn^{2+}, and Zn^{2+}) was investigated for three different initial concentrations (5, 10 and 25 mg/L). For these experiments, adsorbent dose, 2 g/L and pH 5 were kept constant. The graphs revealed that the metal adsorption rate initially increased drastically until about 100 min, and thereafter it became constant for all the studied initial concentrations (Figures 6.2 (a) to (c)). This indicates that the adsorption sites are vacant at the beginning of the adsorption process whereas it progressively became saturated after a particular time during the adsorption reaction; that is, the adsorption phase reached equilibrium. As shown in Figure 6.2(a), 1 mg/L solution of all the heavy metals were completely removed within 140 min. The 100%

removal of Pb^{2+}, Cd^{2+}, Mn^{2+}, and Zn^{2+} were achieved at 100, 140, 90, and 40 min, respectively. It is evident from the figures that, with an increase in the initial concentration of metal ion solution from 1 to 25 mg/L, the percentage removal (%) of all the ions were decreased. In the case of Pb^{2+} the maximum percentage removal (%) for 10 and 25 mg/L initial concentrations were 95% and 88%, respectively (Figures 6.2 (b) and (c)). When 10 mg/L cadmium solution was used, 60 % of Cd was removed within 130 min; whereas, only 55 % of Cd was removed from 25 mg/L in 130 min. With increasing the initial manganese concentration from 1 to 10 mg/L and 10 to 25 mg/L, the removal efficiency was decreased from 100% to 99% and 99% to 93%, respectively. The adsorbent was able to adsorb 100 % of the zinc ions from 10 mg/L zinc solution within 140 min and >97% from the 25 mg/L solution within 120 min.

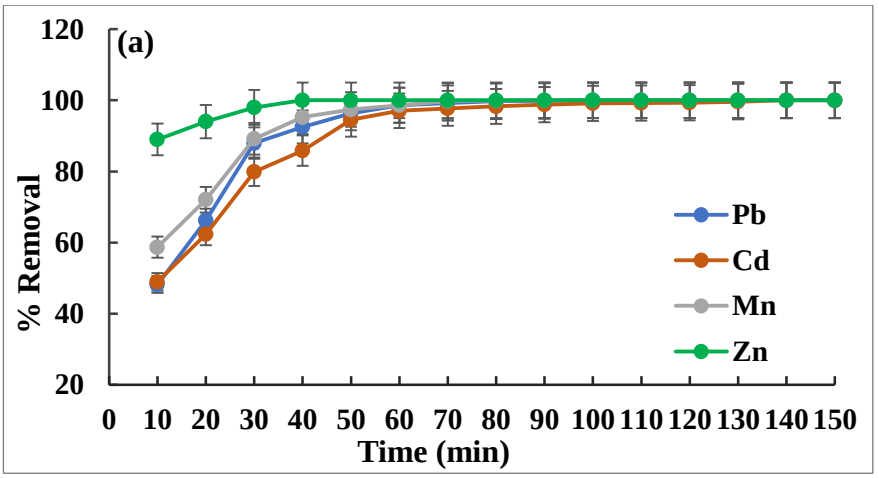

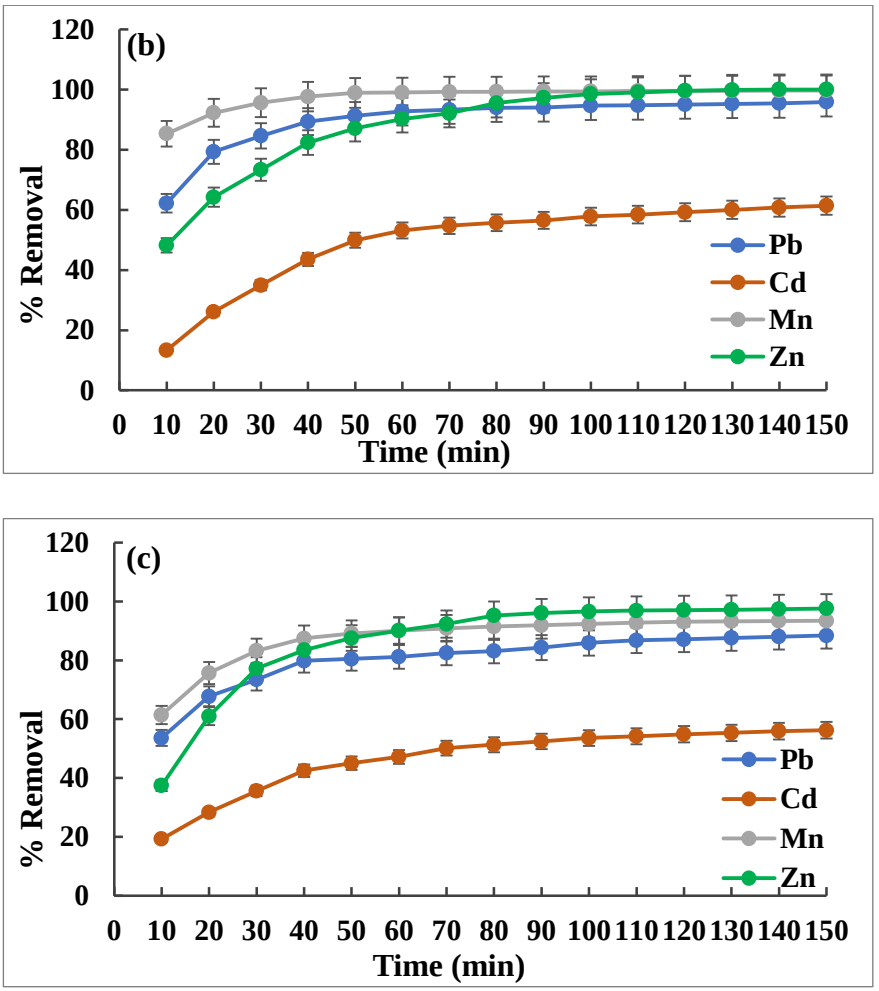

Figure 6.2: Effect of contact time on percentage removal of lead (adsorbent dosage, 2 g/L; pH, 5; 200 rpm), cadmium (adsorbent dosage, 2 g/L; pH, 7; 200 rpm), manganese (adsorbent dosage, 2 g/L; pH, 7; 200 rpm) and zinc (adsorbent dosage, 1.5 g/L; pH, 7; 200 rpm) ions with initial metal concentrations of (a) 1 mg/L, (b) 10 mg/L and (c) 25 mg/L.

Significant variations in adsorption were observed for different heavy metals. The highest adsorption was achieved for zinc and manganese. The amount of cadmium adsorbed was notably lower than

that of the other three metals. The experimental differences in the removal percentage of different heavy metal ions were considered due to the difference in their chemical affinity, the charge-to-radius ratio of the cations, and their ion exchange capacity (Giammar et al., 2007; Vidal et al., 2009). The results of this work were consistent with the findings established from our previous study (Chapter 4 and Harikumar, and Hridya, 2019).

6.3.2. Kinetic adsorption experiments

The adsorption kinetics experiments were carried out using 10 mg/L metal solutions of Pb^{2+}, Cd^{2+}, Mn^{2+}, and Zn^{2+}. The plots of chemical kinetics; pseudo-first-order and pseudo-second-order models for the adsorption were drawn and mentioned in Figures 6.3 (a) to (d) and the calculated pseudo-first-order and pseudo-second-order kinetic parameters were listed in Table 6.4.

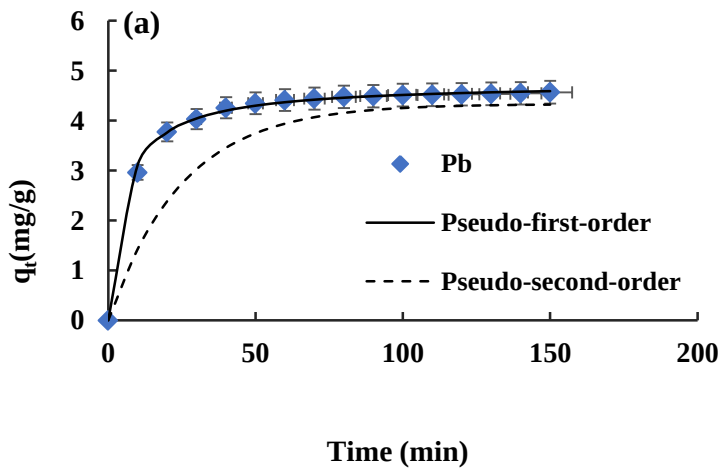

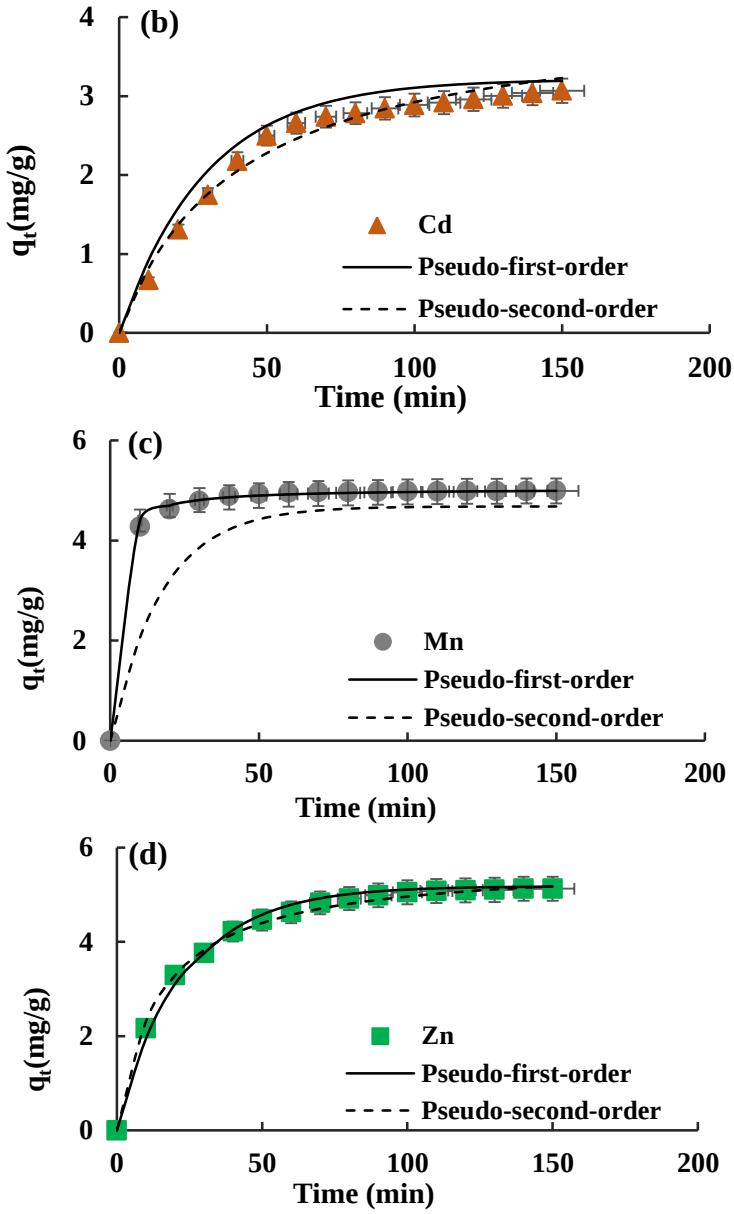

Figure 6.3: Chemical kinetics curves of (a) lead, (b) cadmium, (c) manganese, and (c) zinc adsorption by P(St-DVB)/CuNi BNC microspheres (initial concentration, 10 ppm; adsorbent dosage, 2 g/L for Pb, Cd and Mn, and 1.5 for Zn; pH, 5 for Pb and 7 for Cd, Mn and Zn; 200

High correlation coefficient (R^2) values were obtained for both pseudo-first-order and pseudo-second-order kinetic models. Results showed that, the calculated amounts of metal adsorbed (q_t,cal) by the pseudo-first-order kinetic model is more appropriate to explain the adsorption kinetics onto the P(St-DVB)/CuNi BNC. Considering our previous study, we can conclude that, both the P(St-DVB)/CuNi BNC and CuNi BNPs are following pseudo-first-order kinetics and the rate constants k_1 and k_2 are almost the same (Chapter 4 and Harikumar, and Hridya, 2019). The optimum equilibrium times of 120, 130, 110, and 140 min for Pb^{2+}, Cd^{2+}, Mn^{2+}, and Zn^{2+}, respectively, were selected for further investigation.

Table 6.3

Calculated parameters of pseudo-first-order and pseudo-second-order kinetic models.

Metal	q_e,exp (mg/g)	Pseudo-first-order			Pseudo-second-order		
		q_e,cal (mg/g)	K_1 (min^{-1})	R^2	q_e,cal (mg/g)	K_2 (g/mg min)	R^2
Pb	4.52	4.34	0.04	0.99	4.75	0.04	0.98
Cd	3.00	3.21	0.03	0.99	4.07	0.006	0.97
Mn	4.98	4.88	0.05	0.99	5.07	0.13	0.99
Zn	5.10	5.18	0.04	0.99	5.69	0.01	0.99

6.3.3. Effect of pH on adsorption

Our previous results indicate that, the pH of metal solution plays an important role in the adsorption process and also it can affect the adsorption capacity. Therefore, we studied the effect of pH on the adsorption of metal ions at a pH range of 3–9. Figure 6.4 shows the percentage removal of metal ions versus initial solution pH. As shown

in the figure, with increasing pH of the solution from 3 to 7, the removal percentage of Pb^{2+}, Cd^{2+}, Mn^{2+}, and Zn^{2+} increased respectively, from 69 to 95%, from 42 to 60%, from 91 to 99% and from 85 to 100%. The low adsorption at low pH is due to the competition between hydrogen ions and metal ions for the same adsorption sites. Further increase in the pH enhances the metal adsorption rate of $Cd^{2+}$and Mn^{2+}, this may be due to the precipitation of the appropriate salt or the predominant presence of hydrated species of heavy metals. Based on these results, the optimum pH for the adsorption of lead is considered to be 5-7 and in the case of cadmium, manganese, and zinc it is pH 7.

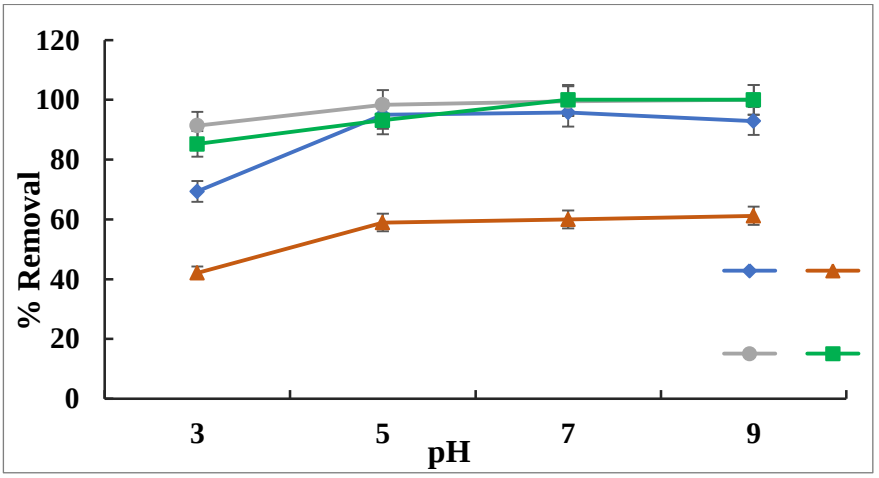

Figure 6.4: Effect of pH on percentage removal of metals (contact time, 120, 130, 110 and 140 min for Pb, Cd, Mn and Zn respectively; adsorbent dosage, 2 g/L for Pb, Cd and Mn, and 1.5 for Zn; initial concentration, 10 ppm; 200 rpm).

6.3.4. Effect of adsorbent dosage

The effect of adsorbent dosage on the uptake of heavy metals onto P(St-DVB)/CuNi BNC was studied and it is shown in Figure 6.5. In this experiment, different amounts of adsorbent (0.5, 1.0, 1.5, 2, 3, and 4 g/L) were added to metal solutions with an initial concentration of 10 mg/L and at pH 7. The samples were collected at appropriate equilibrium times of each metal. The results showed that, initially the percentage removal of metals increases with an increase in the amount of adsorbent up to 2 g/L for Pb^{2+}, Cd^{2+}, and Mn^{2+} and 1.5 g/L in the case of Zn^{2+}. This behaviour can be attributed to the availability of extra surface area and a larger number of adsorption sites by the increased amount of adsorbent. With further increase in adsorbent dosage, little change in adsorption was observed due to the saturation of the adsorbent surface. Therefore, 2g/L is taken as the optimum dosage of adsorbent for Pb^{2+}, Cd^{2+}, and Mn^{2+} and 1.5 g/L for Zn^{2+}. The maximum percentage removal of Pb^{2+}, Cd^{2+}, Mn^{2+}, and Zn^{2+} was found to be 96, 82, 100, and 100, respectively.

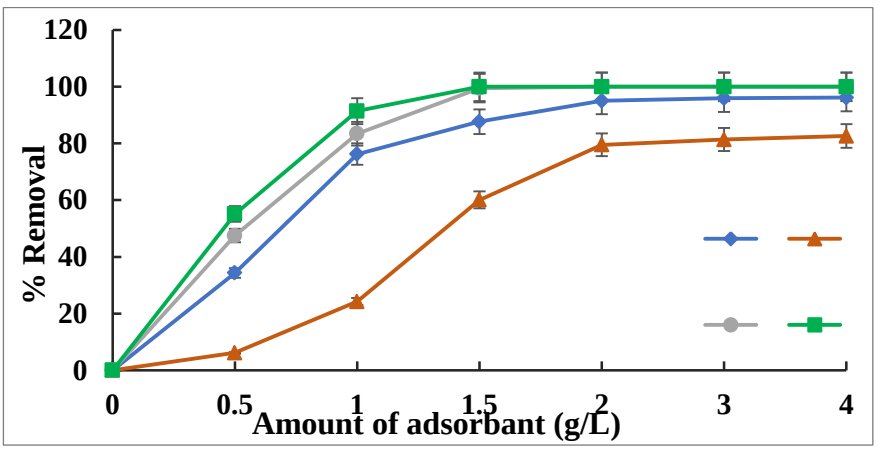

Figure 6.5: Effect of adsorbent dosage on percentage removal of metals (contact time, 120, 130, 110 and 140 min for Pb, Cd, Mn and Zn respectively; pH, 5 for Pb and 7 for Cd, Mn and Zn; initial concentration, 10 ppm; 200 rpm).

6.3.5. Equilibrium adsorption experiments

Adsorption is usually described through isotherm models such as Langmuir and Freundlich. The fitted plots of Langmuir and Freundlich adsorption models are given in Figures 6.6 (a) and (b), respectively. Different parameters and correlation coefficients (R^2) derived from these plots are presented in Table 6.5.

Table 6.4

Langmuir and Freundlich adsorption isotherm parameters for Pb(II), Cd(II), Mn(II) and Zn(II).

Heavy metals	Langmuir			Freundlich		
	q_{max} (mg/g)	K_L (L/mg)	R^2	K_f (mg/g) $(L/mg)^{1/n}$	n	R^2
Pb	15.60	0.83	0.99	6.43	2.46	0.95
Cd	5.28	0.76	0.96	2.30	3.24	0.98
Mn	22.42	1.52	0.98	12.10	3.41	1.0
Zn	20.57	1.52	0.98	10.82	3.45	0.95

Results revealed that, both the Langmuir and Freundlich models were fit to the experimental data very well with high correlation coefficients and linear plots were obtained in both cases, which indicates the applicability of these two isotherms on the current adsorption process.

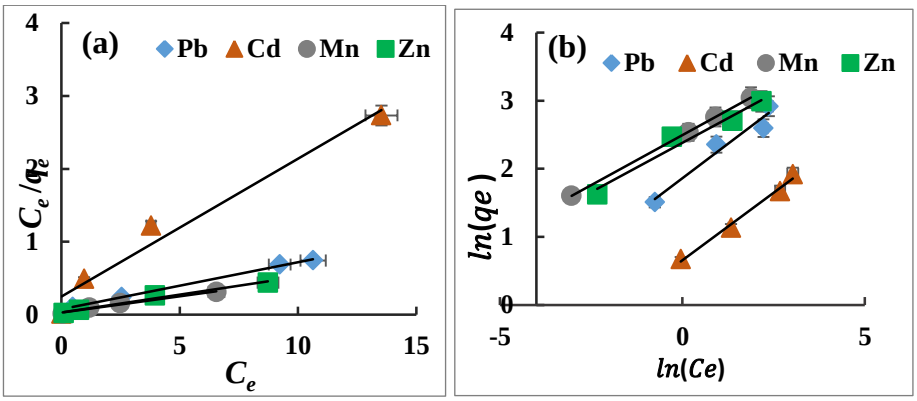

Figure 6.6: (a) Langmuir and (b) Freundlich adsorption isotherm of Pb(II), Cd(II), Mn(II) and Zn(II) (contact time, 120, 130, 110 and 140 min for Pb, Cd, Mn and Zn respectively; pH, 5 for Pb and 7 for Cd, Mn and Zn; adsorbent dosage, 2 g/L for Pb, Cd and Mn, and 1.5 for Zn; 200 rpm).

To find the most appropriate model for the adsorption; experimental isotherms data were fitted to Langmuir and Freundlich models and the result shown that, the Langmuir adsorption isotherm was closely fitted to experimental data than the Freundlich model. The Langmuir isotherm is valid for adsorbents having a homogeneous distribution of active sites which is available for adsorption on the adsorbent surface. It suggests that the adsorbent preferably follows monolayer adsorption of metals on the flat surface of the P(St-DVB)/CuNi BNC. Theoretical maximum values of monolayer adsorption capacity given by Langmuir isotherms are 15.60, 5.28, 22.42, and 20.57 mg/g for Pb, Cd, Mn and Zn respectively. The order of maximum adsorption capacity for metal ions are found to decrease in the order Mn^{2+}> Zn^{2+}> Pb^{2+}> Cd^{2+}. This trend fitted satisfactory with the experimental one. The favourable nature of Langmuir

adsorption isotherm can be expressed in terms of a dimensionless constant called separation factor or equilibrium parameter (R_L), which can be expressed as:

$$R_L = \frac{1}{1 + K_L C_0}$$

where K_L is the Langmuir constant and C_0 is the initial concentration of the adsorbate in solution. The R_L values between 0 and 1 indicate favourable adsorption and the obtained R_L values in this study are less than 1, confirming the favourable adsorption. The values of Freundlich coefficient (n) for all the metals were in between1 and 10, which represent favourable adsorption. The Freundlich constant (K_f) represents the ability of an adsorbent to adsorb heavy metals In Freundlich model. With increasing K_f, the maximum adsorption capacity increased and it follows the order Mn^{2+}> Zn^{2+}> Pb^{2+}> Cd^{2+}. Furthermore, the value of n can be used to validate the type of adsorption accurately. The physical adsorption process occurs when the value of n >1. Consequently, chemical adsorption occurs if the value of n < 1. If n=1, then the adsorption process is said to be linear. Here, the obtained value of n >1 for all cases, suggesting a good adsorption and a favorable physical process. This denoted that the adsorption system is endothermic in nature.

6.3.6. Desorption Studies

Desorption of heavy metals from P(St-DVB)/CuNi BNC was successfully achieved by using alkali solution. 0.1 and 0.5 M NaOH

solution were used for this study and the results of desorption experiments were presented in Table 6.5. The results reviled that, the maximum desorption rates of heavy metals increase with an increase in the NaOH concentration. 100% desorption of Cd ions was happening when 0.5 M NaOH solution was used, while for Pb, Mn, and Zn it was 78%, 85%, and 83%, respectively. With the 0.1 M NaOH solution, the amount become 51%, 87%, 43%, and 49%, respectively, for Pb, Cd, Mn, and Zn. This experiment suggests that there is less possibility of metal desorption from this bimetallic nanocomposite at the natural pH of normal water (6.5 to 8). 20 ml water samples were filtered after each cycle of adsorption experiment and digested it with concentrated HNO_3 and $HClO_4$, and analysed to find whether the Cu or Ni ions were released from the P(St-DVB)/CuNi BNC after adsorption. The presence of Cu or Ni ions were not observed in the collected water samples and it suggests that, the ions were not released from the composite even after the adsorption/desorption cycles. Therefore, the synthesised P(St-DVB)/CuNi BNC can be effective and potentially use as a practical adsorbent to remediate heavy metals from contaminated water.

Table 6.5

Desorption studies of the studied ions from P(St-DVB)/CuNi BNC microspheres.

Metal Ion	Adsorption	Desorption (0.1 M NaOH)	Desorption (0.5 M NaOH)
Pb	95%	51%	78%
Cd	60%	87%	100%

Mn	99%	43%	85%
Zn	100%	49%	83%

6.4. Conclusion

A batch adsorption study were conducted to evaluate the efficiency of the prepared nanocomposite for the removal of Pb^{2+}, Cd^{2+}, Mn^{2+}, and Zn^{2+} ions from synthetic water. The results revealed that the removal efficiency of adsorbent increased with increase in contact time and adsorbent mass, and decreased with increase in initial metal concentration. The maximum lead adsorption was obtained at pH 5-7, and the maximum adsorption of cadmium, manganese, and zinc were obtained at pH 7. Results from this study showed that the optimum dosage of adsorbent for the removal of Zn^{2+} was 1.5g/L, while for Pb^{2+}, Cd^{2+} and Mn^{2+} it was 2g/L. The experimental maximum adsorption capacity of P(St-DVB)/CuNi BNC for metals was 15.60 mg Pb(II)/g, 5.28 mg Cd(II)/g, 22.42 mg Mn(II)/g and 20.57 mg Zn(II)/g. The Langmuir isotherm model provided a better fit of the equilibrium adsorption data than the Freundlich model, while the process kinetics followed the pseudo-first-order. Desorption of heavy metals from P(St-DVB)/CuNi BNC was successfully achieved by using 0.5 M NaOH solution.

The porous nature of the poly(styrene-divinylbenzene) allows good contact between the heavy metals and the CuNi BNPs. Furthermore, the composite is easily recoverable from the aqueous solutions once the adsorption is complete. Therefore, we can conclude that, the immobilization of CuNi BNPs into porous polymeric material

leads to the more efficient, simpler, and low-cost separation of these used materials from the treated solution. The current invention provides an effective adsorbent for water purification, an adsorbent composite that can be packed in a column and remains stable under normal pH and conductivity of water with minimal leaching of nanoparticles.

Chapter 7

Fixed-bed column study on heavy metals removal from aqueous solutions using porous(styrene-divinylbenzene)/CuNi bimetallic nanocomposite microspheres

7.1. Introduction

Previous studies on heavy metal adsorption were focused on batch equilibrium and kinetic studies. However; batch studies provide useful information about the application of adsorption to the removal of specific waste constituents, such data are limited to a laboratory process for investigating the characteristics of the adsorbent and only a limited volume of contaminated water can treat under equilibrium conditions. Additionally, batch studies do not give any authentic scale-up data and may not be applicable to most of the long-term treatment systems (Agrawal and Bajpai, 2011; Li et al., 2011). In most large-scale applications of the adsorption process, fluid flows continuously through a column of adsorbent or a packed bed. Continuous column studies provide the most practical data for real field applications of the adsorbents in wastewater treatment process and also the columnar operation allows more efficient utilization of the adsorptive capacity than the batch process. Continuous flow process is simple in operation, obtain a high yield, treat large quantities of wastewater, and can be easily scaled up from a laboratory scale to industrial scale (Aksu and Gönen, 2004).

Among various technics in column studies, fixed-bed column is the most applicable and efficient arrangement for cyclic adsorption and desorption, hence the requirement of adsorbent is reduced (Kumar et al., 2011). Moreover, fixed bed column is the most used technique for contacting wastewater with the adsorbent. Down flow fixed beds are used more commonly to lessen the chance of accumulating particulate material in the bottom of the bed, where the particulate material would be difficult to remove by backwashing. The additional advantage of a down flow design is that adsorption of heavy metals and filtration of suspended solids are accomplished in a single step. The efficiency of fixed-bed adsorption process is affected by various operational factors such as contact time, influent metal concentration, flow rate and bed height, etc, and it is definitely more challenging to determine the effect of several parameters on the efficiency of the process. Therefore, it is important to study the dynamic behaviour in a fixed bed column condition for the removal of Pb, Cd, Zn, and Mn from contaminated water using porous (styrene-divinylbenzene)/CuNi nanocomposite microspheres (P(St-DVB)/CuNi BNC microspheres).

The objectives of this study are to perform continuous fixed-bed column study for the removal of Pb, Cd, Zn, and Mn. To investigate the metal removal efficiencies and adsorption capacities of P(St-DVB)/CuNi BNC microspheres for different heavy metals. To explore and optimise the impact of operation variables such as contact time, influent metal concentration, flow rate, and bed height, and to

analyse the obtained breakthrough curve using existing model equations.

7.2. Experimental

7.2.1. Materials

All chemicals used were of analytical reagent grade and purchased from Merck. Heavy metal analysis was conducted using a Thermofisher M series atomic absorption spectrophotometer (AAS). Distilled water was used throughout the experiment for all solution preparation. Stock solutions of heavy metals were purchased from Merck. Contaminated aqueous solutions were artificially prepared by diluting the metal stock solution with deionized water to bring the desired concentration.

7.2.2. Fixed-bed column studies

Continuous adsorption studies were conducted to evaluate the performance of a fixed bed adsorption column. Column experiments on laboratory scale were carried out using a glass column of internal diameter of 2 cm and length of 30 cm and were operated in an unsaturated gravity down flow manner. The column was designed based on our previous batch scale studies. Desired quantity of P(St-DVB)/CuNi BNC microspheres were packed as an interlayer between two supporting layers of glass wool to prohibit any loss of adsorbent during elution. After filling, the columns were initially flushed with distilled water in a down-flow mode for 1 h, in order to rinse and

equilibrate the adsorbent particles. The experiments were performed by pumping the heavy metal solutions of different initial concentrations vertically through the column at room temperature (298 K) and optimum pH. To ensure uniform flow throughout the experiment, the flow rate (mL/min) was noted periodically by collecting the effluent solution in a measuring cylinder for one minute. The effluent was collected from the outlet of the column periodically and stored for analysis. The experiments were conducted till the adsorbent gets exhausted. The concentration of heavy metal in the column effluent samples was measured using atomic absorption spectrometry. The effects of various process parameters such as initial concentration, flow rate, and bed height on the breakthrough curves and the amount of metal removed were investigated. Experimental conditions as per Table 7.1 were varied to quantitatively evaluate their effects on metal adsorption.

Table 7.1

Experimental conditions for fixed-bed column study.

Metals	Initial metal concentration (mg/L)	Flow rate (mL/min)	Bed height (cm)	pH
Pb	10, 50,100	2	2	5
	50	1,2,3	2	5
	50	2	2,4,6	5
Cd	10, 50,100	2	2	7
	50	1,2,3	2	7
	50	2	2,4,6	7
Mn	10, 50,100	2	2	7

	50	1,2,3	2	7
	50	2	2,4,6	7
	10, 50,100	2	2	7
Zn	50	1,2,3	2	7
	50	2	2,4,6	7

7.2.2.1. Breakthrough analysis

The adsorption column performance is conveniently described through the concept of the breakthrough curve (Aksu et al., 2007). A plot of the ratio of effluent concentration (C_t) and influent concentration (C_0) versus time (t) or volume (v) of the effluent is known as breakthrough curve (C_t/C_0 vs time). The breakthrough curves illustrate the performance of fixed-bed column and the time to reach breakthrough and shape of breakthrough curve are the key characteristics for evaluating the adsorption capacity of a column because they directly affect the feasibility and economics of the adsorption process (Ahamad et al., 2010). An ideal breakthrough curve has a symmetrical, sigmoidal shape (S-shape) and the breakthrough point time (t_b) was defined as the time necessary for the effluent concentration to be 10% of the feed concentration (C_t/C_0 = 0.1). Table 7.2 represents various breakthrough parameters and their equations for determination (Luo et al., 2011; Nuic et al., 2013; Yagub et al., 2015).

Table 7.2

Breakthrough parameters and their equations for determination.

Breakthrough parameters	**Equations**	
Breakthrough time, t_b (min)	Time at $\frac{C_t}{C_0} = 0.1$	C_t is the effluent metal ion concentration and C_0 is the influent metal ion concentration (mg/L).
Exhaust time, t_e (min)	Time at $\frac{C_t}{C_0} = 0.9$	
Column capacity, q_c (mg)	$q_c = \frac{QA}{1000} = \frac{Q}{1000}\int_0^t C_{ad}.dt$	Q and A are the flow rate (mL/min) and the area under the breakthrough curve, respectively. $C_{ad} = C_0 - C_t$
.Total amount of metal ions sent to the column, m (mg)	$m = QC_0t_e$	
Percentage removal of metals (%R).	$\%R = \frac{q_c}{m} \times 100$	
Adsorption capacity, q_e (mg/g)	$q = \frac{q_c}{X}$	X is the total mass of the adsorbent in the column (g).
Length of Mass Transfer Zone, MTZ (cm).	$MTZ = H\left(1 - \frac{t_b}{t_e}\right)$	H is the total depth of the adsorbent in the column (cm).

7.2.2.2. Effect of influent metal concentration

The influent metal concentration has a significant effect on the breakthrough point. To elucidate the effect of influent metal

concentration on the performance of P(St-DVB)/CuNi BNC, different concentrations of heavy metal solutions (10, 50 and 100 mg/L) were used. For this experiment, the flow rate and bed height were kept constant at 2 mL/min and 2 cm, respectively. The effluent was collected at every 30 min time interval and then analysed. The significant effect of initial metal concentration on the breakthrough curves were also studied.

7.2.2.3. Effect of flow rate

Flow rate is one of the significant parameters in designing a fixed bed adsorption column and it determines the contact time of the adsorbate with the adsorbent in a fixed bed column. The effect of flow rate on the breakthrough curves was studied for three different flow rates (1, 2, and 3 mL/min) at a constant initial heavy metal concentration of 50 mg/L and at a fixed bed height of 2 cm.

7.2.2.4. Effect of bed height

The adsorption of heavy metals in a fixed-bed adsorption column depends on the bed depth as it determines the number of active sites available for adsorption. Experiments for the effect of bed height on the adsorption of heavy metal using P(St-DVB)/CuNi BNC were carried out at constant metal concentration of 50 mg/L, flow rate of 2mL/min and by varying the bed height from 2 to 6 cm. Low bed heights were used because long exhaustion times were observed at larger values.

7.2.3. Theoretical models

Prediction of the breakthrough curve is important for scaling up the adsorption column. The mathematical models were proposed to investigate the mechanism of adsorption and the successful design of fixed-bed adsorption column for industrial applications. The breakthrough curves obtained for initial metal ion concentration, flow rate, and bed height were studied using three well-known empirical models such as Thomas, Yoon–Nelson, and Bohart–Adams models.

7.2.3.1. Thomas model

Thomas model is one of the most general and widely used models to describe the column performance and predict the breakthrough curve of metal adsorption in a fixed bed column (Thomas et al., 1944). The Thomas model follows the Langmuir adsorption-desorption model, i.e., no axial dispersion and described by pseudo-second-order reversible reaction kinetics. This model used to predict the breakthrough curves and maximum adsorption capacity of the adsorbent. The linearized form can be expressed as

$$\ln\left(\frac{C_0}{C_t} - 1\right) = \frac{k_{Th} q_0 m}{Q} - k_{Th} C_0 t \qquad (1)$$

where k_{Th} is the Thomas rate constant (ml/min mg); q_0 is the adsorption capacity (mg/g); C_0 is the influent adsorbate concentration (mg/L); C_t is the effluent concentration at time t (mg/L); m is the mass of adsorbent (g) and Q is the flow rate (mL/min). The values of k_{Th} and

q_0 can be determined from the slope and intercept of $\ln[(C_0/C_t) - 1]$ against time t.

7.2.3.2. Yoon-Nelson model

Yoon and Nelson proposed a relatively simple model based on the assumption that the rate of decrease in the probability of adsorption for each adsorbate molecule was proportional to the probability of adsorbate and the probability of adsorbate breakthrough on the adsorbent (Yoon and Nelson, 1984). This model can be applied to evaluate the exhaustion time and the behavior of the adsorption process for a given adsorbate concentration. The linearized form of the model is expressed as:

$$\ln\left(\frac{C_t}{C_0 - C_t}\right) = k_{YN}t - \tau k_{YN} \quad \textbf{(2)}$$

where k_{YN} is the Yoon–Nelson rate constant (min^{-1}) and τ is the time required for 50% adsorbate breakthrough (min). The values of τ and k_{YN} were determined from the intercept and slope of the linear plot of ln[Ct/(C0–Ct)] against t.

7.2.3.3. Adams-Bohart model

The Adams-Bohart model was proposed by Bohart and Adams (1920) based on the surface reaction theory and they developed an equation which successfully described the relationship between C_t/C_0 and t in a continuous flow system of adsorption (Bohart and Adams, 1920). It is based on the assumption that the equilibrium is not

instantaneous, and the rate of adsorption is proportional to the metal concentration. This model explains the initial part of the breakthrough curve and it is used to describe the relationship between C_t/C_0 and t in the continuous systems. The model equation is expressed as

$$\ln\left(\frac{C_t}{C_0}\right) = k_{AB}C_0 t - k_{AB}N_0\left(\frac{Z}{U_0}\right) \quad (3)$$

where k_{AB} is the Adams-Bohart rate constant (L mg^{-1} min^{-1}); N_0 is the adsorption capacity per unit volume of bed (mg/L); z is the bed height (cm) and U_0 is the linear velocity (cm/min).

7.2.4. Desorption experiments

To regenerate the adsorbent for further use, the columns were flushed with 0.5 M NaOH at a flow rate of 3.0 mL min. After elution, the adsorbent bed was rinsed with deionized water for another 1 h with the same flow rate and the regenerated bed was reused in another cycle.

7.3. Results and Discussions

7.3.1. Fixed bed column studies

Unlike the batch adsorption, in column studies, the adsorbent at the inlet end is contacted continuously with the contaminated water. The change in heavy metal concentration at each succeeding layer is small and accordingly the adsorbent in the column will acts like a series of layers, in which each layer is in contact with a fresh solution

of constant heavy metal concentration. This continuous adsorption of the solute in the bed will results in maximum loading of the adsorbent (high *x/M* on the adsorption isotherm) at constant heavy metal concentration. This condition does not exist in batch studies and in contrast to the column adsorption, a continuously declining solute concentration is there in batch processes. The mass transfer zone (MTZ) is the active surface of the adsorbent material where the heavy metal adsorption takes place. As the volume of heavy metal solution passing through the column increases, the mass transfer zone moves downward through the bed. After some time, the effluent concentration starts to rise and when the MTZ reaches the exit of the bed, the effluent concentration becomes equal to the influent concentration. Hence, the breakthrough and exhaustion are defined as the phenomena when the ratios of effluent-to-influent concentrations are 10% and 90%, respectively.

The breakthrough curves for different column operations such as initial concentration, flow rate, and bed height were investigated. In all cases, the adsorption capacity (q_c) and the breakthrough point time (t_b) were determined and the breakthrough curves were used to validate the models.

7.3.1.1. Effect of influent metal concentration

In the present study, the effect of influent concentration of Pb, Cd, Zn, and Mn was investigated using synthetic solution containing 10, 50, and 100 mg/L of metal ions at the optimised flow rate (2

mL/min) and bed height (2 cm). The breakthrough curves of Pb, Cd, Zn, and Mn were depicted in Figures 7.1, 7.2, 7.3, and 7.4, respectively, and the values of the experimental breakthrough parameters were tabulated in Table 7.3.

The breakthrough curves demonstrated that, the breakthrough time and exhaustion time were inversely related with influent metal concentration. At higher initial concentration, the breakthrough curves shift to the left side and early breakthrough points are observed. This behavior may be explained by the fact that the available adsorbent sites become saturated more quickly at higher influent metal ion concentrations and which results in reduced breakthrough time. In addition, it was observed that the adsorption capacity and the height of MTZ were increased with the increase in initial metal concentration, whereas the removal efficiency was substantially decreased. It can be explained by the fact that when the fixed bed column reaches saturation, the amount of metal ions adsorbed is very low in comparison to the amount of metal ions passing through the column. The difference in the metal removal efficiencies between 50 and 100 mg/L is less than the removal efficiencies between 50 and 10 mg/L. This could be explained by the fact that, a higher inlet concentration provides a higher driving force for adsorption due to the increased concentration gradient between the surface of the sorbent and the solution. And also the increase in the diffusion coefficient or mass transfer coefficient, due to this larger concentration gradient, will leads

to the faster transport and hence increase the adsorption capacity (Ravikumar et al., 1944).

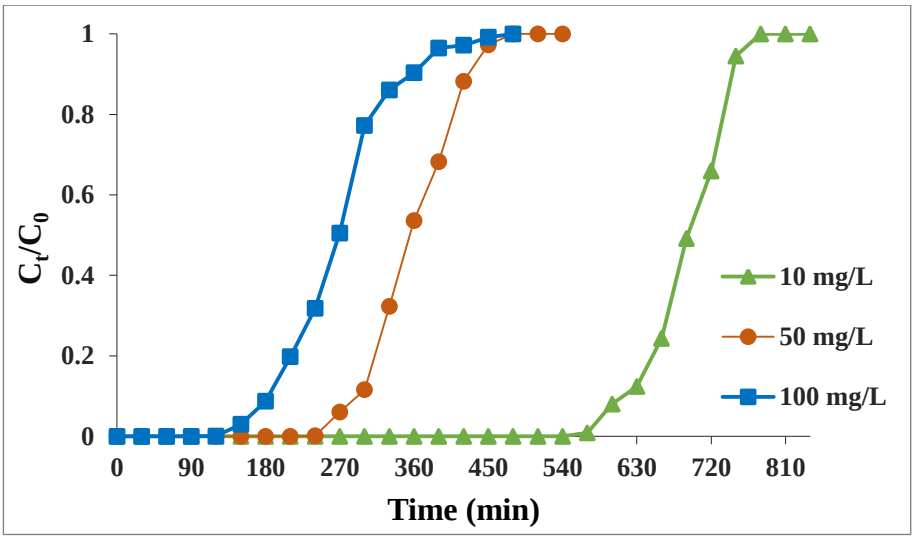

Figure 7.1: Effect of initial Pb(II) concentration on breakthrough curves (flow rate:2.0 mL/min, bed height: 2.0 cm, pH 5).

The breakthrough curves at various influent concentrations of Pb(II) aqueous solutions are shown in Figure 7.1. The curves clearly show that the breakthrough and exhaustion times were dropped with increase in the initial Pb(II) concentration. The breakthrough: exhaustion time for 10, 50, and 100 mg/g were achieved at 600:750, 270:420, and 180:360 min, respectively. It was found that with the increase in Pb(II) concentration from 10 to 100 mg/L, the corresponding adsorption capacity (q_e) increased from 10.33 to 42.30 mg/g. The percentage removal (%R) were computed and found to be 89, 72, and 69% for the initial Pb(II) concentration of 10, 50, and 100

mg/L, respectively. As the influent concentration was increased, the MTZ length increased from 0.1 cm to 1.0 cm for 10 mg/L and 100 mg/L, respectively (Table 7.3).

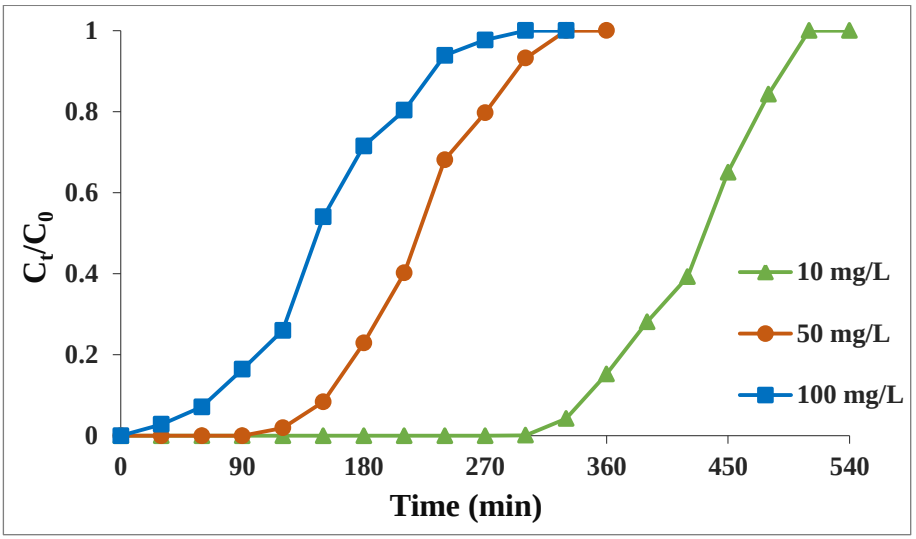

Figure 7.2: Effect of initial Cd(II) concentration on breakthrough curves (flow rate:2.0 mL/min, bed height: 2.0 cm, pH 7).

The adsorption capacity increased from 6.40 to 22.84 mg/g when the initial Cd(II) concentration increased from 10 to 100 mg/L. The %R at 10, 50, and 100 mg/L Cd(II) concentrations were 77, 64, and 61%, respectively, and the MTZ were 0.62, 1, and 1.42 cm. It is also observed that the values of t_b and t_e decrease with decrease in metal concentration (Figure 7.2). The breakthrough: exhaustion time were 330:480, 150:300, and 90:210 min for 10, 50, and 100 mg/L Cd(II) concentration, respectively.

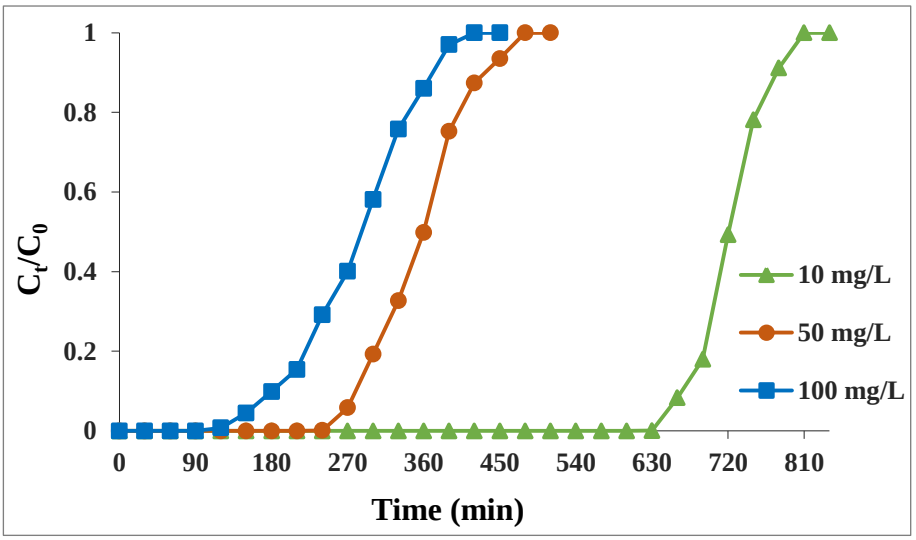

Figure 7.3: Effect of initial Zn(II) concentration on breakthrough curves (flow rate:2.0 mL/min, bed height: 2.0 cm, pH 7).

The adsorption capacity was increased from 10.81 to 23.03 mg/g and from 23.03 to 47.56 mg/g with increasing initial concentration from 10 to 50 mg/L and from 50 to 100 mg/L respectively for Zn(II). It was also noted that the %R was decreased from 88 to 78% with increase in the Zn(II) concentration. The MTZ obtained were 0.30, 0.71, and 0.77 cm for the initial concentrations of 10, 50, and 100 mL/min, respectively. The breakthrough time were found to be 660, 270, and 240 min, and the exhaustion time were 780, 390, and 360 for the 10, 50, and 100 mg/L Zn(II) concentrations, respectively (Figure 7.3).

Table 7.3

Parameters obtained from the breakthrough curves of the fixed bed column.

Metal	Influent metal concentration (mg/L)	t_b (min)	t_e (min)	q_e (mg/g)	%R	MTZ (cm)
Pb	10	600	750	10.33	89	0.4
	50	270	420	23.34	72	0.71
	100	180	360	42.30	69	1
Cd	10	330	480	6.40	77	0.62
	50	150	300	15.05	64	1
	100	90	210	22.84	61	1.42
Zn	10	660	780	10.81	88	0.30
	50	270	390	23.03	76	0.61
	100	240	360	47.56	72	0.67
Mn	10	630	750	10.58	89	0.32
	50	270	390	23.07	76	0.62
	100	210	390	42.65	70	0.92

Figure 7.4 displays the breakthrough curves for different influent concentrations of Mn(II). From the figure it is clear that the breakthrough and exhaustion times were inversely related to the initial Mn(II) concentration and with the increase in Mn(II) concentration from 10 to 100 mg/L, the corresponding t_b and t_e decreased from 630 to 210 min, and 750 to 390 min respectively. The adsorption capacity and MTZ length were increased from 10.58 to 42.65 cm and from 0.32 to 0.92 cm, respectively, with the increase in initial metal concentration from 10 to 100 mg/L, whereas the %R was decreased from 89 to 70%.

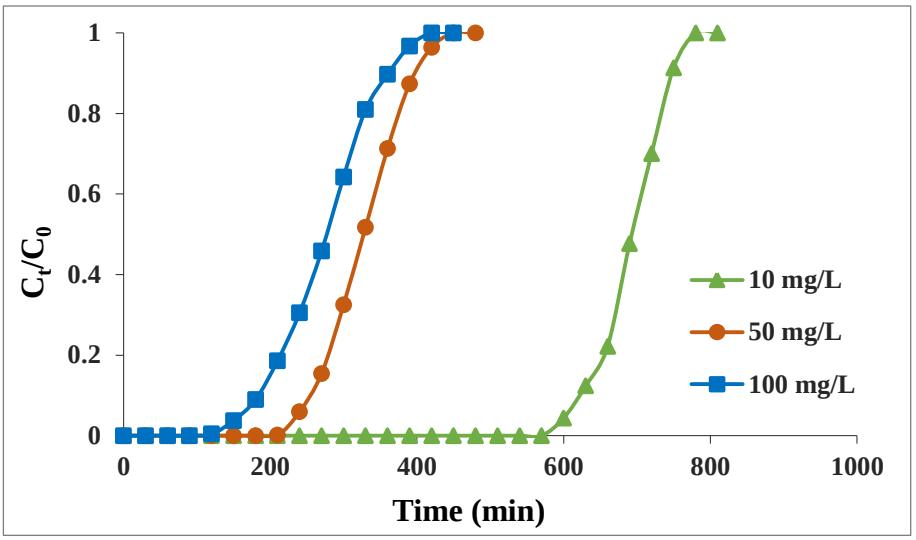

Figure 7.4: Effect of initial Mn(II) concentration on breakthrough curves (flow rate:2.0 mL/min, bed height: 2.0 cm, pH 7).

After analysing the effects of the initial metal concentration on Pb, Cd, Mn and Zn removal and considering the concentration of real industrial wastewater, the optimum concentration was determined as 50 mg/L and it was chosen for the following experiments.

7.3.1.2. Effect of flow rate

The effect of flow rate on the adsorption of Pb, Cd, Zn and Mn using P(St-DVB)/CuNi BNC were evaluated by varying the flow rate (1, 2, and 3 mL/min) while the influent metal ion concentration was kept constant at 50 mg/L and the bed height was 2 cm. The parameters determined from breakthrough curves at different flow rates are given in Table 7.4.

The breakthrough curves clearly show that, the breakthrough occurred significantly faster with increase in flow rate (Figure 7.5 to 7.8). This might be due to the inadequate residence time of the heavy metals in the column and decreased diffusion of heavy metals into the pore of the adsorbent at higher flow rates (Bulgariu and Bulgariu, 2013; Han et al., 2009). Meanwhile, the calculated values of the adsorption capacity and the removal efficiency were found to be decreases with an increase in flow rate from 1 to 3 mL/min. The reduction in q_e values at higher flow rates can also be attributed to the insufficient contact time required for the heavy metals to interact with the adsorbent. The mass transfer zone (MTZ) increased with increasing flow rate and similar observation was reported by Bulgariu and Bulgariu (2013) ((Bulgariu and Bulgariu, 2013).

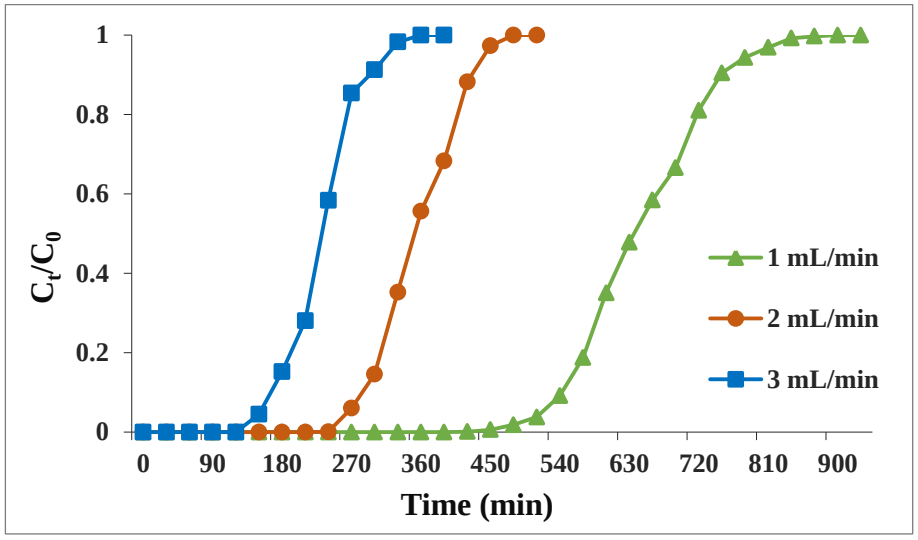

Figure 7.5: Effect of flow rate on breakthrough curves (initial Pb(II) concentration: 50 mg/L, bed height: 2.0 cm, pH 5).

It can be seen from Figure. 7.5, as the flow rate increases from 1 mL/min to 3 mL/min, time to reach the lead breakthrough time decreases from 540 to 150 min. Similarly, the saturation time was also observed to decrease from 750 to 300 min. The estimated lead removal efficiencies were 86, 72 and 64% for flow rates of 1, 2 and 3 mL / min, respectively. It was also found that, the adsorption capacity of the column decreases from 24.06 to 23.34 mg/g and 23.34 to 22.55 mg/g with increased flow rate.

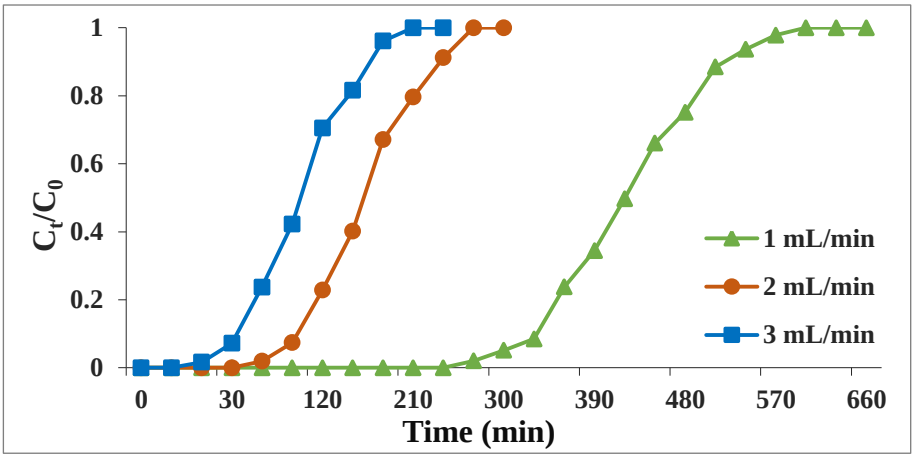

Figure 7.6: Effect of flow rate on breakthrough curves (initial Cd(II) concentration: 50 mg/L, bed height: 2.0 cm, pH 7).

Similar results were also obtained for cadmium ions and it was shown in Figure 7.6. As the flow rate of cadmium ions increases from 1 mL/min to 3 mL/min, the t_b and t_e decreases respectively from 330 to 30 min and 510 to 180 min. The adsorption capacities for flow rates of 1, 2 and 3 mL / min were 16.70, 15.05 and 11.86 mg/g, respectively and the percentage removal obtained for corresponding flow rates were 78, 64 and 54%, respectively.

Table 7.4

Parameters obtained from the breakthrough curves of the fixed bed column.

Metal	Flow rate (mL/min)	t_b (min)	t_e (min)	q_e (mg/g)	%R	MTZ (cm)
Pb	1	540	750	24.06	86	0.56
	2	270	420	23.34	72	0.71
	3	150	300	22.55	64	1.0
Cd	1	330	510	16.70	78	0.70
	2	150	300	15.05	64	1.0
	3	30	180	11.86	54	1.6
Zn	1	570	750	25.79	84	0.48
	2	270	390	23.03	76	0.61
	3	180	300	22.94	67	0.80
Mn	1	570	760	24.13	81	0.50
	2	270	390	23.07	76	0.62
	3	170	290	22.86	69	0.83

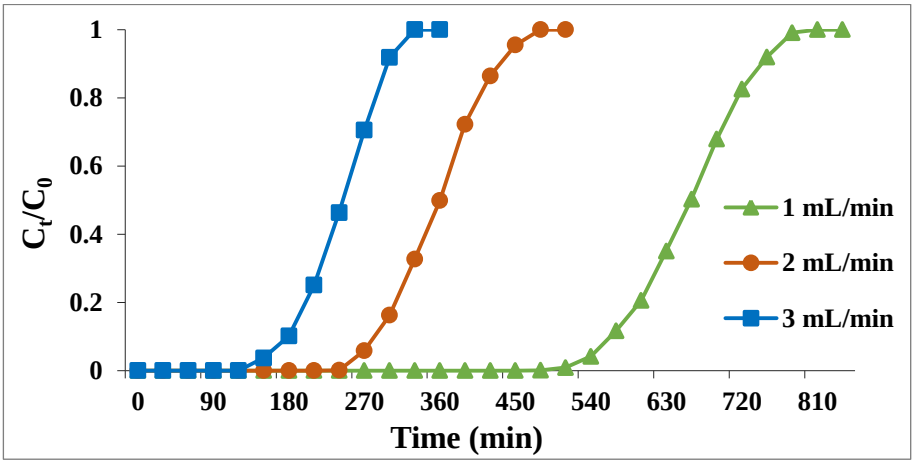

Figure 7.7: Effect of flow rate on breakthrough curves (initial Zn(II) concentration: 50 mg/L, bed height: 2.0 cm, pH 7).

The Zn(II) adsorption capacity for tested flow rates of 1, 2 and 3 mL/min were25.79, 23.03 and 22.94 mg/g, respectively, and the q_e for Mn(II) were 24.13, 23.07 and 22.86 mg/g, respectively. The percentage removal obtained for zinc were 84, 76 and 67% for the flow rates of 1, 2 and 3 mL/min, respectively. Whereas, for manganese it was 81, 76 and 69%. Specifically, at the higher flow rate of 3 mL/min the breakthrough of zinc was reached earlier (180 min) compared to the lower flow rate of 1 mL/min (570 min) (Figure 7.7). In the case of manganese, the breakthrough occurred at 170 min and 570 min for flow rates of 3 and 1 mL / min, respectively (Figure 7.8). As the flow rate increased from 1 to 3 mL/min, the exhaust time was found to decrease from 750 to 300 min and 760 to 290 min, respectively, for zinc and manganese.

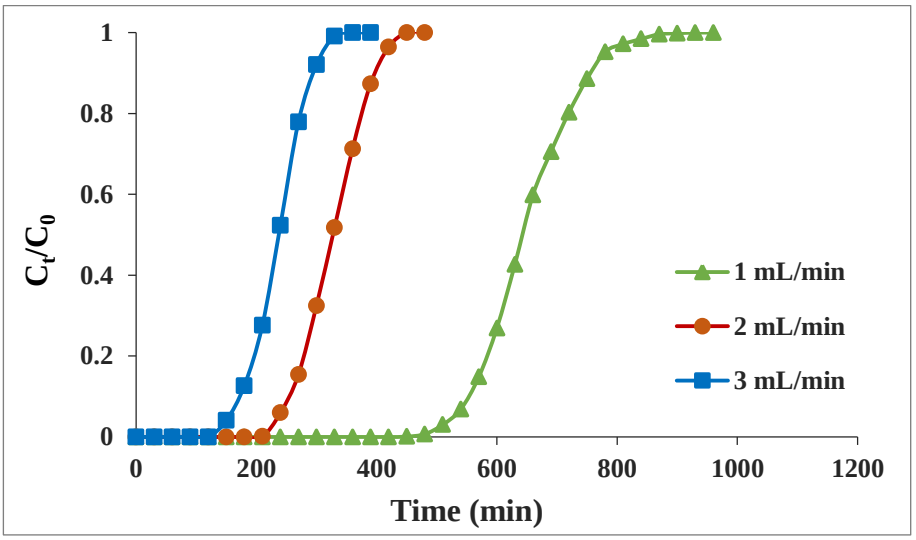

Figure 7.8: Effect of flow rate on breakthrough curves (initial Mn(II) concentration: 50 mg/L, bed height: 2.0 cm, pH 7).

Considering the results, the best performance was obtained at the lowest flow rate of 1.0 mL/min. Nevertheless, at this flow rate, the run time and energy costs were very high, so the flow rate of 2.0 mL/min was applied to the next experiments.

7.3.1.3. Effect of bed height

The effect of bed heights was studied by increasing it from 2 to 6 cm at a constant flow rate of 2 mL/min and an inlet heavy metal concentration of 50 mg/L. The resulting lead, cadmium, zinc, and manganese breakthrough curves obtained at three different adsorbent masses can be observed in Figures. 7.9, 7.10, 7.11 and 7.12, respectively, and the values of the experimental breakthrough parameters are summarized in Table 7.5.

An increase in t_b, q_e and %R was observed with an increase in bed height. This could be attributed to the fact that, there is an increase in the dose of absorbents in larger beds, which provide greater surface area as well as higher number of adsorption sites (Sarkar and Das, 2016; Baral et al., 2009). Jain *et al.* (2013) also reported a positive correlation between the adsorption capacity and bed height (Jain et al., 2013). It was also observed that the values of MTZ increased with an increase in bed height and this may be due to the increase in contact time for metal adsorption because of the higher adsorbent dosage.

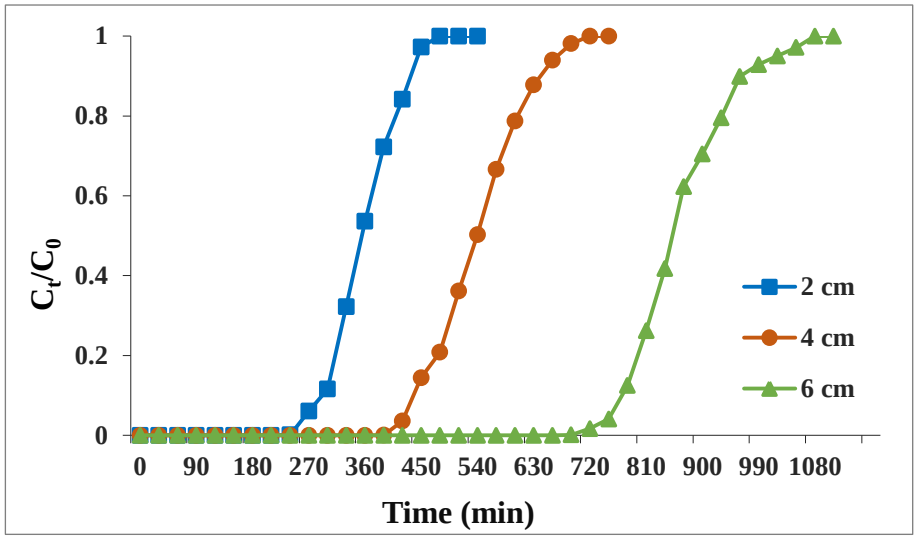

Figure 7.9: Effect of bed height on breakthrough curves (flow rate: 2.0 mL/min, initial Pb(II) concentration: 50 mg/L, pH 5).

In the present study, the breakthrough time of lead and its adsorption capacity were increased from 23.34 to 25.66 mg/g and from 270 to 780 min, respectively, with increasing bed heightfrom 2-6 (Figure 7.9). It was also observed that, the lower bed depth saturated earlier (t_e: 420 min) than the higher bed depth (t_e: 990 min). 72% to 87% of lead was removed by P(St-DVB)/CuNi BNC when bed height of the adsorbent varied from 2-6 cm.

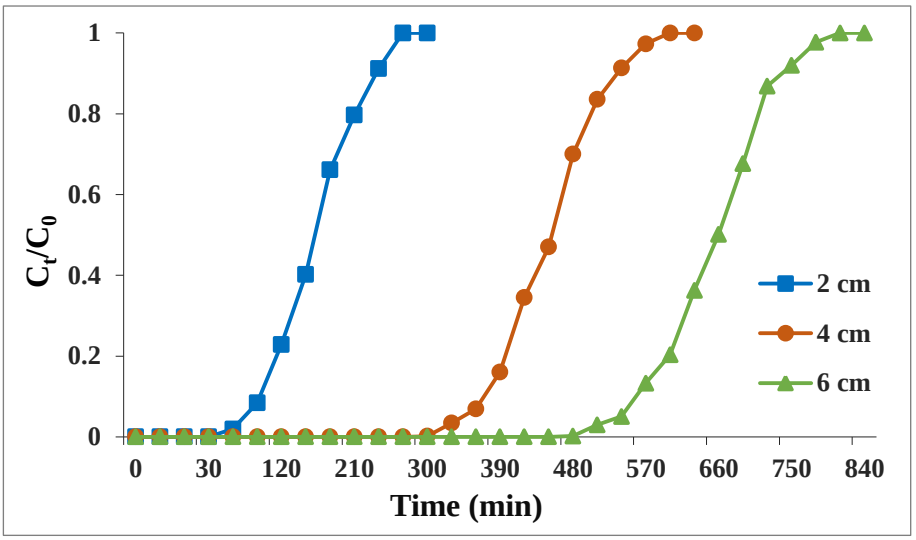

Figure 7.10: Effect of bed height on breakthrough curves (flow rate: 2.0 mL/min, initial Cd(II) concentration: 50 mg/L, pH 7).

The breakthrough: exhaustion time of Cd(II) were 150:300, 360:540, and 570:750 min for 2, 4 and 6 cm bed height, respectively (Figure 7.10). The calculated values of the adsorption capacities were shown that it was increasing from 15.05 to 20.68 mg/g with increasing bed height from 2 to 6 cm, respectively, for cadmium. The results also revealed that by increasing bed height from 2 cm to 6 cm the percentage Cd removal increased from 64% to 87% and the length of MTZ were increased from 1 to 1.44 cm.

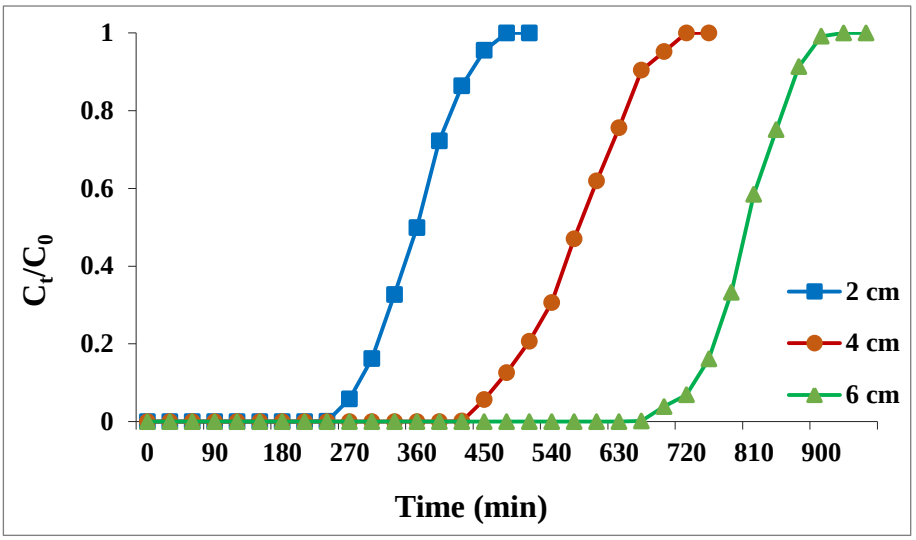

Figure 7.11: Effect of bed height on breakthrough curves (flow rate: 2.0 mL/min, initial Zn(II) concentration: 50 mg/L, pH 7).

In the case of zinc ions the adsorption capacity was found increasing from 23.03 to 26.06 mg/g with increasing bed depth from 2 to 6 cm respectively. As the bed height increased from 2 cm to 6 cm, the breakthrough time of zinc was found to increase from 270 to 720 min (Figure 7.11) and the percentage removal of Zn(II) were 76%, 86% and 92% for bed heights 2, 4 and 6 cm, respectively. These results are consistent with other observations throughout the study.

Table 7.5

Parameters obtained from the breakthrough curves of the fixed bed column.

Metal	Bead hight (cm)	t_b (min)	t_e (min)	q_e (mg/g)	%R	MTZ (cm)
Pb	2	270	420	23.34	72	0.71
	4	450	660	24.68	82	1.27
	6	780	990	25.66	87	1.27
Cd	2	150	300	15.05	64	1
	4	360	540	19.38	78	1.33
	6	570	750	20.68	87	1.44
Zn	2	270	390	23.03	76	0.61
	4	510	660	25.19	86	0.91
	6	720	870	26.06	92	1.03
Mn	2	270	390	23.07	76	0.62
	4	480	660	25.46	92	1.09
	6	750	930	26.05	95	1.16

In the case of manganese ions, the t_b:t_e were 270:390, 480:660, and 750:930 min for 2, 4 and 6 cm bed height, respectively (Figure 7.12). It was also observed that, the breakthrough time, %R and its adsorption capacity were increased from 23.07 to 26.05 mg/g, from 76 to 95% and from 270 to 750 min, respectively, with increasing bed height from 2 to 6.

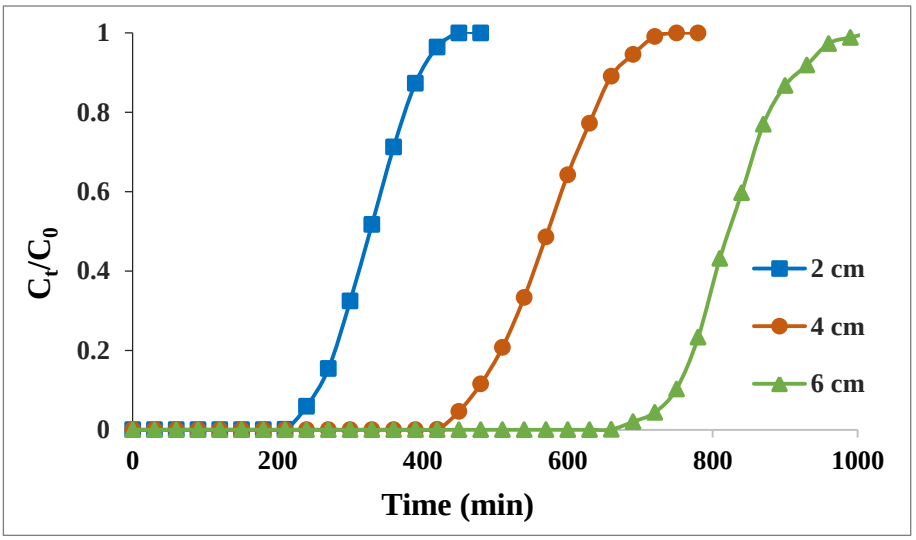

Figure 7.12: Effect of bed height on breakthrough curves (flow rate: 2.0 mL/min, initial Mn(II) concentration: 50 mg/L, pH 7).

After analysing the effects of bed height on heavy metal removal and considering the amount of adsorbent needed, 2 cm was chosen as the optimum bed height.

From the fixed bed column and breakthrough parameters, it was concluded that zinc and manganese required the longest time period to reach the breakthrough concentration and cadmium required the least time, which revealed that adsorption of Zn ~ Mn is highest, and cadmium is lowest onto P(St-DVB)/CuNi BNC among the four metals. These results were consistent with the findings established from our batch study. Furthermore, for the same initial metal ion concentration (10 mg/L), the adsorption capacities of the nanocomposite in column experiment for Pb (q_e: 10.33), Cd (q_e: 6.40), Zn (q_e: 10.81) and Mn (q_e: 10.58) were higher than its corresponding

equilibrium adsorption capacity (q_e: 4.52, 3.0, 5.10 and 5.98, respectively, for Pb, Cd, Zn and Mn) in batch experimental system (2g/L P(St-DVB)/CuNi BNC dose). The discrepancy between the adsorption capacities in batch and column experimental systems may be due to the reason that the pores of the nanocomposite favour improved solid-state diffusion in fixed bed column mode compared to the batch operation (Gupta et al., 2001).

Hence, to conclude, the lower influent concentration, lower flow rate, and higher bed height increased the adsorption of metal ions into the P(St-DVB)/CuNi BNC microspheres.

7.3.2. Theoretical Models

Thomas, Yoon–Nelson and Adams–Bohart models were applied to the breakthrough curves obtained for different initial metal ion concentration, flow rate, and bed height in order to predict the breakthrough behaviour. The values of characteristic parameters are presented in Tables 7.6, 7.7 and 7.8 respectively.

7.3.2.1. Thomas model

The experimental column data was fitted to the Thomas model to determine the Thomas rate constant (k_{Th}) and maximum adsorption capacity (q_0). The values of k_{Th}, q_0 and regression coefficient (R^2) at three different initial influent metal ion concentrations, flow rates and bed heights are listed in Table 7.6. As observed in Table 7.6, the values of q_0 calculated from Thomas model [Eq. (1)] were comparable to the experimental q_e values. It was found that the values of q_0 increased

with increasing influent metal ion concentration and bed depth but decreased with increase in flow rate. This can be interpreted as the fact that for a given bed depth, the adsorption capacity would increase with a lower flow rate and higher influent metal ion concentration. On the other hand, k_{Th} values decrease significantly with increasing influent metal ion concentration, because the adsorption driving force is given by the concentration difference between the adsorbed metal ion on the adsorbent and its concentration in the solution, and the obtained results correlate with the data of other researchers (Sarin et al., 2006; Wu and Yu, 2008). Furthermore, k_{Th} increased with increasing flow rates, whereas it reduced with increasing bed height. At higher flow rates, the increase in k_{Th} values can be attributed to the decrease in the mass transport resistance and the decrease in k_{Th} values with increase in bed height may be due to increase in mass transport resistance. Maximum Thomas adsorption capacities were achieved up to 42.75, 23.04, 47.71 and 42.35 mg/g for heavy metals, Pb, Cd, Zn and Mn, respectively.

The correlation coefficient R^2 values range from 0.971 to 0.996 for lead, 0.979 to 0.999 for cadmium, 0.966 to 0.996 for zinc and 0.974 to 0.997 for manganese. This indicates that, the Thomas model exhibited an excellent fit to the experimental data for all the parameters studied. The Thomas model predicts monolayer adsorption/desorption reaction kinetics, which is also confirmed by our earlier batch sorption studies, where the experimental data fitted very well with the Langmuir isotherm. Hence, we can conclude that the experiment follows monolayer adsorption and also external and internal diffusions were not the rate-limiting steps (Chen et al., 2012; Han et al., 2009).

Table 7.6

Parameters of the Thomas model under different conditions.

Parameters	Pb			Cd			Zn			Mn		
	k_{Th} (mL/min mg)	q_0 (mg/g)	R^2	k_{Th} (mL/min mg)	q_0 (mg/g)	R^2	k_{Th} (mL/min mg)	q_0 (mg/g)	R^2	k_{Th} (mL/min mg)	q_0 (mg/g)	R^2
Influent metal conc. (mg/L)												
10	3.50	10.79	0.971	3.05	6.90	0.979	3.58	11.41	0.982	3.48	11.04	0.990
50	0.66	23.38	0.989	0.66	16.22	0.996	0.65	23.52	0.996	0.62	25.15	0.992
100	0.26	42.75	0.996	0.29	23.04	0.999	0.27	47.71	0.978	0.30	42.35	0.979
Flow rate (mL/min)												
1	0.50	24.18	0.985	0.48	17.11	0.994	0.59	25.91	0.972	0.49	25.48	0.990
2	0.66	23.38	0.989	0.66	16.22	0.996	0.65	23.52	0.996	0.62	25.15	0.992
3	0.76	22.34	0.995	0.72	12.01	0.991	0.74	23.14	0.994	0.82	24.62	0.974
Bead height (cm)												
2	0.66	23.38	0.989	0.66	16.22	0.996	0.65	23.52	0.996	0.62	25.15	0.992
4	0.49	24.96	0.992	0.55	19.85	0.998	0.46	25.12	0.992	0.47	25.63	0.997
6	0.43	25.88	0.977	0.52	20.64	0.993	0.42	25.83	0.966	0.45	27.86	0.997

7.3.2.2. Yoon–Nelson model

The Yoon–Nelson model was applied to investigate the breakthrough behaviour of Pb(II), Cd(VI), and Zn(II) adsorption on P(St-DVB)/CuNi BNC. The values of the Yoon-Nelson model rate constant k_{YN}, 50 % breakthrough time τ and the regression coefficient (R^2) obtained for all breakthrough curves are given in Table 7.7. It is clear from the obtained results that, the k_{YN} was lower at higher influent metal ion concentrations. This is because the competition between the adsorbate species for the adsorption sites increases when the metal ion concentration increases, which ultimately results in a higher rate of retention. Moreover, the values of k_{YN} were found to increase with an increase in flow rates, whereas a reverse trend is observed for bed heights. However, the values of τ, was found to be significantly decreased with increasing initial influent concentration and flow rate, while the τ values of increased with an increase in bed height. This is due to the fact that, the saturation of the column was attained quickly when the initial influent concentration and flow rate increase, but considerably slower saturation of the column occurs at higher bed heights. Moreover, the correlation coefficient values were found to be between 0.974 and 0.996 for lead, 0.979 and 0.999 for cadmium, 0.966 and 0.996 for zinc and 0.974 to 0.997 for manganese, which shows the Yoon-Nelson model fitted well to the experimental data along with the Thomas model.

Table 7.7

Parameters of the Yoon–Nelson model under different conditions.

Parameters	Pb			Cd			Zn			Mn		
	k_{YN} (min^{-1})	τ (min)	R^2	k_{YN} (min^{-1})	τ (min)	R^2	k_{YN} (min^{-1})	τ (min)	R^2	k_{YN} (min^{-1})	τ (min)	R^2
Influent metal conc. (mg/L)												
10	0.035	618.56	0.974	0.041	425.00	0.979	0.036	721.82	0.982	0.035	689.29	0.990
50	0.032	303.07	0.989	0.033	225.35	0.996	0.031	326.31	0.996	0.031	324.11	0.992
100	0.027	268.90	0.996	0.029	147.94	0.999	0.027	307.00	0.978	0.029	303.53	0.979
Flow rate (mL/min)												
1	0.025	563.59	0.981	0.024	423.12	0.994	0.030	654.0	0.972	0.025	645.19	0.990
2	0.032	303.07	0.989	0.033	225.76	0.996	0.031	326.31	0.996	0.031	324.11	0.992
3	0.038	192.33	0.995	0.036	96.50	0.991	0.037	212.85	0.994	0.042	224.11	0.974
Bead height (cm)												
2	0.032	303.07	0.989	0.033	225.76	0.996	0.031	326.31	0.996	0.031	324.11	0.992
4	0.024	534.57	0.992	0.028	450.56	0.998	0.025	571.58	0.992	0.030	568.52	0.980
6	0.022	848.88	0.977	0.026	654.28	0.993	0.023	792.94	0.966	0.027	827.50	0.997

Table 7.8

Parameters of the Adams-Bohart model under different conditions.

Parameters	Pb			Cd			Zn			Mn		
	$k_{AB}\times10^{-3}$ (L/mg min)	N_0 (mg/L)	R^2	$k_{AB}\times10^{-3}$ (L/mg min)	N_0 (mg/L)	R^2	$k_{AB}\times10^{-3}$ (L/mg min)	N_0 (mg/L)	R^2	$k_{AB}\times10^{-3}$ (L/mg min)	N_0 (mg/L)	R^2
Influent metal conc. (mg/L)												
10	1.48	2448.99	0.951	1.82	1561.83	0.929	1.73	2493.21	0.963	2.00	2377.48	0.960
50	0.299	6198.84	0.901	0.403	4054.01	0.878	0.336	5661.61	0.895	0.278	6395.76	0.923
100	0.118	11837.1	0.832	0.165	6835.08	0.916	0.126	12789.4	0.935	0.116	12876.8	0.872
Flow rate (mL/min)												
1	0.269	6376.22	0.78	0.243	4147.48	0.888	0.312	5898.80	0.849	0.274	6544.63	0.720
2	0.299	6198.84	0.901	0.403	4054.01	0.878	0.336	5661.61	0.895	0.278	6395.76	0.923
3	0.332	5856.28	0.865	0.442	3699.80	0.805	0.422	5463.48	0.949	0.346	6183.06	0.890
Bead height (cm)												
2	0.299	6198.84	0.901	0.403	4054.01	0.878	0.336	5661.61	0.895	0.278	6395.76	0.923
4	0.247	6146.78	0.836	0.276	4308.68	0.897	0.225	5318.43	0.926	0.210	5403.83	0.871
6	0.214	5419.16	0.781	0.277	3989.25	0.894	0.321	4668.57	0.925	0.252	4982.15	0.840

7.3.2.3. Adams-Bohart model

The values of kinetic constant, k_{AB} and saturation concentration, N_0 were calculated from the linear plots with respect to influent heavy metal concentration, flow rate, and bed height using the Adams-Bohart model is given in Table 7.8 along with their correlation coefficients (R^2). The value of k_{AB} decreased with both increasing influent concentration and depth of the column bed depth, while it increased with increasing flow rate. At the same time the N_0 values were reduced with increasing bed height and flow rate, nevertheless; it increased with increasing influent metal concentration. This trend can be explained by the fact that as the bed height increases, more active sites become accessible for adsorption, resulting in a higher overall metal absorption but lower adsorption per unit volume. However, at higher flow rates, the amount of adsorbate entering the column was higher, which resulted an early saturation of the bed. Higher values of N_0 at higher influent metal ion concentration may be due to higher loading of metal ions on the adsorbent during the limited contact time. The value of R^2 fluctuates from 0.781 to 0.951 for lead, 0.805 to 0.929 for cadmium, 0.849 to 0.963 for zinc, and 0.720 to 0.960 for manganese. The R^2 values show that the experiment data are fairly well described by the model, but it's not the most suitable model to describe the experimental breakthrough curve.

In a comparison of predicted models, it is observed that the R^2 values of the Thomas and Yoon–Nelson models are higher than the Adams–Bohart model. Therefore, it can be concluded that both Thomas and Yoon–Nelson models can be used to predict the removal

of metal ions by a fixed-bed column packed with P(St-DVB)/CuNi BNC microbeads.

7.3.3. Desorption Experiments

The desorption of heavy metals from P(St-DVB)/CuNi BNC microbeads was performed with 0.5 M concentrations of NaOH solution because this concentration of NaOH showed good desorption efficiency of heavy metal ions in batch desorption experiments. Desorption studies were conducted in up to three successive adsorption–desorption cycles. From sorption–desorption data, it was indicated that, the removal efficiency (%) decreased with each adsorption-desorption cycle progress for all instigated metals. Total regeneration was not achieved due to incomplete desorption of metal ions from the adsorbent (Table 7.9). The removal efficiency decreased from 70% to 56%, 63% to 50%, 73% to 59%, and 74% to 53%, respectively, for Pb, Cd, Zn and Mn, respectively, from the first to the fourth cycle. This preliminary study suggests that the P(St-DVB)/CuNi BNC microbeads is a potential adsorbent for the removal of heavy metal ions in a fixed bed column with repeated usage.

Table 7.9

Desorption studies of the studied ions from P(St-DVB)/CuNi BNC microspheres.

Metals	**Removal efficiency (%)**			
	Cycle 1	**Cycle 2**	**Cycle 3**	**Cycle 4**
Pb	70%	67%	63%	56%
Cd	63%	61%	57%	50%
Zn	73%	70%	66%	59%
Mn	74%	69%	62%	53%

7.4. Conclusion

This study concludes that the removal of heavy metals such as lead, cadmium, zinc, and manganese onto the P(St-DVB)/CuNi BNC microbeads in a fixed bed column was feasible and effective. The effects of different process parameters such as initial metal concentration, flow rate, and bed height on the performance of the adsorption column were investigated, and the breakthrough curves were plotted. The experimental breakthrough parameters were calculated, and we have found that adsorption capacity was increased with increasing initial metal concentration and with bed height; and decreasing flow rate. From breakthrough curves and parameters, we can conclude that lower influent concentration, lower flow rate, and higher bed height increased the adsorption of metal ions into the P(St-DVB)/CuNi BNC microspheres. The breakthrough obtained and the column kinetic parameters were successfully predicted with mathematical models such as the Thomas, Yoon-Nelson, and Adams–Bohart models and both Thomas and Yoon–Nelson models were shown to be in good agreement with the experimental results for all the operating conditions studied. Successful desorption of heavy metals from P(St-DVB)/CuNi BNC microbeads were performed using NaOH solution and showed good reusability of the adsorbent in the bed column during four adsorption–desorption cycles. The results show that P(St-DVB)/CuNi BNC microbeads is an effective and low-cost adsorbent and can be used in real time large scale industrial wastewater treatment processes for the removal of heavy metals.

Chapter 8

Fabrication of a low-cost water filter for the removal of heavy metals

8.1 Introduction

An affordable point-of-use domestic water purifier is one of the essential requirements for human life. The most important goal of any such innovation should be to increase the effectiveness and reduce the cost of water purification. There are products on the market with similar goals, but no efficient solution has been found due to the ineffectiveness and high cost of purifying materials, membranes, and designs.

In a study, Sankar et al. demonstrated an affordable water purification device based on iron oxyhydroxide-chitosan granular composite materials and could be able to filter 400 L of water spiked with 1 ppm of arsenic (As^{5+}) using 20 grammes of granular composite at a flow rate of 50 mL/min (Sankar et al., 2013).

In a different study, Kumar *et al*. have developed an affordable water filtration system using confined metastable 2-line ferrihydrite (CM2LF) as a potential solution to remove arsenic from drinking water. They showed that As(III), As(V), and As(mix) were eliminated below the World Health Organization (WHO) limit of 10 g L^{-1} for 1100 L synthetic and natural tap water samples using 60 g of the

composite at a flow rate of 12 to 15 mL/min and this only cost US $2 (Kumar et al., 2017).

TATA developed a water purifier system TATA Swach that uses Rice Husk Ash (RHA) impregnated with silver nanoparticles to kill waterborne pathogens. In addition to silver nanoparticles, TATA also produces water purifiers that use ultraviolet (UV) radiation. As it can filter 3-4 litres of water per hour, this device is quite useful in the kitchen. However, it does not have the capacity for chemical treatment. The Tata Swach Cristella Plus (total 18 L) costs Rs. 1700 and comes with a 9-litre storage unit (Swach, 28.10.2014).

HUL Pureit Classic is a domestic water purifier that incorporates numerous water treatment techniques. Feed water is processed by a clarifier, activated carbon module, a microfiber filter, and gradual chlorine dispenser. It has a 9L storage capacity and costs Rs 2600 (Pureit, 28.10.2014).

Another similar product is Aquasure Xtra Tuff, which costs Rs 2000 and has an 8 L water storage capacity. It draws in up to 10 NTU of water and filters it through a carbon block, sediment filter, particulate filter and an unspecified disinfectant (Aquasure, 28.10.2014).

Our previous studies have shown that, the synthesized bimetallic nanocomposites are efficient in removing bacteria and heavy metals from water. Moreover, the granular bimetallic nanocomposite material can be easily packed in a prototype cartridge and could be used to

create a hand-held water filter that allows polluted water to flow continuously in an antigravity fashion for a longer contact time without using any external energy. Therefore, in this chapter, we are describing the fabrication of a simple, low-cost, and portable water purification device based on the synthesised P(St-DVB)/CuNi bimetallic nanocomposite microspheres for the removal of heavy metals.

8.2. Experimental

8.2.1. Materials

All chemicals used were of analytical reagent grade and purchased from Merck. Heavy metal analysis was conducted using the Thermofisher M series atomic absorption spectrophotometer (AAS). Distilled water was used throughout the experiment for all solution preparation unless otherwise noted. Heavy metal stock solutions were purchased from Merck. The cartridge, filtration unit, and the water storage tank/container were purchased from Amazon, India. The water tap was purchased from local suppliers.

8.2.2. Fabrication of a Water Filter

After the performance of the P(St-DVB)/CuNi BNC microspheres was evaluated in column experiments, a portable water purification device was developed. The entire set-up comprises three major assemblies, a storage container, tap, and a filtration unit (Figure 8.1). The storage container is a cylindrical-shaped fibre container that was used to store polluted water. It has a cover that can be removed to

add raw water to the container. A fiber tap was attached to the storage container and it connects the storage container to the filtration unit.

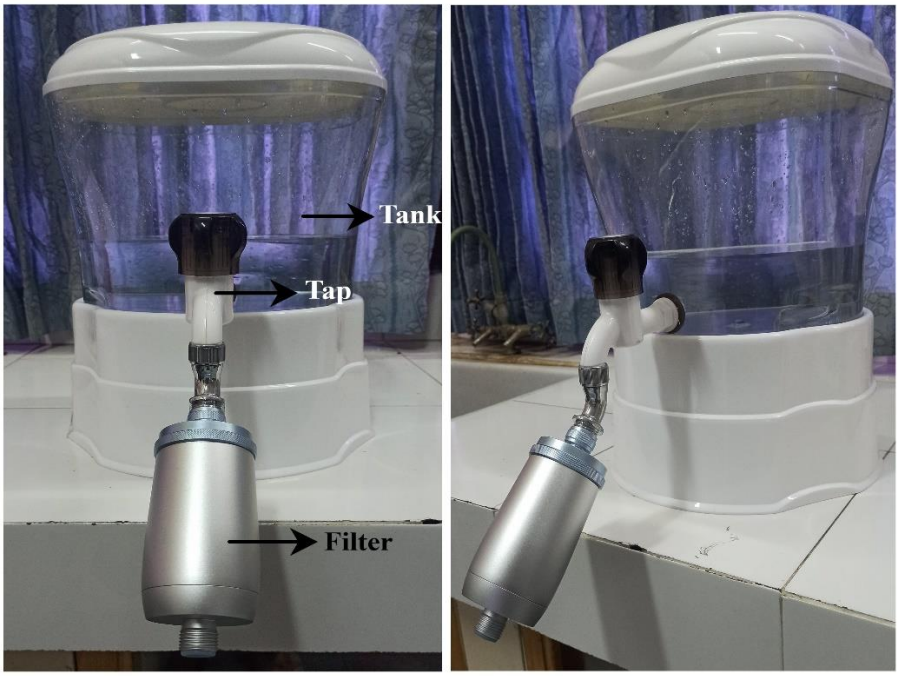

Figure 8.1: Photographs of the apparatus for the water purification device used for filtration containing lead, cadmium, manganese, and zinc contaminated water.

Filtration includes a cylindrical shaped hollow steel jar and a water purification cartridge (Figure 8.2 and Figure 8.3(a)). The cartridge is placed inside the steel jar. The steel jar had openings on both sides (Figure 8.2 (b)), and the cartridge was inserted into the jar through that opening (Figure 8.2 (c)). Both sides of the steel jar have a screw-threaded socket adapted to fit on a water supply outlet tap.

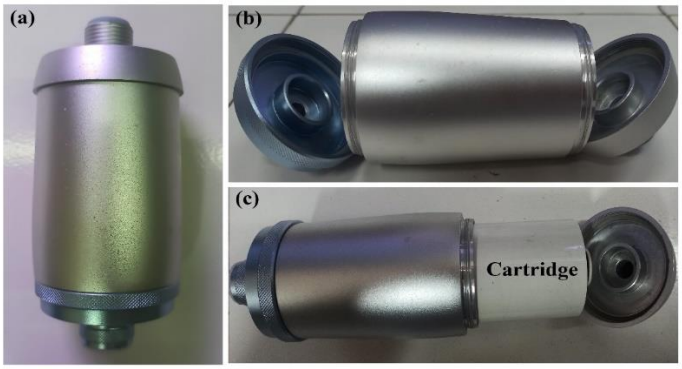

Figure 8.2: Photographs of the water filter include (a) a side view of the filter, (b) a view of the apertures, and (c) the filter after the cartridge has been partially inserted.

The cartridge is made of fibre and has a cylindrical shape with a diameter of 50 mm and a height of 100 mm (Figure 8.3 (a)). One side of the cartridge has an opening and through that opening, approximately 20 g of the composite (particle size: 110 m) were packed into the cartridge together with small pebbles, coarse sand, and fine sand (Figure 8.4). Each layer is separated with medical grade cotton and Gauze.

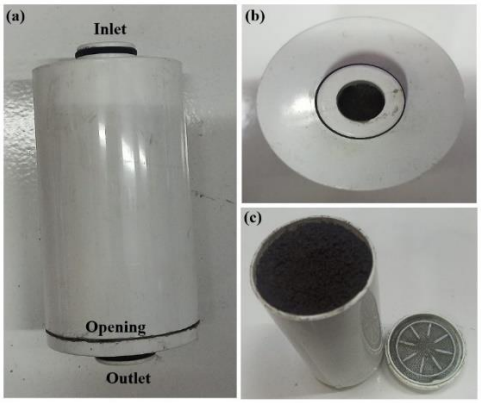

Figure 8.3: Photographs of the cartridge used in the filtration unit for the study (b) top view of the cartridge.

After that, the cartridge was placed inside the steel jar and the filtration unit was then assembled in an antigravity fashion. In a typical use, the polluted water is poured into the tank. When we turn on the tap, the pressure due to the water head in the tank drives the water into the water filter via the water tap, and the water flow can be adjusted with the help of the tap. The treated water was collected from the outlet of the filtration unit (Figure 8.1).

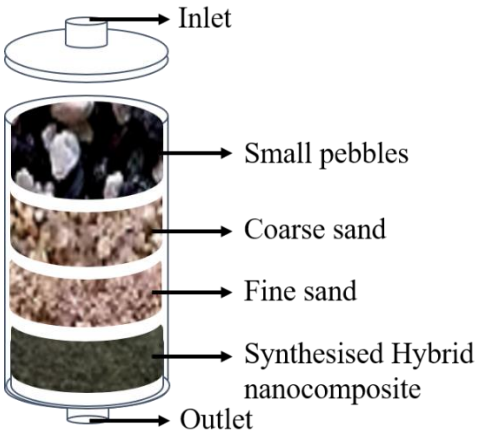

Figure 8.4: Schematic diagram of the cartridge.

8.2.2.1. Removal of heavy metals using the fabricated water filter

The input water contains 1 mg/L of Pb(II), Cd(II), Mn(II), and Zn (II), and it was passed at a flow rate of 25 mL/min. The flow rates were optimised for the best performance, and a slight fluctuation in the pressure head of the input water container caused the flow rate to vary somewhat during the long experiment. The filtrate collected from the

filter was analysed using an inductively coupled plasma optical emission spectrometer (ICP-OES).

8.3. Results and Discussion

8.3.1. Removal of heavy metals using the fabricated water filter

The cartridge consists of four layers in which small pebbles, coarse sand, fine sand, and encapsulated nanocomposite microbeads were arranged from top to bottom, respectively. Therefore, the filter filters water in four stages by the filter as it moves from pebbles to coarse sand to fine sand to encapsulated nanocomposite microbeads. Pebbles are lightweight, porous and contain numerous crevasses, providing a great surface area for trapping tiny bugs, sediments, and other large particles present in water. The fine pores in the ceramic candle remove fine dirt particles from the contaminated water. Sand is one of the oldest known methods of treating water, and it is still used in most municipal water treatment plants to remove impurities and flocculation remains. To "drive" the water through the filtering material, there must be a driving pressure. Since we desire to use gravitational force in the system. The main benefit of the fabricated filter is its lower cost of production and lighter weight, owing to the use of fewer components.

The water filtration unit has two stages of water purification. A first stage of purification involves filtering untreated water using a combination of pebbles and sand to remove coarse and fine particulate matter, such as suspended particles and mud. A second stage of

purification involves the removal of any heavy metals by treating the water with porous P(St-DVB)/CuNi BNC microbeads, which have disinfection as well as adsorption properties. Usually, during the passage of water through the cartridges, contaminants in the water come into contact with the adsorbent inside the cartridges and are ultimately removed from the water. Therefore, BNC microbeads can adsorb heavy metals present in contaminated water as it passes through the porous microbeads.

After fabrication was completed, the system was tested to check for performance in terms of how efficient it is in terms of heavy metal removal. The test was carried out by passing contaminated water through the water filter. Freshly prepared feed water containing 1 mg/L of Pb(II), Cd(II), Mn(II), and Zn(II) was fed through the composite at a flow rate of 25 mL/min. The treated water was collected from the filter outlet at every 1hr time interval and analysed for Pb(II), Cd(II), Mn(II), and Zn(II) using ICP-OES. Furthermore, the performance of the water purification system was tested by comparing the concentrations in the purified water and the untreated water, as shown in Figure 8.5 (a) to (d).

The filter was run for 70.5 L of contaminated water and the results obtained are given in figure 8.5 (a) to (d). It was found that Pb(II), Cd(II), Mn(II), and Zn(II) were removed below the limit of the World Health Organization (WHO) in 66 litters of synthetic contaminated water samples using 20 g of the composite without any reactivation. The breakthrough was achieved in between 44 and 45

hours (67 - 67.5 L) for all the four metals, that is, from time t = 0 to 44 hr, all metal ions introduced into the water filter are completely absorbed by the adsorbent present in the filter. As time increases, the adsorbent's binding sites become occupied with metal ions, and most of the ions passes through the adsorbent bed without being adsorbed. Therefore, a sudden increase in the concentration of metal ions was observed in the effluent after 45 hrs. Once the adsorbent is completely saturated, the metal ion concentration in the effluent levels out at around the same concentration as the contaminated water introduced into the column (C_0).

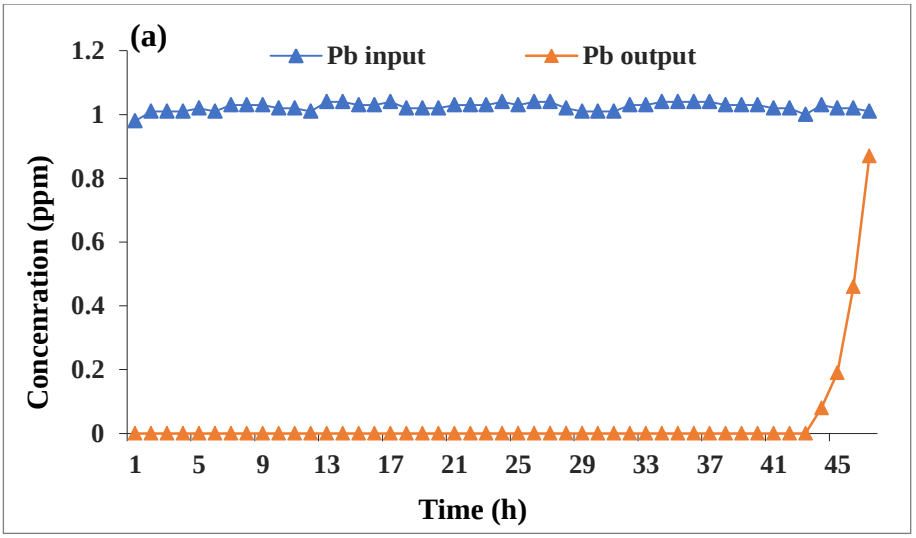

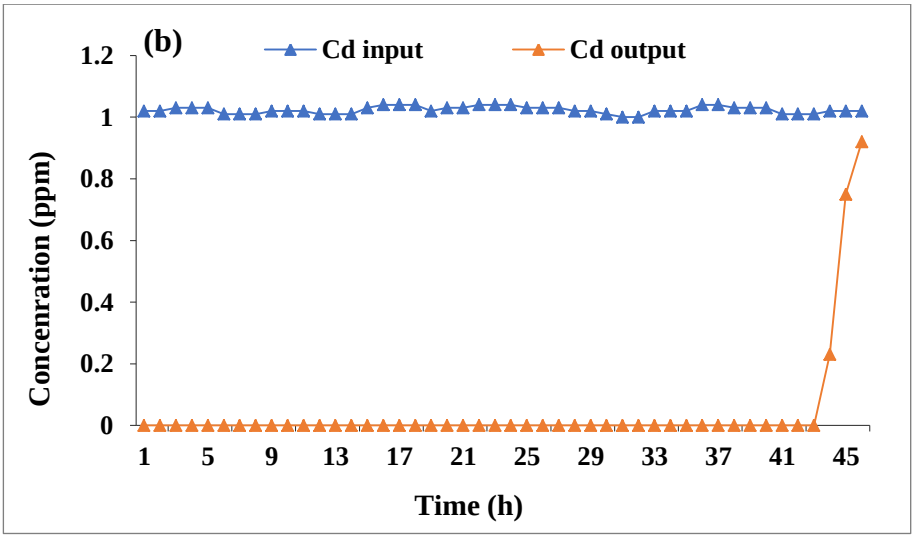
(b)
Cd input
Cd output
Concenration (ppm)
1.2
1
0.8
0.6
0.4
0.2
0
1
5
9
13
17
21
25
29
33
37
41
45
Time (h)

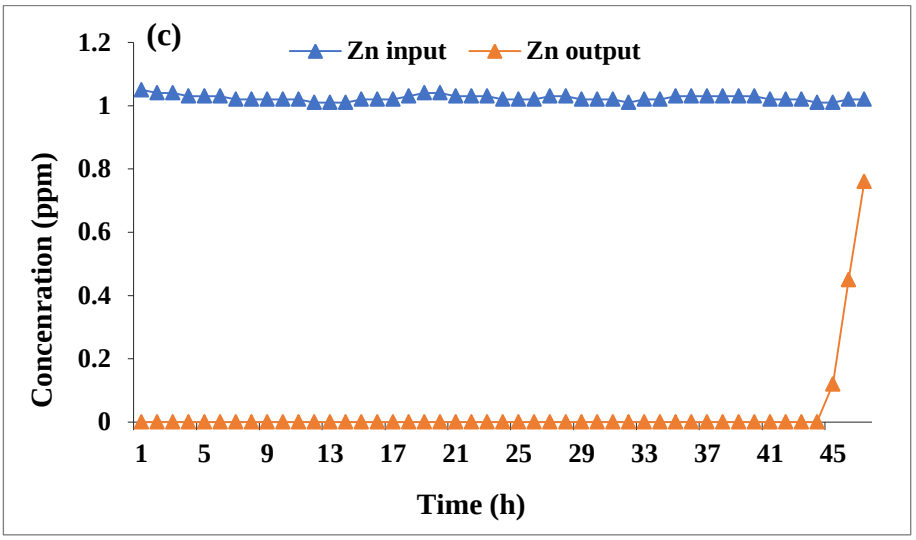
(c)
Zn input
Zn output
Concenration (ppm)
1.2
1
0.8
0.6
0.4
0.2
0
1
5
9
13
17
21
25
29
33
37
41
45
Time (h)

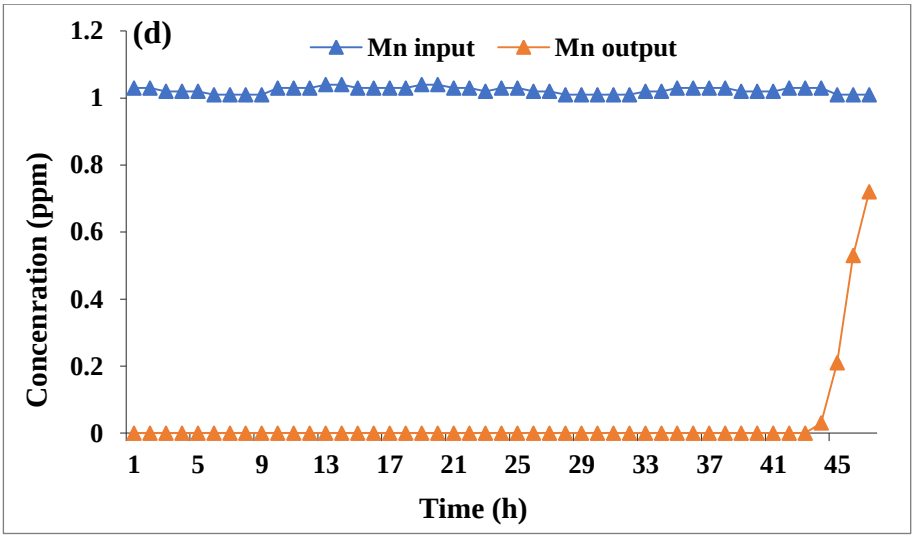

Figure 8.5: Breakthrough curves obtained (a) Pb(II), (b) Cd(II), (c) Zn(II), and (d) Mn(II)**.**

8.3.1.1. Advantageous

The most beneficial aspect of our filter was its potential to simultaneously remove all four heavy metals from 66 litres of contaminated water. Most of the other studies were concentrated on the removal of a single metal at a time. Moreover, these BNC microbeads have both disinfection and adsorption properties, which allows them to generate water that is free of microorganisms and heavy metals (Figure 8.6). Furthermore, the water purifying system is compact and portable and does not require an external source of energy to operate. Another advantage of this model is that the screw-threaded outlet neck of the filter may easily fit into the mouth of a water supply outlet such as a tap.

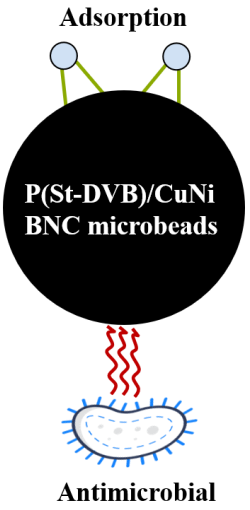

Figure 8.6: Schematic representation of the simultaneous adsorption and antimicrobial action of P(St-DVB)/CuNi BNC.

8.3.1.2. Affordability

This filter only costs less than Rs. 600/- even after all costs associated with chemicals, sediment prefilter, plastic assembly, and cartridge were taken into account. The cartridge's lifespan can be further extended by reactivating the composite, and this will reduce the cost even more. Therefore, it is intended that the invention will provide an incredibly simple yet highly efficient and affordable water purification device.

8.3.1.3. Disposal of waste

The disposal of the used/heavy metal adsorbed BNCs can be done in leach-free landfills after being subjected to multiple regenerations by suitable base treatment like 0.5 M NaOH. Toxicity

Characteristic Leaching Procedure (TCLP) suggests safe disposal of the adsorbent after saturation loading.

8.4. Conclusion

Successfully fabricated a low-cost, portable, and simple water purification device using the synthesised P(St-DVB)/CuNi BNC microspheres. It was found that Pb(II), Cd(II), Mn(II), and Zn(II) were removed below the limit of the World Health Organization (WHO) for about 66 L of water with an average flow rate of 25 mL/min using 20 g of the composite without any regeneration of the material. Additionally, BNC microbeads can inactivate microbiological pollutants and adsorb heavy metals present in contaminated water as it passes through the porous microbeads. Furthermore, the robustness of the BNCs prevents leaching of the CuNi BNPs, making them an excellent option for an industrially practicable material for providing safe water across the affected regions.

Chapter 9

Insights into the environmental impact of nanocomposite by assessing the morphological changes that have occurred in various plant and animal species

9.1 Introduction

Although nanotechnology has immense advantages in the field of drinking water treatment, there are still challenges to overcome, particularly with regard to the safe disposal of used nanomaterials and their potential risk to public health and the ecosystem. Therefore, the impact of a nanomaterial must be assessed not only in terms of its use but also in terms of its potential toxicity when released into the environment. A surface coating made of polymer or natural organic matter might reduce the toxicity of nanoparticles by preventing them from adhering to cells (Li et al., 2010). Therefore, addressing the impact of any functionalisation or stabilisation of the nanoparticles that might be performed during the synthesis process may also be important. Few studies indicate that the environmental fate and ecotoxicity of nanoparticles depends on a number of factors including particle size, shape, dose, duration of exposure, mode of administration, etc. (Kuang et al., 2016; Lei et al., 2016; Tiede et al., 2009). Composites based on less toxic materials may be useful for the purification of water in a wide range of geographical locations without the need for large input of energy.

In this chapter, we investigate the impact of both P(St-DVB)/CuNi BNC microspheres and CuNi BNPs on different species like Chlorella vulgaris, Mosquito ferns, Water Hyacinth, Water Hyssop, Ostracods, and Guppy. The results attained from all the toxicity studies are expected to add a new vision for understanding of its nanotoxicity on flora and fauna. All experiments were conducted using controls to compare the results.

9.2. Experimental

9.2.1. Materials

Test systems

(a) Algae: Chlorella vulgaris

(b) Plant systems: Mosquito ferns (*Azolla*), Water Hyacinth (*Eichhornia crassipes), and* Water Hyssop (*Bacopa monnieri).*

(c) Zooplankton: *Ostracoda*

(d) Animal systems: Guppy (*Poecillia reticulata*)

Eichhornia crassipes and *Bacopa monnieri* were among the aquatic plants that were taken from the cannoli canal near the Sarovaram Bio-Park in Calicut, and the zooplanktons were collected from the Malabar Botanical Garden Research Institute, Calicut, respectively. The azolla plant and the freshwater field guppy fish (*P. reticulata)* were obtained from a local freshwater pond at the water

heritage museum of CWRDM. All collected species were maintained in the laboratory for further study.

9.2.2. Environmental impact study of synthesised P(St-DVB)/CuNi BNC microspheres

The impact of synthesised P(St-DVB)/CuNi BNC on selected species was investigated by evaluating their growth/morphological changes that occurred in each system. Three aquatic plant species, two animal species including zooplankton and fish, and one algal species were selected to check the toxicity of P(St-DVB)/CuNi BNC. The results were then compared with the toxicological effects of CuNi BNPs for the same group of organisms at similar concentrations. Such comparison data will help us to understand whether the BNPs were gradually released from the composite microsphere or not.

9.2.2.1. Evaluation of the dose-dependent effect of P(St-DVB)/CuNi BNC on Algal growth

Initially, the collected algal samples were cultured in Tris-Acetate-Phosphate Medium (TAP) for algal growth as described by Andersen, 2005. TAP medium was prepared by mixing the required quantities (Volume) of stock solutions (SL) prepared at the specified concentrations, as described in Table 8.1, to 850 mL of dd-H_2O. Then finally, the tank was filled to 1000 mL and autoclaved at 121°C for 20 min (Andersen, 2005). The algae samples were cultured in test tubes having 10 ml of TAP medium next after collection under cool white fluorescent lamp at an intensity of 400-700 nm at 24±2°C for 10-15

days. The cultured algal samples were then streaked on petri plates with 25 mL of Agar-TAP solidified medium in the laminar air flow chamber and placed in the culture room. After 7-10 days of streaking, single cells obtained within the petri-plates were observed under the microscope and cultured again in the test tubes. This process was repeated until the single strain was isolated. The obtained algal strain was then placed in a conical flask of 250 mL, along with 200 mL of TAP media, and it was allowed to grow for 15 days. The cultured algae were then used for further studies.

Table 9.1

Composition of TAP medium.

Stock Solution (SL)	Component	Quantity/ Volume	Concentration in SL
Trisbase	$H_2NC(CH_2OH)_3$ Tris(hydroxymethyl)-aminomethan	2.42 g	
TAP-salts	NH_4Cl $MgSO_4 \cdot 7H_2O$ $CaCl_2 \cdot 2H_2O$	25 mL	15 g/L 4 g/L 2 g/L
Phosphate solution	K_2HPO_4 KH_2PO_4	1 mL	28.8 g/100 mL 14.4 g/100 mL
Trace elements solution (Hutner's trace elements)	$Na_2EDTA \cdot 2H_2O$ (Titriplex III) $ZnSO_4 \cdot 7H_2O$ H_3BO_3 $MnCl_2 \cdot 4H_2O$ $FeSO_4 \cdot 7H_2O$ $CoCl_2 \cdot 6H_2O$ $CuSO_4 \cdot 5H_2O$ $(NH_4)_6Mo_7O_{24}.4H_2O$	1 mL	5.00 g/100 mL 2.20 g/100 mL 1.14 g/100 mL 0.50 g/100 mL 0.50 g/100 mL 0.16 g/100 mL 0.16 g/100 mL 0.11 g/100 mL
Acetic acid, conc.	CH_3COOH	1 mL	

To test the effect of P(St-DVB)/CuNi BNC microspheres on algae, 1, 2, 3, 4, and 5 g of the synthesised BNCs were introduced to 200 mL TAP media, followed by the addition of 5 mL of previously cultivated algal media to each conical flask. TAP medium without BNC was used as control. The flasks were then kept for 12 days in the culture room to promote algal growth. After the 12^{th} day, algae growth was monitored using a Thermo Scientific Eutech TN-100 turbidimeter. To eliminate the turbidity of added BNC, the same amount of BNCs was added in to a conical flask which contains 200 mL od TAP solution. After 12 days, the final turbidity was calculated using the following equation.

$$Turbidity = (Turbidity\ of\ TAP\ medium + algae + BNC) - (turbidity\ of\ TAP\ medium + BNC)$$

A similar set of experiments were conducted with CuNi BNPs also to compare the environmental impact of the two systems. For that, 200 mL of TAP media were mixed with 0.5, 1, 2, and 3 g of CuNi BNPs followed by 5 mL of algal media. The flasks were then kept for 12 days in the culture room, and the growth of algae was monitored by measuring the turbidity.

9.2.2.2. Evaluation of the dose-dependent effect of P(St-DVB)/CuNi BNC on morphological changes in aquatic plants

The nanotoxicity effect of synthesised P(St-DVB)/CuNi BNC microspheres was investigated on three aquatic plant species i.e.,

Mosquito ferns, Water hyacinth, and Water Hyssop. Analysis mainly focused on morphological changes that occurred.

(a) Mosquito ferns

10 L plastic trays were used to carry out the experiments and among all the first tray was used as a control. 2, 4, 6, and 8 g/L of the synthesised BNCs were added to the other four trays and used to check the effect of P(St-DVB)/CuNi BNC microspheres on plant morphology. The trays were filled with 6 L of water that was taken from Canoli canal. Similarly, 2, 4, 6, and 8 g/L CuNi BNPs were added to four additional sets of trays to understand the direct effect of nanoparticles on the plant. After that, nearly equal amounts of the collected plants were placed in each tray, including the control. The plants were observed for up to 8 days.

(b) Water Hyssop

Water Hyssop plants of similar size were exposed to a concentration of 2, 4, 6, and 8 g/L concentration of P(St-DVB)/CuNi BNC microspheres, along with the control, in a tray with 6L of water from Canoli Canal. To explore the direct impact of CuNi BNPs, the same amount of BNPs (2, 4, 6, and 8 g/L) was added to another four trays. Then all the plants were maintained at room temperature and monitored for up to 8 days.

(c) Water Hyacinth

The collected plants of similar size were put in trays containing 6 L of water from Canoli canal along with a control. The plants were exposed different amounts of P(St-DVB)/CuNi BNC microspheres (8, 10, and 12 g/L). Unlike the other two plants, the water hyacinth pant did not exhibit significant differences at BNC concentrations of 2, 4, and 6 g/L. Therefore, we utilized higher concentrations to determine the impact of BNC microspheres on water hyacinth plants. All plants were kept at room temperature and monitored for 8 days.

9.2.2.3. Evaluation of the dose-dependent effect of P(St-DVB)/CuNi BNC on Zooplanktons

The ostracods were collected and placed in 50 mL Petri plates with 0.1, 0.2, 0.3, and 0.4 g of P(St-DVB)/CuNi BNC microspheres and 20 mL of water collected from the same pond. A control was also prepared for analysis without the addition of BNCs. The same amounts of CuNi BNPs were added to the remaining four Petri dishes along with the zooplankton. The Zooplanktons were examined under a compound microscope for 4 days to detect any morphological changes that may have resulted from interaction with the nanoparticles.

9.2.2.4. Evaluation of the dose-dependent effect of P(St-DVB)/CuNi BNC on Guppy

All fish species were acclimatised for one week in stock aquifers and then randomly graded into different experimental glass tanks. To test the effect of P(St-DVB)/CuNi BNC microspheres on

Guppy fish, an equal number of fish were exposed to varying concentrations of P(St-DVB)/CuNi BNC microspheres (2, 4, 6, and 8 g/L). A glass tank without the addition of BNC was used as control. Similarly, an equal number of fish were put in various glass tanks containing 2, 4, 6, and 8 g/L CuNi BNPs to evaluate their effects on fish. The water level was maintained carefully so that the fish species were partially immersed. All tanks were then kept at room temperature with a proper supply of food and aeration. The fish species were monitored for 8 days.

9.3. Results and Discussion

9.3.1. Impact study of synthesised P(St-DVB)/CuNi BNC microspheres

9.3.1.1. Evaluation of the dose-dependent effect of P(St-DVB)/CuNi BNC on Algal growth

The collected algae species, *Chlorella vulgaris*, was allowed to grow in conical flasks with 200 mL of TAP medium which contains 1, 2, 3, 4 and 5 g of P(St-DVB)/CuNi BNC along with a control. Algal growth was observed for 8 days and a visible difference in green colour / algal growth was found for up to 5-6 days. During the initial days, less algal development was noticed in the conical flasks containing P(St-DVB)/CuNi BNC microspheres than in the control. A progressive decline in algae growth was also observed with increase in the concentration of BNCs (Figure 9.1). The growth in the conical

flasks that contain 1 and 2 g of BNC had shown a growth rate that is nearly identical to that of the control. This suggests that lower concentrations of BNC concentrations have less impact on algal growth.

Figure 9.1: Dose-dependent study of P(St-DVB)/CuNi BNC microspheres on Algal growth, where (a), (b), (c), (d), and (e) displaying the effects of 1, 2, 3, 4 and 5 g of BNC, respectively, on the 6^{th} day.

It was found that, as the number of days increased, the colour difference between the conical flasks became less visible. On the concentrations of 12^{th} day, the algae in the 1 and 2 g of BNC possess almost same color as the control (Figure 9.2). However, there was a visible change in algal growth after 3 g of BNC and the lighter green colour of algae at concentrations 3, 4 and 5 g of BNC was indicating a retarded algal growth at the higher concentrations (Figure 9.2).

Figure 9.2: Dose-dependent study of P(St-DVB)/CuNi BNC microspheres on Algal growth, where (a), (b), (c), (d), and (e) displaying the effects of 1, 2, 3, 4 and 5 g of BNC, respectively, on the 12^{th} day

The results were further conformed by turbidity analysis. It is evident from the turbidity readings that the turbidity value decreases at increased BNCs concentrations (Figure 9.3). Higher turbidity readings represent high algal concentration or high algal growth. A significant difference in turbidity was observed when the concentration exceeded 3 g. Therefore, we can conclude that the growth of the algae is not much affected at lower BNC concentrations. However, higher concentrations slow down algal development, resulting in a faded green colour. This might be because increased BNC concentrations result in a stronger interaction between the algal cell surface and BNC particles. As a result of these interactions, algal cells undergo oxidative stress. Another crucial characteristic that was discovered to increase with the dose of NPs concentration was, turbidity of the media, which has previously been reported to generate a shading effect (Choi et al., 2014). Furthermore, the uptake of essential nutrients must have been hindered by the presence of these particles in the medium. The

deposition of particles on the surface of algal cells was another mechanism related toxicity (Aruoja et al., 2014). According to the findings, it is notable that the inhibitory effect of P(St-DVB)/CuNi BNC microspheres decreased as the exposure duration increased, showing that time is also an important factor in determining toxicity.

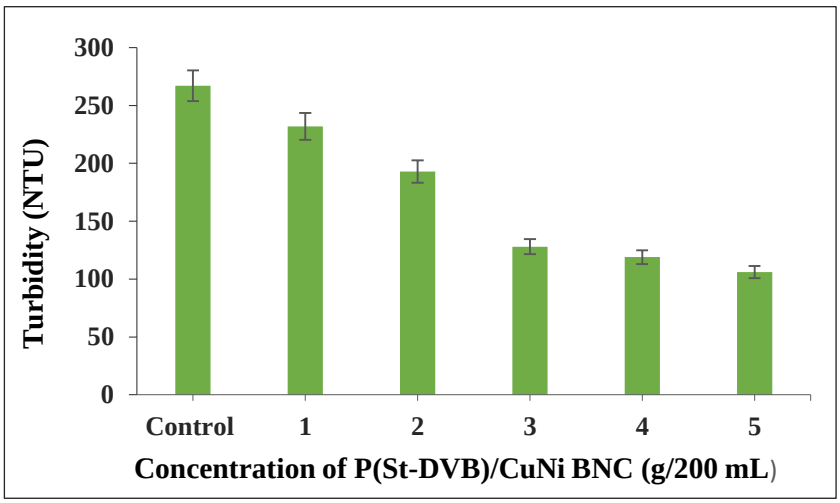

Figure 9.3: Turbidity studies on the dose-dependent effect of P(St-DVB)/CuNi BNC microspheres on Algal growth.

To compare the effects of CuNi BNPs on algae, a similar set of studies was also carried out with CuNi BNPs. In this case, 200 mL of TAP medium was mixed with 5 mL of algal medium and 0.5, 1, 2, and 3 g of previously produced BNPs. Figure 9.4 shows the growth of the algae observed on the eighth day. In contrast to P(St-DVB)/CuNi BNC microspheres, CuNi BNPs have a more significant and visible effect on algae. The figure clearly illustrates how the growth decreases as BNP concentration increases. At both the 0.5 and 1 g concentrations of

BNP, the algae grew in a way that was nearly identical to the control. The impact was greater when 2 and 3g of BNP were present. Very less algal growth was observed in the flask, which is treated with 3g of CuNi BNPs.

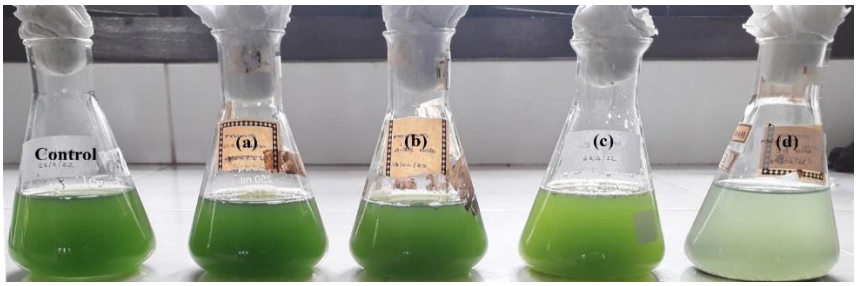

Figure 9.4: Dose-dependent study of CuNi BNPs on Algal growth, where (a), (b), (c), and (d) are displaying the effects of 0.5, 1, 2, and 3 g of BNC, respectively, on the 12^{th} day.

Similar results were also obtained from the turbidity analysis. Turbidity data clearly show that the turbidity drops at higher concentrations of CuNi BNPs (Figure 9.5). A noticeable change in turbidity was observed when the concentration exceeded 1 g. A sudden decrease in the turbidity value was found when the BNP concentration increased to 3g/200 mL.

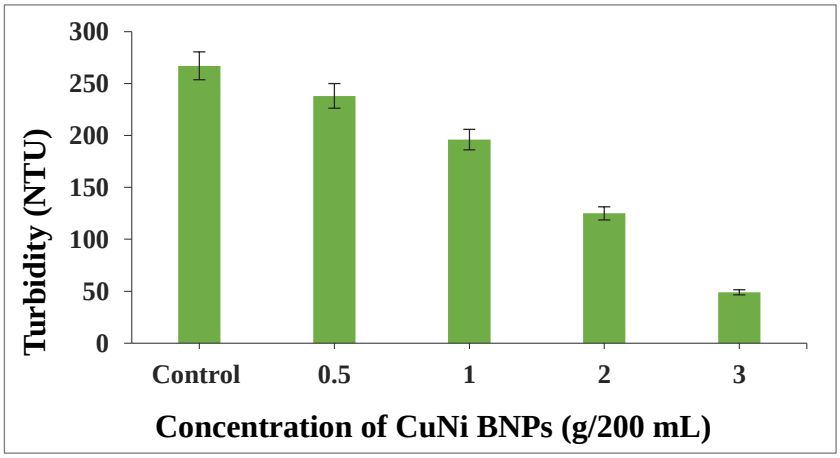

Figure 9.5: Turbidity studies on the dose-dependent effect of CuNi BNPs on Algal growth.

9.3.1.2. Evaluation of the dose-dependent effect of P(St-DVB)/CuNi BNC on morphological changes in aquatic plants

(a) Mosquito ferns

The plant morphology was analysed to check the effect of the P(St-DVB)/CuNi BNC microspheres and the changes were compared with the control. Variations in plant morphology have been observed with increasing concentrations of BNCs and can be seen in Figure 9.6. After 8 days, it was discovered that the plant morphology at concentrations of 2 and 4 g/L of BNC was not affected and the growth was almost similar to that of control. That is, there were no adverse impacts on the plant growth at these concentrations and the plants grew as healthily as the control.

However, plants began to wilt as the BNC concentration increased, and the impact became more pronounced when the concentration exceeded 6 g/L (Figure 9.6 (a)). At a 6 g concentration of BNC, it was observed that as the number of days increased, the plant began to exhibit a few minor differences when compared to the control. A slight change in the colour of leaves from green to brown was observed at 8 g/L of BNC concentration and the plants were also started to wilt (Figure 9.6 (b)). Although most of leave was green.

Compared to control and BNC, plants exposed to 8 g/L of CuNi BNPs showed more variations in leaf colour. Blackening, yellowing, and withering of the leaves were also noted (Figure 9.6 (c)).

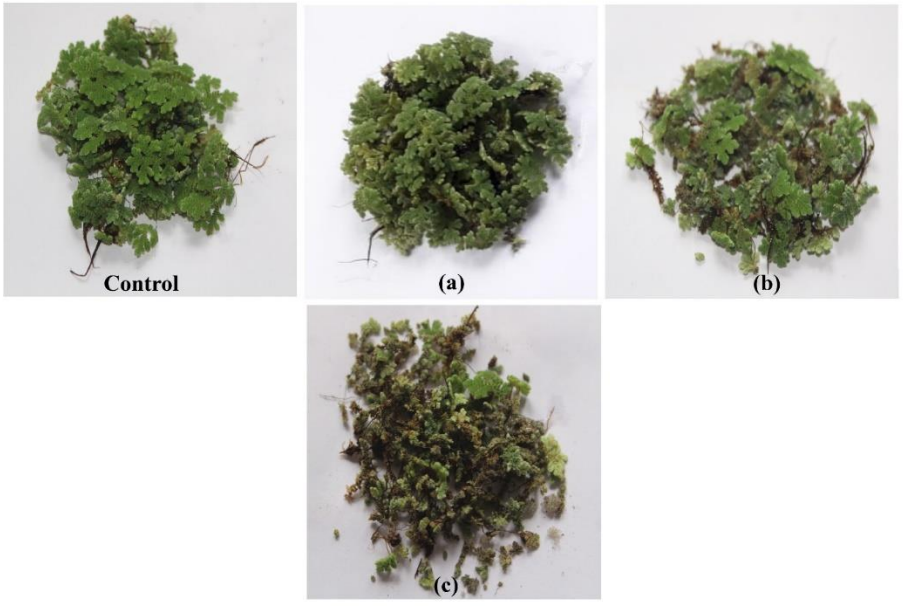

Figure 9.6: Dose-dependent study on Mosquito ferns plant. (a) and (b) represents the 6 and 8 g/L of P(St-DVB)/CuNi BNC, respectively, on the 8th day and (c) represents the 8 g/L of CuNi BNP on the 8th day.

(b) Water Hyssop

The morphological parameters of the Water Hyssop plants under the influence of different concentrations of P(St-DVB)/CuNi BNC microspheres and CuNi BNPs (2, 4, 6, and 8 g/L) were compared with the control. The study revealed that neither P(St-DVB)/CuNi BNC nor CuNi BNPs had a significant impact on plant development. Although some effects of BNCs on plant morphology was evident and were found increased with increasing concentration of BNCs, which could easily be easily observed by visual examination (Figure 9.7).

No discernible morphological differences were observed between plants which were treated with 2 and 4 g/L of BNC compared to the control even after 8 days of exposure. But as the concentration increased from 4 g/L, some changes were observed. Yellowing of some parts of the Water Hyssop plant leaf was observed at 6 g/L BNCs. The curling of the leaves and stem in the top part of the plant was also noticed (Figure 9.7 (a)). However, all other leaves were found healthy.

Among the tested concentrations of P(St-DVB)/CuNi BNC microspheres, significant change in leaf morphology was observed at 8 g/L BNC. The curling of the leaves was further extended to the bottom part of the plant at this concentration and no other changes were observed (Figure 9.7 (b)).

Figure 9.7: Dose-dependent study of P(St-DVB)/CuNi BNC microspheres on Water Hyssop plant. (a) and (b) represents the 6 and 8 g/L of BNC respectively on the 8th day.

However, plants treated with CuNi BNPs showed more adverse effects. Curling of the leaves and stem of the entire plant was noticed when treated with 8 g/L of CuNi BNP and blackening of the lower part of the stem was also observed at this concentration (Figure 9.8 (a)).

Figure 9.8: Dose-dependent study of CuNi BNPs on Water Hyssop plant. (a) represents the 8 g/L of BNPs on the 8th day.

(c) Water Hyacinth

Unlike the other two plants, the water hyacinth pant did not show significant differences at 2, 4, and 6 g/L concentrations of BNC and CuNi BNPs. Therefore, higher concentrations were used for the study. The collected plant was exposed to 8, 10, and 12 g/L of both BNPs P(St-DVB)/CuNi BNC microspheres and CuNi, and the morphological parameters of the plants were analysed for 8 days to check their effects compared to the control.

Figure 9.9 shows the effects of P(St-DVB)/CuNi BNC on the morphology of the water hyacinth plant on the eighth day. According to visual observations, no significant differences were recorded in plants morphology which were treated with up to 12 g/L of BNC (figure 9.9 (a)).

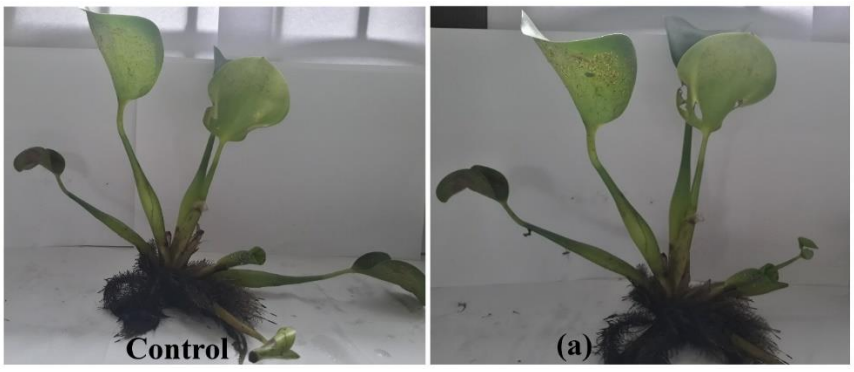

Figure 9.9: Dose-dependent study of P(St-DVB)/CuNi BNC microspheres on Water Hyacinth plant. (a) represents the 12 g/L of BNC on the 8th day.

Although the water hyacinth plant showed certain morphological abnormalities in the presence of 12 g/L of CuNi BNPs, including rotting stems, curled leaves and dried leaves (Figure 9.10). Blackening of the leaves and shoots was also evident from the visual observations compared to control plants. Early effects were detected on 4th day such as blackening the leaves. Further, curling and rotting of the plants was observed on 6th day. On 7th day, the plant leaves had started to dry. However, complete damage to the plant was not observed at this concentration. The plants treated with the lower concentration of CuNi BNPs microspheres were found healthy and green in colour as control plants.

Figure 9.10: Dose-dependent study of 12 g/L CuNi BNPs on Water Hyacinth plant on the 8th day.

9.3.1.3. Evaluation of the dose-dependent effect of P(St-DVB)/CuNi BNC on Zooplankton

The ostracoda have an exterior carapace that includes the left and right valves and can be observed under a microscope (Figure 9.11 (a)). Normally, they continuously open and shut its valves, and also move its appendages rapidly. However, some alterations in these movements were noticed after exposure to the P(St-DVB)/CuNi BNC microspheres and they respond differently when the concentration of BNC microspheres increases. Compared to the control, the free movement of their appendage was found to be retarded when the concentration increased. After being exposed to 0.4 g of BNC, its carapace was permanently left slightly open, as seen in figure 9.11 (b).

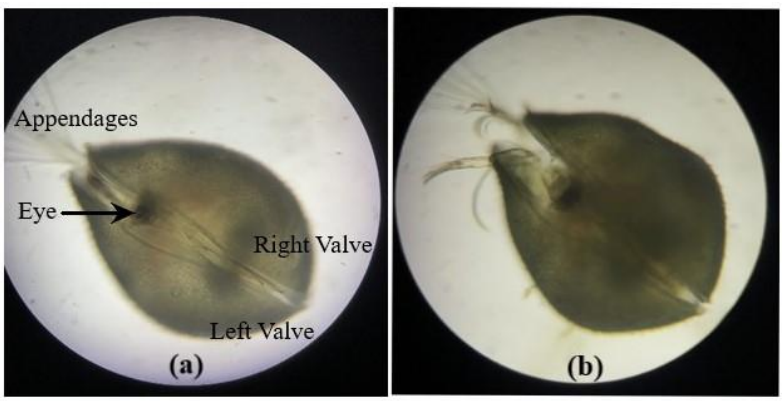

Figure 9.11: Dose-dependent study of P(St-DVB)/CuNi BNC microspheres on Zooplanktons. (a) and (b) represents the 0.3 and 0.4 g/L of BNC respectively on the 8th day.

In the case of CuNi BNPs, some of them were found inactive after 3 days of exposure to the highest dose, that is, 0.4 g of BNPs.

Their carapace was mostly exposed and no movement of appendage was visible (Figure 9.12).

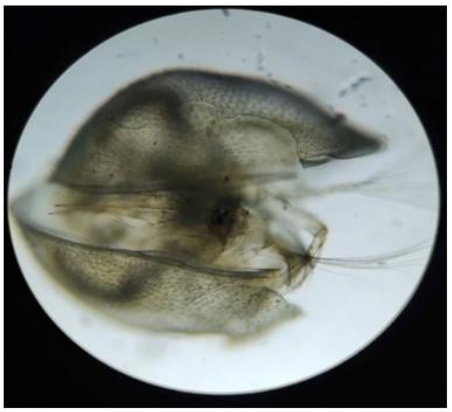

Figure 9.12: Dose-dependent study of 0.4 g CuNi BNPs on Zooplanktons on the 8th day.

9.3.1.4. Evaluation of the dose-dependent effect of P(St-DVB)/CuNi BNC on Guppy

The guppy fish were exposed to 2, 4, 6 and 8 g/L of both P(St-DVB)/CuNi BNC microspheres and CuNi BNPs for 8 days. No significant changes in the guppy fish were observed compared to the control after exposure to BNCs. But after three days, the movement of fish was found slowed down and were become less active at concentrations higher than 8 g/L of BNC, which was the only noticeable change that could be seen.

After being exposed to 8 g/L of CuNi BNPs for seven days, one out of five fish was discovered dead and the remaining were found

alive. The movement of all the fish was slow and any other morphological changes were not observed.

9.4. Conclusion

The present study investigated the toxicity of both P(St-DVB)/CuNi BNC microspheres and CuNi BNPs in different species like Chlorella vulgaris, Mosquito ferns, Water Hyacinth, Water Hyssop, Ostracods, and Guppy. The results showed that the CuNi BNPs had a greater impact on algal growth than P(St-DVB)/CuNi BNC microspheres at similar concentrations. In the case of aquatic plants, among the tested concentrations of BNCs, the concentration of 8 g/L displayed highest toxic effect on both mosquito ferns and water hyssop plants, while in the case of water hyacinth, no detrimental effects were not observed up to 12g/L concentration of BNCs. Whereas, at higher concentrations of CuNi BNPs, all studied organisms showed a significant toxic impact on morphological parameters such as drying, blackening, yellowing, and withering of the leaves, curling of the leaves and stem, and so on. Furthermore, some of them were found to be inactive after 3 days of exposure with 0.4 g of CuNi BNPs. The toxicity study reveals that P(St-DVB)/CuNi BNC had less detrimental effects on both flora and fauna than CuNi BNPs at the same dose. Therefore, we can conclude that very few amounts of CuNi BNPs were gradually released from the BNCs over time and, therefore, they can be used for the water treatment applications.

Chapter 10

Summary and future works

10.1. Summary

The main objective of this work was to develop an efficient and affordable organo-inorganic hybrid nanocomposite material for the treatment of water contaminated with heavy metals and bacteria. In this thesis, porous(Styrene-divinylbenzene)/CuNi bimetallic nanocomposite were synthesised, evaluated as adsorbents for the removal of heavy metals, and their potential use as an antibacterial agent was investigated. The research resulted in technological prototypes for water purification, using the synthesised bimetallic nanocomposite, that have the potential to be commercially viable. Finally, considerable attempt was made to understand the environmental impact of the bimetallic nanocomposite in some detail. The outcome of our research is summarised below.

In Chapter 3, the synthesis, characterisation, and antibacterial activity of the CuNi bimetallic nanoparticle is described. A chemical reduction method has been utilised for the synthesis. It is simple, easy to operate, cost-effective and allows high purity of the products with reproducible results. Moreover, the procedure can be applied at room temperature under ordinary pressure and in aqueous solution. SEM and TEM studies of the synthesised CuNi BNPs revealed a spherical morphology with a particle size of around 38.4 nm. Clear lattice fringes with an interplanar distance of 2.0 Å support the presence of the (111) plane

and were further confirmed by XRD. The BET surface area of the BNP was found to be 31 m^2/g. The antibacterial activity of CuNi BNP was tested using *Escherichia coli* (*E.coli*), *Aeromonas hydrophila* (*A.hydrophila*), and *Vibrio alginolyticus (V. alginolyticus)* by the spread plate counting method and showed remarkable antibacterial activity against all three tested bacteria. A relatively higher antimicrobial activity was observed against *A. hydrophila* and *V. alginolyticus* compared with *E. coli* and it can be attributed to the different cell wall composition of the bacteria. Lastly, antibacterial activity of individual Cu NPs and Ni NPs was analysed and observed that the CuNi BNPs exhibited more antibacterial activity than the individual Cu and Ni NPs.

In Chapter 4, CuNi BNPs have been applied for the removal of heavy metals such as Cd^{2+}, Pb^{2+}, Zn^{2+} and Mn^{2+} from aqueous solutions under various operational conditions. The batch study showed significant elimination of heavy metals and all of the reactions fit very well to the Langmuir isotherm model and the pseudo-first-order kinetic model. The result revealed that the adsorption of heavy metals follows the order: $Mn^{2+}>Zn^{2+}>Pb^{2+}>Cd^{2+}$. The percentage of removal of all ions was strongly dependent on pH, and the removal efficiency is enhanced in higher pH values. In addition, the synthesised CuNi bimetallic nanoparticle showed a higher efficiency in adsorption in comparison to individual Cu and Ni NPs. This may be due to the increased surface area of the bimetallic nanoparticle compared to their monometallic counterpart and the synergistic effect between the two metals.

Chapter 5, highlights the immobilization of the CuNi BNPs using styrene and divinylbenzene copolymer. This styrene-divinylbenzene copolymer was selected as it is biocompatible, insoluble in aqueous solutions, and highly porous, making it an ideal matrix for the nanoparticles. The porous nature allows good contact between the nanoparticles and heavy metals for adsorption. Furthermore, the composite is easily recoverable once the adsorption process is complete. The immobilized microspheres were successfully synthesised by oil-in-water emulsion polymerisation of styrene and divinylbenzene in the presence of CuNi BNPs. The SEM image of P(St-DVB)/CuNi BNC indicates the formation of spherical-shaped particles with average diameter of 110 µm. HR-TEM images indicated that CuNi bimetallic NPs were successfully encapsulated in the P(St-DVB) microspheres. EDX spectra showed that Cu and Ni elements were present inside the P(St-DVB) microsphere. The crystalline structure of the nanocomposite was characterised by PXRD and showed prominent peaks at 43.26° (111), 50.44° (200) and 74.03° (220) confirming the crystal planes of CuNi BNPs. According to the BET analysis, the nanocomposite had a specific surface area of 45.88 m^2/g with an average pore diameter of 64.80 nm. Similar to CuNi BNPs, P(St-DVB)/CuNi BNCs also shown remarkable antibacterial activity toward *E. coli*, *A. hydrophila*, and *V. alginolyticus,* although BNCs required a longer contact time to completely inhibit bacterial growth compared to CuNi BNPs.

In Chapter 6, we report batch adsorption studies with P(St-DVB)/CuNi BNC for the removal of heavy metals such as Cd^{2+}, Pb^{2+},

Zn^{2+} and Mn^{2+} from aqueous solutions under various operational conditions. The results revealed that the removal efficiency of the adsorbent increased with increasing contact time and adsorbent mass and decreased with increase in initial metal concentration. The experimental maximum adsorption capacity of the metals was 15.60 mg Pb(II)/g, 7.28 mg Cd(II)/g, 22.42 mg Mn(II)/g and 20.57 mg Zn(II)/g. Similarly, to the CuNi BNP, the pseudo-first-order kinetic model is more appropriate to explain the adsorption kinetics, and the Langmuir adsorption isotherm was more closely fit to experimental data than the Freundlich model. The desorption of heavy metals from P(St-DVB)/CuNi BNC was successfully achieved by using a 0.5 M NaOH solution. Immobilization of CuNi BNPs into porous polymeric material leads to the more efficient, simpler, and low-cost separation of these used materials from the treated solution.

In Chapter 7, the efficiency of the immobilized adsorbent was evaluated by conducting series of fixed-bed column studies. The study showed that the removal of different heavy metals onto P(St-DVB)/CuNi BNC microbeads in a fixed bed column was feasible and effective. System parameters such as initial metal concentration, flow rate, and bed height were optimised for a maximum removal rate and found that adsorption capacity increased with increasing initial metal concentration and bed height; and decreasing flow rate. The breakthrough obtained and the column kinetic parameters were successfully predicted with mathematical models such as the Thomas, Yoon-Nelson, and Adams–Bohart models and both Thomas and Yoon–Nelson models were shown to be in good agreement with the

experimental results for all the operating conditions studied. Successful desorption of heavy metals from the P(St-DVB)/CuNi BNC microbeads were performed using NaOH solution and showed good reusability of the adsorbent in the bed column during four adsorption–desorption cycles. Most NP immobilization techniques result in a partial loss of their activity proportional to the reduction in their active surface area. Whereas, in the case of P(St-DVB)/CuNi BNC, the porous nature of poly(styrene-divinylbenzene) allows good contact between the CuNi BNPs and the heavy metals. Therefore, they could exhibit good adsorption efficiency comparable to that of CuNi BNPs.

Chapter 8, highlights the fabrication of a low-cost, portable, and simple water purification device using the synthesised P(St-DVB)/CuNi BNC microspheres. The packed cartridge showed heavy metal removal (according to WHO standards) for approximately 66 L of water with an average flow rate of 25 mL/min using 20 g of the composite without any regeneration of the material. Furthermore, the robustness of the BNCs prevents leaching of the CuNi BNPs, which makes it an excellent option for an industrially practicable material for supplying inexpensive water across the affected regions.

In chapter 9, we report further insights related to the environmental impact of synthesised P(St-DVB)/CuNi BNC microspheres and CuNi BNPs on different species like Chlorella vulgaris, Mosquito ferns, Water Hyacinth, Water Hyssop, Ostracods, and Guppy. The study was carried out by assessing the morphological changes that have occurred in plant and animal species. The results

demonstrated that P(St-DVB)/CuNi BNC had less detrimental effects on both flora and fauna than CuNi BNPs at the same dose. Therefore, we can conclude that very few amounts of CuNi BNPs were gradually released from the BNCs over time and, therefore, they can be used for the water treatment applications.

10.2. Future works

The future work to extend this study can be listed as follows:

- There is a wide scope of improvement in terms of nanomaterial functionalities, uptake capacities, and robustness for adsorption-based purification techniques.
- Further experiments are necessary to evaluate the efficacy of this treatment technology for the removal of wide range of other heavy metals.
- Performance of the filter should be assessed for its practical application as a domestic filter in treating contaminated water under various environmental parameters affecting the treatment technology.

Further research and significant efforts are required in the scaling-up processes for taking lab-based techniques to pilot scale method with better efficiencies.

Reference

Abbas, S., Nasreen, S., Haroon, A. and Ashraf, M.A., 2020. Synhesis of silver and copper nanoparticles from plants and application as adsorbents for naphthalene decontamination. *Saudi Journal of Biological Sciences*, *27*(4), pp.1016-1023.

Abdelbasir, S.M. and Shalan, A.E., 2019. An overview of nanomaterials for industrial wastewater treatment. *Korean Journal of Chemical Engineering*, *36*(8), pp.1209-1225.

Adeleye, A.S., Conway, J.R., Garner, K., Huang, Y., Su, Y. and Keller, A.A., 2016. Engineered nanomaterials for water treatment and remediation: Costs, benefits, and applicability. *Chemical Engineering Journal*, *286*, pp.640-662.

Agdi, K., Bouaid, A., Esteban, A.M., Hernando, P.F., Azmani, A. and Camara, C., 2000. Removal of atrazine and four organophosphorus pesticides from environmental waters by diatomaceous earth–remediation method. *Journal of environmental monitoring*, *2*(5), pp.420-423.

Agrawal, P. and Bajpai, A.K., 2011. Dynamic column adsorption studies of toxic Cr (VI) ions onto iron oxide loaded gelatin nanoparticles. *Journal of dispersion science and technology*, *32*(9), pp.1353-1362.

Ahmad, A., Li, L., Bao, J., Jia, X., Xu, Y. and Guo, X., 2016. Antibacterial activity of graphene supported FeAg bimetallic nanocomposites. *Colloids and Surfaces B: Biointerfaces*, *143*, pp.490-498.

Ahmad, A.A. and Hameed, B.H., 2010. Fixed-bed adsorption of reactive azo dye onto granular activated carbon prepared from waste. *Journal of hazardous materials*, *175*(1-3), pp.298-303.

Ai, D., Kang, S., Dai, X. and Kwon, H., 2003. Synthesis of nickel nanopowders in microemulsion. *China Particuology*, *1*(3), pp.131-133.

Akin, I., Arslan, G., Tor, A., Cengeloglu, Y. and Ersoz, M., 2011. Removal of arsenate [As (V)] and arsenite [As (III)] from water by SWHR and BW-30 reverse osmosis. *Desalination*, *281*, pp.88-92.

Aksu, Z. and Gönen, F., 2004. Biosorption of phenol by immobilized activated sludge in a continuous packed bed: prediction of breakthrough curves. *Process biochemistry*, *39*(5), pp.599-613.

Aksu, Z., Çağatay, Ş.Ş. and Gönen, F., 2007. Continuous fixed bed biosorption of reactive dyes by dried Rhizopus arrhizus: Determination of column capacity. *Journal of hazardous materials*, *143*(1-2), pp.362-371.

Alberts, B., Johnson, A., Lewis, J., Morgan, D., Raff, M., Roberts, K. and Walter, P., 2017. Molecular biology of the cell., sixth edit ed. *New York: Garland Science*, *2017*.

Albuszis, M., Roth, P.J., Exnowitz, F., Wong, D.L., Pauer, W. and Moritz, H.U., 2016. Synthesis and in-depth characterization of reactive, uniform, crosslinked microparticles based on free radical copolymerization of 4-vinylbenzyl azide. *Polymer Chemistry*, *7*(5), pp.1168-1180.

Al-Ghouti, M.A., Khraisheh, M.A.M., Allen, S.J. and Ahmad, M.N., 2003. The removal of dyes from textile wastewater: a study of the physical characteristics and adsorption mechanisms of diatomaceous earth. *Journal of environmental management*, *69*(3), pp.229-238.

Ali, I. and Gupta, V.K., 2006. Advances in water treatment by adsorption technology. *Nature protocols*, *1*(6), pp.2661-2667.

Ali, S.M.U., Nur, O., Willander, M. and Danielsson, B., 2010. A fast and sensitive potentiometric glucose microsensor based on glucose oxidase coated ZnO nanowires grown on a thin silver wire. *Sensors and Actuators B: Chemical*, *145*(2), pp.869-874.

Alloway, B.J., 1995. Soil processes and the behaviour of metals. *Heavy metals in soils*, *13*, p.3488.

Alluri, H.K., Ronda, S.R., Settalluri, V.S., Bondili, J.S., Suryanarayana, V. and Venkateshwar, P., 2007. Biosorption: An eco-friendly alternative for heavy metal removal. *African journal of Biotechnology*, *6*(25).

Al-Othman, Z.A., Ali, R. and Naushad, M., 2012. Hexavalent chromium removal from aqueous medium by activated carbon prepared from peanut shell: adsorption kinetics, equilibrium and thermodynamic studies. *Chemical engineering journal*, *184*, pp.238-247.

Alvarez-Bastida, C., Martínez-Miranda, V., Vázquez-Mejía, G., Solache-Ríos, M., de Oca, G.F.M. and Trujillo-Flores, E., 2013. The corrosive nature of manganese in drinking water. *Science of the Total Environment*, *447*, pp.10-16.

Alyüz, B. and Veli, S., 2009. Kinetics and equilibrium studies for the removal of nickel and zinc from aqueous solutions by ion exchange resins. *Journal of hazardous materials*, *167*(1-3), pp.482-488.

Andersen, R.A. ed., 2005. *Algal culturing techniques*. Elsevier.

Aquasure, 28.10.2014. Aquasure Xtra Tuff, Eureka Forbes http://www.eurekaforbes.com/Product/Water-Purifiers/AquaSure/Non-Electric/AquasureXtra-Tuff?pid=20.

Argueta-Figueroa, L., Morales-Luckie, R.A., Scougall-Vilchis, R.J. and Olea-Mejía, O.F., 2014. Synthesis, characterization and antibacterial activity of copper, nickel and bimetallic Cu–Ni nanoparticles for potential use in dental materials. *Progress in Natural Science: Materials International*, *24*(4), pp.321-328.

Arora, N., Thangavelu, K. and Karanikolos, G.N., 2020. Bimetallic nanoparticles for antimicrobial applications. *Frontiers in Chemistry*, *8*, p.412.

Aruoja, V., Pokhrel, S., Sihtmäe, M., Mortimer, M., Mädler, L. and Kahru, A., 2015. Toxicity of 12 metal-based nanoparticles to algae, bacteria and protozoa. *Environmental Science: Nano*, *2*(6), pp.630-644.

Babaee, Y., Mulligan, C.N. and Rahaman, M.S., 2018. Removal of arsenic (III) and arsenic (V) from aqueous solutions through adsorption by Fe/Cu nanoparticles. *Journal of Chemical Technology & Biotechnology*, *93*(1), pp.63-71.

Babel, S. and Kurniawan, T.A., 2003. Low-cost adsorbents for heavy metals uptake from contaminated water: a review. *Journal of hazardous materials*, *97*(1-3), pp.219-243.

Bankura, K., Maity, D., Mollick, M.M.R., Mondal, D., Bhowmick, B., Roy, I., Midya, T., Sarkar, J., Rana, D., Acharya, K. and Chattopadhyay, D., 2014. Antibacterial activity of Ag–Au alloy NPs and chemical sensor property of Au NPs synthesized by dextran. *Carbohydrate polymers*, *107*, pp.151-157.

Barakat, M.A., 2011. New trends in removing heavy metals from industrial wastewater. *Arabian journal of chemistry*, *4*(4), pp.361-377.

Baral, S.S., Das, N., Ramulu, T.S., Sahoo, S.K., Das, S.N. and Chaudhury, G.R., 2009. Removal of Cr (VI) by thermally activated weed Salvinia cucullata in a fixed-bed column. *Journal of Hazardous Materials*, *161*(2-3), pp.1427-1435.

Belenov, S.V., Volochaev, V.A., Pryadchenko, V.V., Srabionyan, V.V., Shemet, D.B., Tabachkova, N.Y. and Guterman, V.E., 2017. Phase behavior of Pt–Cu nanoparticles with different architecture upon their thermal treatment. *Nanotechnologies in Russia*, *12*(3), pp.147-155.

Beyth, N., Houri-Haddad, Y., Domb, A., Khan, W. and Hazan, R., 2015. Alternative antimicrobial approach: nano-antimicrobial materials. *Evidence-based complementary and alternative medicine*, *2015*.

Bhardwaj, S. and Sarkar, T., 2020. Core–shell type magnetic Ni/NiO nanoparticles as recyclable adsorbent for Pb (II) and Cd (II) ions: One-pot synthesis, adsorption performance, and mechanism. *Journal of the Taiwan Institute of Chemical Engineers*, *113*, pp.223-230.

BIS, 2012. Bureau of Indian Standards IS: 10500.

Bohart, G.S. and Adams, E.Q., 1920. Some aspects of the behavior of charcoal with respect to chlorine. *Journal of the American Chemical Society*, *42*(3), pp.523-544.

Bohli, T., Ouederni, A. and Villaescusa, I., 2017. Simultaneous adsorption behavior of heavy metals onto microporous olive stones activated carbon: analysis of metal interactions. *Euro-Mediterranean Journal for Environmental Integration*, *2*(1), pp.1-15.

Boholm, Å. and Prutzer, M., 2017. Experts' understandings of drinking water risk management in a climate change scenario. *Climate Risk Management*, *16*, pp.133-144.

Bulgariu, D. and Bulgariu, L., 2013. Sorption of Pb (II) onto a mixture of algae waste biomass and anion exchanger resin in a packed-bed column. *Bioresource technology*, *129*, pp.374-380.

Burguete, M.I., Fraile, J.M., García-Verdugo, E., Luis, S.V., Martínez-Merino, V. and Mayoral, J.A., 2005. Polymer-supported bis (oxazolines) and related systems: toward new heterogeneous

enantioselective catalysts. *Industrial & engineering chemistry research*, *44*(23), pp.8580-8587.

Bustamante-Torres, M., Romero-Fierro, D., Arcentales-Vera, B., Pardo, S. and Bucio, E., 2021. Interaction between filler and polymeric matrix in nanocomposites: Magnetic approach and applications. *Polymers*, *13*(17), p.2998.

Buzea, C., Pacheco, I.I. and Robbie, K., 2007. Nanomaterials and nanoparticles: sources and toxicity. *Biointerphases*, *2*(4), pp.MR17-MR71.

Cady, N.C., Behnke, J.L. and Strickland, A.D., 2011. Copper- based nanostructured coatings on natural cellulose: Nanocomposites exhibiting rapid and efficient inhibition of a multi- drug resistant wound pathogen, A. baumannii, and mammalian cell biocompatibility in vitro. *Advanced Functional Materials*, *21*(13), pp.2506-2514.

Cai, S., Jia, X., Han, Q., Yan, X., Yang, R. and Wang, C., 2017. Porous Pt/Ag nanoparticles with excellent multifunctional enzyme mimic activities and antibacterial effects. *Nano Research*, *10*(6), pp.2056-2069.

Cárdenas-Triviño, G., Elgueta, C., Vergara, L., Ojeda, J., Valenzuela, A. and Cruzat, C., 2017. Chitosan doped with nanoparticles of copper, nickel and cobalt. *International journal of biological macromolecules*, *104*, pp.498-507.

Carrillo-Torres, R.C., García-Soto, M.J., Morales-Chávez, S.D., Garibay-Escobar, A., Hernández-Paredes, J., Guzmán, R., Barboza-Flores, M. and Álvarez-Ramos, M.E., 2016. Hollow Au–Ag bimetallic nanoparticles with high photothermal stability. *RSC advances*, *6*(47), pp.41304-41312.

Chang, Y.N., Zhang, M., Xia, L., Zhang, J. and Xing, G., 2012. The toxic effects and mechanisms of CuO and ZnO nanoparticles. *Materials*, *5*(12), pp.2850-2871.

Chatterjee, A.K., Sarkar, R.K., Chattopadhyay, A.P., Aich, P., Chakraborty, R. and Basu, T., 2012. A simple robust method for synthesis of metallic copper nanoparticles of high antibacterial potency against E. coli. *Nanotechnology*, *23*(8), p.085103.

Chen, D.H. and Wu, S.H., 2000. Synthesis of nickel nanoparticles in water-in-oil microemulsions. *Chemistry of Materials*, *12*(5), pp.1354-1360.

Chen, L., Ji, T., Mu, L., Shi, Y., Brisbin, L., Guo, Z., Khan, M.A., Young, D.P. and Zhu, J., 2016. Facile synthesis of mesoporous carbon nanocomposites from natural biomass for efficient dye adsorption and selective heavy metal removal. *RSC advances*, *6*(3), pp.2259-2269.

Chen, S., Yue, Q., Gao, B., Li, Q., Xu, X. and Fu, K., 2012. Adsorption of hexavalent chromium from aqueous solution by modified corn stalk: a fixed-bed column study. *Bioresource technology*, *113*, pp.114-120.

Chen, Y., Peng, D.L., Lin, D. and Luo, X., 2007. Preparation and magnetic properties of nickel nanoparticles via the thermal decomposition of nickel organometallic precursor in alkylamines. *Nanotechnology*, *18*(50), p.505703.

Cheng, L., Weir, M.D., Xu, H.H., Antonucci, J.M., Kraigsley, A.M., Lin, N.J., Lin-Gibson, S. and Zhou, X., 2012. Antibacterial amorphous calcium phosphate nanocomposites with a quaternary ammonium dimethacrylate and silver nanoparticles. *Dental Materials*, *28*(5), pp.561-572.

Choi, M.H., Hwang, Y., Lee, H.U., Kim, B., Lee, G.W., Oh, Y.K., Andersen, H.R., Lee, Y.C. and Huh, Y.S., 2014. Aquatic ecotoxicity effect of engineered aminoclay nanoparticles. *Ecotoxicology and environmental safety*, *102*, pp.34-41.

Cioffi, N., Torsi, L., Ditaranto, N., Tantillo, G., Ghibelli, L., Sabbatini, L., Bleve-Zacheo, T., D'Alessio, M., Zambonin, P.G. and Traversa, E., 2005. Copper nanoparticle/polymer composites with antifungal and bacteriostatic properties. *Chemistry of Materials*, *17*(21), pp.5255-5262.

Clifford, C.A., Stinz, M., Hodoroaba, V.D., Unger, W.E. and Fujimoto, T., 2020. International standards in nanotechnologies. In *Characterization of Nanoparticles* (pp. 511-525). Elsevier.

Cruces, E., Arancibia-Miranda, N., Manquián-Cerda, K., Perreault, F., Bolan, N., Azócar, M.I., Cubillos, V., Montory, J., Rubio, M.A. and Sarkar, B., 2022. Copper/silver bimetallic nanoparticles supported on aluminosilicate geomaterials as antibacterial agents. *ACS Applied Nano Materials*, *5*(1), pp.1472-1483.

Dang, T.M.D., Le, T.T.T., Fribourg-Blanc, E. and Dang, M.C., 2011. Synthesis and optical properties of copper nanoparticles prepared by a chemical reduction method. *Advances in Natural Sciences: Nanoscience and Nanotechnology*, *2*(1), p.015009.

De Kwaadsteniet, M., Dobrowsky, P.H., Van Deventer, A., Khan, W. and Cloete, T.E., 2013. Domestic rainwater harvesting: microbial and chemical water quality and point-of-use treatment systems. *Water, Air, & Soil Pollution*, *224*(7), pp.1-19.

Ding, X., Yuan, P., Gao, N., Zhu, H., Yang, Y.Y. and Xu, Q.H., 2017. Au-Ag core-shell nanoparticles for simultaneous bacterial imaging and synergistic antibacterial activity. *Nanomedicine: Nanotechnology, Biology and Medicine*, *13*(1), pp.297-305.

Dlamini, N.G., Basson, A.K. and Pullabhotla, V.S.R., 2021. Synthesis and Application of FeCu Bimetallic Nanoparticles in Coal Mine Wastewater Treatment. *Minerals*, *11*(2), p.132.

Dong, H., Jiang, Z., Zhang, C., Deng, J., Hou, K., Cheng, Y., Zhang, L. and Zeng, G., 2018. Removal of tetracycline by Fe/Ni bimetallic nanoparticles in aqueous solution. *Journal of colloid and interface science*, *513*, pp.117-125.

Doulia, D., Leodopoulos, C., Gimouhopoulos, K. and Rigas, F., 2009. Adsorption of humic acid on acid-activated Greek bentonite. *Journal of Colloid and Interface Science*, *340*(2), pp.131-141.

Ealia, S.A.M. and Saravanakumar, M.P., 2017, November. A review on the classification, characterisation, synthesis of nanoparticles and their application. In *IOP conference series: materials science and engineering* (Vol. 263, No. 3, p. 032019). IOP Publishing.

Effenberger, F.B., Sulca, M.A., Machini, M.T., Couto, R.A., Kiyohara, P.K., Machado, G. and Rossi, L.M., 2014. Copper nanoparticles synthesized by thermal decomposition in liquid phase: the influence of capping ligands on the synthesis and bactericidal activity. *Journal of nanoparticle research*, *16*(11), pp.1-10.

Eluri, R. and Paul, B., 2012. Microwave assisted greener synthesis of nickel nanoparticles using sodium hypophosphite. *Materials Letters*, *76*, pp.36-39.

Er, O.F., Caglar, A., Ulas, B., Kivrak, H. and Kivrak, A., 2020. Novel carbon nanotube supported Co@ Ag@ Pd formic acid electrooxidation

catalysts prepared via sodium borohydride sequential reduction method. *Materials Chemistry and Physics*, *241*, p.122422.

Eremenko, A.M., Petrik, I.S., Smirnova, N.P., Rudenko, A.V. and Marikvas, Y.S., 2016. Antibacterial and antimycotic activity of cotton fabrics, impregnated with silver and binary silver/copper nanoparticles. *Nanoscale research letters*, *11*(1), pp.1-9.

Ersahin, M.E., Ozgun, H., Dereli, R.K., Ozturk, I., Roest, K. and van Lier, J.B., 2012. A review on dynamic membrane filtration: materials, applications and future perspectives. *Bioresource technology*, *122*, pp.196-206.

Es-Said, A., Nafai, H., El Hamdaoui, L., Bouhaouss, A. and Bchitou, R., 2020. Adsorptivity and selectivity of heavy metals Cd (II), Cu (II), and Zn (II) toward phosphogypsum. *Desalin water treat*, *197*, pp.291-299.

European Commission, NanoData Landscape Compilation - Environment, 2017, https://doi.org/10.2777/ 031727.

Fang, W., Xu, C., Zheng, J., Chen, G. and Jiang, K., 2015. Fabrication of Cu–Ag bimetal nanotube-based copper silicates for enhancement of antibacterial activities. *RSC Advances*, *5*(49), pp.39612-39619.

Feng, J. and Zhang, C.P., 2006. Preparation of Cu–Ni alloy nanocrystallites in water-in-oil microemulsions. *Journal of colloid and interface science*, *293*(2), pp.414-420.

Feng, X., Wu, Z. and Chen, X., 2007. Removal of metal ions from electroplating effluent by EDI process and recycle of purified water. *Separation and purification Technology*, *57*(2), pp.257-263.

Fernando, S., Gunasekara, T. and Holton, J., 2018. Antimicrobial Nanoparticles: applications and mechanisms of action. *Sri Lankan Journal of Infectious Diseases*, 8(1), pp.2–11.

Ferrando, R. and Jellinek, J., 2009. Nano-particles as a catalysts incatalytic converters, RL Johnston. *Chem. Rev*, *108*, p.845.

Feynman, R.P., 1959, December. Plenty of Room at the Bottom. In *APS annual meeting*.

Feynman, R.P., 1960. *There's Plenty of Room at the Bottom. Engineering and Science*, 23 (5). pp. 22-36.

Fortunelli, A. and Velasco, A.M., 2002. A theoretical study of the catalytic properties of Pt/Fe nanoclusters. *Journal of Molecular Structure: THEOCHEM*, *586*(1-3), pp.17-27.

Freundlich, H., 1907. Über die adsorption in lösungen. *Zeitschrift für physikalische Chemie*, *57*(1), pp.385-470.

Gao, Z., Bandosz, T.J., Zhao, Z., Han, M. and Qiu, J., 2009. Investigation of factors affecting adsorption of transition metals on oxidized carbon nanotubes. *Journal of Hazardous Materials*, *167*(1-3), pp.357-365.

García, A., Rodríguez, B., Giraldo, H., Quintero, Y., Quezada, R., Hassan, N. and Estay, H., 2021. Copper-modified polymeric membranes for water treatment: A comprehensive review. *Membranes*, *11*(2), p.93.

Gawande, M.B., Goswami, A., Felpin, F.X., Asefa, T., Huang, X., Silva, R., Zou, X., Zboril, R. and Varma, R.S., 2016. Cu and Cu-based nanoparticles: synthesis and applications in catalysis. *Chemical reviews*, *116*(6), pp.3722-3811.

Giammar, D.E., Maus, C.J. and Xie, L., 2007. Effects of particle size and crystalline phase on lead adsorption to titanium dioxide nanoparticles. *Environmental Engineering Science*, *24*(1), pp.85-95.

Giannousi, K., Lafazanis, K., Arvanitidis, J., Pantazaki, A. and Dendrinou-Samara, C., 2014. Hydrothermal synthesis of copper based nanoparticles: antimicrobial screening and interaction with DNA. *Journal of Inorganic Biochemistry*, *133*, pp.24-32.

Gomaji Chaudhary, R., A Tanna, J., V Gandhare, N., R Rai, A. and D Juneja, H., 2015. Synthesis of nickel nanoparticles: Microscopic investigation, an efficient catalyst and effective antibacterial activity. *Advanced Materials Letters*, *6*(11), pp.990-998.

González, A.G. and Herrador, M.Á., 2007. A practical guide to analytical method validation, including measurement uncertainty and accuracy profiles. *TrAC Trends in Analytical Chemistry*, *26*(3), pp.227-238.

González, E., Arbiol, J. and Puntes, V.F., 2011. Carving at the nanoscale: sequential galvanic exchange and Kirkendall growth at room temperature. *Science*, *334*(6061), pp.1377-1380.

Grass, G., Rensing, C. and Solioz, M., 2011. Metallic copper as an antimicrobial surface. *Applied and environmental microbiology*, *77*(5), pp.1541-1547.

Gupta, V.K., Gupta, M. and Sharma, S., 2001. Process development for the removal of lead and chromium from aqueous solutions using red mud—an aluminium industry waste. *Water research*, *35*(5), pp.1125-1134.

Gurunathan, S., Han, J.W., Dayem, A.A., Eppakayala, V. and Kim, J.H., 2012. Oxidative stress-mediated antibacterial activity of graphene oxide and reduced graphene oxide in Pseudomonas aeruginosa. *International journal of nanomedicine*, *7*, p.5901.

Gutiérrez, M.F., Malaquias, P., Hass, V., Matos, T.P., Lourenço, L., Reis, A., Loguercio, A.D. and Farago, P.V., 2017. The role of copper nanoparticles in an etch-and-rinse adhesive on antimicrobial activity, mechanical properties and the durability of resin-dentine interfaces. *Journal of Dentistry*, *61*, pp.12-20.

Hajipour, A.R. and Abolfathi, P., 2018. Nickel embedded on triazole-modified magnetic nanoparticles: a novel and sustainable heterogeneous catalyst for Hiyama reaction in fluoride-free condition. *Catalysis Communications*, *103*, pp.92-95

Hajipour, M.J., Fromm, K.M., Ashkarran, A.A., de Aberasturi, D.J., de Larramendi, I.R., Rojo, T., Serpooshan, V., Parak, W.J. and Mahmoudi, M., 2012. Antibacterial properties of nanoparticles. *Trends in biotechnology*, *30*(10), pp.499-511.

Han, R., Zou, L., Zhao, X., Xu, Y., Xu, F., Li, Y. and Wang, Y., 2009. Characterization and properties of iron oxide-coated zeolite as adsorbent for removal of copper (II) from solution in fixed bed column. *Chemical Engineering Journal*, *149*(1-3), pp.123-131.

Han, Y. and Yan, W., 2014. Bimetallic nickel–iron nanoparticles for groundwater decontamination: effect of groundwater constituents on surface deactivation. *Water research*, *66*, pp.149-159.

Hänninen, M.L. and Siitonen, A., 1995. Distribution of Aeromonas phenospecies and genospecies among strains isolated from water, foods or from human clinical samples. *Epidemiology & Infection*, *115*(1), pp.39-50.

Harikumar, P., and AnishaAravind B. P., 2016. Heavy metal removal from waste water using Copper alumina Nanocomposite. *International Journal of Innovative and Applied Research*, 4(1), pp.35- 44.

Harikumar, P.S. and Hridya, T. K., 2021. Application of CuNi bimetallic nanoparticle as an adsorbent for the removal of heavy metals from aqueous solution. *International Journal of Environmental Analytical Chemistry*, *101*(6), pp.869-883.

Harish, K., Renu, R. and Kumar, S.R., 2011. Synthesis of nickel hydroxide nanoparticles by reverse micelle method and its antimicrobial activity. *Res J Chem Sci. ISSN*, *2231*, p.606X.

Hashemizadeh, S.A. and Biglari, M., 2018. Cu: Ni bimetallic nanoparticles: facile synthesis, characterization and its application in photodegradation of organic dyes. *Journal of Materials Science: Materials in Electronics*, *29*(15), pp.13025-13031.

Hassan, S.A. and Ghadam, P., 2020. Bimetallic Nanoparticles with Specific Insight into Nanoremediation.

Haydon, B., 2015. Nanoengineering: A Toolbox of Standards for Health and Safety. In *Nanoengineering* (pp. 557-580). Elsevier.

He, Z., Zhang, Z. and Bi, S., 2020. Nanoparticles for organic electronics applications. *Materials Research Express*, *7*(1), p.012004.

Hilbert, D.W., 2011. Uropathogenic Escherichia coli: the pre-eminent urinary tract infection pathogen. *E. coli Infections: Causes, Treatment and Prevention*.

Ho, Y.S., 2006. Review of second-order models for adsorption systems. *Journal of hazardous materials*, *136*(3), pp.681-689.

Hong, R., Fischer, N.O., Emrick, T. and Rotello, V.M., 2005. Surface PEGylation and ligand exchange chemistry of FePt nanoparticles for biological applications. *Chemistry of materials*, *17*(18), pp.4617-4621.

Hou, Y., Kondoh, H., Ohta, T. and Gao, S., 2005. Size-controlled synthesis of nickel nanoparticles. *Applied Surface Science*, *241*(1-2), pp.218-222.

Hristovski, K., Baumgardner, A. and Westerhoff, P., 2007. Selecting metal oxide nanomaterials for arsenic removal in fixed bed columns: from nanopowders to aggregated nanoparticle media. *Journal of hazardous materials*, *147*(1-2), pp.265-274.

Huang, C.C., Lo, S.L. and Lien, H.L., 2015. Vitamin B12-mediated hydrodechlorination of dichloromethane by bimetallic Cu/Al particles. *Chemical Engineering Journal*, *273*, pp.413-420.

Huang, Q., Liu, W. and Huang, W., 2013. Reductive dechlorination of tetrachlorobisphenol A by Pd/Fe bimetallic catalysts. *Journal of hazardous materials*, *262*, pp.634-641.

Husein, D.Z., Hassanien, R. and Al-Hakkani, M.F., 2019. Green-synthesized copper nano-adsorbent for the removal of pharmaceutical pollutants from real wastewater samples. *Heliyon*, *5*(8), p.e02339.

Inglezakis, V.J., Loizidou, M.D. and Grigoropoulou, H.P., 2003. Ion exchange of Pb2+, Cu2+, Fe3+, and Cr3+ on natural clinoptilolite: selectivity determination and influence of acidity on metal uptake. *Journal of colloid and interface science*, *261*(1), pp.49-54.

International Agency for Research on Cancer, 1993. Cadmium and cadmium compounds. Monographs on evaluation of carcinogenic risks to humans, 58, pp.119-237.

Ivanova, E.P., Hasan, J., Webb, H.K., Gervinskas, G., Juodkazis, S., Truong, V.K., Wu, A.H., Lamb, R.N., Baulin, V.A., Watson, G.S. and Watson, J.A., 2013. Bactericidal activity of black silicon. *Nature communications*, *4*(1), pp.1-7.

Jain, M., Garg, V.K. and Kadirvelu, K., 2013. Cadmium (II) sorption and desorption in a fixed bed column using sunflower waste carbon calcium–alginate beads. *Bioresource technology*, *129*, pp.242-248.

Jena, P., Bhattacharya, M., Bhattacharjee, G., Satpati, B., Mukherjee, P., Senapati, D. and Srinivasan, R., 2020. Bimetallic gold–silver nanoparticles mediate bacterial killing by disrupting the actin cytoskeleton MreB. *Nanoscale*, *12*(6), pp.3731-3749.

Jeyaraj Pandian, C., Palanivel, R. and Dhanasekaran, S., 2016. Screening antimicrobial activity of nickel nanoparticles synthesized using Ocimum sanctum leaf extract. *Journal of Nanoparticles*, *2016*.

Jia, F.L., Zhang, L.Z., Shang, X.Y. and Yang, Y., 2008. Non- Aqueous Sol–Gel Approach towards the Controllable Synthesis of Nickel Nanospheres, Nanowires, and Nanoflowers. *Advanced Materials*, *20*(5), pp.1050-1054.

Jian, W., Ma, Y., Wu, H., Zhu, X., Wang, J., Xiong, H., Lin, L. and Wu, L., 2019. Fabrication of highly stable silver nanoparticles using polysaccharide-protein complexes from abalone viscera and antibacterial activity evaluation. *International journal of biological macromolecules*, *128*, pp.839-847.

Jin, L., Zhao, X., Qian, X. and Dong, M., 2018. Nickel nanoparticles encapsulated in porous carbon and carbon nanotube hybrids from bimetallic metal-organic-frameworks for highly efficient adsorption of dyes. *Journal of colloid and interface science*, *509*, pp.245-253.

Jo, C., Lee, J.I. and Jang, Y., 2005. Electronic and magnetic properties of ultrathin Fe− Co alloy nanowires. *Chemistry of materials*, *17*(10), pp.2667-2671.

Joudeh, N. and Linke, D., 2022. Nanoparticle classification, physicochemical properties, characterization, and applications: a comprehensive review for biologists. *Journal of Nanobiotechnology*, *20*(1), pp.1-29.

Jun, L.Y., Mubarak, N.M., Yee, M.J., Yon, L.S., Bing, C.H., Khalid, M. and Abdullah, E.C., 2018. An overview of functionalised carbon nanomaterial for organic pollutant removal. *Journal of Industrial and Engineering Chemistry*, *67*, pp.175-186.

Kadhom, M. and Deng, B., 2018. Metal-organic frameworks (MOFs) in water filtration membranes for desalination and other applications. *Applied Materials Today*, *11*, pp.219-230.

Kahrizi, H., Bafkar, A. and Farasati, M., 2016. Effect of nanotechnology on heavy metal removal from aqueous solution. *Journal of Central South University*, *23*(10), pp.2526-2535.

Kameda, T., Suzuki, Y. and Yoshioka, T., 2014. Removal of arsenic from an aqueous solution by coprecipitation with manganese oxide. *Journal of Environmental Chemical Engineering*, *2*(4), pp.2045-2049.

Kargozar, S. and Mozafari, M., 2018. Nanotechnology and Nanomedicine: Start small, think big. *Materials Today: Proceedings*, *5*(7), pp.15492-15500.

Kataria, N. and Garg, V.K., 2018. Optimization of Pb (II) and Cd (II) adsorption onto ZnO nanoflowers using central composite design: isotherms and kinetics modelling. *Journal of Molecular Liquids*, *271*, pp.228-239.

Kaushal, A. and Singh, S.K., 2017. Adsorption phenomenon and its application in removal of lead from wastewater: a review. *Int. J. Hydrol*, *1*(2), pp.38-47.

Kim, D.K., Kan, D., Veres, T., Normadin, F., Liao, J.K., Kim, H.H., Lee, S.H., Zahn, M. and Muhammed, M., 2005. Monodispersed Fe–Pt nanoparticles for biomedical applications. *Journal of Applied Physics*, *97*(10), p.10Q918.

King, A.S. and Twyman, L.J., 2002. Heterogeneous and solid supported dendrimer catalysts. *Journal of the Chemical Society, Perkin Transactions 1*, (20), pp.2209-2218.

Kodama, D., Shinoda, K., Sato, K., Konno, Y., Joseyphus, R.J., Motomiya, K., Takahashi, H., Matsumoto, T., Sato, Y., Tohji, K. and Jeyadevan, B., 2006. Chemical synthesis of sub- micrometer- to nanometer- sized magnetic FeCo dice. *Advanced Materials*, *18*(23), pp.3154-3159.

Kornblatt, A.P., Nicoletti, V.G. and Travaglia, A., 2016. The neglected role of copper ions in wound healing. *Journal of inorganic biochemistry*, *161*, pp.1-8.

Kuang, H., Yang, P., Yang, L., Aguilar, Z.P. and Xu, H., 2016. Size dependent effect of ZnO nanoparticles on endoplasmic reticulum stress signaling pathway in murine liver. *Journal of hazardous materials*, *317*, pp.119-126.

Kuang, Y., Du, J., Zhou, R., Chen, Z., Megharaj, M. and Naidu, R., 2015. Calcium alginate encapsulated Ni/Fe nanoparticles beads for simultaneous removal of Cu (II) and monochlorobenzene. *Journal of colloid and interface science*, *447*, pp.85-91.

Kuhn, R., Bryant, I.M., Jensch, R. and Böllmann, J., 2022. Applications of Environmental Nanotechnologies in Remediation, Wastewater Treatment, Drinking Water Treatment, and Agriculture. *Applied Nano*, *3*(1), pp.54-90.

Kumar, A.A., Som, A., Longo, P., Sudhakar, C., Bhuin, R.G., Gupta, S.S., Sankar, M.U., Chaudhary, A., Kumar, R. and Pradeep, T., 2017. Confined metastable 2- line ferrihydrite for affordable point- of- use arsenic- free drinking water. *Advanced Materials*, *29*(7), p.1604260.

Kumar, H., Rani, R. and Salar, R., 2010. Reverse micellar synthesis, characterization & antibacterial study of nickel

nanoparticles. *Advances in Control, Chemical Engineering, Civil Engineering and Mechanical Engineering*, pp.88-94.

Kumar, M. and Deka, S., 2014. Multiply twinned AgNi alloy nanoparticles as highly active catalyst for multiple reduction and degradation reactions. *ACS applied materials & interfaces*, *6*(18), pp.16071-16081.

Kumar, R., Bhatia, D., Singh, R., Rani, S. and Bishnoi, N.R., 2011. Sorption of heavy metals from electroplating effluent using immobilized biomass Trichoderma viride in a continuous packed-bed column. *International Biodeterioration & Biodegradation*, *65*(8), pp.1133-1139.

Kumar, S., Majhi, R.K., Singh, A., Mishra, M., Tiwari, A., Chawla, S., Guha, P., Satpati, B., Mohapatra, H., Goswami, L. and Goswami, C., 2019. Carbohydrate-coated gold–silver nanoparticles for efficient elimination of multidrug resistant bacteria and in vivo wound healing. *ACS applied materials & interfaces*, *11*(46), pp.42998-43017.

Kumari, M.M., Jacob, J. and Philip, D., 2015. Green synthesis and applications of Au–Ag bimetallic nanoparticles. *Spectrochimica Acta Part A: Molecular and Biomolecular Spectroscopy*, *137*, pp.185-192.

Kummu, M., Ward, P.J., de Moel, H. and Varis, O., 2010. Is physical water scarcity a new phenomenon? Global assessment of water shortage over the last two millennia. *Environmental Research Letters*, *5*(3), p.034006.

Langmuir, I., 1918. The adsorption of gases on plane surfaces of glass, mica and platinum. *Journal of the American Chemical society*, *40*(9), pp.1361-1403.

Lei, C., Zhang, L., Yang, K., Zhu, L. and Lin, D., 2016. Toxicity of iron-based nanoparticles to green algae: effects of particle size, crystal phase, oxidation state and environmental aging. *Environmental Pollution*, *218*, pp.505-512.

Leung, Y.H., Ng, A.M., Xu, X., Shen, Z., Gethings, L.A., Wong, M.T., Chan, C.M., Guo, M.Y., Ng, Y.H., Djurišić, A.B. and Lee, P.K., 2014. Mechanisms of antibacterial activity of MgO: non- ROS mediated toxicity of MgO nanoparticles towards Escherichia coli. *Small*, *10*(6), pp.1171-1183.

Lewis, D.L. and Gattie, D.K., 2002. Peer reviewed: pathogen risks from applying sewage sludge to land. *Environmental Science & Technology*, *36*(13), pp.286A-293A.

Li, D., Dong, M., Besenbacher, F., Huang, Y. and Chen, M., 2016. The preparation of a recyclable catalyst of silver nanoparticles dispersed in a mesoporous silica nanofiber matrix. *RSC advances*, *6*(70), pp.65613-65618.

Li, G. and Tang, Z., 2014. Noble metal nanoparticle@ metal oxide core/yolk–shell nanostructures as catalysts: recent progress and perspective. *Nanoscale*, *6*(8), pp.3995-4011.

Li, H., He, Z., Ouyang, Z., Palchoudhury, S., Ingram, C.W., Harruna, I.I. and Li, D., 2020. Modifying electrical and magnetic properties of single-walled carbon nanotubes by decorating with iron oxide nanoparticles. *Journal of Nanoscience and Nanotechnology*, *20*(4), pp.2611-2616.

Li, Q., Mahendra, S., Lyon, D.Y., Brunet, L., Liga, M.V., Li, D. and Alvarez, P.J., 2008. Antimicrobial nanomaterials for water disinfection and microbial control: potential applications and implications. *Water research*, *42*(18), pp.4591-4602.

Li, S., Yan, X., Yang, Z., Yang, Y., Liu, X. and Zou, J., 2014. Preparation and antibacterial property of silver decorated carbon microspheres. *Applied surface science*, *292*, pp.480-487.

Li, W., Yue, Q., Tu, P., Ma, Z., Gao, B., Li, J. and Xu, X., 2011. Adsorption characteristics of dyes in columns of activated carbon prepared from paper mill sewage sludge. *Chemical Engineering Journal*, *178*, pp.197-203.

Li, X., Xu, H., Chen, Z.S. and Chen, G., 2011. Biosynthesis of nanoparticles by microorganisms and their applications. *Journal of Nanomaterials*, *2011*.

Li, Y., Cao, L., Li, L. and Yang, C., 2015. In situ growing directional spindle TiO2 nanocrystals on cellulose fibers for enhanced Pb2+ adsorption from water. *Journal of Hazardous Materials*, *289*, pp.140-148.

Li, Z., Greden, K., Alvarez, P.J., Gregory, K.B. and Lowry, G.V., 2010. Adsorbed polymer and NOM limits adhesion and toxicity of nano scale zerovalent iron to E. coli. *Environmental science & technology*, *44*(9), pp.3462-3467.

Lima, R.A., de Souza, S.L.X., Lima, L.A., Batista, A.L.X., de Araújo, J.T.C., Sousa, F.F.O., Rolim, J.P.M.L. and Bandeira, T.D.J.P.G., 2020. Antimicrobial effect of anacardic acid–loaded zein nanoparticles loaded on Streptococcus mutans biofilms. *Brazilian Journal of Microbiology*, *51*(4), pp.1623-1630.

Lin, C.J., Liou, Y.H. and Lo, S.L., 2009. Supported Pd/Sn bimetallic nanoparticles for reductive dechlorination of aqueous trichloroethylene. *Chemosphere*, *74*(2), pp.314-319.

Lin, Q., Pan, J., Lin, Q. and Liu, Q., 2013. Microwave synthesis and adsorption performance of a novel crosslinked starch microsphere. *Journal of Hazardous Materials*, *263*, pp.517-524.

Lin, Y., Chen, Z., Megharaj, M. and Naidu, R., 2012. Degradation of scarlet 4BS in aqueous solution using bimetallic Fe/Ni nanoparticles. *Journal of colloid and interface science*, *381*(1), pp.30-35.

Lin, Y., Jin, X., Khan, N.I., Owens, G. and Chen, Z., 2022. Bimetallic Fe/Ni nanoparticles derived from green synthesis for the removal of arsenic (V) in mine wastewater. *Journal of Environmental Management*, *301*, p.113838.

Lisiecki, I., Bjoerling, M., Motte, L., Ninham, B. and Pileni, M.P., 1995. Synthesis of copper nanosize particles in anionic reverse micelles: effect of the addition of a cationic surfactant on the size of the crystallites. *Langmuir*, *11*(7), pp.2385-2392.

Liu, L., Zhou, X., Liu, L., Jiang, S., Li, Y., Guo, L., Yan, S. and Tai, X., 2019. Heterogeneous bimetallic Cu–Ni nanoparticle-supported catalysts in the selective oxidation of benzyl alcohol to benzaldehyde. *Catalysts*, *9*(6), p.538.

Liu, S., Mei, J., Zhang, C., Zhang, J. and Shi, R., 2018. Synthesis and magnetic properties of shuriken-like nickel nanoparticles. *Journal of Materials Science & Technology*, *34*(5), pp.836-841.

Liu, W.J., Qian, T.T. and Jiang, H., 2014. Bimetallic Fe nanoparticles: recent advances in synthesis and application in catalytic elimination of environmental pollutants. *Chemical Engineering Journal*, *236*, pp.448-463.

Liu, X., Chen, Z., Chen, Z., Megharaj, M. and Naidu, R., 2013. Remediation of Direct Black G in wastewater using kaolin-supported bimetallic Fe/Ni nanoparticles. *Chemical engineering journal*, *223*, pp.764-771.

Liu, Y., Liang, P. and Guo, L., 2005. Nanometer titanium dioxide immobilized on silica gel as sorbent for preconcentration of metal ions prior to their determination by inductively coupled plasma atomic emission spectrometry. *Talanta*, *68*(1), pp.25-30.

Lo, W., Chua, H., Lam, K.H. and Bi, S.P., 1999. A comparative investigation on the biosorption of lead by filamentous fungal biomass. *Chemosphere*, *39*(15), pp.2723-2736.

Lu, H., Tian, B., Wang, J. and Hao, H., 2017. Montmorillonite-supported Fe/Ni bimetallic nanoparticles for removal of Cr (VI) from wastewater. *Chemical Engineering Transactions*, *60*, pp.169-174.

Lu, X., Wang, L., Lei, K., Huang, J. and Zhai, Y., 2009. Contamination assessment of copper, lead, zinc, manganese and nickel in street dust of Baoji, NW China. *Journal of hazardous materials*, *161*(2-3), pp.1058-1062.

Luo, D., Zhang, G., Liu, J. and Sun, X., 2011. Evaluation criteria for reduced graphene oxide. *The Journal of Physical Chemistry C*, *115*(23), pp.11327-11335.

Luo, X., Deng, Z., Lin, X. and Zhang, C., 2011. Fixed-bed column study for Cu2+ removal from solution using expanding rice husk. *Journal of hazardous materials*, *187*(1-3), pp.182-189.

Mahar, A.M., Alveroglu, E., Balouch, A., Talpur, F.N. and Jagirani, M.S., 2022. Fabrication of Fe/Bi bimetallic magnetic nano-oxides (IBBMNOs) as efficient remediator for hexavalent chromium from aqueous environment. *Environmental Science and Pollution Research*, pp.1-15.

Maheshwari, M., Nelapati, K. and Kiranmayi, B., 2011. Vibrio cholerae-A Review. *Veterinary world*, *4*(9).

Mahmoodi, S., Elmi, A. and Hallaj-Nezhadi, S., 2018. Copper Nanoparticles as Antibacterial Agents. *Molecular Pharmaceutics & Organic Process Research*, 06, pp140.

Mahmoud, A.M., Ibrahim, F.A., Shaban, S.A. and Youssef, N.A., 2015. Adsorption of heavy metal ion from aqueous solution by nickel oxide

nano catalyst prepared by different methods. *Egyptian Journal of Petroleum*, *24*(1), pp.27-35.

Mahmoud, A.M., Ibrahim, F.A., Shaban, S.A. and Youssef, N.A., 2015. Adsorption of heavy metal ion from aqueous solution by nickel oxide nano catalyst prepared by different methods. *Egyptian Journal of Petroleum*, *24*(1), pp.27-35.

Mallick, K. and Scurrell, M.S., 2003. CO oxidation over gold nanoparticles supported on TiO_2 and TiO_2-ZnO: catalytic activity effects due to surface modification of TiO_2 with ZnO. *Applied Catalysis A: General*, *253*(2), pp.527-536.

Maqbool, Q., Iftikhar, S., Nazar, M., Abbas, F., Saleem, A., Hussain, T., Kausar, R., Anwaar, S. and Jabeen, N., 2017. Green fabricated CuO nanobullets via Olea europaea leaf extract shows auspicious antimicrobial potential. *IET nanobiotechnology*, *11*(4), pp.463-468.

Marcus, Y., 1988. Ionic radii in aqueous solutions. *Chemical Reviews*, *88*(8), pp.1475-1498.

Marg, B.Z., 2011. Hazardous metals and minerals pollution in India: Sources, toxicity and management. *A Position Paper, Indian National Science Academy, New Delhi*.

Markova, Z., S□is□ková, K.M., Filip, J., C□uda, J., Kolár□, M., S□afár□ová, K., Medr□ík, I. and Zbor□il, R., 2013. Air stable magnetic bimetallic Fe–Ag nanoparticles for advanced antimicrobial treatment and phosphorus removal. *Environmental science & technology*, *47*(10), pp.5285-5293.

Maruthupandy, M., Zuo, Y., Chen, J.S., Song, J.M., Niu, H.L., Mao, C.J., Zhang, S.Y. and Shen, Y.H., 2017. Synthesis of metal oxide nanoparticles (CuO and ZnO NPs) via biological template and their optical sensor applications. *Applied Surface Science*, *397*, pp.167-174.

Matlock, M.M., Howerton, B.S. and Atwood, D.A., 2002. Chemical precipitation of heavy metals from acid mine drainage. *Water research*, *36*(19), pp.4757-4764.

Mattei, G., de Julián Fernández, C., Mazzoldi, P., Sada, C., De, G., Battaglin, G., Sangregorio, C. and Gatteschi, D., 2002. Synthesis, Structure, and Magnetic Properties of Co, Ni, and Co− Ni Alloy Nanocluster-Doped

SiO2 Films by Sol− Gel Processing. *Chemistry of materials*, *14*(8), pp.3440-3447.

Mauter, M.S. and Elimelech, M., 2008. Environmental applications of carbon-based nanomaterials. *Environmental science & technology*, *42*(16), pp.5843-5859.

McNabb, D.E., 2019. Alternative Sources of Water Supply. In *Global Pathways to Water Sustainability* (pp. 251-262). Palgrave Macmillan, Cham.

McNabb, D.E., 2019. The population growth barrier. In *Global pathways to water sustainability* (pp. 67-81). Palgrave Macmillan, Cham.

Mekonnen, M.M. and Hoekstra, A.Y., 2016. Four billion people facing severe water scarcity. *Science advances*, *2*(2), p.e1500323.

Meunier, N., Drogui, P., Montané, C., Hausler, R., Mercier, G. and Blais, J.F., 2006. Comparison between electrocoagulation and chemical precipitation for metals removal from acidic soil leachate. *Journal of hazardous materials*, *137*(1), pp.581-590.

Midander, K., Cronholm, P., Karlsson, H.L., Elihn, K., Möller, L., Leygraf, C. and Wallinder, I.O., 2009. Surface characteristics, copper release, and toxicity of nano- and micrometer- sized copper and copper (II) oxide particles: a cross- disciplinary study. *Small*, *5*(3), pp.389-399.

Milly, P.C.D., Wetherald, R.T., Dunne, K.A. and Delworth, T.L., 2002. Increasing risk of great floods in a changing climate. *Nature*, *415*(6871), pp.514-517.

Mishra, S.P., 2014. Adsorption–desorption of heavy metal ions. *Current Science*, pp.601-612.

Mittal, A.K., Kumar, S. and Banerjee, U.C., 2014. Quercetin and gallic acid mediated synthesis of bimetallic (silver and selenium) nanoparticles and their antitumor and antimicrobial potential. *Journal of colloid and interface science*, *431*, pp.194-199.

Momeni, S., Ahmadi, R., Safavi, A. and Nabipour, I., 2017. Blue-emitting copper nanoparticles as a fluorescent probe for detection of cyanide ions. *Talanta*, *175*, pp.514-521.

Mondal, A., Arora, M., Dubey, B.K. and Mumford, K., 2022. Comparative assessment of the characteristics and Cr (VI) removal activity of the

bimetallic Fe/Cu nanoparticles pre-and post-coated with carboxymethyl cellulose. *Chemical Engineering Journal*, *444*, p.136343.

Montazer, M., Shamei, A. and Alimohammadi, F., 2012. Stabilized nanosilver loaded nylon knitted fabric using BTCA without yellowing. *Progress in Organic Coatings*, *74*(1), pp.270-276.

Moritz, M. and Geszke-Moritz, M., 2013. The newest achievements in synthesis, immobilization and practical applications of antibacterial nanoparticles. *Chemical Engineering Journal*, *228*, pp.596-613.

Morones, J.R., Elechiguerra, J.L., Camacho, A., Holt, K., Kouri, J.B., Ramírez, J.T. and Yacaman, M.J., 2005. The bactericidal effect of silver nanoparticles. *Nanotechnology*, *16*(10), p.2346.

Morris, J. and Willis, J., 2007. US Environmental Protection Agency nanotechnology white paper. *US Environmental Protection Agency, Washington, DC*.

Musee, N., Thwala, M. and Nota, N., 2011. The antibacterial effects of engineered nanomaterials: implications for wastewater treatment plants. *Journal of Environmental Monitoring*, *13*(5), pp.1164-1183.

Nagpal, V., Bokare, A.D., Chikate, R.C., Rode, C.V. and Paknikar, K.M., 2010. Reductive dechlorination of γ-hexachlorocyclohexane using Fe–Pd bimetallic nanoparticles. *Journal of hazardous materials*, *175*(1-3), pp.680-687.

Nagy, A., Harrison, A., Sabbani, S., Munson Jr, R.S., Dutta, P.K. and Waldman, W.J., 2011. Silver nanoparticles embedded in zeolite membranes: release of silver ions and mechanism of antibacterial action. *International journal of nanomedicine*, *6*, p.1833.

Ni, S.Q. and Yang, N., 2014. Cation exchange resin immobilized bimetallic nickel–iron nanoparticles to facilitate their application in pollutants degradation. *Journal of colloid and interface science*, *420*, pp.158-165.

Niu, H.L., Chen, Q.W., Lin, Y.S., Jia, Y.S., Zhu, H.F. and Ning, M., 2004. Hydrothermal formation of magnetic Ni–Cu alloy nanocrystallites at low temperatures. *Nanotechnology*, *15*(8), p.1054.

NNI, The national nanotechnology initiative supplement to the president's 2020 budget, Available at: https://www.whitehouse.gov/wp-

content/uploads/2018/08/The-National-Nanotechnology-Initiative-Supplement-to-the-President%E2%80%99s-2019-Budget.pdf, 2020.

Noyes, P.D., McElwee, M.K., Miller, H.D., Clark, B.W., Van Tiem, L.A., Walcott, K.C., Erwin, K.N. and Levin, E.D., 2009. The toxicology of climate change: environmental contaminants in a warming world. *Environment international*, *35*(6), pp.971-986.

Nriagu, J.O. and Pacyna, J.M., 1988. Quantitative assessment of worldwide contamination of air, water and soils by trace metals. *nature*, *333*(6169), pp.134-139.

Nuić, I., Trgo, M., Perić, J. and Medvidović, N.V., 2013. Analysis of breakthrough curves of Pb and Zn sorption from binary solutions on natural clinoptilolite. *Microporous and Mesoporous Materials*, *167*, pp.55-61.

Ojha, N.K., Zyryanov, G.V., Majee, A., Charushin, V.N., Chupakhin, O.N. and Santra, S., 2017. Copper nanoparticles as inexpensive and efficient catalyst: A valuable contribution in organic synthesis. *Coordination Chemistry Reviews*, *353*, pp.1-57.

Olvera, R.C., Silva, S.L., Robles-Belmont, E. and Lau, E.Z., 2017. Review of nanotechnology value chain for water treatment applications in Mexico. *Resource-Efficient Technologies*, *3*(1), pp.1-11.

Omer, A., Elagib, N.A., Zhuguo, M., Saleem, F. and Mohammed, A., 2020. Water scarcity in the Yellow River Basin under future climate change and human activities. *Science of the Total Environment*, *749*, p.141446.

Omori, T., Ando, K., Okano, M., Xu, X., Tanaka, Y., Ohnuma, I., Kainuma, R. and Ishida, K., 2011. Superelastic effect in polycrystalline ferrous alloys. *Science*, *333*(6038), pp.68-71.

Ou, J.H., Sheu, Y.T., Tsang, D.C., Sun, Y.J. and Kao, C.M., 2020. Application of iron/aluminum bimetallic nanoparticle system for chromium-contaminated groundwater remediation. *Chemosphere*, *256*, p.127158.

Pal, S.L., Jana, U., Manna, P.K., Mohanta, G.P. and Manavalan, R., 2011. Nanoparticle: An overview of preparation and characterization. *Journal of applied pharmaceutical science*, (Issue), pp.228-234.

Pan, C., Qian, J., Fan, J., Guo, H., Gou, L., Yang, H. and Liang, C., 2019. Preparation nanoparticle by ionic cross-linked emulsified chitosan and its antibacterial activity. *Colloids and Surfaces A: Physicochemical and Engineering Aspects*, *568*, pp.362-370.

Pandey, A. and Manivannan, R., 2015. A study on synthesis of nickel nanoparticles using chemical reduction technique. *Recent Patents on Nanomedicine*, *5*(1), pp.33-37.

Pandey, J. and Pandey, U., 2009. Atmospheric deposition and heavy metal contamination in an organic farming system in a seasonally dry tropical region of India. *Journal of Sustainable Agriculture*, *33*(4), pp.361-378.

Pang, H., Lu, Q., Li, Y. and Gao, F., 2009. Facile synthesis of nickel oxide nanotubes and their antibacterial, electrochemical and magnetic properties. *Chemical Communications*, (48), pp.7542-7544.

Pehlivan, E., Yanık, B.H., Ahmetli, G. and Pehlivan, M., 2008. Equilibrium isotherm studies for the uptake of cadmium and lead ions onto sugar beet pulp. *Bioresource technology*, *99*(9), pp.3520-3527.

Pelgrift, R.Y. and Friedman, A.J., 2013. Nanotechnology as a therapeutic tool to combat microbial resistance. *Advanced drug delivery reviews*, *65*(13-14), pp.1803-1815.

Perdikaki, A., Galeou, A., Pilatos, G., Karatasios, I., Kanellopoulos, N.K., Prombona, A. and Karanikolos, G.N., 2016. Ag and Cu monometallic and Ag/Cu bimetallic nanoparticle–graphene composites with enhanced antibacterial performance. *ACS Applied Materials & Interfaces*, *8*(41), pp.27498-27510.

Perdikaki, A., Galeou, A., Pilatos, G., Karatasios, I., Kanellopoulos, N.K., Prombona, A. and Karanikolos, G.N., 2016. Ag and Cu monometallic and Ag/Cu bimetallic nanoparticle–graphene composites with enhanced antibacterial performance. *ACS applied materials & interfaces*, *8*(41), pp.27498-27510.

Pokropivny, V.V. and Skorokhod, V.V., 2008. New dimensionality classifications of nanostructures. *Physica E: Low-dimensional Systems and nanostructures*, *40*(7), pp.2521-2525.

Pradeep, T., 2009. Noble metal nanoparticles for water purification: a critical review. *Thin solid films*, *517*(24), pp.6441-6478.

Prasse, C., Zech, W., Itanna, F. and Glaser, B., 2012. Contamination and source assessment of metals, polychlorinated biphenyls, and polycyclic aromatic hydrocarbons in urban soils from Addis Ababa, Ethiopia. *Toxicological & Environmental Chemistry*, *94*(10), pp.1954-1979.

Prüss- Ustün, A., Bartram, J., Clasen, T., Colford Jr, J.M., Cumming, O., Curtis, V., Bonjour, S., Dangour, A.D., De France, J., Fewtrell, L. and Freeman, M.C., 2014. Burden of disease from inadequate water, sanitation and hygiene in low- and middle- income settings: a retrospective analysis of data from 145 countries. *Tropical Medicine & International Health*, *19*(8), pp.894-905.

Pureit, 28.10.2014. HUL Pureit Classic 23L. Hindustan Unilever Limited http://www.pureitwater.com/IN/products%E2%80%8E/pureit-classic-23l.

Qu, X., Alvarez, P.J. and Li, Q., 2013. Applications of nanotechnology in water and wastewater treatment. *Water research*, *47*(12), pp.3931-3946.

Quezada, R., Quintero, Y., Salgado, J.C., Estay, H. and García, A., 2020. Understanding the phenomenon of copper ions release from copper-modified TFC membranes: A mathematical and experimental methodology using shrinking core model. *Nanomaterials*, *10*(6), p.1130.

Raffi, M., Mehrwan, S., Bhatti, T.M., Akhter, J.I., Hameed, A. and Yawar, W., 2010. Investigations into the antibacterial behavior of copper nanoparticles against Escherichia coli. *Annals of microbiology*, *60*(1), pp.75-80.

Raghav, S., Nair, M. and Kumar, D., 2019. Tetragonal prism shaped Ni-Al bimetallic adsorbent for study of adsorptive removal of fluoride and role of ion-exchange. *Applied Surface Science*, *498*, p.143785.

Rahimi, M., Pourmortazavi, S.M., Zandavar, H. and Mirsadeghi, S., 2021. Recyclable methodology over bimetallic zero-valent Mg: Zn composition for hexavalent chromium remediation via batch and flow systems in industrial wastewater: An experimental design. *Journal of Materials Research and Technology*, *11*, pp.1-18.

Rajesh, K.M., Ajitha, B., Reddy, Y.A.K., Suneetha, Y. and Reddy, P.S., 2018. Assisted green synthesis of copper nanoparticles using

Syzygium aromaticum bud extract: Physical, optical and antimicrobial properties. *Optik*, *154*, pp.593-600.

Rao, C.N.R., Kulkarni, G.U., Thomas, P.J. and Edwards, P.P., 2003. Size-dependent chemistry: properties of nanocrystals. In *Advances In Chemistry: A Selection of CNR Rao's Publications (1994–2003)* (pp. 227-233).

Ravikumar, K.V.G., Kubendiran, H., Ramesh, K., Rani, S., Mandal, T.K., Pulimi, M., Natarajan, C. and Mukherjee, A., 2020. Batch and column study on tetracycline removal using green synthesized NiFe nanoparticles immobilized alginate beads. *Environmental Technology & Innovation*, *17*, p.100520.

Ravikumar, K.V.G., Singh, A.S., Sikarwar, D., Gopal, G., Das, B., Mrudula, P., Natarajan, C. and Mukherjee, A., 2019. Enhanced tetracycline removal by in-situ NiFe nanoparticles coated sand in column reactor. *Journal of environmental management*, *236*, pp.93-99.

Reddad, Z., Gerente, C., Andres, Y. and Le Cloirec, P., 2002. Adsorption of several metal ions onto a low-cost biosorbent: kinetic and equilibrium studies. *Environmental science & technology*, *36*(9), pp.2067-2073.

Ren, X., Li, J., Tan, X., Shi, W., Chen, C., Shao, D., Wen, T., Wang, L., Zhao, G., Sheng, G. and Wang, X., 2014. Impact of Al2O3 on the aggregation and deposition of graphene oxide. *Environmental science & technology*, *48*(10), pp.5493-5500.

Riaz, N., Chong, F.K., Dutta, B.K., Man, Z.B., Khan, M.S. and Nurlaela, E., 2012. Photodegradation of Orange II under visible light using Cu–Ni/TiO2: Effect of calcination temperature. *Chemical Engineering Journal*, *185*, pp.108-119.

Ribeiro, M.S., de Melo, L.S., Farooq, S., Baptista, A., Kato, I.T., Nunez, S.C. and de Araujo, R.E., 2018. Photodynamic inactivation assisted by localized surface plasmon resonance of silver nanoparticles: In vitro evaluation on Escherichia coli and Streptococcus mutans. *Photodiagnosis and Photodynamic Therapy*, *22*, pp.191-196.

Rijsberman, F.R., 2006. Water scarcity: fact or fiction?. *Agricultural water management*, *80*(1-3), pp.5-22.

Roduner, E., 2006. Size matters: why nanomaterials are different. *Chemical Society Reviews*, *35*(7), pp.583-592.

Roselina, N.N. and Azizan, A., 2012. Ni nanoparticles: study of particles formation and agglomeration. *Procedia Engineering*, *41*, pp.1620-1626.

Saberi, A., 2012. Comparison of Pb^{2+} removal efficiency by zero valent iron nanoparticles and Ni/Fe bimetallic nanoparticles. *Iranian (Iranica) Journal of Energy & Environment*, *3*(2).

Sadrolhosseini, A.R., Abdul Rashid, S., Zakaria, A. and Shameli, K., 2016. Green fabrication of copper nanoparticles dispersed in walnut oil using laser ablation technique. *Journal of Nanomaterials*, *2016*.

Safonov, A., Sulyaeva, V., Timoshenko, N. and Starinskiy, S., 2017. Synthesis of copper nanoparticles in a fluoropolymer matrix by annealing in vacuum. *Physics Letters A*, *381*(25-26), pp.2103-2106.

Saleh, T.A., 2020. Nanomaterials: Classification, properties, and environmental toxicities. *Environmental Technology & Innovation*, *20*, p.101067.

Salem, S.S., Hammad, E.N., Mohamed, A.A. and El-Dougdoug, W., 2022. A comprehensive review of nanomaterials: Types, synthesis, characterization, and applications. *Biointerface Res. Appl. Chem*, *13*(1), p.41.

Sandia, D., 2003. water purification roadmap–a report of the executive committee, US Department of the Interior, Bureau of Reclamation and Sandia National Laboratories.

Sankar, M.U., Aigal, S., Maliyekkal, S.M., Chaudhary, A., Anshup, Kumar, A.A., Chaudhari, K. and Pradeep, T., 2013. Biopolymer-reinforced synthetic granular nanocomposites for affordable point-of-use water purification. *Proceedings of the National Academy of Sciences*, *110*(21), pp.8459-8464.

Santo, C.E., Taudte, N., Nies, D.H. and Grass, G., 2008. Contribution of copper ion resistance to survival of Escherichia coli on metallic copper surfaces. *Applied and environmental microbiology*, *74*(4), pp.977-986.

Sarin, V., Singh, T.S. and Pant, K.K., 2006. Thermodynamic and breakthrough column studies for the selective sorption of chromium from industrial effluent on activated eucalyptus bark. *Bioresource technology*, *97*(16), pp.1986-1993.

Sarkar, S. and Das, S.K., 2016. Removal of Cr (VI) and Cu (II) ions from aqueous solution by rice husk ash—column studies. *Desalination and Water Treatment*, *57*(43), pp.20340-20349.

Sarma, G.K., Sen Gupta, S. and Bhattacharyya, K.G., 2019. Nanomaterials as versatile adsorbents for heavy metal ions in water: a review. *Environmental Science and Pollution Research*, *26*(7), pp.6245-6278.

Schwarzenbach, R.P., Egli, T., Hofstetter, T.B., Von Gunten, U. and Wehrli, B., 2010. Global water pollution and human health. *Annual review of environment and resources*, *35*(1), pp.109-136.

Scott, J.R. and Barnett, T.C., 2006. Surface proteins of gram-positive bacteria and how they get there. *Annual review of microbiology*, *60*(1), pp.397-423.

Seethapathy, V., Sudarsan, P., Pandey, A.K., Pandiyan, A., Kumar, T.V., Sanjeevi, K., Sundramoorthy, A.K. and Moorthy, S.B.K., 2019. Synergistic effect of bimetallic Cu: Ni nanoparticles for the efficient catalytic conversion of 4-nitrophenol. *New Journal of Chemistry*, *43*(7), pp.3180-3187.

Sepúlveda, P., Rubio, M.A., Baltazar, S.E., Rojas-Nunez, J., Llamazares, J.S., Garcia, A.G. and Arancibia-Miranda, N., 2018. As (V) removal capacity of FeCu bimetallic nanoparticles in aqueous solutions: the influence of Cu content and morphologic changes in bimetallic nanoparticles. *Journal of colloid and interface science*, *524*, pp.177-187.

Shannon, M.A., Bohn, P.W., Elimelech, M., Georgiadis, J.G., Marinas, B.J. and Mayes, A.M., 2010. Science and technology for water purification in the coming decades. *Nanoscience and technology: a collection of reviews from nature Journals*, pp.337-346.

Sharma, G., Kumar, A., Sharma, S., Naushad, M., Dwivedi, R.P., ALOthman, Z.A. and Mola, G.T., 2019. Novel development of nanoparticles to bimetallic nanoparticles and their composites: A review. *Journal of King Saud University-Science*, *31*(2), pp.257-269.

Sharma, G., Naushad, M., Kumar, A., Devi, S. and Khan, M.R., 2015. Lanthanum/Cadmium/Polyaniline bimetallic nanocomposite for the photodegradation of organic pollutant. *Iranian Polymer Journal*, *24*(12), pp.1003-1013.

Shi, T., Jia, S., Chen, Y., Wen, Y., Du, C., Guo, H. and Wang, Z., 2009. Adsorption of Pb (II), Cr (III), Cu (II), Cd (II) and Ni (II) onto a vanadium mine tailing from aqueous solution. *Journal of hazardous materials*, *169*(1-3), pp.838-846.

Silva, A.R., Freitas, M.M.A., Freire, C., de Castro, B. and Figueiredo, J.L., 2002. Heterogenization of a functionalized copper (II) Schiff base complex by direct immobilization onto an oxidized activated carbon. *Langmuir*, *18*(21), pp.8017-8024.

Silva, N., Ramírez, S., Díaz, I., Garcia, A. and Hassan, N., 2019. Easy, quick, and reproducible sonochemical synthesis of CuO nanoparticles. *Materials*, *12*(5), p.804.

Simeonidis, K., Martinez-Boubeta, C., Zamora-Perez, P., Rivera-Gil, P., Kaprara, E., Kokkinos, E. and Mitrakas, M., 2018. Nanoparticles for heavy metal removal from drinking water. In *Environmental Nanotechnology* (pp. 75-124). Springer, Cham.

Simeonidis, K., Martinez-Boubeta, C., Zamora-Pérez, P., Rivera-Gil, P., Kaprara, E., Kokkinos, E. and Mitrakas, M., 2019. Implementing nanoparticles for competitive drinking water purification. *Environmental Chemistry Letters*, *17*(2), pp.705-719.

Singh, A. and Prasad, S.M., 2015. Remediation of heavy metal contaminated ecosystem: an overview on technology advancement. *International Journal of Environmental Science and Technology*, *12*(1), pp.353-366.

Singh, H.P., Gupta, N., Sharma, S.K. and Sharma, R.K., 2013. Synthesis of bimetallic Pt–Cu nanoparticles and their application in the reduction of rhodamine B. *Colloids and Surfaces A: Physicochemical and Engineering Aspects*, *416*, pp.43-50.

Singh, N. and Gupta, S.K., 2016. Adsorption of heavy metals: a review. *Int. J. Innov. Res. Sci. Eng. Technol*, *5*(2), pp.2267-2281.

Singh, P.P., 2003. Relativity and magnetism in Ni–Pd and Ni–Pt alloys. *Journal of magnetism and magnetic materials*, *261*(3), pp.347-352.

Singh, R., Gautam, N., Mishra, A. and Gupta, R., 2011. Heavy metals and living systems: An overview. *Indian journal of pharmacology*, *43*(3), p.246.

Singh, S., Joshi, H.C., Srivastava, A., Sharma, A. and Verma, N., 2014. An efficient antibacterial multi-scale web of carbon fibers with asymmetrically dispersed Ag–Cu bimetal nanoparticles. *Colloids and Surfaces A: Physicochemical and Engineering Aspects*, *443*, pp.311-319.

Sistemática, D., Gabriela, S.S., Daniela, F.R. and Helia, B.T., 2016. Copper nanoparticles as potential antimicrobial agent in disinfecting root canals. A systematic review. *Int. J. Odontostomat*, *10*(3), pp.547-554.

Sobal, N.S., Ebels, U., Möhwald, H. and Giersig, M., 2003. Synthesis of core− shell PtCo nanocrystals. *The Journal of Physical Chemistry B*, *107*(30), pp.7351-7354.

Sondi, I. and Salopek-Sondi, B., 2004. Silver nanoparticles as antimicrobial agent: a case study on E. coli as a model for Gram-negative bacteria. *Journal of colloid and interface science*, *275*(1), pp.177-182.

Srinoi, P., Chen, Y.T., Vittur, V., Marquez, M.D. and Lee, T.R., 2018. Bimetallic nanoparticles: enhanced magnetic and optical properties for emerging biological applications. *Applied Sciences*, *8*(7), p.1106.

Su, Y., Adeleye, A.S., Huang, Y., Sun, X., Dai, C., Zhou, X., Zhang, Y. and Keller, A.A., 2014. Simultaneous removal of cadmium and nitrate in aqueous media by nanoscale zerovalent iron (nZVI) and Au doped nZVI particles. *Water research*, *63*, pp.102-111.

Sudhasree, S., Shakila Banu, A., Brindha, P. and Kurian, G.A., 2014. Synthesis of nickel nanoparticles by chemical and green route and their comparison in respect to biological effect and toxicity. *Toxicological & Environmental Chemistry*, *96*(5), pp.743-754.

Sun, Y., Yang, S., Chen, Y., Ding, C., Cheng, W. and Wang, X., 2015. Adsorption and desorption of U (VI) on functionalized graphene oxides: a combined experimental and theoretical study. *Environmental science & technology*, *49*(7), pp.4255-4262.

Swach, 28.10.2014. Tata Swach Cristella Plus. Tata Chemicals Limited http://www.tataswach.com/shopping/product_index.aspx#.

Tabakci, M. and Yilmaz, M., 2008. Sorption characteristics of Cu (II) ions onto silica gel-immobilized calix [4] arene polymer in aqueous

solutions: batch and column studies. *Journal of Hazardous Materials*, *151*(2-3), pp.331-338.

Taner, M., Sayar, N., Yulug, I.G. and Suzer, S., 2011. Synthesis, characterization and antibacterial investigation of silver–copper nanoalloys. *Journal of Materials Chemistry*, *21*(35), pp.13150-13154.

Tang, C., Shu, Y., Zhang, R., Li, X., Song, J., Li, B., Zhang, Y. and Ou, D., 2017. Comparison of the removal and adsorption mechanisms of cadmium and lead from aqueous solution by activated carbons prepared from Typha angustifolia and Salix matsudana. *RSC advances*, *7*(26), pp.16092-16103.

Tarafdar, J.C., Sharma, S. and Raliya, R., 2013. Nanotechnology: Interdisciplinary science of applications. *African Journal of Biotechnology*, *12*(3).

Tchounwou, P.B., Yedjou, C.G., Patlolla, A.K. and Sutton, D.J., 2012. Heavy metal toxicity and the environment. *Molecular, clinical and environmental toxicology*, pp.133-164.

Thakur, S., Sharma, S., Thakur, S. and Rai, R., 2018. Green synthesis of copper nano-particles using Asparagus adscendens roxb. Root and leaf extract and their antimicrobial activities. *Int. J. Curr. Microbiol. Appl. Sci*, *7*(4), pp.683-694.

Thomas, H.C., 1944. Heterogeneous ion exchange in a flowing system. *Journal of the American Chemical Society*, *66*(10), pp.1664-1666.

Tian, Q., Yu, D., Zhu, K., Hu, G., Zhang, L. and Liu, Y., 2016. Multi-hollow polymer microspheres with enclosed surfaces and compartmentalized voids prepared by seeded swelling polymerization method. *Journal of colloid and interface science*, *473*, pp.44-51.

Tiede, K., Hassellöv, M., Breitbarth, E., Chaudhry, Q. and Boxall, A.B., 2009. Considerations for environmental fate and ecotoxicity testing to support environmental risk assessments for engineered nanoparticles. *Journal of chromatography A*, *1216*(3), pp.503-509.

Tiwari, D.K., Behari, J. and Sen, P., 2008. Application of nanoparticles in waste water treatment 1.

Toshima, N. and Yonezawa, T., 1998. Bimetallic nanoparticles—novel materials for chemical and physical applications. *New Journal of Chemistry*, *22*(11), pp.1179-1201.

Tripathi, R., Sodaye, S. and Sudarshan, K., 2015. Non-compound nucleus fission in actinide and pre-actinide regions. *Pramana*, *85*(2), pp.315-322.

Turnlund, J.R., 1998. Human whole-body copper metabolism. *The American journal of clinical nutrition*, *67*(5), pp.960S-964S.

Tyagi, I., Gupta, V.K., Sadegh, H., Ghoshekandi, R.S. and Makhlouf, A.H., 2017. Nanoparticles as adsorbent; a positive approach for removal of noxious metal ions: a review. *Science Technology and Development*, *34*(3), pp.195-214.

Udikovic-Kolic, N., Wichmann, F., Broderick, N.A. and Handelsman, J., 2014. Bloom of resident antibiotic-resistant bacteria in soil following manure fertilization. *Proceedings of the National Academy of Sciences*, *111*(42), pp.15202-15207.

USEPA (U.S. Environmental Protection Agency), 2008. Draft nanomaterial research strategy. EPA/600/S-08/002. Washington, DC: U.S. Environmental Protection Agency, Office of Research and Development.

USEPA (U.S. Environmental Protection Agency), 2019. Drinking Water Health Advisories for PFOA and PFOS.

USEPA; Antimicrobial Copper Alloys Group. Available online: https://www3.epa.gov/pesticides/chem_search/ppls/082012-00002-20101110.pdf (accessed on 28 January 2021).

Van der Horsta, C., Silwanaa, B., Makombea, M., Iwuohab, E. and Somerseta, V., 2021. Application of a chitosan bimetallic nanocomposite for the simultaneous removal of cadmium, nickel, and lead from aqueous solution. *Desalination and Water Treatment*, *220*, pp.168-181.

Vidal, M., Santos, M.J., Abrão, T., Rodríguez, J. and Rigol, A., 2009. Modeling competitive metal sorption in a mineral soil. *Geoderma*, *149*(3-4), pp.189-198.

Vincent, M., Duval, R.E., Hartemann, P. and Engels- Deutsch, M., 2018. Contact killing and antimicrobial properties of copper. *Journal of applied microbiology*, *124*(5), pp.1032-1046.

Vodyanitskii, Y.N., 2010. The role of iron in the fixation of heavy metals and metalloids in soils: a review of publications. *Eurasian Soil Science*, *43*(5), pp.519-532.

Wadhawan, S., Jain, A., Nayyar, J. and Mehta, S.K., 2020. Role of nanomaterials as adsorbents in heavy metal ion removal from waste water: A review. *Journal of Water Process Engineering*, *33*, p.101038.

Walsh, F.C. and Reade, G.W., 1994. Electrochemical techniques for the treatment of dilute metal-ion solutions. In *Studies in environmental science* (Vol. 59, pp. 3-44). Elsevier.

Wang, B., Wan, Y., Zheng, Y., Lee, X., Liu, T., Yu, Z., Huang, J., Ok, Y.S., Chen, J. and Gao, B., 2019. Alginate-based composites for environmental applications: a critical review. *Critical reviews in environmental science and technology*, *49*(4), pp.318-356.

Wang, H., Sheng, K.C., Lan, T., Adl, M., Qian, X.Q. and Zhu, S.M., 2010. Role of surface treatment on water absorption of poly (vinyl chloride) composites reinforced by Phyllostachys pubescens particles. *Composites Science and Technology*, *70*(5), pp.847-853.

Wang, H., Zhou, Y., Jiang, X., Sun, B., Zhu, Y., Wang, H., Su, Y. and He, Y., 2015. Simultaneous capture, detection, and inactivation of bacteria as enabled by a surface- enhanced Raman scattering multifunctional chip. *Angewandte Chemie*, *127*(17), pp.5221-5225.

Wang, J. and Chen, C., 2009. Biosorbents for heavy metals removal and their future. *Biotechnology advances*, *27*(2), pp.195-226.

Wang, L., Hu, C. and Shao, L., 2017. The antimicrobial activity of nanoparticles: present situation and prospects for the future. *International journal of nanomedicine*, *12*, p.1227.

Wang, S. and Peng, Y., 2010. Natural zeolites as effective adsorbents in water and wastewater treatment. *Chemical engineering journal*, *156*(1), pp.11-24.

Wang, T., Jiao, Y., He, M., Ouyang, W., Lin, C. and Liu, X., 2022. Facile co-removal of As (V) and Sb (V) from aqueous solution using Fe-Cu

binary oxides: Structural modification and self-driven force field of copper oxides. *Science of The Total Environment*, *803*, p.150084.

Wang, T., Jiao, Y., He, M., Ouyang, W., Lin, C., Liu, X. and Xie, H., 2022. Deep insight into the Sb (III) and Sb (V) removal mechanism by Fe–Cu-chitosan material. *Environmental Pollution*, *303*, p.119160.

Wang, X., Guo, Y., Yang, L., Han, M., Zhao, J. and Cheng, X., 2012. Nanomaterials as sorbents to remove heavy metal ions in wastewater treatment. *J. Environ. Anal. Toxicol*, *2*(7), pp.154-158.

Wang, Y., Zhao, X., Gao, W., Chen, L., Chen, S., Wei, M., Gao, M., Wang, C., Zhang, Y. and Yang, J., 2015. Au/Ag bimetal nanogap arrays with tunable morphologies for surface-enhanced Raman scattering. *RSC advances*, *5*(10), pp.7454-7460.

Wang, Z., Huang, W. and Fennell, D.E., 2015. Rapid dechlorination of 1, 2, 3, 4-TCDD by Ag/Fe bimetallic particles. *Chemical Engineering Journal*, *273*, pp.465-471.

Wang, Z., Shen, Q., Xue, J., Jia, H., Xu, B., Liu, X. and Li, Q., 2020. Annealing temperature effect on 3D hierarchically porous NiO/Ni for removal of trace hexavalent chromium. *Materials Chemistry and Physics*, *240*, p.122140.

Water, U.N., 2018. 2018 UN World Water Development Report, Nature-based Solutions for Water.

Weber, B. and Holz, F., 1991. Landfill leachate treatment by reverse osmosis. In *Effective industrial membrane processes: benefits and opportunities* (pp. 143-154). Springer, Dordrecht.

Wen, M., Liu, Q.Y., Wang, Y.F., Zhu, Y.Z. and Wu, Q.S., 2008. Positive microemulsion synthesis and magnetic property of amorphous multicomponent Co-, Ni-and Cu-based alloy nanoparticles. *Colloids and Surfaces A: Physicochemical and Engineering Aspects*, *318*(1-3), pp.238-244.

Weng, X., Lin, S., Zhong, Y. and Chen, Z., 2013. Chitosan stabilized bimetallic Fe/Ni nanoparticles used to remove mixed contaminants-amoxicillin and Cd (II) from aqueous solutions. *Chemical engineering journal*, *229*, pp.27-34.

WHO, 2008. *Guidelines for drinking-water quality: second addendum. Vol. 1, Recommendations*. World Health Organization.

WHO, G., 2011. Guidelines for drinking-water quality. *World health organization*, *216*, pp.303-304.

WHO, U. and UNICEF, 2017. Progress on drinking water, sanitation and hygiene. *Joint Monitoring Programme*.

WHO. Edition, F. (2011). Guidelines for drinking-water quality. WHO chronicle, 38(4), 104-108.

Wolny-Koładka, K.A. and Malina, D.K., 2017. Silver nanoparticles toxicity against airborne strains of Staphylococcus spp. *Journal of Environmental Science and Health, Part A*, *52*(13), pp.1247-1256.

WHO, 2017. Guidelines for Drinking Water Quality–Fourth Edition Incorporating the First Addendum, 2017.

WHO, 2019. *Global status report on alcohol and health 2018*. World Health Organization.

Wu, J. and Yu, H.Q., 2008. Biosorption of 2, 4-dichlorophenol from aqueous solutions by immobilized Phanerochaete chrysosporium biomass in a fixed-bed column. *Chemical Engineering Journal*, *138*(1-3), pp.128-135.

Wu, S.H. and Chen, D.H., 2003. Synthesis and characterization of nickel nanoparticles by hydrazine reduction in ethylene glycol. *Journal of Colloid and Interface Science*, *259*(2), pp.282-286.

Wu, X., Xing, W., Zhang, L., Zhuo, S., Zhou, J., Wang, G. and Qiao, S., 2012. Nickel nanoparticles prepared by hydrazine hydrate reduction and their application in supercapacitor. *Powder technology*, *224*, pp.162-167.

Xia, J., Duan, Q.Y., Luo, Y., Xie, Z.H., Liu, Z.Y. and Mo, X.G., 2017. Climate change and water resources: Case study of Eastern Monsoon Region of China. *Advances in Climate Change Research*, *8*(2), pp.63-67.

Xing, Y., Chen, X. and Wang, D., 2007. Electrically regenerated ion exchange for removal and recovery of Cr (VI) from wastewater. *Environmental science & technology*, *41*(4), pp.1439-1443.

Xiu, Z.M., Zhang, Q.B., Puppala, H.L., Colvin, V.L. and Alvarez, P.J., 2012. Negligible particle-specific antibacterial activity of silver nanoparticles. *Nano letters*, *12*(8), pp.4271-4275.

Xu, P., Zeng, G.M., Huang, D.L., Feng, C.L., Hu, S., Zhao, M.H., Lai, C., Wei, Z., Huang, C., Xie, G.X. and Liu, Z.F., 2012. Use of iron oxide nanomaterials in wastewater treatment: a review. *Science of the Total Environment*, *424*, pp.1-10.

Xu, W., Liew, K.Y., Liu, H., Huang, T., Sun, C. and Zhao, Y., 2008. Microwave-assisted synthesis of nickel nanoparticles. *Materials letters*, *62*(17-18), pp.2571-2573.

Yadav, N., Jaiswal, A.K., Dey, K.K., Yadav, V.B., Nath, G., Srivastava, A.K. and Yadav, R.R., 2018. Trimetallic Au/Pt/Ag based nanofluid for enhanced antibacterial response. *Materials Chemistry and Physics*, *218*, pp.10-17.

Yagub, M.T., Sen, T.K., Afroze, S. and Ang, H.M., 2015. Fixed-bed dynamic column adsorption study of methylene blue (MB) onto pine cone. *Desalination and Water Treatment*, *55*(4), pp.1026-1039.

Yang, Y., Liao, H., Tong, Z. and Wang, C., 2015. Porous Ag/polymer composite microspheres for adsorption and catalytic degradation of organic dyes in aqueous solutions. *Composites Science and Technology*, *107*, pp.137-144.

Ye, J., Wang, Y., Xu, Q., Wu, H., Tong, J. and Shi, J., 2021. Removal of hexavalent chromium from wastewater by Cu/Fe bimetallic nanoparticles. *Scientific reports*, *11*(1), pp.1-11.

Yoon, K.Y., Byeon, J.H., Park, J.H. and Hwang, J., 2007. Susceptibility constants of Escherichia coli and Bacillus subtilis to silver and copper nanoparticles. *Science of the Total Environment*, *373*(2-3), pp.572-575.

Yoon, Y.H. and Nelson, J.H., 1984. Application of gas adsorption kinetics I. A theoretical model for respirator cartridge service life. *American industrial hygiene association journal*, *45*(8), pp.509-516.

You, J., Zhao, C., Cao, J., Zhou, J. and Zhang, L., 2014. Fabrication of high-density silver nanoparticles on the surface of alginate microspheres for application in catalytic reaction. *Journal of Materials Chemistry A*, *2*(22), pp.8491-8499.

Zaleska-Medynska, A., Marchelek, M., Diak, M. and Grabowska, E., 2016. Noble metal-based bimetallic nanoparticles: the effect of the structure on the optical, catalytic and photocatalytic properties. *Advances in colloid and interface science*, *229*, pp.80-107.

Zamboulis, D., Peleka, E.N., Lazaridis, N.K. and Matis, K.A., 2011. Metal ion separation and recovery from environmental sources using various flotation and sorption techniques. *Journal of Chemical Technology & Biotechnology*, *86*(3), pp.335-344.

Zha, T., Song, L., Chen, P., Nie, W. and Zhou, Y., 2015. Nonsolvent/solvent-induced phase separation to multi-porous sulfonated polystyrene/chitosan/silver particles and their application in adsorbing chromium ion (III) and reduction of methylene blue. *Colloids and Surfaces A: Physicochemical and Engineering Aspects*, *481*, pp.423-430.

Zhang, D., Li, G. and Jimmy, C.Y., 2010. Inorganic materials for photocatalytic water disinfection. *Journal of materials chemistry*, *20*(22), pp.4529-4536.

Zhang, F., Chen, X., Wu, F. and Ji, Y., 2016. High adsorption capability and selectivity of ZnO nanoparticles for dye removal. *Colloids and Surfaces A: Physicochemical and Engineering Aspects*, *509*, pp.474-483.

Zhang, G., Li, J., Zhang, G. and Zhao, L., 2015. Room-temperature synthesis of Ni nanoparticles as the absorbent used for sewage treatment. *Advances in Materials Science and Engineering*, *2015*.

Zhang, M., Zhang, K., De Gusseme, B. and Verstraete, W., 2012. Biogenic silver nanoparticles (bio-Ag0) decrease biofouling of bio-Ag0/PES nanocomposite membranes. *Water research*, *46*(7), pp.2077-2087.

Zhang, Y., Wu, B., Xu, H., Liu, H., Wang, M., He, Y. and Pan, B., 2016. Nanomaterials-enabled water and wastewater treatment. *NanoImpact*, *3*, pp.22-39.

Zhang, Z., Shen, Q., Cissoko, N., Wo, J. and Xu, X., 2010. Catalytic dechlorination of 2, 4-dichlorophenol by Pd/Fe bimetallic nanoparticles in the presence of humic acid. *Journal of Hazardous Materials*, *182*(1-3), pp.252-258.

Zhao, L., Wang, H., Huo, K., Cui, L., Zhang, W., Ni, H., Zhang, Y., Wu, Z. and Chu, P.K., 2011. Antibacterial nano-structured titania coating

incorporated with silver nanoparticles. *Biomaterials*, *32*(24), pp.5706-5716.

Zhou, S., Li, Y., Chen, J., Liu, Z., Wang, Z. and Na, P., 2014. Enhanced Cr (VI) removal from aqueous solutions using Ni/Fe bimetallic nanoparticles: characterization, kinetics and mechanism. *RSC Advances*, *4*(92), pp.50699-50707.

Zhou, X., Xue, X. and Jiang, W., 2011, February. Study on adsorption of heavy metal ion in metallurgical wastewater by sepiolite. In *Proceeding of 2011 2nd International Conference on Environmental Science and Development. IPCBEE* (Vol. 4, pp. 100-104).

APPENDIX I

PUBLICATIONS

Patents

- Hridya T K and P S Harikumar. "A Method to Prepare a Porous Bimetallic Nanocomposite Microsphere" [Indian Patent Application No. 202241028652].

Journals

- Hridya T K, Rosmin Antu and Harikumar, P.S., (2023). Remediation of Pb (II), Cd (II), and Zn (II) from aqueous solutions using porous (styrene–divinylbenzene)/Cu–Ni bimetallic nanocomposite microspheres: continuous fixed-bed column study. *Water Science and Technology*, *87*(9), pp.2277-2291. DOI: 10.2166/wst.2023.101.
- Hridya, T.K., Varghese, E. and Harikumar, P.S., 2021. Removal of heavy metals from aqueous solution using porous (Styrene-divinylbenzene)/CuNi bimetallic nanocomposite microspheres. *Environmental Nanotechnology, Monitoring & Management*, *16*, p.100606. DOI: 10.1016/j.enmm. 2021.100606.
- Harikumar, P.S and Hridya, T.K., 2019. Application of CuNi bimetallic nanoparticle as an adsorbent for the removal of heavy metals from aqueous solution. *International Journal of Environmental Analytical Chemistry*, *101*(6), pp.869-883. DOI: 10.1080/03067319.2019.1673383.

Conferences

- Hridya, T. K., & Harikumar, P. S. (2022). *Fixed-Bed Column Study on Lead Removal from Aqueous Solutions Using Porous (Styrene-Divinylbenzene)/Cu-Ni Bimetallic Nanocomposite Microspheres.* Proceedings of the International Conference on Water and Environmental Management, 22-24-June, CWRDM, Kozhikode, Kerala.
- Hridya, T. K., & Harikumar, P. S. (2020). *Poly(Styrene-DVB) Encapsulated CuNi Bimetallic nanoparticles as an Adsorbent for the Removal of Heavy Metals from Aqueous Solution.* Proceedings of the International Conference on Water Resources, 16-17 October 2020, Central University of Karnataka in virtual mode.
- Hridya, T. K., & Harikumar, P. S. (2020). *Application of Poly(Styrene-DVB) Encapsulated CuNi Bimetallic Nanomaterials for the Removal of Mercury from Waste Water.* Proceedings of the Third Indian National Groundwater Conference, 18-20 February 2020, CWRDM, Kozhikode, Kerala.
- Hridya, T. K., & Harikumar, P. S. (2018). *Removal of Heavy Metals from Aqueous Solution Using CuNi Bimetallic Nanoparticle.* Proceedings of the International Symposium on Advances in Materials Science, 24-25 October 2018, Sree Sankara College, Kalady, Kerala.